



**Constraints on the Upper Permian  
to Upper Triassic marine carbon isotope curve.  
Case studies from the Tethys**

**Thèse de doctorat**

présentée à la

Faculté des Sciences de  
l'Université de Lausanne

par

**Nicu-Viorel ATUDOREI**

Diplomé en Géologie  
Université de Bucarest

**Jury**

Prof. Jacques Dubochet, Président  
Prof. Jean GUEX, Rapporteur  
Dr. Aymon BAUD, Directeur de thèse  
Prof. Maurice RENARD, Expert  
Prof. Zachary SHARP, Expert

LAUSANNE

1998

*Imprimatur*  
*Université de Lausanne*  
*Faculté des Sciences*

*Vu le rapport présenté par le jury d'examen, composé de*  
*MM.* M. le Dr Aymon BAUD, directeur de thèse, MM. les Profs  
Jean GÜEX, Maurice RENARD, Zachary SHARP, experts,  
M. le Prof. Jacques DUBOCHET, président.

*le Conseil de Faculté autorise l'impression de la thèse de Monsieur*  
Nicu-Viorel ATUDOREI, géologue diplômé de l'Université de Bucarest,  
Roumanie  
*intitulée*                    CONSTRAINTS ON THE UPPER PERMIAN  
TO UPPER TRIASSIC MARINE CARBON ISOTOPE CURVE.  
CASE STUDIES FROM THE TETHYS

*Lausanne, le* 16 décembre 1998

pour *Le doyen de la Faculté des Sciences*  
Professeur Jacques DUBOCHET

*J. Dubochet*

# CONTENTS

<b>Foreword</b> .....	<i>i</i>
<b>Acknowledgements</b> .....	<i>i</i>
<b>Abstract</b> .....	1
<b>Résumé</b> .....	2
<b>Chapter 1.</b>	
<b>Introduction</b> .....	3
<b>Chapter 2.</b>	
<b>Controls on the stable isotope record in marine carbonate sediments</b> .....	9
<b>2.1 Inorganic (carbonate) carbon isotope</b> .....	10
2.1.1 Carbon isotope variations in the modern ocean and in carbonate sediments.....	10
2.1.2 The effect of diagenesis on $\delta^{13}\text{C}$ values of carbonates.....	11
2.1.3 Secular variations.....	12
<b>2.2 Organic carbon isotopes</b> .....	14
<b>2.3 Sulfur isotopes</b> .....	15
<b>2.4 Strontium isotopes</b> .....	15
<b>Chapter 3.</b>	
<b>Supporting data, methods and analytical techniques</b> .....	17
<b>3.1 Constraining the carbon isotope seawater curve using bulk carbonate samples</b> .....	17
<b>3.2 The Upper Permian to Upper Triassic time scale</b> .....	18
3.2.1 Subdivisions.....	20
3.2.2 Biostratigraphy.....	21
3.2.3 Radiometric calibration.....	21
<b>3.3 Methods</b> .....	23
<b>3.4 Analytical techniques</b> .....	23
3.4.1 Carbonate and organic carbon content.....	23
3.4.2 Carbonate carbon and oxygen isotopes.....	24
3.4.3 Organic carbon isotopes.....	24
3.4.4 Strontium isotope measurements.....	24

<b>Chapter 4.</b>	
<b>Constraints from the Permian-Triassic of the Tethyan Himalaya.....</b>	<b>27</b>
4.1 Introduction.....	27
4.2 Salt Ranges.....	29
4.2.1 Nammal Gorge section.....	29
4.2.2.Landu Nala section.....	34
4.3 Kashmir.....	36
4.3.1 Guryul Ravine section.....	36
4.3.2 Palgham section.....	40
4.4 Spiti.....	40
4.4.1 Losar section.....	40
4.5 Nepal.....	46
4.5.1 Thini Chu section.....	46
4.6 Conclusions.....	48
<b>Chapter 5.</b>	
<b>Constraints from the Permian-Triassic of Oman.....</b>	<b>51</b>
5.1 Introduction.....	51
5.2 Shallow-water settings: the Akhdar Group.....	53
5.2.1 Wadi Sahtan section.....	53
5.3 Carbonate platform margin settings: the Sumeini Group.....	58
5.3.1 Wadi Maqam section.....	58
5.4 Deeper water settings: the Oman exotics and sediments of the Hawasina Group.....	60
5.4.1 Wadi Alwa.....	60
5.4.2 Wadi Wasit.....	63
5.4.3 Wadi Musjah.....	65
5.5 Conclusions.....	67
<b>Chapter 6.</b>	
<b>Constraints from the the Triassic of North Dobrogea.....</b>	<b>71</b>
6.1 Geological settings and stratigraphy.....	71
6.1.1 Geological settings.....	71
6.1.2 The Triassic of the Tulcea Unit.....	73
6.1.3 Lithostratigraphy.....	74
6.2 Stratigraphy, carbon and oxygen isotope data.....	79
6.2.1 Shallow water settings.....	79
6.2.2 Deeper water settings.....	84

## *Contents*

6.2.3 Basinal settings.....	104
6.2.4 Other localities.....	110
<b>6.3 Interpretation of carbon and oxygen isotope data .....</b>	<b>113</b>
6.3.1 Carbonate platforms versus basin isotopic signatures.....	110
6.3.2 The preservation of the stable isotope record.....	113
6.3.3 Stratigraphic trends.....	114
<b>6.4 Strontium isotope data.....</b>	<b>119</b>
6.4.1 Samples.....	119
6.4.2 Results.....	119
6.4.3 Stratigraphic trends.....	120
<b>Chapter 7.</b>	
<b>Constraints from the the Triassic of Albania.....</b>	<b>127</b>
7.1 Kçira section.....	127
<b>Chapter 8.</b>	
<b>The Upper Permian to Upper Triassic carbon isotope curve.....</b>	<b>129</b>
8.1 Late Permian.....	129
8.2 The Permian/Triassic boundary.....	132
8.3 Early Triassic.....	133
8.4 The Lower-Middle Triassic boundary.....	134
8.5 Middle - Late Triassic.....	136
8.6 Strontium and sulfur isotope curves.....	136
<b>References.....</b>	<b>141</b>
<b>Appendix.....</b>	<b>161</b>
Plates (1 to 5)	
Tables (1 to 27)	

## Foreword

This dissertation would have not been possible without the financial support of the Swiss National Science Foundation through grants 20 - 33'448.92 and 2000 - 045455.95, the Geological Museum of Lausanne, the Institute of Mineralogy and Petrography and the Institute of Geology and Paleontology, University of Lausanne. Part of the fieldwork in Romania was funded by the Peritethys Program. Fieldwork in Oman was greatly facilitated by the Oman Ministry of Commerce and Industry and I am grateful to Dr. Hilal Bin Mohammed Al Azry , Deputy Director General of Minerals. Thanks also to Dr. Jean-Paul Breton, Head of the Oman Branch of the BRGM and to Françoise, for their valuable help.

Given the interdisciplinary aspect of the present work, bordering stable isotope geochemistry, stratigraphy, sedimentology and paleoceanography, it could not have been completed without the support of several individuals who shared samples, basic stratigraphic data, technical expertise and contributed to the interpretations expressed herein through discussions. These generous contributors include: Aymon Baud, Hugo Bucher, Maurizio Gaetani, Eugen Gradinaru, Jean Guex, Elena Mirauta, Maurice Renard, Zachary Sharp, Graham Shields and Sofia Zerrari. Particularly, Eugen Gradinaru provided a large amount of basic data (including litho and biostratigraphy) which constitutes the framework for chapter 6; the reader should be aware that most of these data were not published previously and that they represent an original contribution by Eugen Gradinaru.

## Acknowledgements

I sincerely believe that Lausanne represents an ideal place to study the Permian-Triassic chemostratigraphy. The Institute of Geology and Paleontology from the University of Lausanne has a well established tradition in the study of Permian and (mostly) Triassic. The Geological Museum of Lausanne (which has particularly strong ties with the former through location and research activities) hosts large and unique collections of Permian and Triassic sedimentary rocks, many of them from remote areas or inaccessible today. In addition, the Institute of Mineralogy and Petrography is equipped with modern facilities, including a state-of-the-art stable isotope laboratory. Therefore, I consider myself fortunate to have had the opportunity to complete a dissertation on this particular subject and in this particular place.

I am extremely grateful to Aymon Baud, my thesis adviser, who offered me the possibility to complete this work. I always appreciated his constant support, availability, and patience as well as his vast knowledge of Permian-Triassic stratigraphy. Many discussions with Aymon (including disagreements) helped shape many of the ideas presented in the following pages. Special thanks go to Jean Guex, who taught me to think critically and be a better scientist. I already miss our long discussions about the Triassic timescale and geochronology in general (among so many others). Zachary Sharp influenced me in more ways than he knows. He not only taught me stable isotope geochemistry and “infected” me (as well as anyone around) with his energy and enthusiasm; he unwillingly (or maybe not...) taught me different ways to structure my research and to be less conventional. I had the advantage to collaborate with Maurice Renard, whose insightful comments were extremely stimulating and inspirational. I also appreciate very much that he accepted to act as a referee for my dissertation.

I owe very much to Eugen Gradinaru who had a major contribution to my formation as a geologist and opened my eyes to the Triassic stratigraphy and to the fascinating North Dobrogea. Without his generous contribution, the “heart” of the dissertation (the chapter 6) could not be possibly completed.

I am grateful to many individuals for their effective help and exchange of ideas. Johannes Hunziker constantly encouraged this work and made possible unlimited access to the stable isotope laboratory. Graham Shields and Peter Stille (Strasbourg) provided the strontium isotope measurements. The trace elements studies on samples from Dobrogea by Sofia Zerrari and Maurice Renard (Paris) were very helpful in evaluating the stable isotope data. Hugo Bucher (Lyon) shared samples and unpublished stratigraphic data from Spiti and sustained stimulating discussions on various aspects of the dissertation. Elena Mirauta kindly identified the conodont faunas and shared her vast knowledge on the Triassic of North Dobrogea. Prof. Maurizio Gaetani (Milano) shared samples from Albania and constantly encouraged this work. Discussions with Gérard Stampfli on various aspects of Triassic geology were always inspirational. Alain Pillevuit offered valuable data and ideas for the Oman sections. Philippe Thélin and Liliane Dufresne kindly helped with acquisition of XRD data. Nicholas Meisser always shared his remarkable expertise in mineralogy and chemistry and constantly advised me in chemicals handling. Laurent Nicod executed an impressive number of thin sections. Jean-Claude Lavanchy and Hans-Rudolf Pfeifer made possible coulometric determinations. Peter Baumgartner, Graham Shields and Jim O’Neil contributed in one way or another to my understanding of paleoceanography and stable isotope geochemistry.

Many colleagues made my stay in Lausanne extremely pleasant. I enjoyed all the time I spent with the team from the Geological Museum, including Nejia, Odile, Aymon, Daniel, Gilles, Michel, Nicholas, Stephane and Stephan. I do not have to write special thanks to my Italian friends and colleagues. Ana-Chiara, Bianca Neve, Mizzi, Sabrina, Andreea, Antonio, Giovanni, Guido, Lorenzo, Luigi, Raffaele, and all the others, know how much I enjoyed their company. The same holds true for Yannis, Olman and Pierre. I also spent enjoyable time with Carole, Irina, Pascale, Tatiana, Alain, Dave, Francois, Jean-Claude, Jon, Marcus, Mike, Robin and Romano. Thanks to all of you!

And finally, I would like to thank Adriana, Ana, Ileana, Michaela, Micheline, Raluca, Sultana, Veronique, Dan, Eugen, Gabi, Gérard, Horatiu, Ionut, Sorin and Traian for making me feel in Lausanne like at home and to my parents for their love.

## Abstract

Secular variations of the seawater carbon isotopic composition provide evidence for paleoceanographic and paleoclimatic changes and may serve for chemiostratigraphic correlations. The present study aimed to improve the current knowledge on the Upper Permian and Triassic segment of the Phanerozoic marine carbon isotope curve, whose Triassic part was poorly constrained by previous studies. Profiles of inorganic carbon isotopes are provided for sections from Himalaya (Salt Range, Kashmir, Spiti and Nepal), Oman and North Dobrogea (Romania) on the basis of whole-rock carbonate analysis.

The data acquired, together with a literature compilation confirmed that most of the Upper Permian is characterized by high  $\delta^{13}\text{C}$  values (averaging +4‰) but failed to detect a positive excursion as suggested by recent compilations. In the light of these observations, the large drop in  $\delta^{13}\text{C}$  values associated with the end-Permian mass extinction appears to be driven by a sudden transfer of previously stocked  $\delta^{13}\text{C}$  depleted carbon, rather than by the overturn of a Late Permian stratified ocean.

The Triassic data-set outlines significant secular variations. The best documented is a carbon isotope positive excursion just across the Lower-Middle Triassic boundary, globally developed since it was detected in various paleogeographic settings. It is interpreted to reflect variations in surface ocean chemistry, possibly related to increased primary productivity, at times when the biotic recovery after the end-Permian mass-extinction began to accelerate significantly and when a sharp rise in seawater  $\delta^{34}\text{S}$  values occurred globally. Strontium isotope data obtained from well preserved biogenic phosphates allow a refinement of the Middle Triassic segment of the seawater strontium isotope curve and show a major inflexion point of the seawater strontium isotope curve also near the Lower Triassic - Middle Triassic boundary. These facts suggest that the transition from the Early to the Middle Triassic was a time of revolutionary global change which represented an important step in the evolution of Mesozoic marine environments.

A tentative carbon isotope curve for the Upper Permian to Upper Triassic time interval is proposed. Its major features are:

- high but constant  $\delta^{13}\text{C}$  values during the Late Permian
- a sharp drop in  $\delta^{13}\text{C}$  values in the latest Permian
- subsequent recovery of  $\delta^{13}\text{C}$  values
- a short-lived positive excursion across the Early-Middle Triassic boundary
- a gradual rise in  $\delta^{13}\text{C}$  values starting in the Late Ladinian or in the Early Carnian

It is foreseen that these fluctuations of the carbon isotope curve may serve as chronostratigraphic markers and further assist in the correlation of Permian and Triassic carbonate deposits.



## Résumé

Les variations séculaires de la proportion relative des isotopes stables de l'eau de mer permettent de mettre en évidence des changements paléo-océanographiques et paléoclimatiques et peuvent également servir pour des corrélations chemostratigraphiques. La présente étude a pour but d'apporter des nouvelles données sur le segment Permien supérieur - Trias de la courbe isotopique du carbone marin relativement mal contraint jusqu'à présent. Des profils isotopiques du carbone inorganique basés sur les analyses de roche totale des carbonates ont été établis sur des coupes lithologiques provenant de l'Himalaya (Salt Range, Kashmir, Spiti and Nepal), d'Oman, et de la Dobrogea du Nord (Roumanie).

Les nouvelles données compilées avec celles disponibles dans la littérature confirment que la majeure partie du Permien supérieur est caractérisé par de hautes valeurs  $\delta^{13}\text{C}$  (en moyenne +4‰) mais par contre, ne permettent pas de détecter une excursion positive comme suggéré par de récentes études. A la lumière de ces observations, l'importante chute du  $\delta^{13}\text{C}$  associée à l'extinction en masse de la fin du Permien serait la conséquence d'un transfert massif de carbone léger antérieurement stocké sous la forme de matière organique, plutôt que par un phénomène de mélange d'un océan stratifié durant le Permien tardif.

Les données provenant de couches marines d'âge triasique mettent en évidence des fluctuations importantes de la courbe isotopique. Un événement isotopique positif très bien documenté et retrouvé dans des coupes éloignées se situe à la limite Trias inférieur - Trias moyen. Il est interprété comme reflétant des variations de la chimie des eaux de surface, variations probablement liées à l'augmentation de la productivité primaire. Ceci intervient au moment où la biomasse se diversifie de manière significative, bien après l'extinction en masse de la fin du Permien. Au même moment une très rapide augmentation des valeurs du  $\delta^{34}\text{S}$  de l'eau de mer se marque sur l'ensemble du globe. Les données des isotopes du strontium obtenues sur des phosphates biogéniques bien préservés permettent un affinement de la courbe isotopique du strontium marin pour le Trias moyen et montrent aussi un point d'inflexion majeur de celle-ci, proche de la limite Trias inférieur - Trias moyen. Ces faits suggèrent qu'au passage du Trias inférieur au Trias moyen un changement global radical intervient. Il représente un pas important dans l'évolution des environnements marins mésozoïques.

Une courbe synthétique des valeurs isotopiques du carbone ( $\delta^{13}\text{C}$ ) pour l'intervalle Permien supérieur - Trias supérieur est présentée. Les points les plus marquants sont:

- des valeurs du  $\delta^{13}\text{C}$  élevées et relativement constantes durant le Permien supérieur
- une chute très marquée des valeurs du  $\delta^{13}\text{C}$  à la fin du Permien suivi d'un retour à des valeurs intermédiaires
- une excursion positive de courte durée à la limite Trias inférieur - Trias moyen
- une augmentation graduelle du  $\delta^{13}\text{C}$  à partir du Ladinien supérieur ou du Carnien inférieur

Les fluctuations enregistrées sur la courbe isotopique du carbone offrent potentiellement une aide non négligeable aux corrélations entre les dépôts carbonatés du Permien et du Trias de régions éloignées.

# CHAPTER 1

## INTRODUCTION

The end of the Paleozoic and the beginning of the Mesozoic, that is the Late Permian and the Early Triassic, was a time of profound biotic crisis in the history of the Earth. Much of the Paleozoic marine biota was affected by the most devastating mass extinction in the Earth history, the end-Permian mass extinction (Raup, 1979; Raup and Sepkoski, 1986; Erwin, 1993, 1994). The Late Permian - Early Triassic is characterized by a series of features that, all together, have never been encountered in the history of the Earth. Following the end-Permian mass extinction, the full recovery of the marine biota was delayed with several millions years (Erwin, 1993). No reef communities (corals, green algae, sphinctozoans) are known in the Early Triassic (Flügel, 1994; Flügel and Senowbari-Darian, 1996). The Early Triassic reef gap was paralleled on land by a coal gap (Faure et al., 1995; Rettalack et al., 1996). Along with the dramatic reduction of marine biota, the aftermath of the end Permian mass extinction was a flourishing of disaster forms as microbial communities (Schubert and Bottjer, 1992; Baud et al, 1997) and fungi (Eshet et al, 1995; Visscher et al, 1996).

The Late Permian - Triassic was also a time of maximum continental aggregation (the supercontinent Pangea) characterized by a warm, dry climate as suggested by both geological evidence (e.g. Parrish, 1993) and modelling studies (Wilson et al., 1994; Fawcett et al., 1994). In addition, climate models predict extreme continentality and monsoonal circulation (Crowley et al., 1989).

During the last decades, carbon isotopes became increasingly used in paleoceanographic and paleoclimatic reconstructions. Secular variations in carbon, sulfur and strontium isotopic composition of marine sediments were detected and Phanerozoic age curves have been constructed (Fig. 1). However, the curves available for Phanerozoic delineate only the major trends, numerous short term variations were documented and superpose on the long term trends (see review by Holser et al., 1995). As far as the Permian and Triassic periods are concerned, the isotopic composition of seawater carbon, sulfur and strontium underwent large variations (Holser and Magaritz, 1987). Most of the previous carbon isotope studies focused on the Upper Permian and the lower part of the Lower Triassic (Baud et al., 1989; Magaritz and Holser, 1991; and many others); very few considered in detail the remainder of the Lower Triassic and the Triassic in general. Therefore, the Triassic segment of the frequently cited Phanerozoic carbon isotope curve (Holser, 1988), or even of the Scholle's (1995) more recent compilation is poorly constrained.

The number of marine sections with a good chronostratigraphic coverage for this time interval is relatively small and restricted to some areas. Probably the best sedimentary marine record is found along the Tethyan margins, presently in the Alpine-Himalayan Belt and in adjacent areas. Other marine sections across the Permian-Triassic boundary can be found in the Arctic domain (Arctic Canada, Svalbard Basin). Most of the deep sea sediments have been consumed through subduction processes; the deep sea record is known only from some accreted terrains in Japan and in British Columbia (Isozaki, 1994). The existing whole-rock carbonate carbon isotope data-set is based mainly on sections from the Tethys Ocean, which was the major site for the deposition of carbonate rocks during the Permian to Triassic time interval.

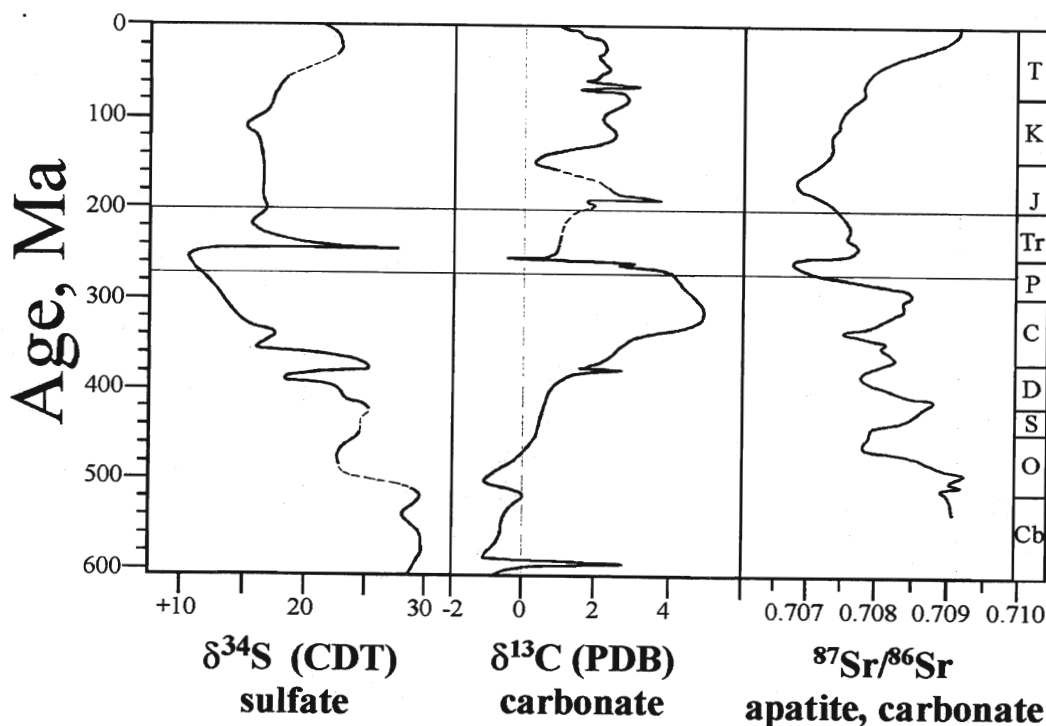


**Fig. 1** Phanerozoic age curves of sulfur isotopes ( $\delta^{34}\text{S}$ ) in sulfates, carbon isotopes ( $\delta^{13}\text{C}$ ) in carbonates and strontium isotopes ( $^{87}\text{Sr}/^{86}\text{Sr}$ ) in carbonates and phosphates. After Holser (1984).

An outline of C, S, and Sr isotopic curves near the Permian-Triassic boundary as well as the basic problems related to their interpretations are given in a keynote paper by Holser and Magaritz (1987). The most significant contributions to the knowledge of carbon isotope variations near the Permian/Triassic boundary are those reported by Baud et al. (1989a) and Magaritz and Holser (1991). Baud et al. (1989a) provided carbon isotope profiles for the Upper Permian and Lower Triassic time-interval for numerous sections from the Tethys and proposed a carbon isotope curve for that period (fig. 2). Magaritz and Holser (1991) focused on the Permian-Triassic transition in a core section from the Southern Alps and provided a high resolution carbon isotope curve.

In two recent reviews (Grossman, 1994; Scholle, 1995), the Carboniferous to Triassic carbonate carbon and oxygen isotope data set is critically evaluated. Scholle (1995) compiled a large number of Late Carboniferous to Early Jurassic carbonate carbon isotope data. He processed separately carbon isotope data from whole-rock micritic limestones, dolomites, marine cements and brachiopods and constructed isotopic curves by smoothing through the most positive clusters of data points, assuming that in most situations diagenetic overprint acts toward lower  $\delta^{13}\text{C}$  values (fig. 3). Given the poor chronostratigraphic coverage of the existing data set, the general trend outlined by Scholle (1995) may obscure short term variations.

During the last years further insights have been provided by organic carbon isotope data (e.g. Magaritz and Holser, 1992). Although the controls on natural variations of carbon isotopes from organic matter are complex (Popp et al., 1997; Foster et al., 1997), variations consistent with carbonate carbon data have been found across the Permian/Triassic boundary (Wang et al, 1994).

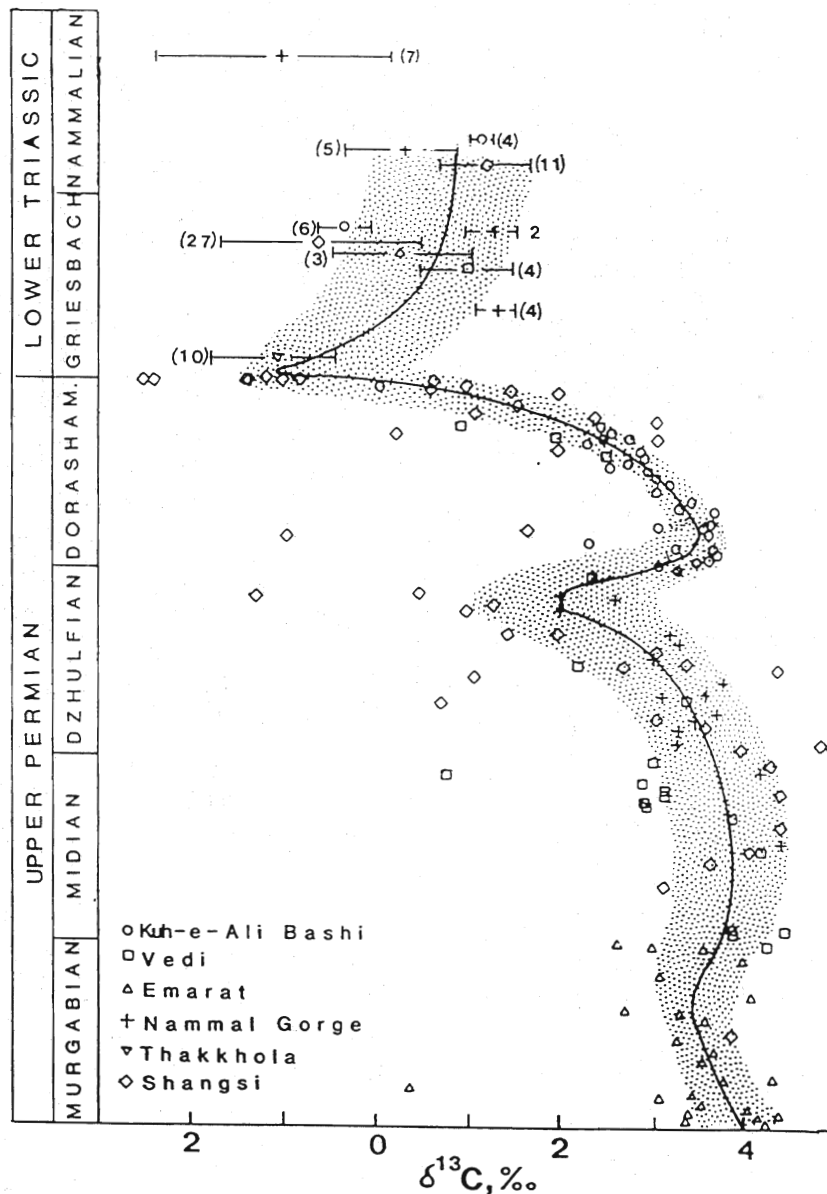


**Fig. 2** Late Permian and Early Triassic carbon isotope data based on Tethyan carbonates. After Baud et al. (1989a).

Strontium and sulfur isotope seawater curves for the Upper Permian and Triassic time interval were proposed by Koepnick et al. (1990), Denison and Koepnick (1995) and Claypool et al. (1980).

Much less attention has been paid to the Triassic seawater curve, although a number of papers considered various aspects of origin, paleoclimate or diagenesis using carbon and oxygen isotopes from Triassic carbonates (e.g. Scherer, 1977; Henrich and Zankl, 1986; Frisia-Bruni and Weissert, 1989; Spötl and Burns, 1991; Litnerova, 1992; Bernasconi, 1993; Bellanca, 1995; Al-Aasm, 1995; Mutti and Weissert, 1995; Loreau, 1995; Zeeh et al., 1995; Zeeh et al., 1997).

One of the few studies that present in detail carbon isotope variations along measured Triassic profiles are presented in Steuber (1991) and Simon and Steuber (1993). The data were obtained on a Middle Triassic to Lower Jurassic section from the Helicon Mountains, Greece. No well defined fluctuations were observed in  $\delta^{13}\text{C}$  values of the carbonates, instead, a gradual increase in  $\delta^{13}\text{C}$  values of organic matter from Ladinian to Norian was found. More recently, Böhm and Gawlick (1997) reported a

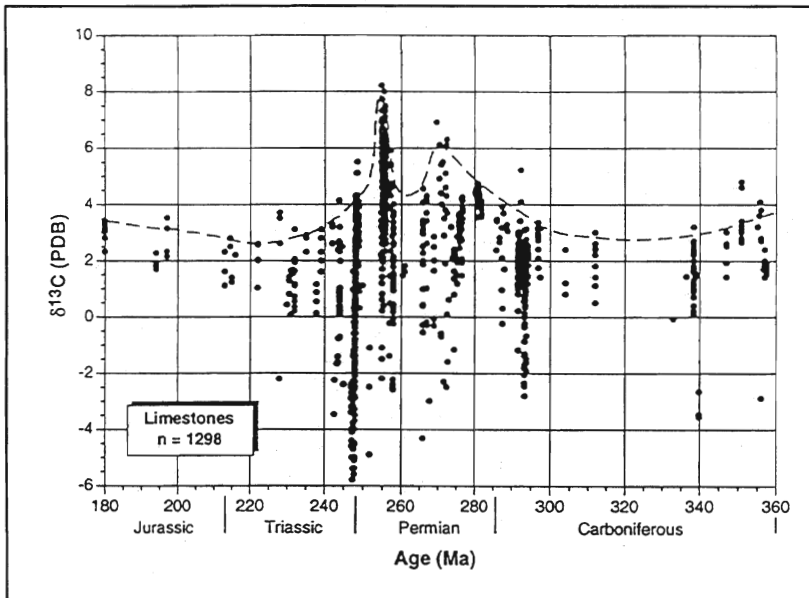


**Fig. 3** *Secular variations of  $\delta^{13}\text{C}$  values of Carboniferous to Jurassic marine micritic limestones. After Scholle (1995).*

Triassic carbon cycling and its partitioning between the major reservoirs, with significant implications for paleoceanographic and paleoclimatic reconstructions, and secondly it may potentially serve as a reference for stratigraphic correlations.

Profiles of inorganic carbon isotopes were studied in several sections from the Tethyan Permo-Triassic. The studied sections are representatives of three main paleogeographic areas within the Tethys: the Northern Indian margin (presently in the Himalayan belt), the Omanese margin and the North Dobrogean margin (fig. 4).

positive carbon isotope excursion in the Upper Triassic based on data obtained on a section from the Northern Calcareous Alps.

The main goal of the present study is to ameliorate the current knowledge on the Upper Permian and Triassic segment of the Phanerozoic marine carbon isotope curve and to propose an improved carbon isotope curve. The interest in establishing a carbon isotope curve for this period of time is twofold. First, it may improve our understanding of Permian and

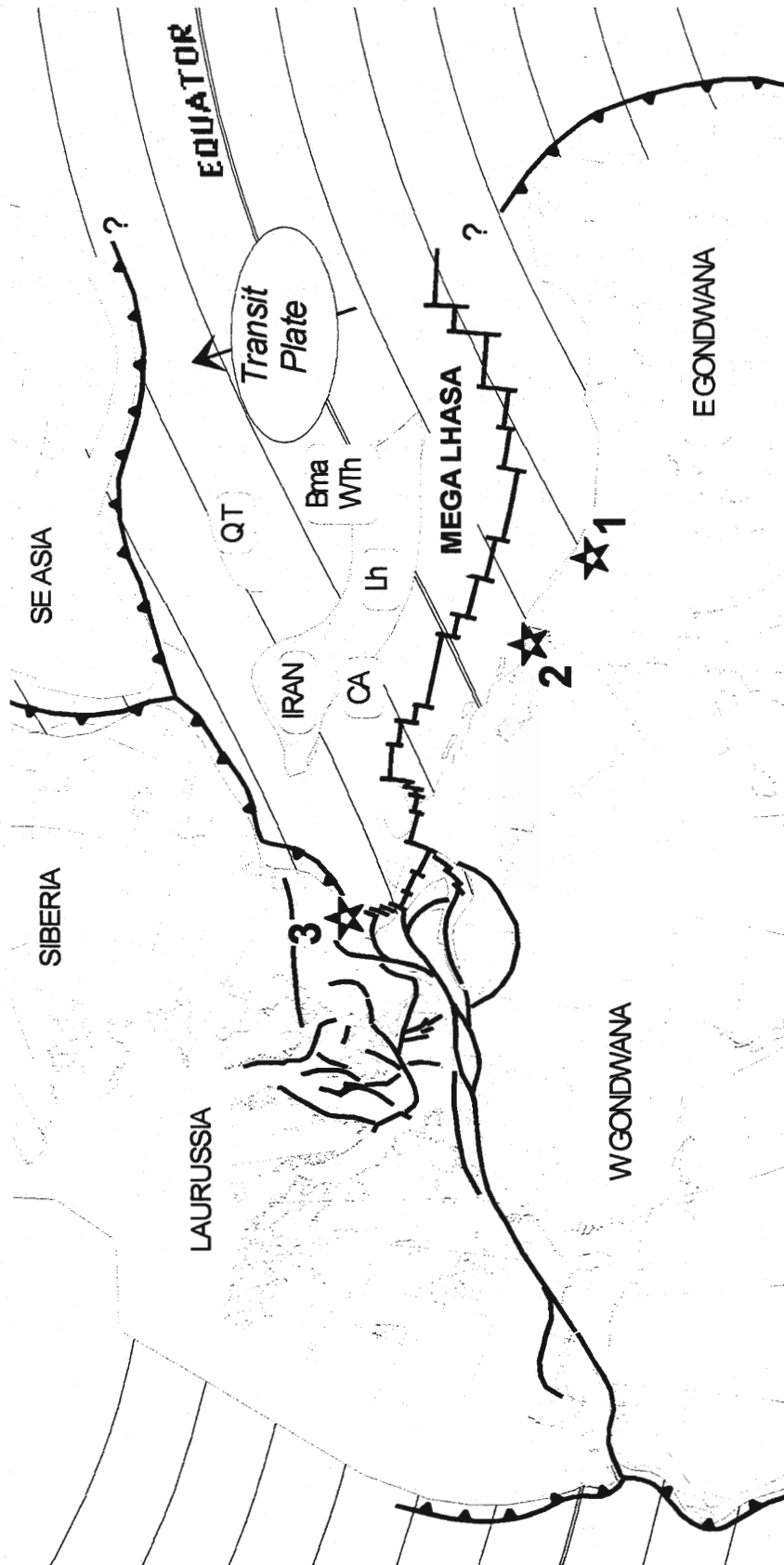


**Fig. 4** Paleogeographic map of the Tethyan domain for the Late Anisian, showing the location of the Northern Indian margin (1), Oman margin (2) and North Dobrogea margin (3) (Ricou et al., 1992 and Marcoux et al., 1993).



## CHAPTER 2

# CONTROLS ON THE STABLE ISOTOPE RECORD IN CARBONATE SEDIMENTS

The purpose of this chapter is to briefly discuss the factors controlling the carbon, sulfur and strontium isotope composition in marine environments and in carbonate rocks. There are many papers which review the applications of stable isotope geochemistry in sedimentary geology. General considerations can be found in Hoefs (1987, or later editions), Chester (1990) and Bowen (1991) and more specific applications are reviewed in various papers in Arthur et al. (1983), Schidlowski et al. (1983), Reeder (1983), Kyser (1987), Gregor et al. (1988) and Clauer and Chaudhuri (1992). Figure 5 represents schematically the major sources of variations of the isotopes of carbon, sulfur and strontium in the exogenic cycle. Herein, only some general features are presented, more detailed discussions are provided for those aspects which are considered significant for the interpretation of the Permian to Triassic isotope record. Someway, this chapter reflects the author's view onto the still controversial field of the stable isotope stratigraphy.

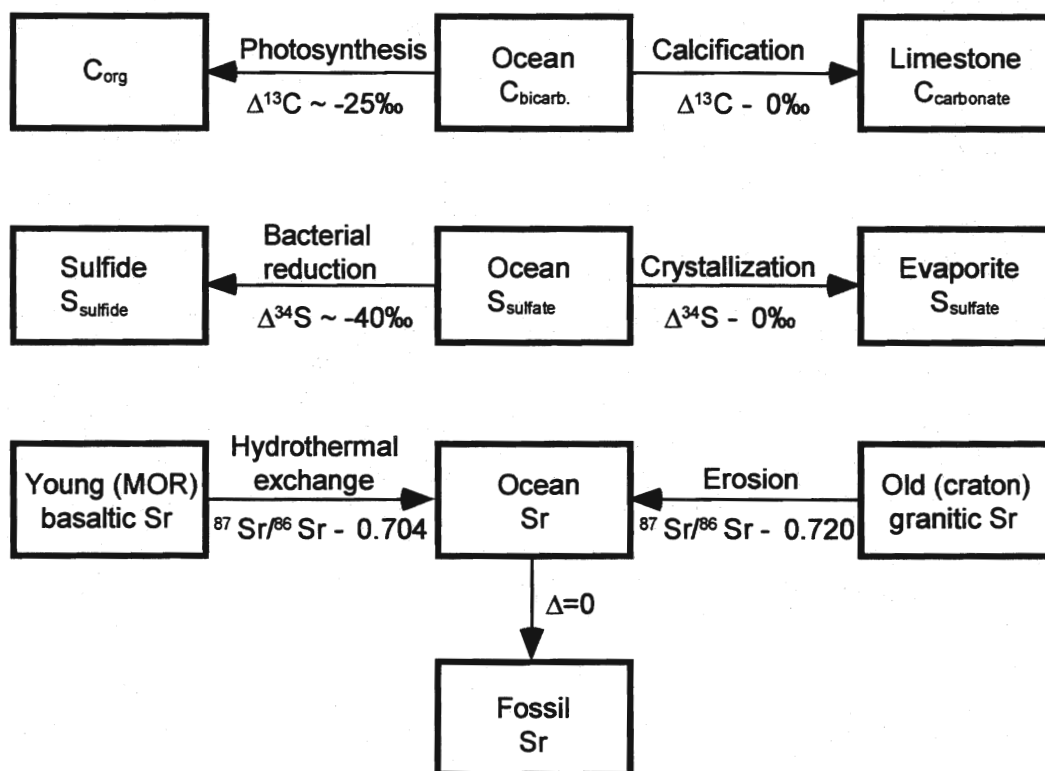


**Fig. 5** The major sources of secular variations of C, S and Sr isotopes in marine environments (adapted after Holser et al., 1984).

marine environments (adapted after Holser et al., 1984).



## 2.1. Inorganic (carbonate) carbon isotopes

Marine carbonates are sensitive recorders of ancient oceanic and atmospheric chemistry. Carbon isotopes, for instance are widely used in paleoceanographic and paleoclimatic reconstructions. Reviews concerning the marine carbonate carbon isotopes can be found in Anderson and Arthur (1983), Veizer (1983), Holser et al. (1988), Land (1992), Marshall (1992), Grossman (1994) and Holser (1997).

### 2.1.1. Carbon isotope variations in the modern ocean and in carbonate sediments

In the modern ocean, the carbon isotopic composition of the **Dissolved Inorganic Carbon (DIC)** is not homogeneous, both vertical and horizontal variations being reported (Broecker and Peng, 1982). The range of variations of  $\delta^{13}\text{C}$  in the open ocean DIC is relatively small, less than 1‰ (Kroopnick, 1980); however, in carbonate platforms and in more restricted marine basins the  $\delta^{13}\text{C}$  of the seawater DIC may be up to 4‰ lower relative to the open ocean as a result of evaporation, freshwater input and respiration of organic matter (Patterson and Walter, 1994).

The most important process affecting carbon isotopic composition of dissolved carbonate in the seawater is photosynthesis which strongly discriminates against  $^{13}\text{C}$ , preferentially incorporating  $^{12}\text{C}$  in organic matter. Thus, changes in phytoplankton productivity, or bacterial oxidation of organic matter in the water column, will significantly affect surface water  $\delta^{13}\text{C}$  values (Berger and Vincent, 1986).

In the present day ocean the dissolved bicarbonate in surface seawater is relatively enriched in  $^{13}\text{C}$  as a result of the preferential uptake of  $^{12}\text{C}$  during photosynthesis. In contrast, deep waters are relatively depleted in  $^{13}\text{C}$  due to the respiration and oxidation of the sinking isotopically light organic matter. Therefore, there is a marked carbon isotopic gradient in dissolved bicarbonate between the surface and bottom water masses. In the well mixed modern ocean, the surface-to-deep gradient is in the order of 1-3‰ (Kroopnick et al., 1970), but in anoxic basins, such as the Black Sea, it can be as high as 7‰ (Deuser, 1970).

The carbon isotopic composition of **carbonate sediments** is controlled by the isotopic composition of the carbonate dissolved in the seawater. Both biological and chemical precipitation of calcium carbonate are generally associated with a relatively small but constant fractionation of carbon isotopes, virtually independent of temperature (Emrich, 1970). The magnitude of the fractionation is determined by the mineralogy of the resulting carbonate (Grossman and Ku, 1986) and by the carbonate ion concentration (Spero et al., 1997). The  $\text{HCO}_3^-$  - calcite and  $\text{HCO}_3^-$  - aragonite fractionation are  $1.0 \pm 0.1\text{‰}$  and  $2.7 \pm 0.2\text{‰}$ , respectively (Romanek et al., 1992). Consequently,  $\delta^{13}\text{C}$  values of the calcite will be about 1.7‰ lower than  $\delta^{13}\text{C}$  values of the aragonite precipitated from the same waters. However, biological carbonates often precipitate out of isotopic equilibrium with ambient waters, as a result of either kinetic or metabolic processes (McConnaughey, 1989), the so-called "vital-effect". The magnitude of the "vital effect" for both carbon and oxygen isotopes may vary among groups of carbonate secreting organisms or within one group (see Wefer and Berger, 1991, for a review). Studies on individual components of recent carbonate sediments also revealed heterogeneity in the carbon isotopic composition (Gonzales and Lohmann, 1985).

Thus, it appears that in the present day ocean the carbon isotopic composition of the seawater and of the carbonate sediments is heterogeneous. However, taking into consideration only the open marine carbonate sediments the variability is greatly reduced.

### 2.1.2. The effect of diagenesis on $\delta^{13}\text{C}$ values of carbonates

Previous studies demonstrated that the original isotopic composition of carbonates may be modified during diagenesis (for reviews see Hudson, 1977; Dickson and Coleman, 1980; Brand and Veizer, 1981; Marshall, 1992; Grossman, 1994 and Kaufman et al., 1995). Diagenetic overprint usually lower both the  $\delta^{18}\text{O}$  and  $\delta^{13}\text{C}$  values of the original carbonate (there are some exceptions, however) because the diagenetic fluids are commonly depleted in  $^{13}\text{C}$  and  $^{18}\text{O}$  with respect to the seawater (and the marine carbonates). The amount of oxygen present in diagenetic fluids is considerable and therefore the  $\delta^{18}\text{O}$  composition of the carbonate can be easily modified; in turn carbon is only rarely affected by diagenesis in carbonate rocks because there is much more carbon in carbonates than in diagenetic fluids and thus the carbon isotopic composition of fluids is buffered by that of the host carbonates (Magaritz, 1983). Mass balance calculations showed that extremely high water volumes are required to shift  $\delta^{13}\text{C}$  values in carbonate-rich rocks (Banner and Hanson, 1990). In addition, the diagenetic fluids interacting with the carbonates prior to lithification have a carbon isotopic composition dominated by the seawater.

There are, however, some situations when the  $\delta^{13}\text{C}$  values of the carbonates can be substantially modified. During the **meteoric diagenesis** both  $\delta^{13}\text{C}$  and  $\delta^{18}\text{O}$  values of the carbonate can be shifted to lower values (Allan and Mathews, 1977, 1982). When dealing with normal marine sequences meteoric diagenesis is rather the exception and exposure surfaces can be relatively easily recognized through sedimentologic and geochemical criteria; the cross-plot of  $\delta^{13}\text{C}$  and  $\delta^{18}\text{O}$  values of cements exhibit a typical inverted "J" trend (Lohmann, 1987).

The most significant diagenetic processes which can alter the carbon isotopic composition of carbonates are those involving the breakdown of organic matter (Irwin et al., 1977; Curtis and Coleman, 1986). During the **anoxic early diagenesis**, cements with extremely variable  $\delta^{13}\text{C}$  values can be precipitated as the endproduct of a process comprising bacterial sulfate reduction of organic matter and  $\text{CO}_2$  production. The  $\delta^{13}\text{C}$  values of organic matter are very low (average values are about -25‰) and therefore the addition of cements incorporating carbon derived from the decomposition of organic matter can affect the bulk carbonate  $\delta^{13}\text{C}$  values. It should be noted that  $^{13}\text{C}$  enriched cements can also be formed during the early anoxic diagenesis, in the methanogenesis zone of Irwin et al. (1977). Carbonate cements with low  $\delta^{13}\text{C}$  values can be formed also during **burial diagenesis**, also in relation with the breakdown of the organic matter which can be decomposed under increased temperatures (Heydari, 1997). It is questionable, however, if the bulk carbonate  $\delta^{13}\text{C}$  values will be significantly affected, as carbonates are usually lithified before attaining burial diagenetic depths and porosity related open spaces reduced. Burial diagenetic products are laid down mainly along veinlets which are usually avoided during sampling.

It appears thus that the carbon isotopic composition of **organic rich sediments** is prone to diagenetic alteration, more than any other type of normal marine carbonate sediments (e.g. Grant, 1992). A survey of the published whole-rock  $\delta^{13}\text{C}$  data from organic-rich sediment, show that  $^{13}\text{C}$  depletion do not always occur as a simple function of the organic carbon content. The  $C_{\text{carbonate}}/C_{\text{organic}}$  ratio is probably more meaningful than the organic carbon content alone. This has been demonstrated by Jenkyns and Clayton (1997) through simple mass balance calculations. However, the  $C_{\text{carbonate}}/C_{\text{organic}}$  ratio should be estimated for the entire pile of sediments and not only at a hand sample scale, as carbonate-rich samples are preferentially collected for carbon isotope stratigraphies.  $^{13}\text{C}$  depleted cements may derive also from adjacent organic rich sediments. In this context, another parameter somehow difficult to evaluate, is whether the diagenetic transformations took place in open or close systems (Marshall, 1992).

The carbon isotopic composition of carbonate rocks can be altered also during **metamorphism** by decarbonation reactions in the presence of siliciclastic components (Kaufman and Knoll, 1995). This process occur only if silicates are present in the rock; pure carbonate rocks may preserve their carbon isotopic composition even during high-temperature processes (e.g. Sharp et al., 1995).

A number of criteria have been proposed in order to evaluate the preservation of the isotopic composition, as reviewed by Marshall (1992) and Holser et al. (1995). So far, diagenetic overprints have been detected using textural evidence, trace element data, cathodoluminescence studies, strontium isotope analysis (Renard, 1979; Brand and Veizer, 1981; Popp et al., 1986; Veizer et al., 1986; Adlis et al., 1988; Veizer et al., 1997a). Accordingly, best preserved samples should have trace element concentrations similar to those reported for modern ocean (Mn, Sr, Fe, Mg and the Sr/ Mg, Sr/Mn ratios are believed to be the most meaningful) and the  $^{87}\text{Sr}/^{86}\text{Sr}$  ratios should be close to the seawater ratios for the time period concerned (Burke et al., 1982). Crossplots of trace element data and isotopic ratios may indicate diagenetic alteration, when patterns of covariance are displayed. Brand and Veizer (1981) proposed that using such crossplots original isotopic composition may be calculated through backstripping. So far, few works (if any) have attempted to correct the measured  $\delta^{13}\text{C}$  values through backstripping for "adjusting" carbon isotope stratigraphic profiles. Widely used are  $\delta^{13}\text{C} - \delta^{18}\text{O}$  cross plots, the covariance of the two parameters being interpreted as a result of diagenetic alteration; however, they may also reflect primary variations (Marshall, 1992)

Finally, a critical evaluation of the published carbon isotope stratigraphies leads to the conclusion that the best way to prove that stratigraphic variations observed in individual sections reflect changes in seawater chemistry is to demonstrate by biostratigraphical means that they reproducible laterally at a global scale (Renard, 1986; Holser et al., 1995; Saltzman et al., 1998).

### 2.1.3. Secular variations

The isotopic heterogeneity in Dissolved Inorganic Carbon and carbonate sediments documented in the modern ocean (as shown above) as well as examples showing that the carbon isotopic signature may be altered diagenetically, led many scientists to treat the whole-rock based isotopic data as unreliable. However, the large number of studies published during the past 20 years showed that bulk carbonates may accurately record the carbon isotope composition of the water in which they formed. This may be due to the fact that early diagenesis tends to average the isotopic composition of the individual components (average which appears to approximate the composition of the seawater) and later diagenetic processes have little effect on the carbon isotopic composition, as discussed above. Stratigraphic trends have been confirmed to be correlative and carbon isotope reference curves have been established for several time-windows (see references cited in Holser et al., 1995).

There is a general consensus that long term variations (i.e. longer than the residence time of carbon in the ocean - about  $10^5$  years) are the due to changes in the partition between the main isotopically different carbon reservoirs: the oxidized carbon reservoir (essentially the carbonate reservoir) and the reduced carbon reservoir (organic material). Several processes are responsible for the changing fluxes between the two reservoirs. The most important of them are briefly discussed bellow. Recent reviews can be found in Holser et al. (1995) and Holser (1997).

#### **Carbon isotope trends and organic carbon burial**

For any given time the  $\delta^{13}\text{C}$  composition of surface waters DIC is determined by the photosynthetic reduction of oxidized carbon to organic carbon. The  $^{13}\text{C}$  depleted organic material produced in surface waters is transferred to the deep ocean leaving the surface waters relatively enriched in  $^{13}\text{C}$ . At steady-state conditions, the burial of organic carbon is balanced by the input of  $^{13}\text{C}$  depleted from others

reservoirs (basically through recycling of reduced organic carbon). Hence, if the burial of organic carbon exceeds the recycling of organic carbon, the  $\delta^{13}\text{C}$  values of surface waters will increase.

Accordingly, carbon isotope excursions have been related to changes in burial rates through time. Examples from the geological record have showed that positive carbon isotope excursions are correlated with black shales deposition (Scholle and Arthur, 1980, among many others). Likewise, a relative decrease in organic carbon burial is mirrored by a decrease in surface water DIC  $\delta^{13}\text{C}$  (Holser, 1997). In the oceanic realm, increasing rates of organic carbon burial can be related to increased marine productivity (Pedersen and Calvert, 1990), to low oxygen levels in deep and intermediate waters (Canfield, 1994), to elevated sedimentation rates or to a combination of them.

An important point is that the oceanic waters will record also changes in burial fluxes on both continents and oceans, because atmospheric and oceanic  $\text{CO}_2$  levels are in equilibrium. Important amounts of organic carbon may be stored in terrestrial environments. For example, Dean and Gorham (1998) estimated that in the present day the rate of accumulation of organic carbon in lakes and peatlands is higher than the rate of organic carbon accumulation in the global ocean.

### **Carbon isotope trends and marine primary productivity**

The relation of secular variations in carbon isotope trends with marine productivity was postulated already by the early workers in carbon isotope stratigraphy (e.g. Scholle and Arthur, 1980). During times of increased primary productivity, more  $^{12}\text{C}$  is removed from the surface waters (Berger and Vincent, 1986) and leaving the dissolved carbonate enriched in  $^{13}\text{C}$ . Thus, periods of increased productivity should coincide with positive excursion of  $\delta^{13}\text{C}$  values in carbonates.

Because nutrient concentration in the seawater is a limiting factor for marine productivity, the nutrient cycling was often recalled in interpreting carbon isotope excursions (eg. Förlmi et al., 1994; Martin, 1996). The main sources of nutrients in surface waters are runoff from surrounding land masses and recycling through a feed-back mechanism involving the breakdown of organic matter, the latter being probably the most important, because of mass-balance requirements. The mechanisms of nutrients recycling are complex. An important issue to address in relation with primary productivity and carbon isotope excursions is whether nutrient recycling is prevailing during periods of ocean stratification, as proposed by Van Cappellen and Ingall (1994) or in well mixed oceans, driven by massive upwelling of deep-waters (Thiede and Suess, 1983; Martin, 1996). Both alternatives are widely invoked.

Magaritz (1989) observed that the major mass-extinctions are correlated with a negative shift in marine  $\delta^{13}\text{C}$  values and explain the latter by a reduction of biomass. Kump (1991) noted that the oceanic biomass represents an insignificant carbon reservoir (compared to the total oceanic carbon reservoir) and argued that changes in oceanic biomass should not influence the  $\delta^{13}\text{C}$  record. Following his arguments, at timescales longer than the residence time of carbon in the ocean ( $10^5$  years) only changes in organic burial/weathering rates will be recorded isotopically. Thus, changes in primary productivity can be recorded only as very short events (the transient excursions of Holser et al., 1995), unless they are coupled with organic carbon burial.

### **Carbon isotope trends and sea-level changes**

A positive correlation between the relative sea-level changes and carbon isotope trends (positive carbon isotope trends corresponding to rising sea level) has been noted by several studies (Scholle and Arthur, 1980; Renard et al., 1982; Woodruff and Savin, 1985; Weissert and Lini, 1991; Förlmi et al., 1994; Baud et al., 1996; Jenkyns, 1996; Mitchel et al., 1996; Grötsch et al., 1998). It was explained as a result of increasing primary productivity and organic carbon burial fluxes during highstand levels because of increased areas covered by the sea and hence increased net organic production (Mitchel et

al., 1996) or as a more complex interplay between climate, nutrient cycling, primary productivity and organic carbon burial (Förlmi et al., 1994; Bartolini et al., 1996). When comparing relative sea-level changes with carbon isotopes patterns we must be aware of the source of carbon isotope data because the  $\delta^{13}\text{C}$  signature may record paleobathymetry, as suggested by Berger and Vincent (1986), Baum et al., (1994), Vahrenkamp (1996), among others. Generally speaking,  $\delta^{13}\text{C}$  values of whole-rock shallow-water limestones may be higher than their deep-water counterparts because the  $^{13}\text{C}$  depleted benthic skeletal component is present only in deep-water carbonates which, in addition, undergo early diagenesis in the presence of  $^{13}\text{C}$  depleted deep-waters. Therefore, shifts to higher  $\delta^{13}\text{C}$  in shallowing upward sequences may reflect decreasing water depths, and not necessarily changes in surface-water DIC  $\delta^{13}\text{C}$  values.

Although sea-level changes are often correlated with carbon isotope trends, they are not directly related. This statement is demonstrated by the numerous examples when sea-level changes are not correlated with carbon isotope excursion and when carbon isotope excursion are not correlated with sea-level changes. The ultimate cause of secular variations in carbon isotope values of carbonates are organic carbon burial fluxes (related or not to primary productivity) or inputs from other major carbon reservoirs (Kump, 1991), as riverine influx, recycling of previously formed organic carbon reservoirs, maybe also abrupt and massive inputs of volcanic  $\text{CO}_2$ .

## 2.2. Organic carbon isotopes

The carbon isotopic composition of organic carbon in marine environments was reviewed recently by Sackett (1989), Hayes (1993), Meyers (1994, 1997), Tyson (1995), De Leeuw et al. (1995) and Popp et al. (1997).

Organic matter consists of a variety of components with a wide range of  $\delta^{13}\text{C}$  values and variable resistance to degradation (Hayes et al., 1983). The major factors that control the variations of  $\delta^{13}\text{C}$  values of marine organic matter are, according to Popp (1997):

- concentrations of oceanic (and atmospheric)  $\text{CO}_2$
- phytoplankton productivity
- physiology of marine phytoplankton

In the interpretation of bulk samples of organic carbon from stratigraphic section it is hypothesized that temporal fluctuations of organic carbon isotope ratios, as recorded by well-preserved marine sediments, are determined primarily by the shallow water productivity and dissolved  $\text{CO}_2$  levels.

The organic matter produced presently in terrestrial environments has  $\delta^{13}\text{C}$  values lower than the marine organic matter (Tyson, 1995). Likewise, the carbon isotopic composition of bulk organic matter in marine sediments has also related to sea level changes. Variations in  $\delta^{13}\text{C}$  values of organic matter are interpreted as the result of mixing between the two major isotopically distinctive sources (marine versus terrestrial). Bulk organic matter  $\delta^{13}\text{C}$  values from lowstand deposits should be higher than their counterparts from transgressive, highstand deposits, reflecting a stronger terrestrial influence for the former.

It has been shown that global shifts of carbon isotope ratios recorded in marine carbonates are paralleled by those derived from organic carbon in coeval rocks (Magaritz et al. 1992, Wang et al., 1994, Morante et al, 1996). Because it is unlikely that diagenetic processes would alter carbon isotope ratios in carbonate and inorganic carbon in the same direction, the parallelism of  $\delta^{13}\text{C}_{\text{carb}}$  and  $\delta^{13}\text{C}_{\text{org}}$

values is regarded as evidence for the primary origin of the observed variations (Morante and Hallam, 1996; Joackimski, 1997).

Given the variety of factors controlling the carbon isotopic composition of organic material, chemostratigraphic studies based on bulk organic matter should be made in conjunction with other studies (e.g. organic petrology).

### 2.3. Sulfur isotopes

Sulfur isotopic systematics in sedimentary environments was reviewed recently by Holser (1988), Nielsen (1989) and Strauss (1997).

There is only a minor isotopic fractionation associated with the precipitation of sulfates from the seawater (Longinelli, 1989), therefore the sulfur isotopic composition of sulfates can be used to determine global variations of the seawater sulfate through time. The main process leading to isotopic fractionation of sulfur in marine environments is the sulfate reduction through processes mediated by bacteria. Basically, seawater sulfate is reduced to dissolved sulfide ( $\text{H}_2\text{S}$ ), which is further reacting with detrital iron minerals to produce iron monosulfides or/and pyrite. Because bacteria discriminate against the  $^{34}\text{S}$ , sedimentary sulfides are enriched in  $^{32}\text{S}$  relative to the seawater sulfate. The magnitude of this fractionation is controlled mainly by the sulfate reduction rate which in turn may be dependent by a variety of factors, such as the organic carbon supply, redox conditions or sediment deposition rates (Berner, 1984; Canfield, 1991). However, Kajiwara (1992), Canfield and Teske (1996), Habicht and Canfield (1997) showed that bacterial sulfate reduction cannot fully explain the sulfur isotopic composition of marine sulfides. They argued that the initial  $^{34}\text{S}$  depletion resulted from the bacterial reduction of sulfate, is followed by further  $^{34}\text{S}$  depletion during the oxidation of sulfides. Thus, larger fractionation of sulfur isotope are achieved through repeated cycles of bacterial sulfate reduction and oxidation. Therefore, sulfur isotope data from sedimentary sulfides may provide paleoenvironmental information.

The Phanerozoic seawater  $\delta^{34}\text{S}$  curve relies on the analysis of sulfate minerals, mainly from evaporitic deposits, assuming that the sulfur isotopic composition of the seawater is homogenous (Claypool et al., 1980). Secular variations are related to variations of the sulfur redox cycle, similar to the carbonate carbon. High  $\delta^{34}\text{S}$  values of surface water sulfates should reflect periods of extensive burial of reduced sulfur (commonly pyrite).

### 2.4. Strontium isotopes

Strontium isotopic composition, mainly the  $^{87}\text{Sr}/^{86}\text{Sr}$  ratio, has proved to be particularly useful in tracing geological processes (Faure, 1977). Strontium has a relatively high concentration in seawater and a residence time much longer than the oceanic mixing time; therefore the seawater  $^{87}\text{Sr}/^{86}\text{Sr}$  ratios is very homogenous at any one time. The strontium isotopic composition of the seawater is determined primarily by the balance between the "radiogenic strontium" (high  $^{87}\text{Sr}/^{86}\text{Sr}$  ratio) delivered to the oceans via continental weathering and "nonradiogenic strontium" (low  $^{87}\text{Sr}/^{86}\text{Sr}$  ratio) delivered to the oceans via the mid-ocean ridge hydrothermal systems (Elderfield, 1986). Secular variations in the seawater strontium isotope curve is driven by changes in the mass flux and isotopic composition of these two sources, provided there is negligible contribution of  $^{87}\text{Sr}$  from  $^{87}\text{Rb}$  decay. Simply stated, hydrothermal circulation decreases the  $^{87}\text{Sr}/^{86}\text{Sr}$  of marine Sr, while continental weathering increase it.

The considerable amount of data acquired during the last 15 years demonstrated the utility of strontium isotopes as a stratigraphic tool (Elderfield, 1986; McArthur, 1994; Veizer et al., 1997; Stille and Shields, 1998). A Phanerozoic strontium isotope curve was proposed by Burke (1982), based on whole-rock carbonate analysis, further refined by the "Ottawa-Bochum research group" (Veizer et al., 1997) through the analysis of low magnesium calcite shells and conodonts. The advantage of using biogenic carbonates or phosphates is due to the fact that their state of preservation can be more easily estimated. Unlike the light elements (e.g. C, O) strontium does not experience any isotopic fractionation or "vital effect" during shell growth.

# CHAPTER 3

## SUPPORTING DATA, METHODS AND ANALYTICAL TECHNIQUES

Any attempt to prospect chemostratigraphic trends should meet several basic requirements:

- The biostratigraphic control of the samples used must be reliable. In spite of the advent of many "non-biostratigraphic" techniques for the correlation of sedimentary sequences, biostratigraphy remains the most reliable correlation tool, at least for Permian and Triassic times. For Triassic sediments, ammonoids are the most useful age diagnostic fossils and we should be able to relate any geochemical trend to an ammonoid based zonation. However, there is no single generally accepted "standard" ammonoid zonation for the Upper Permian to Upper Triassic time interval and one has to choose among the proposed zonations the one which can be used for a given paleogeographic area.
- The timing and the duration of "isotope events" should be well constrained in order to understand their origin. When evidence for geological events to be related with the "isotope events" is lacking (situations occurring often when dealing with pre-Cretaceous sediments, as a result of an increased consumption of older oceanic sediments through subduction processes), it is useful to have good estimates of their duration for mass balance requirements (Kump, 1991; Holser et al., 1997) and therefore we need a good radiometric calibration of the time scale used.
- A good knowledge of the samples to be analysed is essential in order to evaluate the quality of the geochemical results. Simply stated, we should know what we measure: primary seawater signal or a mixture of primary and diagenetic signals.
- Analytical procedures employed are important to be well understood and accurately reported. Although carbon and oxygen isotope analysis are routinely measured presently, confusion may be introduced at this stage through inappropriate reporting of the calibration methods and standardization.

Specific aspects which apply to the present work are discussed in the following section.

### 3.1. Constraining the carbon isotope seawater curve using bulk carbonate samples

There are basically two approaches employed for reconstructing pre-Jurassic secular variations of carbon isotope ratios, as discussed in Grossman (1994) and Scholle (1995). The first considers only the



data recorded from carefully selected carbonate components, like marine cements and mainly nonluminescent brachiopod shells, which are more likely to preserve primary signatures. The second one relies on the use of whole-rock micritic limestones or dolomites assuming, through mass-balance criteria, that inorganic carbon isotopes are affected to only a small degree by diagenetic alteration in carbonate rich sediments (diagenetic processes are buffered by the carbonate in which concerns carbon isotopes); oxygen isotopes have been, in most cases, reset during diagenesis.

The scarce occurrence of well preserved thick shelled brachiopods in Triassic deposits seriously limits the acquisition of "high-confidence" carbon and oxygen isotope data. In addition, due to the current correlation problems that are posed (mainly to the Lower and Middle Triassic), an isotopic curve with a good chronostratigraphic coverage must be obtained from sections that are well calibrated by biostratigraphic means. For this reasons, in the present work bulk carbonates were used exclusively and it is assumed that their carbon isotopic composition approximate that of the Dissolved Inorganic Carbon of the waters in which they formed. The problem of the record and preservation of primary signatures in bulk carbonates is discussed in more detail in the previous chapter. There are more and more studies which show that whole-rock inorganic carbon may preserve original seawater isotopic signatures and that parallel stratigraphic trends may serve for correlations.

A different approach to the problem of seawater carbon isotope evolution was undertaken by several research groups who tried to overcome the problem of diagenesis by analysing exclusively unaltered brachiopods shells and belemnite rostra (Popp et al., 1986; Veizer et al., 1986; Grossman et al., 1991; Grossman et al., 1993; Veizer et al., 1997; Wenzel and Joachimski, 1996), following a scrutiny check of the state of preservation using standard techniques (see Grossman, 1994). The major drawback of this approach is the spotty occurrence of well preserved brachiopods (Grossman, 1992), which result in a poor stratigraphic resolution and coverage. In addition, brachiopods do not always precipitate their shells in equilibrium with the seawater (Carpenter and Lohmann, 1995) and a high number of analysis are required for each level in order to estimate the magnitude of the "vital effect". Undoubtly, brachiopods offer much better alternatives for the study of seawater oxygen and strontium isotopes; as far as the carbon isotopes are concerned, brachiopods may be useful in defining long term trends, but considered from the perspective of carbon isotope stratigraphy their utility is limited.

The Phanerozoic carbon isotope data based on brachiopods published by Veizer et al. (1997) show an important data spread (up to 8‰ for a given stratigraphic level) and actually, the general trends confirm the bulk carbonate based record published 30 years before (Keith and Weber, 1964). The poor stratigraphic coverage represents a drawback also for the record based on marine cements (Carpenter and Lohmann, 1989; 1997). In addition, both brachiopods and marine cements based methods require minute and time consuming work for sample preparation and screening, and often microanalytical techniques are required (nowadays the latter issue is no more relevant because of the advent of automated devices for the analysis of microsamples of carbonates).

### **3.2. The Upper Permian to Upper Triassic time scale**

Choosing an appropriate time scale for the Upper Permian to Upper Triassic time interval has proved to be a difficult task. There are currently many local stage names employed, correlations between the main biogeographic provinces are sometimes difficult and the radiometric age calibration of the time scale appears to pose major problems. The adopted time scale is certainly a compromise. As all the sections examined for the present study are from the Tethys, the stage names and ammonoid zonation selected are mostly from the Tethys as well. It is acknowledged, however, that for several time-intervals the ammonoid zonation used is not the best.

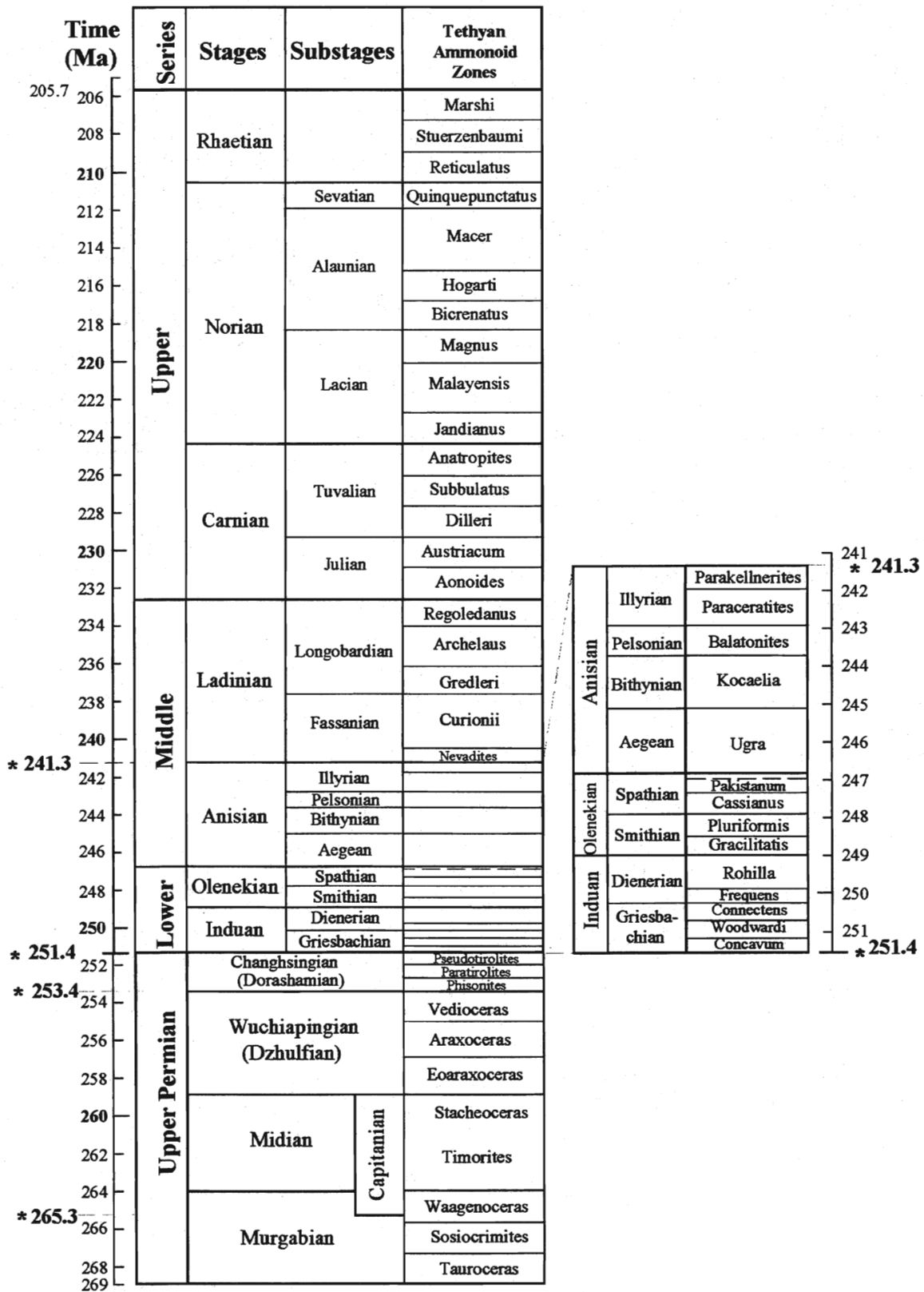


Fig. 6 The Upper Permian and Triassic timescale which serves as standard for the present study (see text for source of data)

### 3.2.1. Subdivisions

The Upper Permian and Triassic chronostratigraphic subdivisions are represented in fig. 6. The names of Permian subdivisions have been recently approved by the Subcommittee of Permian Stratigraphy (Yugan et al., 1997). They recommend a threefold division of the Permian in Cisuralian, Guadalupian and Lopingian, the Lopingian (the Upper Permian, accordingly) being further divided into Wuchiapingian and Changhsingian. However, in the present work the Upper Permian term usage follows Ross et al., (1994), with Murgabian, Midian, Wuchiapingian and Changhsingian as stages. The same source (Ross et al., 1994) was used for the correlation with the North American time scale.

The Lower Triassic is divided in two stages, Induan and Olenekian, following the recommendations of the Subcommittee of Triassic Stratigraphy (Gaetani, 1992); however, the standard subdivisions of Tozer (1967), i.e., in ascending order, Griesbachian, Dienerian, Smithian and Spathian, are used at a substage status. It is assumed that the Induan - Olenekian boundary coincides with the Dienerian - Smithian boundary. The Middle and Upper Triassic subdivisions are more or less standard; the Rhaetian is used as the uppermost stage of the Triassic. Substage names defined in the Mediterranean-Alpine Tethys are used occasionally. For the Anisian, the early Anisian is equated with the "Aegean", the middle Anisian includes both the "Bithynian" and "Pelsonian" and the late Anisian is the equivalent of "Illyrian". Not all stage boundaries are thoroughly defined yet, thereby some of them (those which are relevant to the present work) are briefly discussed in the following.

#### The Permian-Triassic boundary

Considering the major changes that affected the biosphere during the end Permian mass extinction one may believe from a simplistic standpoint that the Permian-Triassic boundary is easily recognisable biostratigraphically. However, the precise definition of the Permian/Triassic boundary has been the subject of a long lasting debate (see for example Tozer, 1988) and neither presently there is not a consensus achieved. Frequently, a marked lithological change occur at the Permian to Triassic transition. The biostratigraphically defined Permian/Triassic boundary do not always coincide with the lithological break, as it is the case, for instance in South China, (one of the best place in the world where to study the Permian-Triassic transition, see for example papers in Yin, 1996). Moreover, gaps are often recorded at the P/T transition as a consequence of the high amplitude sea level fall that characterized the Late Permian. Often they are easily recognisable through sedimentological criteria, but sometimes they are discrete and thereby controversial. The working definition of the base of the Triassic is taken at the first occurrence of the conodont *Hindeodus parvus* (Mei, 1996; papers in Yin, 1996; see also comments by Orchard, 1996 and Baud, 1996). The value of species of *Otoceras* for the placement of the Permian-Triassic boundary is discussed in Tozer (1994a).

#### The Lower-Middle Triassic boundary

The definition of the Lower/Middle Triassic boundary (also referred to as the Olenekian/Anisian or Spathian/Anisian boundary) is one of the current tasks of the Submission of Triassic Stratigraphy (Gaetani, 1994). However, continuous sections with a well established ammonoid-based stratigraphy for this time interval are rather scarce. According to Gaetani (1994), the best candidate sections are in Chios (Assereto et al., 1980; Fantini Sestini, 1981; Gaetani et al., 1992), Nevada (Bucher, 1989), Oman (Tozer and Callon, 1990), Kçira, Albania (Muttoni et al., 1996; Germani, 1997) and finally in North Dobrogea, Romania (Gradinaru, 1993; Crasquin-Soleau and Gradinaru, 1996). In the present work the base of the Anisian is taken at the base of the *Aegeiceras ugra* beds. Correlation between the Tethyan, North American and boreal ammonoids associations around the Lower/Middle Triassic boundary awaits further refinements in regional ammonoid zonations. In North Dobrogea, for instance, the equivalent of the *Keyserlingites subrobustus* zone, considered to be the youngest Spathian biozone in the North American Triassic (Tozer, 1994b) is not known (Gradinaru, 1993). The same holds true

for the conodont zonation (Orchard and Tozer, 1997a, b). The range of several conodonts species from the Lower - Middle Triassic transition are seemingly diachronous (Orchard, 1995). The first appearance of *Chiosella timorensis*, for instance, is only in the early Anisian in the North American Triassic, while in North Dobrogea it was found together with Late Spathian ammonoids (Mirauta and Gradinaru, unpublished data). The First Appearance Datum (FAD) of *Neogondolella regale* is apparently not synchronous worldwide as well (Orchard, personal communication).

Following the Tethyan ammonoid zonation by Mietto and Manfrin, (1995) the **Anisian - Ladinian** boundary is taken at the base of *Nevadites* beds, although Brack and Rieber (1993) recommended the placement of the *Nevadites* zone into the Anisian stage. Similarly, the **Ladinian - Carnian** boundary is taken at the base of *Trachyceras aon* zone and not at the base of *Daxatina canadiensis* as recently proposed by Broglio Loriga et al. (1998). Both Anisian - Ladinian and Ladinian - Carnian boundary awaits formal definitions by the Subcommission of Triassic Stratigraphy.

### 3.2.2. Biostratigraphy

The biostratigraphic time scale for the Late Permian and Triassic is established mainly on the basis of ammonoids and conodonts biozones (Tozer, 1984; Orchard and Tozer, 1997; Yugan et al., 1997), which are assumed to be isochronous worldwide. While most of the Triassic stage and substage definition is based on ammonoids, for some intervals in the late Permian and the early Triassic conodonts are preferred, as conodonts are the group less affected by the end-Permian mass extinction and they are ubiquitous in strata close to the Permian/Triassic boundary. For the Upper Permian the ammonoid zonation of Yang and Li (1992), as cited by Baud et al. (1996) is used, in agreement with Yugan et al. (1997). For the Triassic, the Tethyan ammonoid zonation of Mietto and Manfrin as cited by Gradstein et al. (1995) is used.

It is important to mention here that in the Anisian strata of North Dobrogea, ammonoids originally described in the North American Triassic occur at several levels (Gradinaru, 1993). Their fine scale correlation with the Tethyan zonation is yet uncertain and therefore several assumptions have been made. It is the case mainly in the Middle Anisian, where several subzones of the *Hyatti* and *Taylori* zones (Bucher, 1992a) have been recognized. It is assumed in this work that these ammonoids have a synchronous range in Nevada and in North Dobrogea and that they are subzones within the *Kocaelia* zone from the Tethys (see Bucher, 1992a for a detailed discussion). This approximation, suggested by the overall stratigraphic distribution of ammonoid faunas in North Dobrogea (Gradinaru, 1993) should be considered only as a working hypothesis.

### 3.2.3. Radiometric calibration

Assigning absolute ages to a biochronological scale is a rather uncertain process. Although the dating analytical techniques have been considerably improved during the last decade and analytical errors diminished consequently, the absolute age rating of sedimentary sequences is strongly dependent on the availability of biostratigraphic constraints and on the knowledge of the exact time of formation for the minerals used for dating.

The numerical calibration of the Upper Permian to Upper Triassic time scale was accomplished by combining the relative duration of stages and biozones of Gradstein et al., (1995) to the most recent radiometric dates reported from sections well constrained biostratigraphically by Mundil et al., (1996) and Bowring et al., (1998). The anchor points are: the base of the Capitanian, the base of Changhsingian, the Permian/Triassic boundary and the Anisian/Ladinian boundary.

The maximum estimate for the base of the Capitanian is 265.3  $\pm$  0.2 Ma (Bowring et al., 1998) on the basis of U/Pb dates on zircons, in agreement with the 266 Ma age used by Ross et al., (1994). The same authors (Bowring et al., 1998) proposed an age of 253.4  $\pm$  0.2 Ma as the best estimate for the base of the Changhsingian stage, in his stratotype area in South China, also on the basis of U/Pb dates on zircons.

The radiometric age attributed to the Permian - Triassic boundary vary considerably between the most cited time scales (see a recent review in Menning, 1995). However, the data obtained during the last years from sections well constrained biostratigraphically (Bowring et al., 1998) confirm the 251 Ma. age proposed by Claeu Long et al. (1992) on the basis of SHRIMP dating of zircons from the South China. The 251.4  $\pm$  0.3 Ma. date (Bowring et al., 1998) was adopted herein, in contrast with the 248.2 Ma. from Gradstein et al. (1996).

The radiometric calibration of the Triassic time scale is based on two major tie points: the Permian-Triassic boundary (as discussed above) and the Anisian-Ladinian boundary. The Anisian/Ladinian boundary was dated by Hellmann and Lippolt (1981) in the Southern Alps as 232  $\pm$  9 Ma. on the basis of K/Ar and Ar/Ar dates on alkali feldspars from tuff layers in the basal part of the *Nevadites* zone. This age was used in most of the time scales available and absolute age estimates for the other Triassic stage boundaries were determined by interpolation. More recently, single-grain zircon U/Pb age dates from tuff layers in the same area gave a considerably older age for the base of the Ladinian (the base of *Nevadites* zone): 241.3  $\pm$  0.8 Ma (Mundil et al., 1996). Supplementary dates from biostratigraphically well constrained levels within the Ladinian (Mundil et al., 1996) are all older than the age values of Hellmann and Lippolt (1981). The age of 241.3 for the base of the Ladinian is preferred herein, because the data provided by Mundil et al., (1996) appear to be more robust and they are based on a more reliable method (see also Brack et al., 1996 and Hardie and Hinnov, 1997). It is also significant that the same authors (using the same methods) obtained a 252.3  $\pm$  0.5 Ma age for the Permian-Triassic boundary in South East China (Mundil et al., 1997), very close to the generally accepted age of the Permian/Triassic boundary. The age assigned for the Triassic/Jurassic boundary vary from 200 to 213 Ma.; a 205.7 Ma age was taken from Gradstein et al. (1996).

The Triassic time scale calibrated with the dates mentioned above displays some intriguing features. The duration of the Lower Triassic and Anisian appears to be extremely short when comparing with the remainder of the Triassic. The duration of the entire Lower Triassic would be of only a few million years, about the same as that of the Rhaetian stage, which is an unexpected feature, the status of the Rhaetian as a stage being contested by several scientists (e.g. Tozer, 1993). Even if we admit that the interpolation methods used for determining the relative duration of the Rhaetian are erroneous, the problem still stands: it is very difficult to admit that the duration of the Lower Triassic and the Anisian represents only a quarter of the Ladinian and the Upper Triassic. The number of biozones separated for the two time periods compared are about the same. It is mainly the duration of the Norian and Rhaetian which seems to be overestimated, although Kent and Olsen (1998) argue for a long duration of the Late Triassic on the basis of cyclostratigraphic and paleomagnetic studies.

The short duration of the Lower Triassic and the Anisian do not result necessarily from the adoption of Mundil et al, (1996) dates, as the Permian-Triassic boundary is also shifted to older ages according to the new data. The duration of the Early Triassic appears to be underestimated, irrespective of whether the Hellmann and Lippolt (1981) or Mundil et al., (1996) are used. In the majority of the widely cited time scales the duration of the Early Triassic is inferior to 10 Ma. However, the implications to the timing of the early Triassic events have been overlooked by most of the previous studies.

### 3.3. Methods

Profiles of inorganic carbon isotopes were studied in several sections from the Tethyan Permo-Triassic. For one section (Losar, Spiti)  $\delta^{13}\text{C}$  values of organic were measured in addition to the  $\delta^{13}\text{C}$  values of carbonates. The studied sections are representatives of three main paleogeographic areas within the Tethys: the Northern Indian margin (presently in the Himalayan belt), the Omanese margin and the North Dobrogean margin. In addition, samples from a section located in Albania were analysed. Many of the sections selected are "classical" for the study of the Permian and/or Triassic biostratigraphy and accordingly the age control is among the best within the Tethys. In this respect, the present study benefited by the input of several collaborators as acknowledged in each particular case. Biostratigraphy is mostly ammonoid based. For the sections from North Dobrogea, the bio and litho stratigraphic groundwork was made available by Prof. E. Gradinaru, University of Bucharest, who provided a wealth of unpublished information. For some critical intervals conodonts have been extracted from limestone samples using conventional methods, by formic or acetic acid dissolution followed by sieving, drying and hand picking. Identification of the conodonts from Dobrogea has been undertaken by Elena Mirauta (Geological Institute of Romania, Bucharest). All samples from the Himalayan sections have been collected and made available by co-workers (A. Baud, J. Guex, H. Bucher); a part of the samples from Oman and the integrity of the samples from Dobrogea were collected specifically for the present study. A better stratigraphic coverage is available for the Lower and the Middle Triassic; the Upper Permian carbon isotope record is better known from previous studies (e.g. Baud et al., 1989).

The various sections studied underwent markedly different diagenetic histories which potentially could have modify the carbon isotopic composition at various degrees. Therefore, only samples with a high carbonate content were analysed, as it was shown that carbonate-rich samples may retain their carbon isotopic signature even at high temperature metamorphic processes (Sharp et al., 1995). Carbonate and organic carbon content was determined on samples from critical profiles (where the initial qualitative appreciation suggested a possible correlation with the carbon isotope variations). For the samples from North Dobrogea a large data set containing carbonate and trace-element concentrations was available as the result of a parallel geochemical study carried out at the Université Paris VI (M. Renard and S. Zerrari). For most of the samples thin sections were prepared (for the Himalayan profiles many of them were already available). Prior to the isotopic investigation, thin section examination eliminated samples that had suffered coarse or extensive recrystallization.

### 3.4 Analytical techniques

#### 3.4.1. Carbonate and organic carbon content

Both total and inorganic **carbon content** were determined using a LECO coulometer at "Centre d'Analyse Minérale (CAM)". The inorganic carbon concentrations were converted to calcium carbonate assuming that the inorganic carbon was present as calcite. The organic carbon content was calculated as the difference between total carbon and inorganic carbon. The relative proportions of calcite and dolomite have been determined for several samples from Salt Range through standard X-Ray diffraction techniques at the XRD Laboratory of the "Institut de Minéralogie et Pétrographie" in Lausanne.

### 3.4.2. Carbonate carbon and oxygen isotopes

For homogenous samples, interior unweathered parts free from veins and voids were cleaned, crushed and ground to fine powders. For heterogeneous samples, fine-grained carbonate was selectively drilled from the most homogenous regions using a dental burr.

The resulting calcite powder (typically between 5mg and 10mg) was then reacted under vacuum for one hour with purified orthophosphoric acid at 50°C (a reduced number of calcite samples were reacted at 25°C for 12 hours). Dolomite samples were reacted at 50°C overnight. Samples of coexisting calcite and dolomite were analysed using the selective acid extraction method of Al-Aasm et al., (1990). Apparently, the organic matter present in some of the carbonate samples do not react with the phosphoric acid. Organic-rich powders reacted with a 5% sodium hypochlorite solution (in order to remove the organic material) prior to the CO<sub>2</sub> extraction gave the same  $\delta^{13}\text{C}$  and  $\delta^{18}\text{O}$  values as untreated powder (within the normal reproducibility). The configuration of the Lausanne off-line system for the extraction of CO<sub>2</sub> gas from carbonates allows the process of 8 carbonate samples for every run. An internal laboratory calcite standard (Carrara Marble) was processed for each batch. The CO<sub>2</sub> evolved was cryogenically purified and sealed into glass tubes and the isotopic composition of the CO<sub>2</sub> gas was measured either on a Finnigan MAT 251 or on a Finnigan MAT Delta S isotope ratio mass spectrometer. Isotope ratios were corrected for <sup>17</sup>O contribution. Oxygen isotope data were corrected using the following carbonate - phosphoric acid fractionation factors: 1.01025 for calcite at 25°C (Sharma and Clayton, 1965); 1.00931 for calcite at 50°C (Swart et al., 1991); 1.0106 for dolomite at 50°C (Rosenbaum and Shepard, 1986). The results were normalized against a laboratory working standard calibrated against NBS 19. For NBS-19,  $\delta^{13}\text{C}$  is +1.95‰ and  $\delta^{18}\text{O}$  is -2.20‰ (Coplen et al., 1983). Reproducibility on replicated samples and the Carrara Marble standard is better than 0.1‰ for  $\delta^{13}\text{C}$  and 0.15‰ for  $\delta^{18}\text{O}$ .

The results are reported using the conventional  $\delta$  notation, relative to PDB. The  $\delta$  value is defined as:

$$\delta \text{ in } \text{‰} = (\text{R}_{\text{sample}} - \text{R}_{\text{standard}}) / \text{R}_{\text{standard}} \times 1000, \text{ where R represents the isotope ratio.}$$

### 3.4.3. Organic carbon isotopes

Powders containing both carbonates and organic carbon were reacted with 1N HCl until all the carbonate was removed then rinsed and centrifuged in distilled water until neutral. Aliquots of the resulting powder were weighed and embedded in tin capsules and placed in the Autosampler of a Carlo Erba Elemental Analyser which was coupled to a Finnigan Mat Delta S isotope ratio mass spectrometer. Isotopic measurements were performed in continuous flow (Mathews and Hayes, 1978; see Brand, 1996 for a recent review) with helium as carrier gas. Both standards and samples (gas) were introduced in the mass spectrometer via an open split interface. The standard gas is calibrated against NBS 21 (for which  $\delta^{13}\text{C}$  is -28.1‰). Reproducibility was better than 0.1‰ for standards and 0.2‰ for sediment samples. Most of the samples were analysed in duplicate.

### 3.4.4. Strontium isotope measurements

Conodont samples used for strontium isotope measurements were extracted exclusively from carbonate rich-limestones by dissolution of carbonate in a 10% solution of acetic acid for 24 hours, sieving, drying at 40°C and hand-picking. About 20 elements from each sample, were cleaned ultrasonically until no adhering clay particles were observed under the microscope. Subsequent preparations and measurements were carried out in the "Centre de Géochimie de la Surface" in Strasbourg through an

exchange project with G. Shields and P. Stille. Conodont samples were washed initially in acetic acid and thereafter dissolved in 1N HNO<sub>3</sub> for analysis. Initial experiments with acetic acid showed that only minor quantities of phosphatic conodonts are dissolved by even prolonged ultrasonic treatment at 60°C. Bulk samples were washed initially in dilute HCl and thereafter dissolved in acetic acid for analysis. Sr was concentrated using standard exchange column and resin techniques, with HCl as solute and ammonium citrate as a complexing agent to remove calcium from the sample.

Sr concentrates were loaded with 2% HNO<sub>3</sub> on tungsten filaments with Ta<sub>2</sub>O<sub>5</sub> as activator. All Sr isotope analyses were carried out on a VG Sector multicollector using five collector cups in dynamic mode. This mode provides high internal precision with 2σ errors no higher than 0.000020 and commonly < 0.000010. Regular measurement of the international NBS standard SRM 987 rules out significant fluctuations in machine output, while three standard measurements during the sample analysis yielded 0.710256 (10), 0.710251 (10) and 0.710250 (7), respectively. These values are exactly equivalent to the most commonly quoted NBS SRM 987 Sr isotope ratio of 0.710250 within machine reproducibility and error (McArthur, 1994) and all literature data cited are normalised against this ratio.

Rb/Sr ratios for Rb corrections and REE concentrations were measured using ICP-MS on the same 1N HNO<sub>3</sub> solutions that were used for isotopic analysis. Errors on the ratios are insignificant as most sources of error cancel out when measuring ratios.



# CHAPTER 4

## CONSTRAINTS FROM THE PERMIAN-TRIASSIC OF THE TETHYAN HIMALAYA

### 4.1. Introduction

Localities presented in this chapter derive from four areas of the Northern Indian margin: Salt Ranges, Kashmir, Spiti and Central Nepal (fig. 7). The results from the Salt Range, Kashmir and Nepal have been already published in Baud et al. (1996) and very little is added to the discussion presented therein.

Recent paleogeographic maps and description of the late Murgabian and late Anisian paleoenvironments of the Northern Indian margin are given in the Tethys Atlas by Baud et al. (1993) and by Marcoux et al. (1993).

From the geodynamical point of view, the northern part of the Great-India was subjected to an early rifting phase in the late Paleozoic, just at the end of the large scale Gondwanian glaciations. The beginning of the rifting process is marked by large hiatuses and discontinuities (paraconformities) between the early or middle Paleozoic sedimentary succession and the discontinuous late Paleozoic transgressive sediments. The asymmetric rifting geometry consists of a northern Lower Plate - the present Ladakh Karakoram and Transhimalaya continental crust with their former sedimentary cover, and a southern upper plate - the present High and Lower Himalaya and small part of the Indian craton and its sedimentary cover.

A sketch map of the geodynamic evolution of an asymmetric rift and a figure showing the different part of the N Indian Permian rift are given in Stampfli *et al.* (1991, figs. 1 and 5). If the lower plate evolved into an active margin during the late Mesozoic, the upper Plate corresponds to the future Mesozoic - early Cenozoic Indian passive margin. From the Indian craton to the rift proper, the rift geometry is hidden in the presently largely deformed underthrust - overthrust Indian margin. The rim basin (landward of the shoulder) is well developed in the Pottawar - Salt Range area. The rift shoulder is found in the Pir Panjal and High Himalayan Ranges, and part of it should be found in the underthrust Lower Himalaya. The blocks facing the central part of the rift are represented now in the Zaskar - Spiti sedimentary belt and elements of the highstand blocks that appeared during the earliest drifting stage have been found in the exotics of the Indus - Yarlung suture zone or in the allochthonous coloured melange, for example in the Spongtag klippe area (Reuber and Colchen, 1987).

From rifting to early drifting stages (early late Permian to early Triassic time), the geodynamic and sedimentary evolutions are characterised by at least seven different events (Baud et al., 1989b).

(1) A laterally extensive extrusion of "plateau basalts" (over 100.000km<sup>2</sup>), the Panjal Traps, mainly on the broad rift shoulder during the Kubergandian - early Murgabian times.

(2) A huge carbonate platform (the Wargal Formation) transgressing in the rim basin during late Murgabian - early Midian time. The first upper Permian transgressive - regressive cycle (T-R or second order cycle) is recorded in the growth and demise of this carbonate platform (Midian time).

(3) A block tilting and uplift phase with erosion processes occurring during the early Dzhulfian. A sudden terrigenous influx occurs both on the rift side and on the land side and marks the boundary between the lower and the upper T-R cycles. In the rim basin (Pottawar - Salt Range area), a shallow water mixed carbonate - clastic ramp, the Chhidru Formation, overlies the Wargal carbonate platform (Pakistanese-Japanese Research Group or PJRG, 1985). To the North, in the Kashmir area, a submerged part of the shoulder developed an offshore mixed clastic carbonate deltaic complex, the Zewan Formation (Nakazawa et al., 1975). The Kuling sandstone represents in Zanskar the distal part of this complex (Baud et al., 1984) and turbiditic, flysch like deposits with volcanic clasts of Dzhulfian - Changhsingian? age appear near the present Indus suture zone in the Markha Valley (NE Zanskar, Stutz, 1988).

(4) The marine submersion of the shoulder indicates the beginning of the thermal subsidence and the transition to the drifting stage (late Dzhulfian - early Changhsingian). The main consequences are a general starvation and hiatuses as we can observe in the rim basin (laminated dark silty to sandy deposits of the top of the Chhidru Formation) and on the rift side of the shoulder with phosphatic shales deposits of the upper Kuling Formation (Gaetani et al., 1990; Garzanti et al., 1994c; Nicora et al., 1984). As shown by the study of large exotic blocks (Reuber and Colchen, 1987; Bassoulet et al., 1978) highly microfossiliferous lime packstones (*Colaniella* limestones) grew within trachytic volcano - sedimentary deposits during the youngest Permian (Changhsingian), on uplifted compartments of the intermediate (and oceanic?) crust.

(5) Hiatuses, gaps and local erosion in part of the margin are direct consequences of the worldwide, first order, end of Permian sea-level fall (Holser and Magaritz, 1987); this is the time of the largest extinction phenomenon of the Phanerozoic (see also discussion in Erwin, 1993).

(6) With the following worldwide sea-level rise and transgression, an important change in sedimentation occurs at the Triassic dawn. In the Salt Range, high energy dolomitic grainstones with glauconite (middle Kathwai Member) transgress over dolomites of the lower Kathwai Member or locally, directly on the starved uppermost Chhidru deposits. On the former shoulder (Kashmir), deepening marine conditions are indicated by open marine shales with ammonoids limestone lenses (*Otoceras* beds of the Khunamuh Formation) and fine graded silt of distal pelagites transgressing over lowstand, shallow *Claraia* shales and limestones. Seaward, very condensed cephalopods limestones occur (basal Lilang Group of Zanskar, Nicora et al., 1984). The Lamayuru exotic (Bassoulet et al., 1978) is characterised by a manganese crust deposit on the Changhsingian *Colaniella* limestone.

(7) A generalisation of the pelagic limestone facies is recorded about 1 My later at the transition between early and late Induan time with the cephalopods rich Lower Ceratite limestone deposition in the proximal part of the margin (Salt Range) and thin, condensed limestones and shales in the distal part (Tamba Kurkur Formation of Zanskar-Spiti and Nepal Himalaya). Some of the exotics record the earliest "Hallstatt" type limestone deposits directly on the Mn crust.

The potential of carbon isotope studies as a stratigraphic tool for the Permian-Triassic sequences has been emphasized by previous studies. However, correlations are often difficult in the absence of biostratigraphical constraints. In terms of biozonation and systematic paleontology, the northern Indian margin has been well studied for more than a century and two sections presented in this chapter (Nammal Gorge, Guryul Ravine) are reference sections for the lower Triassic.

Profiles of whole rock inorganic carbon and oxygen isotopes were studied in marine carbonates from the Guryul Ravine and the Palgham sections in Kashmir, the Nammal Gorge and the Landu sections in the Salt Range and the Surghar Range (Pakistan), the Losar section in Spiti and the Thini Chu section in the Kali Gandaki Valley, Central Nepal.

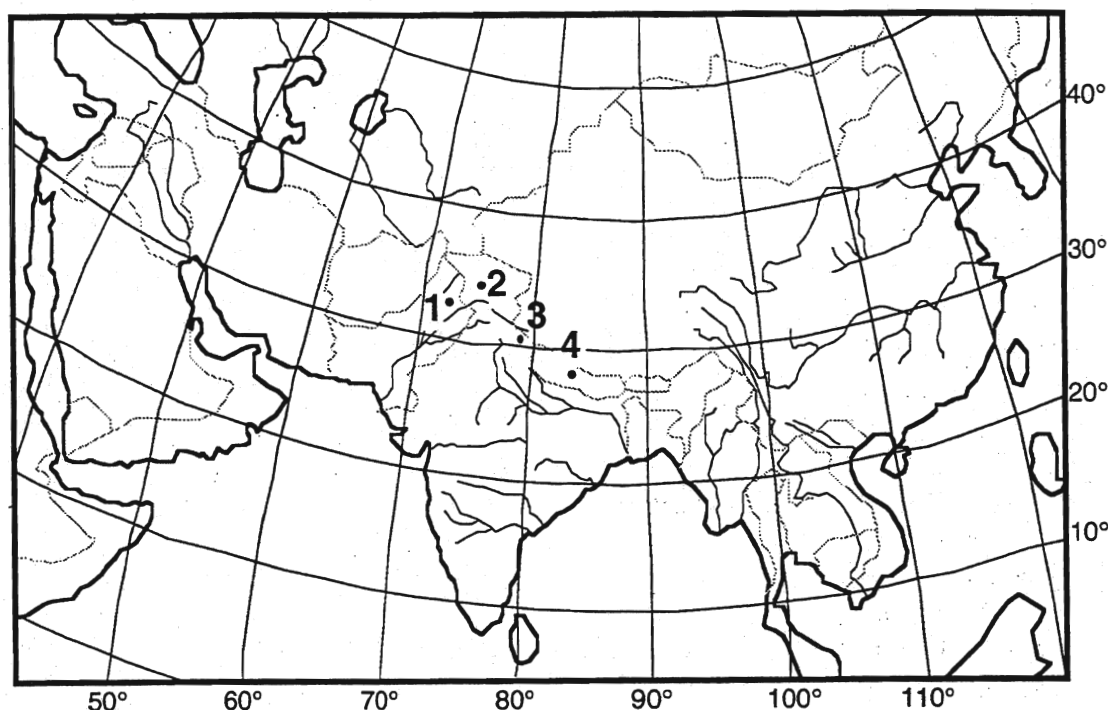


**Fig.7.** Location map of the studied sections. 1. Salt Range and Surghar Range sections. 2. Kashmir sections. 3. Spiti 4. Thakkhola.

## 4.2. Salt Ranges

The upper Permian to lower Triassic succession is well exposed in gorges that dissect the Salt Ranges - Trans-Indus Ranges of Northern Pakistan (fig. 8). The main studies on this area have been summarized in Kummel and Teichert (1970) and part of the recent literature in Wignall and Hallam (1993) and Baud et al. (1996).

A stratigraphic chart is given in fig. 9, with the litho-units, sequences and T-R cycles. The interpretation of a hiatus between the Chhidru and the Mianwali Formation has been expressed in Baud et al. (1989a). With respect to age, we agree with Nakazawa (1993) that part of the early Griesbachian is recorded in the lower and middle Kathwai dolomite. This is also the opinion of Wignall and Hallam (1993), but for the PJRG (1985), the Permian-Triassic boundary occurs between the lower and middle unit of the Kathwai Member (see fig. 9 and 11).

### 4.2.1. Nammal Gorge section

A preliminary carbon isotope profile for the Nammal Gorge section has been published in Baud et al. (1989a), based on analyses performed in Rehovot Laboratory. Also, a preliminary study of the lower Triassic segment for the Nammal Gorge section was carried out by J.-M. Menoud and J. Guex, which outlined the major features of the carbon isotope profile. We present here the results of a more detailed sampling, covering the upper Permian and most of the lower Triassic. In addition, a part of the Landu Nala profile has been analysed to determine whether the variations of  $\delta^{13}\text{C}$  are influenced by diagenetic effects.

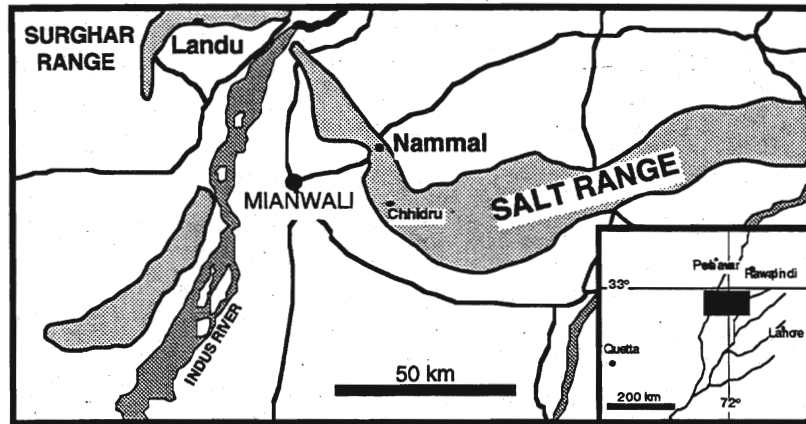


Fig.8. Location map of the Nammal Gorge and Landu sections.

Permian and basal Triassic samples have been collected by A. Baud, C. Jenny and J. Marcoux in December 1987. Additionally, we received a set of samples which were collected for magnetostratigraphic studies from M. Haag (Zürich). Triassic samples came from field work carried out in 1974 by A. Baud, P. Brönnimann, J. Guex and L. Zaninetti (Guex, 1978).

	STAGES	LITHO - UNITS	3-RD ORDER SEQUENCES	T-R CYCLES	
E. TRIASSIC	OLENEKIAN	Topmost limestone	S8	CIII	
		Bivalves beds			S7
		Upper <i>Ceratite</i> lm. <i>Ceratite</i> sandstone			
INDUAN	<i>Ceratite</i> marls	S6			
	Lower <i>Ceratite</i> lm. Kathwai Member				
250 Ma	<b>GAP</b>				
LATE PERMIAN	CHANGHSINGIAN	<b>GAP</b>			
	DZHULFIAN	White sandstone	S5	CII	
		Unit 3 Unit 2 Unit 1	S4		
		Kalabagh Member	S3		
	MIDIAN	<i>Nanlingella</i> beds	S2	CI	
		<i>Neoschwagerina</i> beds	S1		
MURGABIAN	<b>GAP</b>				

Fig.9. Stratigraphic chart showing the lithological units, sequences and T-R cycles in the Salt Range area. Subdivisions after PJRG (1985) for upper Permian and after Guex (1978) for the lower Triassic.

### The Upper Permian T-R cycle CI

Carbon and oxygen isotopic composition of carbonates are plotted against depth on the stratigraphic column in Fig. 10. On the basis of the occurrence of *Neoschwagerina margaritae* in the lower part of the Wargal Formation, the carbonate shallow marine transgression over the lower Permian (Kubergandian) Amb Formation is late Murgabian - early Midian in age (late Permian). The Wargal carbonate platform is subdivided into 5 informal units (1-5) by PJRG (1985) and consists of a second order T-R cycle (CI). Based on field data, the T-R cycle can be subdivided into three shallowing upward third order sequences capped by regressive dolomite, marked S1 to S3 (Fig. 10).

High positive  $\delta^{13}\text{C}$  values (up to 4‰) occur in the S1 transgressive calcarenitic deposits. The boundary between S1 and S2 is the top of the regressive dolostone of the litho-unit 3, where we see an increase of  $\delta^{13}\text{C}$  to values of more than +5‰ in the S2. The boundary between S2 and S3 is linked with regressive dolomites in the upper part of the unit 4a and we note a slight decrease of  $\delta^{13}\text{C}$  values in these highstand dolomites. The transgressive part of the sequence S3 consists of the thick bedded calcarenites of the unit 4b. There is a new increase of  $\delta^{13}\text{C}$  values to a maximum of more than +5.5‰ in the basal transgressive deposits. The decrease of  $\delta^{13}\text{C}$  begins in upper transgressive system. The overlying highstand deposits are represented by the nodular limestone of the Kalabagh Member. The age of this Member is latest Midian to early Dzhulfian, on the basis of its foraminifera and conodont assemblage (PRJG, 1985). It is interesting to note the sudden appearance of abundant *Colaniella gr. minima* Wang (small foraminifera, Jenny-Deshusses and Baud, 1989) above the downlap surface, at the base of the Kalabagh Member. The same species characterise the Zewan transgression in Kashmir. The slight decrease of  $\delta^{13}\text{C}$  continues in these highstand deposits to values about 4‰.

### Upper Permian T-R cycle CII

The overlying Chhidru Formation records the second T-R cycle (cycle II) with a sudden terrigenous influx corresponding to the uplift phase before the break up of the rift. A Dzhulfian age (probably late Dzhulfian) was suggested for this unit by PJRG (1985). Subdivided into 4 informal members (1-4), this Formation consists of a thick lower third order sequence (S4) and a relatively thin upper sequence (S5). The basal part of S4 is composed of proximal predominant carbonate quartzarenites to distal predominant shales of the shelf margin wedge. These grade upward into limestones and calcareous sandstones of the transgressive system tracts (unit 2). The decrease of  $\delta^{13}\text{C}$  stops and we note a slight increase to values near +4‰. Within the calcareous sandstone (unit 3) of the highstand system tracts the  $\delta^{13}\text{C}$  values are decreasing again and the drop accelerates smoothly at the top of the unit 4 to a  $\delta^{13}\text{C}$  value below +2‰. This shift of 2‰ in the late Dzhulfian marine deposits is recorded in many Tethyan sections (Baud *et al.*, 1989a). The overlying sequence boundary is at the base of the lowstand white quartzose arenites (unit 4) and the upper part of this sequence when preserved consists of thin starved silty shales. Emersive conditions with subaerial exposure have been found at the top of this unit in the western part of the area (Kummel and Teichert, 1970). This marks the sequence boundary and allows us to separate the younger Kathwai dolomitic limestone in a new T-R cycle. As noted above, this interpretation differs from Haq *et al.* (1988) who consider that Chhidru and Kathwai Units belongs to the same transgressive system without gap and boundary, but is consistent with Wignall and Hallam (1993).

On a larger scale, the carbon isotope curve for the upper Permian exhibits two positive excursions: the first one is related to the Wargal Formation, and the second one (less marked) is related to the Chhidru Formation. There is a good correlation between these  $\delta^{13}\text{C}$  positive excursions and the second order T-R cycles. Oxygen isotope ratios are less consistent: in some intervals there is a crude correlation with  $\delta^{13}\text{C}$  value variations, but not always. The oxygen isotope profile undergoes a major positive excursion of about 4‰ within the upper part of Kalabagh Member and the base of Chhidru Formation, but we don't

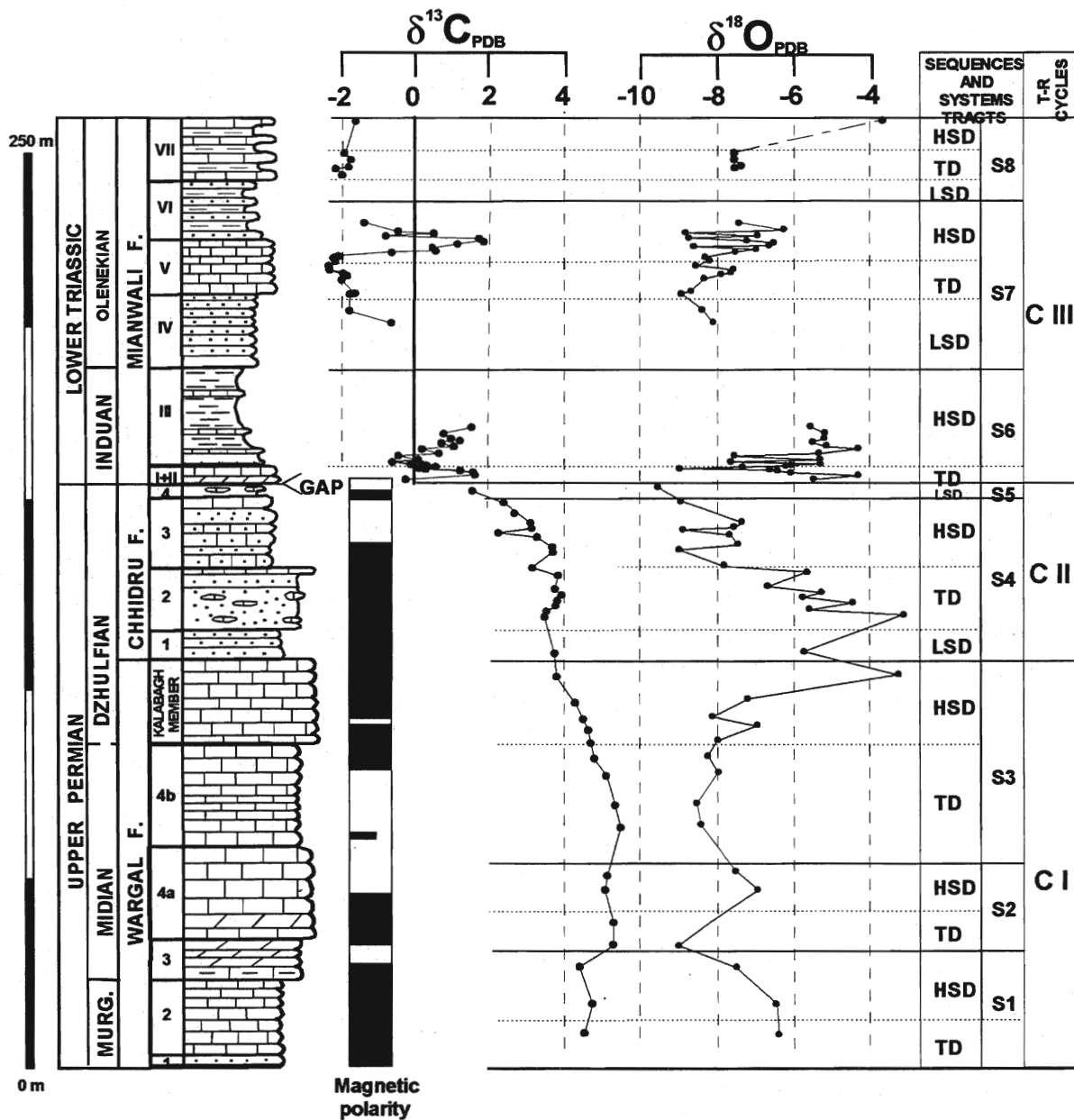


Fig.10. Carbon and oxygen isotope profiles of Nammal Gorge, sequences, systems tracts and T-R cycles. Magnetostratigraphy from Haag (1989). LSD: lowstand deposits; TD: transgressive deposits; HSD: highstand deposits.

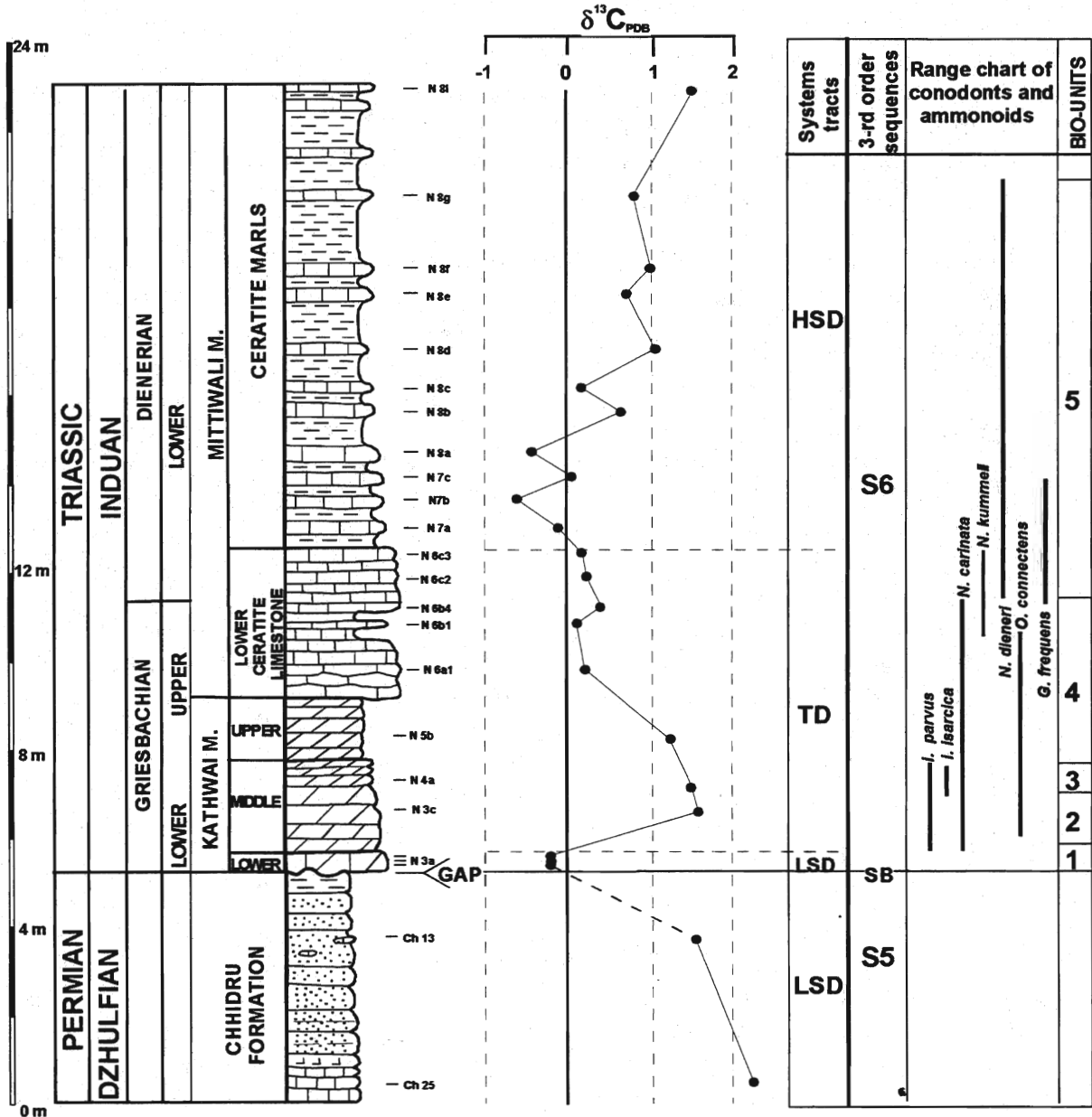


Fig.11. Carbon and oxygen isotope variations across the Permian - Triassic boundary at the Nammal Gorge. LSD: lowstand deposits; TD: transgressive deposits; HSD: highstand deposits. SB: sequence boundary. Range chart of conodonts and ammonoids after PJRG (1985). Bio-units 1 to 5 are corresponding to conodont zones of Nakazawa (1993): 1 = minutus, 2 = parva - minutus, 3 = isarcica - parva, 4 = carinata, 5 = dieneri.

believe this to reflect an original change in the isotopic composition of the seawater. Rather, it is related to diagenesis such as meteoric diagenesis or deep burial diagenesis. The samples most depleted in  $^{18}\text{O}$  are found at the top of Chhidru Formation. This may indicate an exchange with  $^{18}\text{O}$  depleted waters (James and Choquette, 1984) after the end Permian regression phase and before the early Triassic transgression.

The magnetostratigraphic results for the upper Permian obtained by Haag and Heller (1991) from the Nammal Gorge section show 10 magnetic zones corresponding to the base of the Illawara mixed superchron. Due to the gaps at the base of the Wargal and at the top of the Chhidru Formations, the late Permian magnetic polarity time scale is not complete here.

### Lower Triassic T-R cycle CIII

In Haq et al., (1988, their fig. 13), the Mianwali Formation (lower Triassic) at Nammal Gorge has achieved the status of a global reference section in terms of sequence stratigraphy. This Formation consists of one second order T - R cycle (C III) which is subdivided into 3 third order sequences (S6 to S8, fig. 9 and 11).

The Mianwali transgression belongs to the end of the Permian (?) - basal Triassic worldwide, first order transgression. The contact Kathwai-Chhidru shows an erosive relief up to 15 cm (Wignall and Hallam, 1993). The lowstand basal Kathwai dolomite still contains Permian brachiopods (PJR, 1985) and low negative  $\delta^{13}\text{C}$  values are recorded (fig. 11) after a shift of 1.5‰ from the upper Chhidru. A  $\delta^{13}\text{C}$  positive excursion of about 1.5‰ occurs in the middle and upper Kathwai transgressive units of early Induan age (early? - middle Griesbachian *Isarcicella parva* zone, lower *Ophiceras* zone). In the overlying condensed Ceratite limestone (unit III) at the base of Mittiwali Member we note a 1‰ shift of  $\delta^{13}\text{C}$  to values near 0. Downlap surface occurs near the top of this Lower Ceratite limestone and the Ceratite marls (late Induan) consists of highstand deposits. In the lower part  $\delta^{13}\text{C}$  reach its minimum value (-0.8‰) but increase higher to positive +1‰ values. Isotopic data are not available in younger Induan deposits due to the lack of carbonate samples.

The lower Olenekian lowstand Ceratite sandstones (IV) of the overlying S7 sequence are followed by the transgressive and condensed Upper Ceratite limestone (unit V). The local background  $\delta^{13}\text{C}$  values are close to -2‰. In the upper part of the Upper Ceratite limestones, a gradual positive excursion (about 4‰ in magnitude) occurs, just below the early/late Olenekian (Smithian/Spathian) boundary and close to the maximum flooding surface (fig 12). The recovery to background values is very rapid within the highstand deposits of the Lower Bivalve beds (VI). The shift of  $\delta^{13}\text{C}$  is independent of lithology. The last lower Triassic sequence (S8) is of late Olenekian age (Spathian substage). The predominant sandstone of the upper Bivalve beds (VI) forms a relatively thick shelf marine wedge (Haq et al., 1988). The overlying transgressive deposits of the lower Narmia Member (Topmost limestone) still record negative  $\delta^{13}\text{C}$  values (-2‰). The highstand deposits consists of shallowing upward shales and pisolitic limestones overlain by peritidal dolomites at the top, close to the Olenekian - Anisian boundary. This is testified by reports of specimens of *Neospathodus timorensis* from the uppermost beds of Mianwali Formation by both Kummel and Teichert (1970) and PJR (1985).

#### 4.2.2. Landu Nala section

To confirm the Upper Ceratite limestone (lower/upper Olenekian) large carbon isotope positive excursion, the Landu Nala section (about 60 km north-west of Nammal Gorge) was analysed. The same lithological entities are separated, with some differences in thickness. Analyses of the samples from the Unit V (Upper Ceratite limestone) reveal identical  $\delta^{13}\text{C}$  record: a positive excursion with a magnitude of



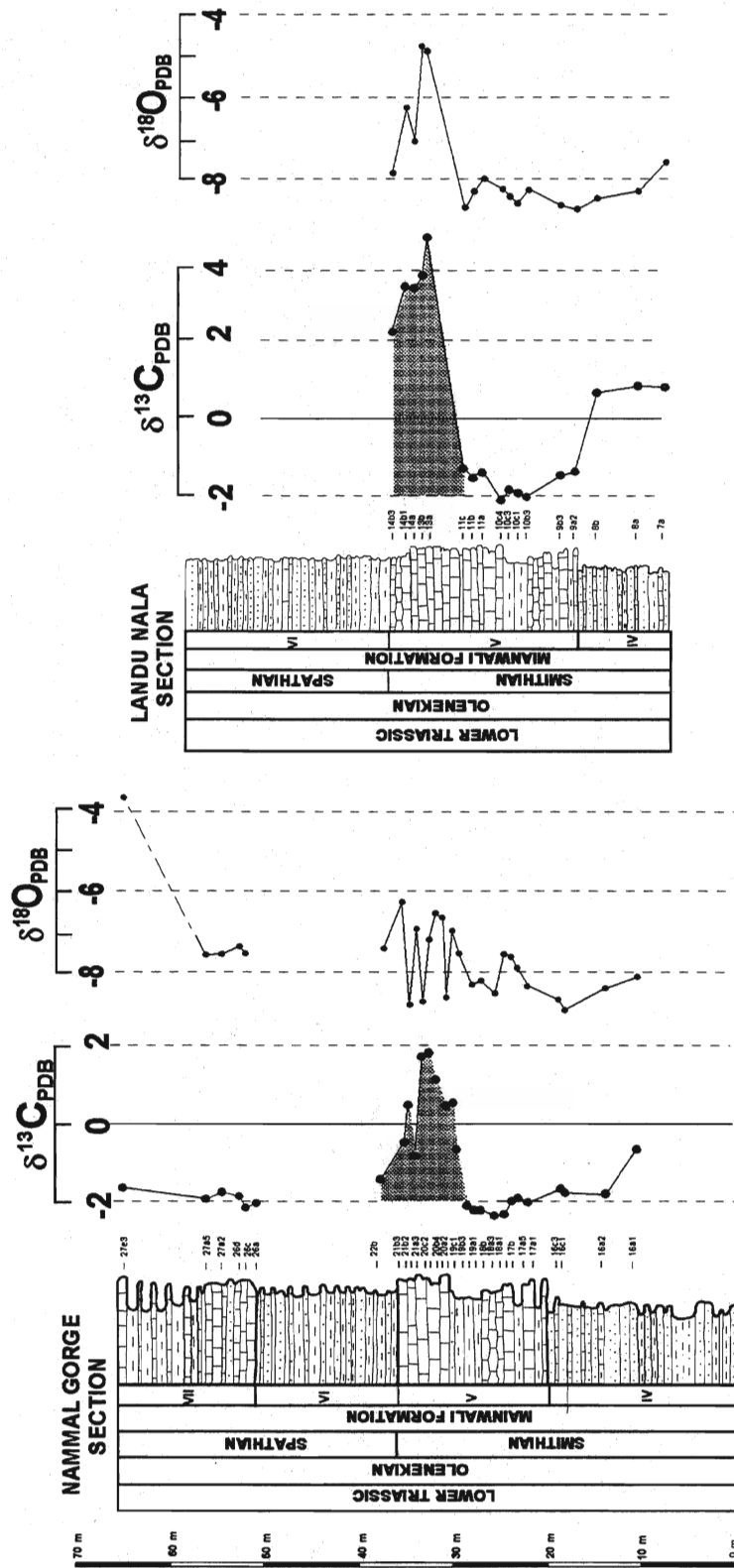


Fig.12. Carbon and oxygen isotope profiles for the upper Mianwali Formation at Nammal Gorge and Landu showing correlative patterns.

about 5‰ just below the Smithian/Spathian boundary. The two isotopic curves are perfectly correlable (fig.12). In both Nammal Gorge and Landu Nala sections the  $\delta^{13}\text{C}$  variation is associated with a positive  $\delta^{18}\text{O}$  excursion. The 4-5‰ shift in  $\delta^{13}\text{C}$  recorded here indicates at least a local dramatic change if not a global one. More data from other basins will demonstrate whether the change was global or restricted to the Indian margin of the Tethys.

### 4.3. Kashmir

Compared with other Tethyan areas, the great interest of Kashmir is the thick development of the *Otoceras* zone with the zonal fossil (basal Triassic), not yet known in the Tethys outside the Himalayan province of the Northern Indian margin.

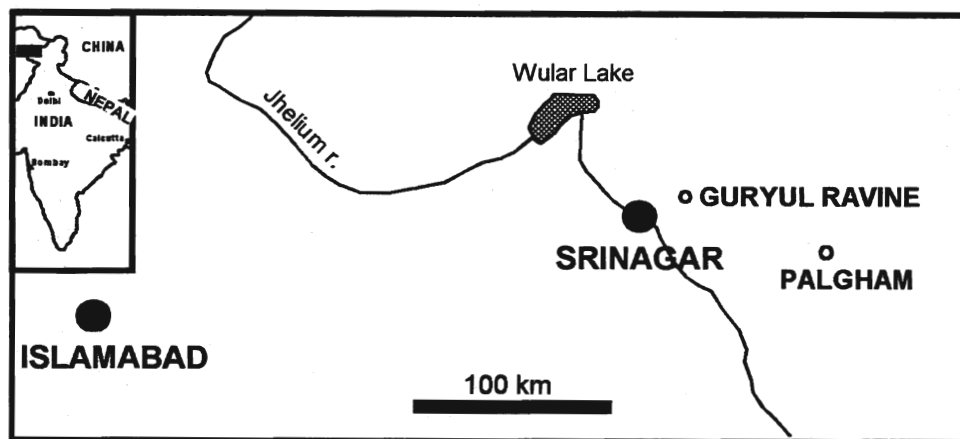


Fig.13. Location map of the Kashmir sections.

Samples from Kashmir sections were collected by Baud in 1987. Part of these samples was analysed by Magaritz, and preliminary results were presented in Baud and Magaritz (1988). We reanalysed and completed all the samples and selected carefully the best preserved carbonate material, following a careful petrographic examination. The two data sets are in agreement.

The Guryul Ravine section is situated about 15km east from Srinagar and Palgham section about 80 km eastwards (fig. 13).

#### 4.3.1. Guryul Ravine section

The Guryul Ravine was selected as a candidate for the Permian-Triassic boundary stratotype section (Wang, 1990). An extensive monography on these sections has been published by Nakazawa and Kapoor, (1981). Stratigraphic units and sequences are plotted against age in fig. 14.

#### Upper Permian

The upper Permian Zewan Formation overlies the Kubergandian to lower Murgabian Panjal Traps and is subdivided into 4 informal units (A to D, fig. 15) by Nakazawa et al. (1975). The transgression of the sandy limestone of the lower Unit A is younger than the transgression in the Salt Ranges and is correlated with the late Midian - early Dzhulfian unit 5 of the Wargal Formation on the basis of the massive appearance of the small Foraminifera "*Colaniella*". Unit A and B belong to a first S1 sequence with arenaceous limestones of the transgressive systems tracts below (Unit A1 to A4) and the shale and

sandy shale of the highstand facies above (Unit B1 and B 2). Positive  $\delta^{13}\text{C}$  values (+2‰) occur in these basal units (fig. 15).

As in the Salt Ranges, the next T-R cycle (CII, Dzhulfian-lower Changhsingian) corresponds to an important terrigenous influx, but here we have the development of an offshore mixed marine clastic-carbonate deltaic complex. The lower part is made of a thin shelf margin wedge with quartzose arenites and silty shales (Unit B3), and calcareous sandstone of the transgressive-systems tracts above (Unit C). Only the top of this unit was sampled and the  $\delta^{13}\text{C}$  values are higher than +3‰. The overlying highstand facies consists of thick-bedded arenaceous limestone and calcareous sandstone (Unit D). A first drop of +1.5‰ in  $\delta^{13}\text{C}$  values occurs between C and base of  $\delta$ units followed by a slight increase to values >+2‰ in the upper part of unit D. Five meters below the top, a large shift of about 3 ‰ of  $\delta^{13}\text{C}$  to a negative value is recorded .

	STAGES	LITHO - UNITS	3-RD ORDER SEQUENCES	T-R CYCLES	
E. TRIASSIC	OLENEKIAN	Unit H	Khunamuh	S4	CIII
		Unit G			
	INDUAN —250 Ma—	Unit F <i>Ophiceras</i> beds E <sup>3</sup> <i>Otoceras</i> beds E <sup>2</sup> <i>Claraia bioni</i> beds E <sup>1</sup>	S3		
LATE PERMIAN	CHANGHSINGIAN	GAP			
	DZHULFIAN	Unit D	Zewan	S2	CII
		Unit C		S1	CI
	MIDIAN	Unit B Unit A			
MURGABIAN	GAP				
	Panjal Traps				

Fig.14. Stratigraphic chart showing the lithological units, sequences and T-R cycles in the Kashmir area. Subdivisions from Nakazawa et al. (1981).

**Early Triassic**

Only the basal part of the next C III T-R cycle has been investigated, that is the third sequence (S3) belonging to the lower Triassic Khunamuh Formation. With the large transgression we note an important change in sedimentation. The lowstand deposits consist of thinly bedded limestones and shales with "Permian Brachiopods" (unit E1). The  $\delta^{13}\text{C}$  values are more or less constant near 0 (PDB), with a slow trend toward positive values. With respect to these local background values, an "anomalous"

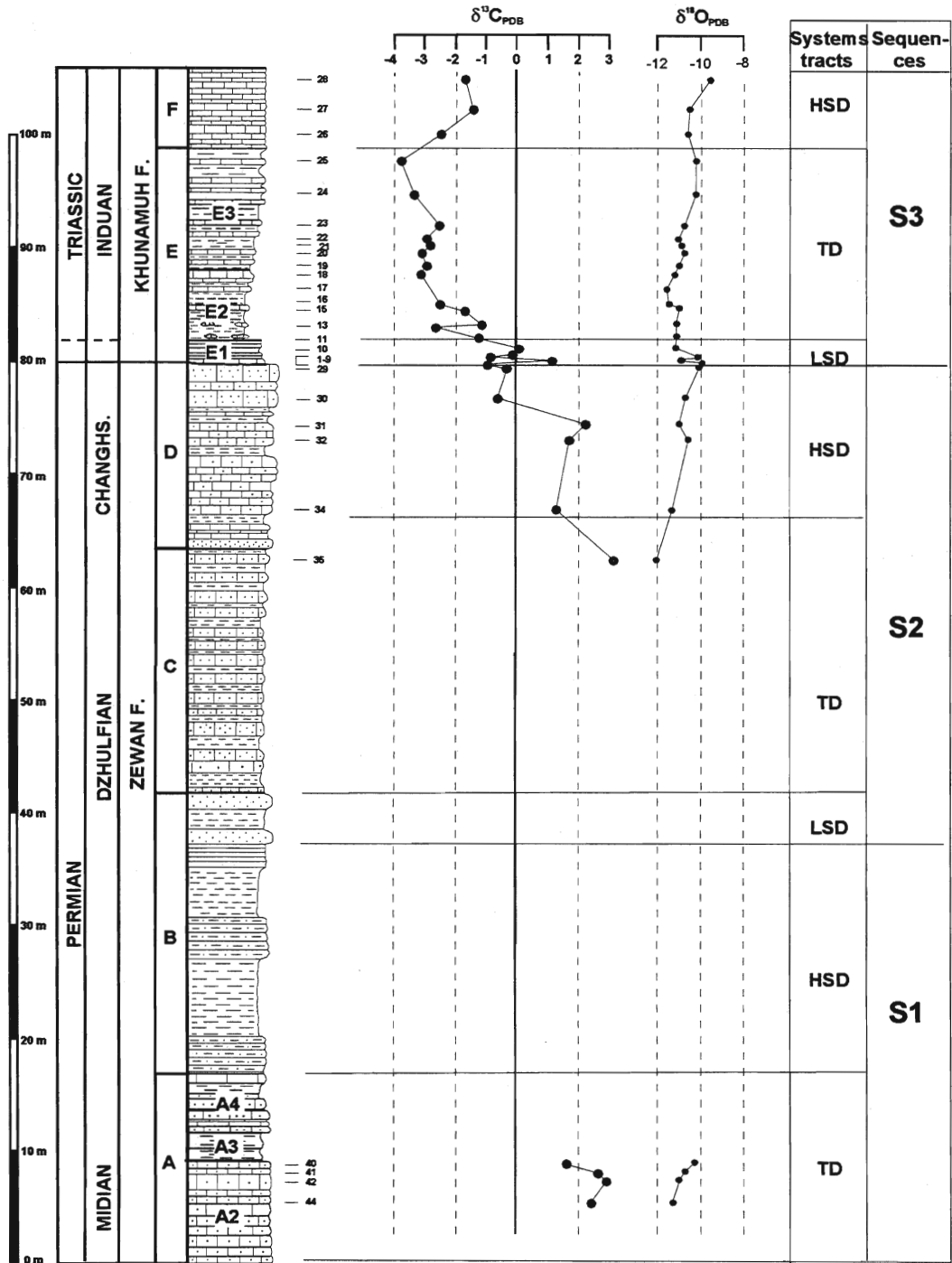


Fig.15. Carbon and oxygen isotope profile at the Guryul Ravine section (Kashmir, India), sequences and systems tracts. LSD: lowstand deposits; TD: transgressive deposits; HSD: highstand deposits.

positive value of +1.4‰ occurs 10 cm above the base of E1 (fig. 11). We interpret this value as being the result of reworking of upper Permian soft lime sediment. In the overlying transgressive black shales with ammonoid limestone lenses ( E2, *Otoceras* zone, E3, *Ophiceras* zone) the downward shift in the  $\delta^{13}\text{C}$  values is gradual and low values (-4‰) are reached near the top of the E3 unit. Biochronological zonation based on the successive appearance of conodonts *Isarcicella? parva* and *I. isarcica* (Matsuda, 1980) allows us to correlate Guryul Ravine E1 to E3 members with Tesero and Mazzin members of the Werfen Formation (Magaritz and Holser, 1991; Schönlaub, 1991). A generalization of the pelagic limestone deposition corresponding to the maximum flooding surface is realized about 1My later at the beginning of the late Induan time (unit F, *Vishnuites* zone) and we note a progressive rise of 2‰ of  $\delta^{13}\text{C}$  (Fig. 10).

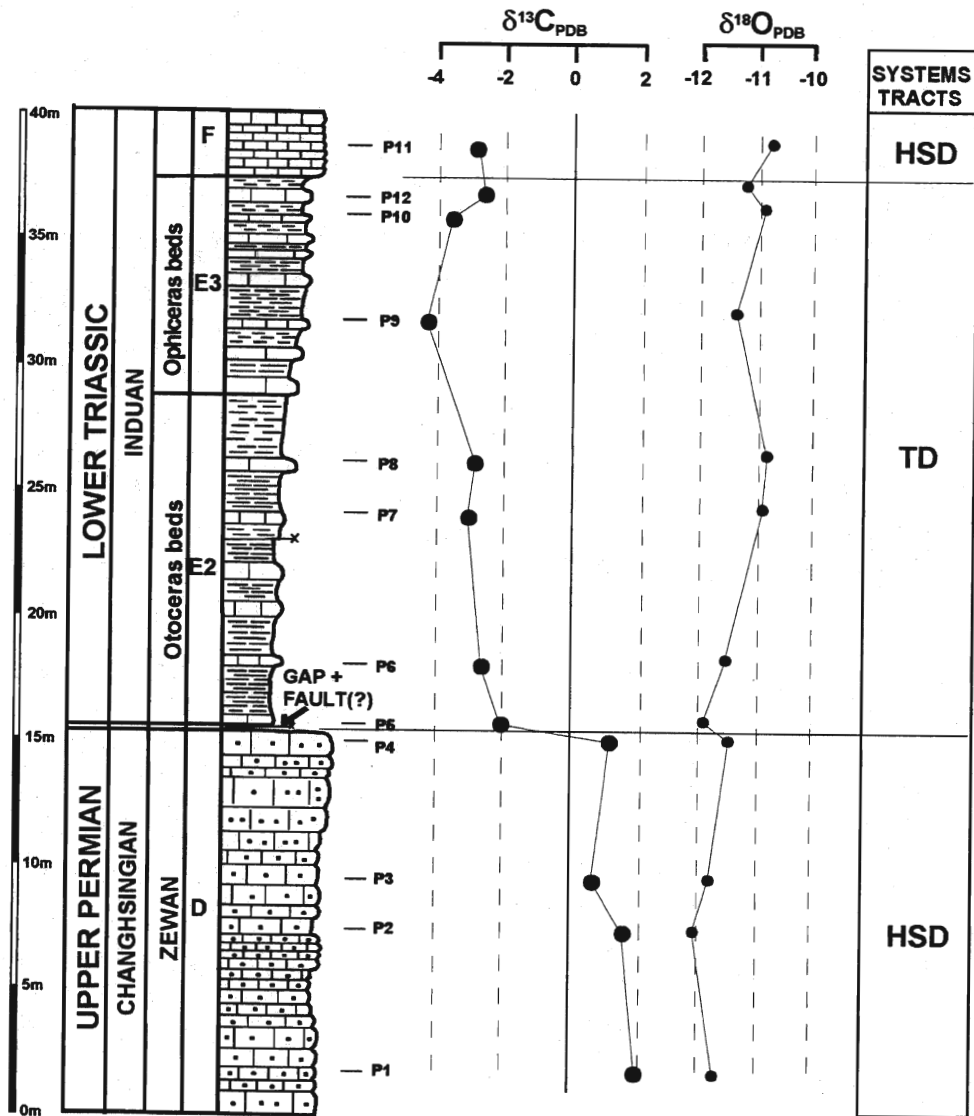


Fig.16. Carbon and oxygen isotope profile at the Palgham section (Kashmir, India), sequences and system tracts. LSD: lowstand deposits; TD: transgressive deposits; HSD: highstand deposits.

### 4.3.2. Palgham section

The Palgham section displays a similar  $\delta^{13}\text{C}$  pattern (fig.12). The drop of the  $\delta^{13}\text{C}$  which occurs here at the base of Khunamuh Formation is abrupt due to the fact that E1 member is missing (tectonically?). The shift is gradual in E2 member and the minima also corresponds to the *Ophiceras* zone with high negative values.

The  $\delta^{18}\text{O}$  values for both sections are very low, ranging from -9.5‰ to -12‰ (PDB) and show no variations in the limestones across the boundary. These very low values can be explained by the thermal metamorphism process of more than 300°C that affected the Kashmir sections, documented by the high Colour Alteration Index of conodonts (Wang, 1990). It is interesting to note that even in such conditions of high temperature metamorphism, the isotopic shift in carbon is preserved, the  $\delta^{13}\text{C}$  pattern is correlable with others recorded for the same time span, although the change in oxygen has been completely obliterated.

## 4.4. Spiti

The Triassic marine strata from Spiti are known for more than a century (for a review of the early works see Diener, 1912) and it was thoroughly investigated for biostratigraphy by both Indian and European workers (see references in Garzanti et al., 1995). Among the most recent works, particularly useful for the present study are Garzanti et al. (1995), Krystyn and Orchard (1996), Balini and Krystyn (1997) and Balini et al. (1998). The geology of Spiti and adjacent areas was recently published by Steck et al. (1998).

In this study, the carbonate carbon and organic carbon isotopic composition of Lower and Middle Triassic sediments was measured along a section located at Losar, examined and sampled in detail by H. Bucher and A. Vogel in 1995. More precise information concerning the location of the section, litho and biostratigraphy will be published in an anticipated collaborative paper (Bucher et al., in preparation). For the present work the litho and biostratigraphic grounds are based on preliminary informations provided by H. Bucher and on the references quoted above.

The Triassic of Spiti is of particular interest for carbon isotope stratigraphy because well constrained biostratigraphically continuous sections with a good chronostratigraphic coverage can be examined. However, the Triassic deposits of Spiti experienced severe diagenetic (metamorphic) histories (Garzanti et al., 1995; Steck et al., 1998) and the original isotopic signature may have been distorted.

The Triassic sedimentary units from Spiti (and generally from the Tethyan Himalaya) are relatively homogeneous laterally and, therefore the stratigraphic nomenclature is quite uniform in the literature. For this work, the informal but practical nomenclature of Hayden (1904) is used together with the acknowledged Tamba Kurkur Formation and Hanse Formation (Srikantia, 1981).

### 4.4.1. Losar section

The section from Losar presented herein includes the Tamba Kurkur Formation and the basal part of the Hanse Formation (Daonella Shales and the basal part of the Daonella Limestone), spanning a most of the Lower and Middle Triassic time interval (fig. 17). The main lithological units sampled are briefly described below.

The Lower Triassic - Anisian **Tamba Kurkur Formation** overlies transgressively the Upper Permian Gungri Shales of the Kuling Formation, the uppermost Permian being absent from the record (Bucher et

al., 1997). The first lithological unit of the Tamba Kurkur Formation is represented by the "**Otoceras beds**", 50 cm thick, made-up of pyrite-rich limestone with moderately rounded extraclasts of black phosphatic nodules and spherical nodules of iron-oxides (Bucher et al., 1997). Ammonoids and conodonts recovered from the "Otoceras beds" indicate a Griesbachian age for its lower part and a Lower Dienerian age for its upper part (Krystyn and Orchard, 1996; Bucher, personal communication). The overlying "**Flemingites beds**", included by Garzanti et al., 1995 into a more comprehensive "Hedenstromia beds" are attributed to the Lower Smithian (Bucher, personal communication), although Garzanti et al. (1995) favour an Upper Dienerian age. The "**Hedenstromia beds**", about 35 m thick consist of black and gray mudrocks interbedded with thin to medium bedded bioclastic limestones (Garzanti et al., 1995) and are attributed to the Smithian substage. A conodont sample collected at Losar by A. Steck, J.-C. Vannay and M. Robyr from the uppermost limestone band of the "Hedenstromia beds", and identified by M. Orchard indicate an Early Spathian age (cf. H. Bucher, personal communication). Accordingly, the Smithian/Spathian boundary occurs likely in the uppermost part of the "Hedenstromia beds". The overlying "**Niti Limestone**", about 15 m thick, consist of medium to thick bedded grey nodular bioclastic limestones (Garzanti et al., 1995). Its age is Spathian, on the basis of conodonts (Garzanti et al., 1995). The same authors mention from the uppermost meter of the "Niti Limestone" the conodont *Chiosella timorensis*. The "**Muschelkalk**", 6 m thick at Losar, represents a strongly condensed interval, and is made up of ammonoid rich dark-grey nodular limestones and interbedded marls. Many successive ammonoid levels indicate an Anisian age (Balini and Krystyn, 1997; Bucher, personal communication). According to Balini and Krystyn (1997) the first two meters are restricted to the Lower Anisian. Their data derive from another section in Spiti, but because the reported thicknesses of the "Muschelkalk" are very similar in various sections, two meters likely approximate the extent of the Lower Anisian in Losar.

From the overlying **Hanse Formation** only samples from the "Daonella Shales" and the basal part of the "Daonella Limestone" were analysed. The "**Daonella Shales**", included by Garzanti et al. (1995) into the Kaga Formation, consist of grey marls interbedded with dark grey marly mudstones. The age of the "Daonella Shales" is Lower Ladinian on the basis of conodonts (Garzanti et al., 1995). The overlying "**Daonella Limestone**", corresponding to the Chomule Formation of Garzanti et al. (1995) consists of dark gray medium-bedded marly mudstones and subordinate marls. The lower part of the "Daonella Limestone" contain the Ladinian-Carnian boundary interval (Balini et al., 1998). Only samples from the first 12 meters of the "Daonella Limestone" were analysed and, comparing with the thickness reported by Balini et al. (1998) this part still belongs to the Upper Ladinian (according to the standard time scale choosed for this study; see chapter 3).

### Carbon and oxygen isotope data

For the Losar section  $\delta^{13}\text{C}$  values from both carbonate fraction and from the associated organic matter were obtained. For the sake of simplicity the  $\delta^{13}\text{C}$  values from the carbonate fraction will be noted as  $\delta^{13}\text{C}_{\text{carb}}$  and for the organic carbon as  $\delta^{13}\text{C}_{\text{org}}$ .

#### Carbonate carbon isotope data

$\delta^{13}\text{C}_{\text{carb}}$  vary over a wide range comprised between -3‰ and +3‰ and display a well-defined stratigraphic trend along the section.  $\delta^{13}\text{C}_{\text{carb}}$  values from the "Otoceras bed" are highly variable, ranging between -1.8‰ and +1.4‰, without any consistent stratigraphic trend. The  $\delta^{13}\text{C}_{\text{carb}}$  values increase from values around -1.5‰ recorded in the top of the "Otoceras bed" to a value of +2.5‰ measured just bellow the base of the "Flemingites beds". Following this local maximal value,  $\delta^{13}\text{C}_{\text{carb}}$  decrease gradually attaining values as low as -3‰ in the middle part of the "Hedenstromia beds". In the upper part of the "Hedenstromia beds"  $\delta^{13}\text{C}_{\text{carb}}$  values increase abruptly reaching local maximal values

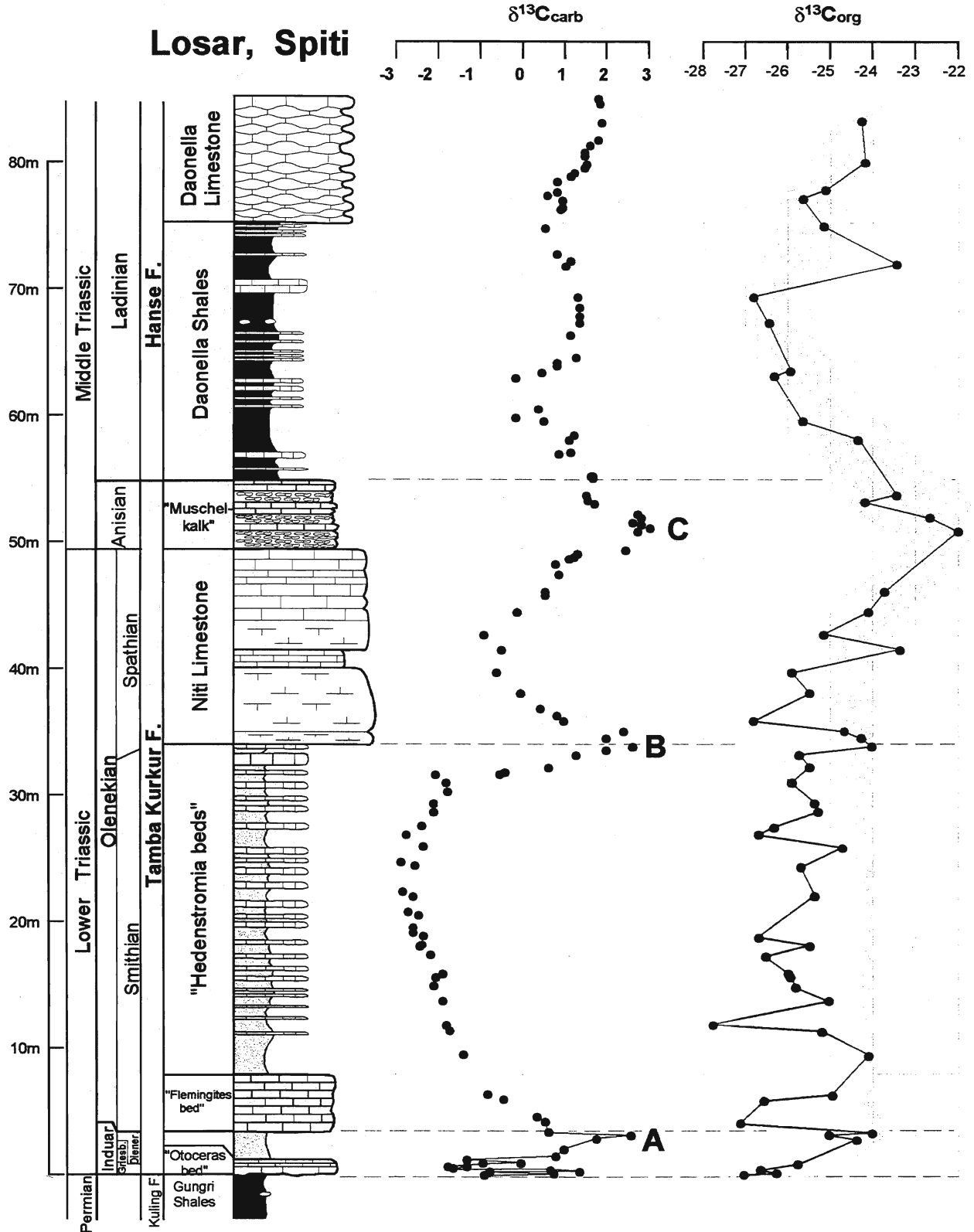


Fig.17  $\delta^{13}C_{carb}$  and  $\delta^{13}C_{org}$  profiles at the Losar section (Spiti Valley)



of +2.5‰ just across the boundary between the "Hedenstromia beds" and the "Niti Limestone", then decrease again to values as low as -1‰ in the middle part of the "Niti Limestone". Over the remainder of the "Niti Limestone"  $\delta^{13}\text{C}_{\text{carb}}$  values increase gradually reaching values around +3‰ in the lower part of the "Muschelkalk", then decrease again, slowly, to values around 0‰ within the "Daonella Shales". Excepting several values around 0‰, the  $\delta^{13}\text{C}_{\text{carb}}$  for the "Daonella Shales" are relatively stable with an average of +1‰, values characterizing also the first 4 meters of the "Daonella Limestone". In the upper part of the "Daonella Limestone" examined for this study the  $\delta^{13}\text{C}_{\text{carb}}$  values display a relatively small (about 1‰) but well marked increase.

Thus, several shifts in  $\delta^{13}\text{C}_{\text{carb}}$  values are apparent from the carbonate carbon isotope profile. Excepting the samples from the "Otoceras bed", the  $\delta^{13}\text{C}_{\text{carb}}$  values show a remarkable low variability for adjacent samples, hence the isotope profile appears to be nicely outlined. Three positive excursions (isotope events) can be distinguished in the profile, named A, B and C. Event A is restricted to the Upper Dienerian, but it is not very well constrained as  $\delta^{13}\text{C}_{\text{carb}}$  values from the underlying "Otoceras bed" are variable. Events B and C are well constrained by data, but both of them are associated with lithological breaks.

A striking feature of the carbon isotope profile of Losar is that the lowest  $\delta^{13}\text{C}_{\text{carb}}$  values are restricted to the "Hedenstromia beds", which are characterized by low carbonate contents and, keeping in mind that these rocks experienced severe thermal overprinting (in addition to diagenesis), one may question whether they preserved primary marine signature. Indeed, in sediments rich in organic matter and siliciclastic components (as it is the case for the "Hedenstromia beds") post-depositional lowering of  $\delta^{13}\text{C}_{\text{carb}}$  values may occur either during various phases of diagenesis through processes related to the degradation of organic matter and subsequent precipitation of  $^{13}\text{C}$  depleted cements (e.g. Marshall, 1992) or during metamorphism by decarbonation reactions in the presence of siliciclastic components (Kaufman and Knoll, 1995). Diagenetic/metamorphic overprint of the carbonates from the "Hedenstromia beds" is further supported by the evidence that such low  $\delta^{13}\text{C}_{\text{carb}}$  values (as low as -3‰) are within the lowermost range of variations for marine carbonates (Anderson and Arthur, 1983), among the lowest  $\delta^{13}\text{C}_{\text{carb}}$  values reported for Phanerozoic carbonates (only from Precambrian rocks negative  $\delta^{13}\text{C}_{\text{carb}}$  values are commonly reported - see Brasier et al., 1996) and out of the Phanerozoic seawater curve (e.g. Holser, 1984).

However, if organic diagenesis or metamorphism is responsible for the  $\delta^{13}\text{C}_{\text{carb}}$  values of the "Hedenstromia beds", we should expect similar  $\delta^{13}\text{C}_{\text{carb}}$  values lowering to occur in carbonates from the "Daonella Shales", also rich in organic-matter and in siliciclastics. Diagenetic/metamorphic conditions must have been similar for the "Daonella Shales" and "Hedenstromia beds"; only early diagenesis might have been different. The  $\delta^{13}\text{C}_{\text{carb}}$  values of carbonates from the "Daonella Shales" are "normal" marine values, within the range of values reported for age-equivalent carbonates arguably less affected by diagenesis (see chapter 6).

Event B from the  $\delta^{13}\text{C}_{\text{carb}}$  occur near the Smithian/Spathian transition and event C appears to be restricted to the ?Upper Spathian and the Early Anisian. Their characteristics will be discussed in the conclusive part of this chapter and in chapter 7. In chapter 7 is discussed also the gradual but well constrained increase in  $\delta^{13}\text{C}_{\text{carb}}$  values from the "Daonella Limestone".

The  $\delta^{18}\text{O}$  values of carbonates from Losar are very low. They vary between -4.5‰ and -15.7‰, but most of them vary between -8‰ and -14‰. They do not covary with the  $\delta^{13}\text{C}_{\text{carb}}$  values (fig. 18a). It is to note, however, that samples from the "Hedenstromia beds" (see the left side of the  $\delta^{18}\text{O}$  -  $\delta^{13}\text{C}$  cross-plot in fig. 18a), characterized by anomalously low  $\delta^{13}\text{C}_{\text{carb}}$  values, have very low and constant  $\delta^{18}\text{O}$

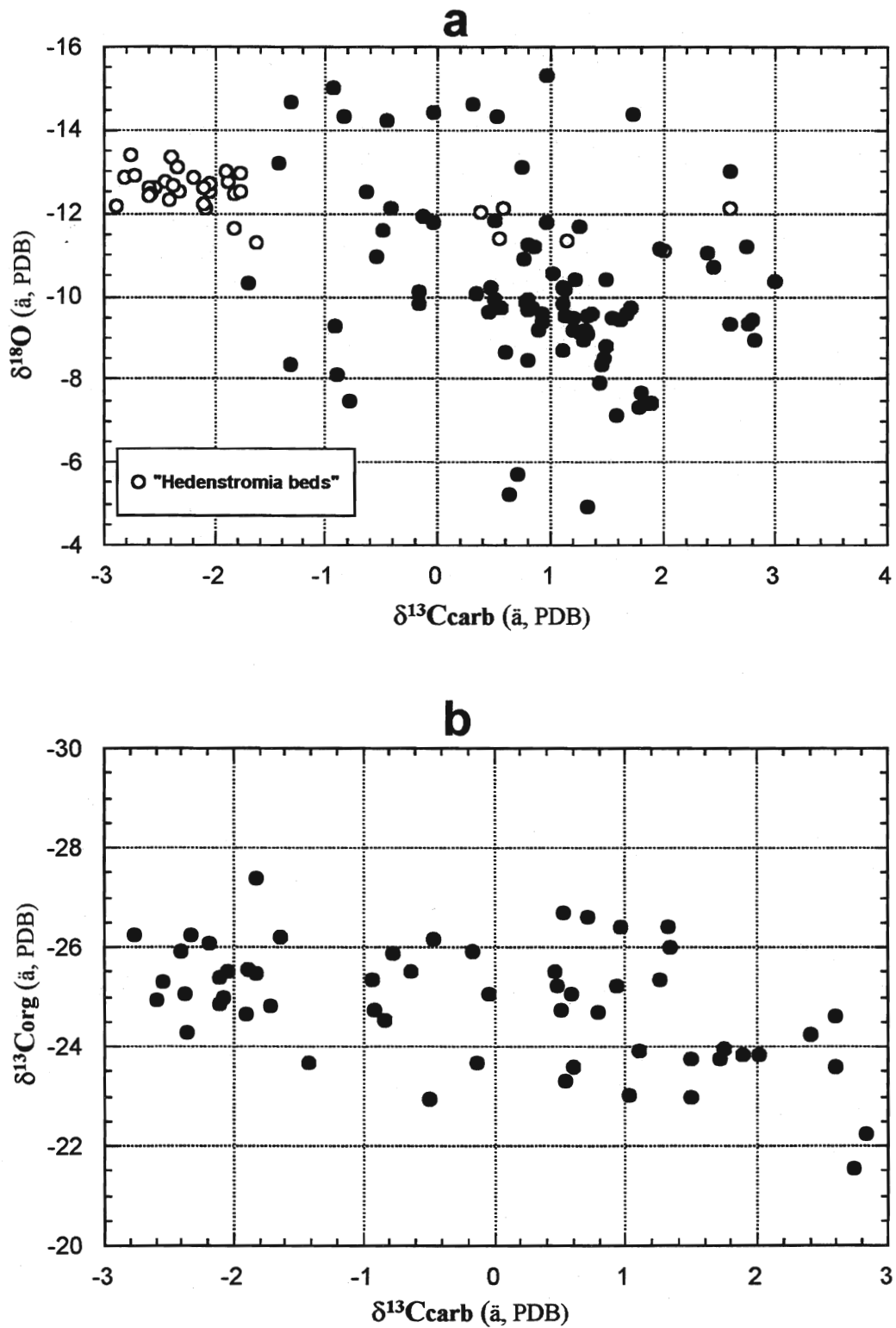


**Fig.18.**  $\delta^{13}\text{C}$  values versus  $\delta^{18}\text{O}$  values (a) and  $\delta^{13}\text{C}_{\text{org}}$  values (b)

values, which also may suggest that diagenetic/metamorphic processes preferentially affected these beds.

### Organic carbon isotope data

Most of the carbon isotope studies devoted to Permian-Triassic rocks dealt with carbonate carbon isotope ratios (Baud, et al., 1989; Magaritz and Holser, 1991; among many others), however organic carbon has been also used (Magaritz et al., 1992; Wang et al., 1994; Morante, R., 1996; Foster et al., 1997; Wignall et al., 1998). It has been shown that global shifts of carbon isotope ratios recorded in marine carbonates are paralleled by those derived from organic carbon in coeval rocks (Magaritz et al. 1992, Wang et al., 1994, Morante et al, 1996). Because it is unlikely that diagenetic processes would alter carbon isotope ratios in carbonate and inorganic carbon in the same direction, the parallelism of  $\delta^{13}\text{C}_{\text{carb}}$  and  $\delta^{13}\text{C}_{\text{org}}$  values is considered as an argument against diagenetic alteration (Hayes et al., 1989; Holser et al., 1995; Morante and Hallam, 1996; Joachimski, 1997).

The significance of stratigraphic variations of bulk organic carbon isotopic composition is difficult to assess, given the multitude of possible sources of variations (e.g. Sackett, 1989; Tyson, 1995). However, it is hypothesized that temporal fluctuations of organic carbon isotope ratios, as recorded by well-preserved marine sediments, are determined primarily by the shallow water productivity and dissolved  $\text{CO}_2$  levels.

The  $\delta^{13}\text{C}_{\text{org}}$  values from Losar section vary between -27.5‰ and -21.5‰, with most of the  $\delta^{13}\text{C}_{\text{org}}$  values between -23‰ and -27‰ (fig. 18b), which is about the normal range of variation of marine organic matter (Tyson, 1995). There is a slight covariant trend between  $\delta^{13}\text{C}_{\text{org}}$  and  $\delta^{13}\text{C}_{\text{carb}}$  values, which can be better observed in fig. 17. In the basal part of the section  $\delta^{13}\text{C}_{\text{org}}$  values increase from a local minimal value of -27‰ in the basal part of the "Otoceras beds" to a value of -24‰ recorded in lowermost part of the "Flemingites beds". At a first approximation this increasing trend parallels the corresponding  $\delta^{13}\text{C}_{\text{carb}}$  pattern. Over the "Flemingites bed" and "Hedenstromia beds" the  $\delta^{13}\text{C}_{\text{org}}$  values are highly variable and do not show any coherent stratigraphic trend. Starting with the base of the "Niti Limestone", the  $\delta^{13}\text{C}_{\text{org}}$  values increase gradually to reach a maximal value of -22‰ in the lower part of the "Muschelkalk", then decrease gently to values averaging -26.5‰ in the middle part of the "Daonella Shales". In the basal beds of the "Daonella Limestone" the  $\delta^{13}\text{C}_{\text{org}}$  values are slightly higher, thus suggesting an increasing trend.

Overall, the  $\delta^{13}\text{C}_{\text{org}}$  profile parallels only partly the  $\delta^{13}\text{C}_{\text{carb}}$  profile. Well defined on both profiles is only the increase near the Lower Triassic/Middle Triassic boundary (event C). For both events A and B there are some similar shifts in  $\delta^{13}\text{C}_{\text{org}}$  values, but the amplitudes are within the overall stratigraphic spread of  $\delta^{13}\text{C}_{\text{org}}$  values and thus these shifts are not clearly marked. Importantly, the  $\delta^{13}\text{C}_{\text{org}}$  profile along the "Hedenstromia beds" do not mirror the  $\delta^{13}\text{C}_{\text{carb}}$  profile.

In summary, the carbonate carbon isotope profile for the Losar section is believed to reflect a mixture of primary and diagenetic signatures. Taking into consideration both  $\delta^{13}\text{C}_{\text{carb}}$  and  $\delta^{13}\text{C}_{\text{org}}$  profiles, and comparing with the carbon isotope record from other sections less affected by post-depositional processes, it appears that at least the Middle Triassic record may be reliable. For the Lower Triassic, at least for the "Hedenstromia beds" preferential re-equilibration of carbon isotopes (likely during metamorphism) is suggested by several lines of evidence:

1.  $\delta^{13}\text{C}_{\text{carb}}$  values are very low and occur in beds containing organic matter and siliciclastic components
2. the  $\delta^{13}\text{C}_{\text{org}}$  and  $\delta^{13}\text{C}_{\text{carb}}$  profiles are not parallel for this segment

3.  $\delta^{18}\text{O}$  values have very low and constant values for the "Hedenstromia beds", unlike for the remainder of the section characterized by highly variable  $\delta^{18}\text{O}$  values, although they are low as well

In this context it is very difficult to postulate a "primary origin" for the variations observed in adjacent beds (ie events A and B). In addition, the event B is not a time equivalent of the isotopic event observed in the Salt Range, as it is discussed in the conclusive part of this chapter.

## 4.5. Nepal

As in the Western Himalayas, similar synrift tectonics with tilting of large blocks occur also in the Tethys Himalaya domain of Nepal (Garzanti and Pagni Frette, 1991) during the late Permian. The central Nepal area has been subjected to numerous stratigraphic studies (Bassoullet and Colchen, 1976; Bodenhausen et al., 1964; Clark and Hatleberg, 1983; Colchen, 1971; Colchen, 1975; Colchen et al., 1986; Garzanti et al., 1994a; Garzanti et al., 1994b; Garzanti et al., 1994c; Garzanti and Pagni Frette, 1991; Hatleberg, 1982; Kapoor and Tokuoka, 1985; Mouterde, 1971; Waterhouse, 1979; Waterhouse, 1987; Nicora et al., 1993; von Rad et al., 1994). Permian stratigraphy is still unclear and, according to the mentioned authors, different names are used for same upper Permian and lower Triassic lithological units, as summarized by Baud et al. (1996) (their fig. 13).

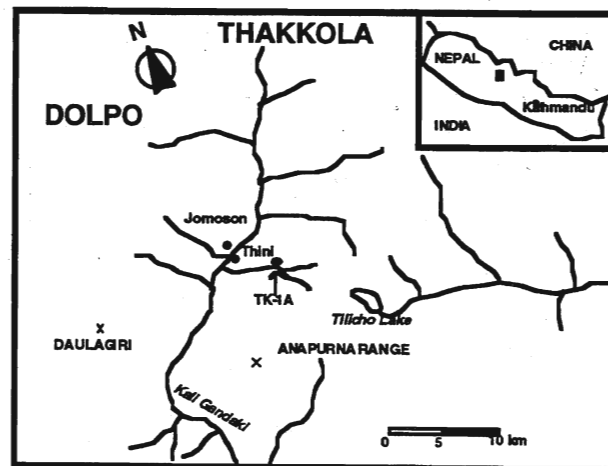


**Fig.19.** Location map of the Thakkhola area (central Nepal). TK-1A: section sampled at Thini Chu.

### 4.5.1 Thini Chu section

Most accessible Permian-Triassic profiles are along the Kali Gandaki Valley, N of the Annapurna (fig.14). The Thini Chu section, sampled in 1994 by A. Baud, is close to the TKa section of (Hatleberg, 1982) and the TK-1A section of von Rad et al. (1994). Unfortunately the upper Permian Kuling Formation lacks carbonate material and, as a consequence, isotopic data are available only for the overlying Tamba Kurkur Formation. Other indication of the isotopic composition of the lower Triassic carbonates from Thakkhola (without profile) are presented in Baud et al. (1989a), based on E. Hatleberg samples, values which are in agreement with the results presented here.

Upper Permian

After Bassoullet and Colchen (1976) and Colchen et al. (1986) thin upper Permian quartzarenites with *Spiriferella rajah* (Dzhulfian) are transgressing the Carboniferous - lower Permian (?) Thini Chu Formation N of the Nilgiri (Annapurna Range). Garzanti and Pagni Frette (1991) correlate these quartzarenites and overlying fine clastics with the Kuling Formation. But here, the exact level of the Kuling transgression is not yet established. There is large gap in the Permian sedimentation of the Kali Gandaki area and only part of the upper T-R cycle is present. As shown by Waterhouse (1987), this is the consequence of middle Permian uplift of the eastern Kali Gandaki block. The Kuling Formation consists of shallow water cross-bedded quartzarenites followed by 1 to 4 m of an alternation of microconglomerate with bryozoans and brachiopods, dark shale and brown-red quartzarenites (= Nisal member of Waterhouse, 1987). Ferruginous alteration at the top of the clastic deposits is interpreted as due to emersive conditions.

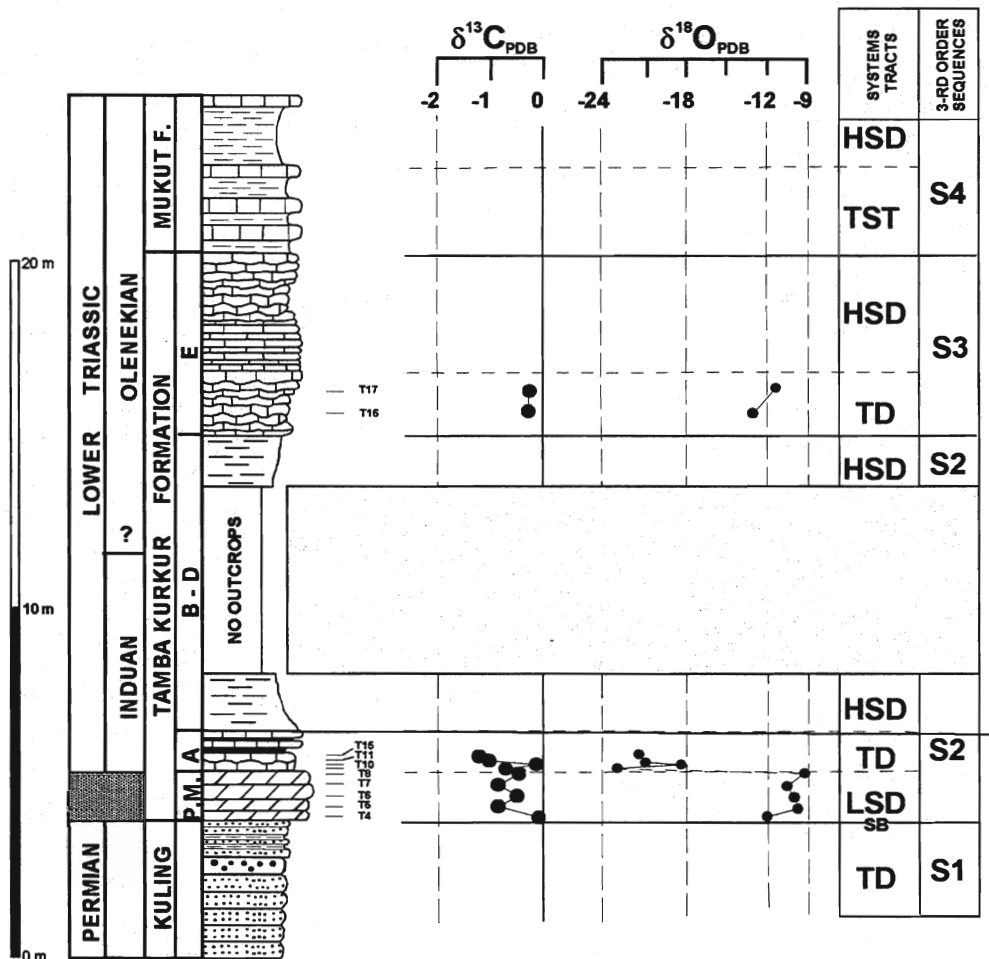


Fig.20. Carbon and oxygen isotope at Thini Chu (central Nepal), sequences and systems tracts.

### Lower Triassic

The following Panjang shallow carbonate unit belongs in our interpretation to the basal part of the lower Triassic T-R cycle, which corresponds to the Tamba Kurkur Formation. Hatleberg (1982) correlates, on the basis of conodonts, the Panjang Unit with the lower Kathwai Member (Salt Ranges) and the E1 unit of the Khunamuh Formation of Kashmir. Garzanti et al. (1994c) interpret as Topmost biocalcarenites the Panjang equivalent in adjacent Marsyandi Valley as end member of his upper Permian Puchenpra Formation.

As in the Salt Range, the lower Triassic T-R cycle is subdivided into three third order sequences (fig.20) with good correlations, see also (Garzanti et al., 1994b; Nicora et al., 1993). Samples from the Panjang member (*sensu* Hatleberg and Clark, 1984) and the lower part of Tamba Kurkur Formation show negative values ( $\delta^{13}\text{C} = -0.5 \pm 0.7\text{‰}$ ) with no significant trend (Fig. 15). A correlation can be made between the Panjang Member and the E1 to E2 units of the Khunamuh Formation from the Kashmir sections (early Induan), using conodont biochronology. Carbon isotope data make possible this correlation.

The  $\delta^{18}\text{O}$  values are very low comparative with Salt Range section and others Tethyan sections ranging from -9‰ to -12‰. High temperature diagenetic processes (Garzanti et al., 1994a) may be responsible for these low  $\delta^{18}\text{O}$  values. In contrast, the much lower  $\delta^{18}\text{O}$  values (from -18‰ to -23‰) that occur at the base of Tamba Kurkur Formation cannot be explained by diagenetic processes alone.

## 4.6. Conclusions

A major problem for carbon isotope studies is whether the measured  $\delta^{13}\text{C}$  values principally reflect the isotopic composition of the seawater from which the carbonate was precipitated, diagenetic inputs, or metamorphism. This problem appears to be particularly important for some sections from the Tethyan Himalaya (sections from Kashmir and Spiti) which experienced severe post-depositional transformations. For both Kashmir and Spiti sections there are lithological units characterized by very low  $\delta^{13}\text{C}$  values, lower than -2‰, atypical for marine carbonates. However, even for these sections, the general pattern of the carbon isotope profiles is similar with published curves for the same time span, proved to reflect primary variations in the seawater.

The results presented in this study chapter confirm the drastic drop of  $\delta^{13}\text{C}$  from the high positive values that characterised the upper Permian to lower values in the lower Triassic. This extraordinary event is documented worldwide and it is thought to be due to the oxidation and removal of the light organic carbon stored on the emerging continental shelf after the large scale regression or/and to a major drop in oceanic productivity at the end of the Permian time (Holser and Magaritz, 1987). Comparison of the upper Permian  $\delta^{13}\text{C}$  curves with sequence stratigraphic analysis shows a close correlation, both for the second order and third order cycles. Higher  $\delta^{13}\text{C}$  values usually occur within the transgressive system tracts, reflecting the deposition of greater amounts of organic matter on the continental shelves during transgressions (Woodruff and Savin, 1985). Similar relationships between the  $\delta^{13}\text{C}$  curve and eustatic level have been reported in the upper Cambrian-lower Ordovician (Ripperdan et al., 1992), in the Cretaceous (Renard, 1986; Mitchell et al, 1997) and in the Tertiary (Woodruff and Savin, 1985; Shackleton and Kennett, 1975).

The most detailed carbon isotope curve for the upper Permian - lower Triassic is given in Magaritz and Holser (1991), based on the study of the Gartnerkopf Core, Southern Alps. The  $\delta^{13}\text{C}$  pattern of this curve for the lower Triassic display a succession of three negative excursions in the Mazzin Member of the Werfen Formation before settling into a more normal phase. A comparison of this curve  $\delta^{13}\text{C}$  curve

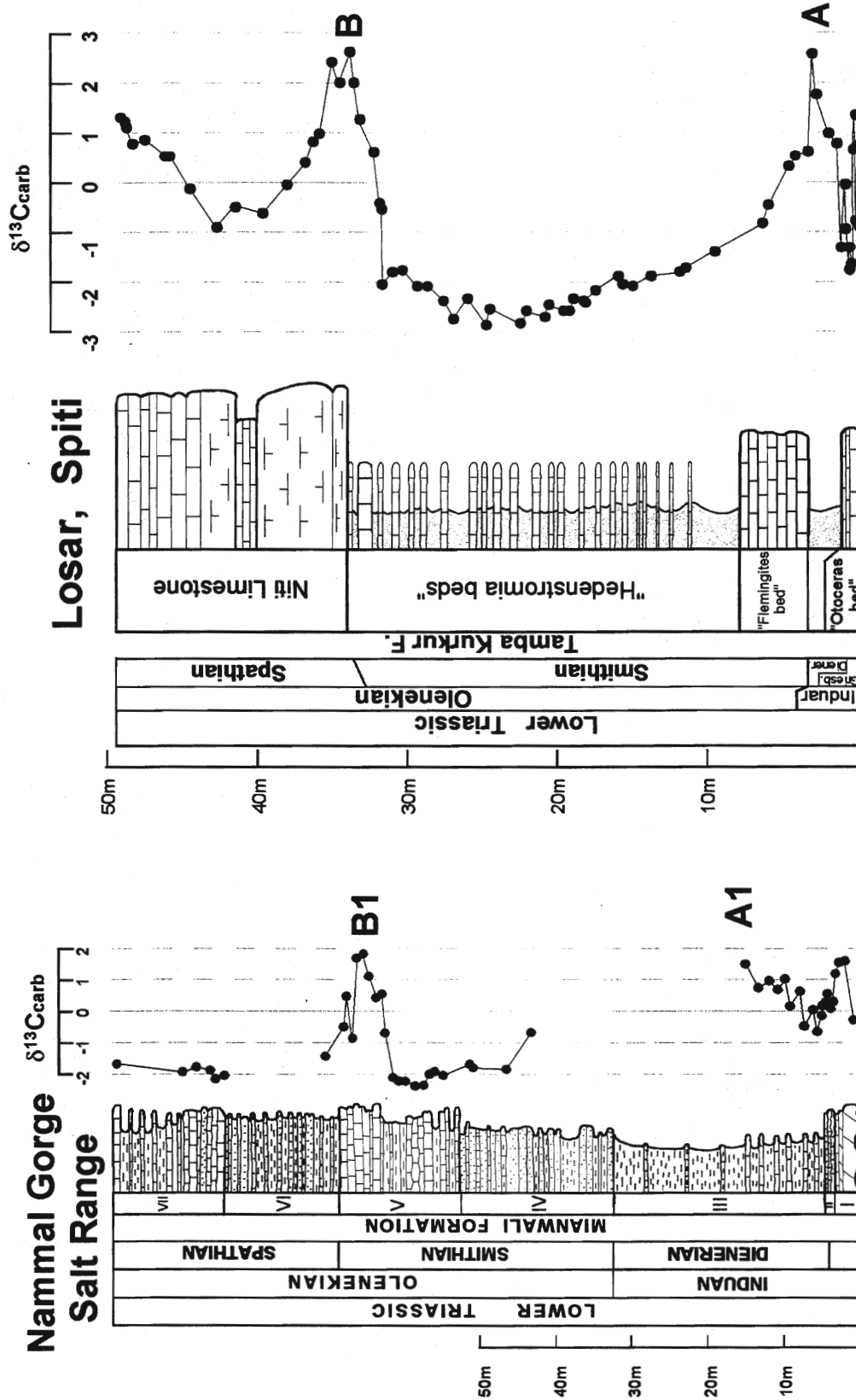


Fig. 21. Comparison of the Lower Triassic Nammal Gorge (Salt Range) and Losar (Spiti) carbon isotope profiles. The shaded areas approximate the extend of the Dienerian and Spathian substages (based on Guex, 1978 and Bucher (personal communication)).

with those from the Northern Indian margin, show some similarities, as well as some discrepancies. The Guryul Ravine profile displays also three negative excursions, that roughly can be correlated with those from the Gartnerkopf Core. Baud et al. (1996) assessed the possibility of correlation of the Guryul Ravine profile with the Gartnerkopf core profile and showed that, although the two peaks are roughly correlatable, they do not overlap perfectly. This may be due to uncertainties in correlations using the recorded range of a limited numbers of taxons.

On the local baseline of low  $\delta^{13}\text{C}$  values, in some Tethyan sections "more positive" values occur (e.g. Guryul Ravine, Member E1 of the Khunamuh Formation - Fig. 11). Isotope data on a very detailed sampling across the boundary show a wide variation of  $\delta^{13}\text{C}$  values at the base of the lower Triassic (Xu and Yan, 1993). It seems unlikely that these large variations in a very short time span are related to changes in the isotopic composition of the seawater. Diagenetic processes cannot be responsible for these higher  $\delta^{13}\text{C}$  values, because the diagenetic alteration is normally reflected in a decrease in  $\delta^{13}\text{C}$  values (Brand and Veizer, 1981). We suggest that a possible explanation of this fact can be the reworking of Permian lime soft sediments with the huge transgression. This hypothesis is sustained by the evidence that in many disputed boundary layers mixed upper Permian and lower Triassic faunas have been found, as in the case of E1 member of the Khunamuh Formation at Guryul Ravine and Kathwai Member in Salt Range.

The positive excursion that occur below the Smithian/Spathian boundary in Salt Ranges is a very short episode, spanning less than a biozone, according to the zonation of Guex (1978) and is characterised by a large magnitude (4-5‰). These two features make it distinctive with respect to other similar events. Other observed positive carbon events have been explained by an increase in the burial ratio of organic carbon to carbonate in marine sediments as a consequence of greenhouse climate conditions resulting from elevated atmospheric  $\text{CO}_2$  levels (Weissert and Lini, 1991) or by an increase in biological productivity (Berger and Vincent, 1986). For the carbon isotope shift below the Smithian/Spathian boundary, an increase in marine productivity appears to be consistent with the fossil record, which shows an important change in ammonoid fauna immediately after the *Anasibirites pluriformis* zone (Guex, personal communication).

A comparison of the carbon isotope profiles of the Nammal Gorge section and the Losar section (two sections which cover the lower Triassic) show some striking similarities (fig. 21). At a first approximation the two isotope profiles appear to be correlatable. In both sections there is an increase in  $\delta^{13}\text{C}$  values in the lower Dienerian (A1 event in Nammal Gorge section and A event in Losar section). For both sections, the background values for the Smithian segment are very low (-2‰ in Nammal Gorge and lower than -2‰ in Losar). As discussed in chapter 4.4.2., for the Losar section the low  $\delta^{13}\text{C}$  values may be explained by diagenetic processes. It is intriguing to find the same low background values in the Salt Range. Unit IV of the Mianwali Formation has very little carbonate. However, low  $\delta^{13}\text{C}$  values are recorded in unit 5, a carbonate rich unit. The sections from the Salt Range do not experienced any thermal metamorphism (Haag, 1991).

The two positive excursions occurring in both sections near the Smithian/Spathian boundary (B and B1) are similar in terms of amplitude and background values. However, the paleontologic data available suggest that they are slightly diachronous. While in Salt Range it occurs within the *Anasibirites pluriformis* zone (Guex, 1978), thus below the Smithian/Spathian boundary, in Losar it extends mainly in the Lower Spathian (Bucher, personal communication). At the time this chapter is being written, more detailed biostratigraphical constrains for the Losar section were not available and therefore a more thorough evaluation is not possible.



## CHAPTER 5

# CONSTRAINTS FROM THE PERMIAN-TRIASSIC OF OMAN

### 5.1. Introduction

The mountainous belt located in the south-eastern part of the Arabian Peninsula, the Oman Mountains, expose a segment of the Neo-Tethys southern margin (Stampfli et al., 1991), interpreted as an upper plate flexural margin (Pillevuit, 1993; Pillevuit et al., 1997; Stampfli et al., in press). The geometry of the Oman margin over a palinspastic cross-section is depicted in figure 22. During Late Permian and Triassic times a large carbonate platform developed on the inner part of the margin: The shallow water facies of the carbonate platform is presently occurring in the Jabal Akhdar Mountains, as part of the "Autochthonous" (Glennie et al., 1974). Carbonates derived from the platform represented the major source for the thick sequence of slope carbonates deposited near the platform margin, cropping out in the Sumeini area. On more distal parts of the Oman margin pelagic sedimentation resulted in various types of carbonate and siliciclastic sediments, presently found in the Hawasina Nappe, which is overthrusting the internal units.

### *Late Triassic - Neotethyan margin - Oman*

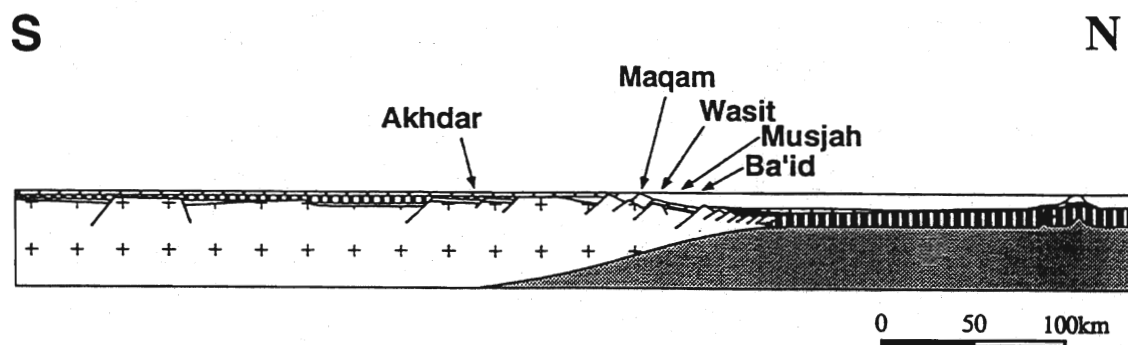


**Fig.22** Late Triassic palinspastic reconstruction of the Oman Neotethyan margin (after Pillevuit, 1993; Stampfli et al., in press)

The main structural units identified in the Oman Mountains are (fig. 23):

- the Autochthonous, the lowest tectonic unit outcropping in Oman, is made up of folded Proterozoic to Paleozoic rocks (the Autochthonous A) and Permian to Cretaceous sediments (the Autochthonous B)
- the Sumeini Nappe (the so-called "Parautochthonous"), consisting of Permian to Cretaceous slope deposits
- the Hawasina Nappes, made-up essentially of Permian to Cretaceous deep water deposits, are subdivided in six groups (see Pillevuit et al., 1997)
- the Semail Ophiolite, a thick Cretaceous oceanic lithospheric slab
- the Mesoautochthonous, the post-tectonic sedimentary cover (Maastrichtian to Miocene)

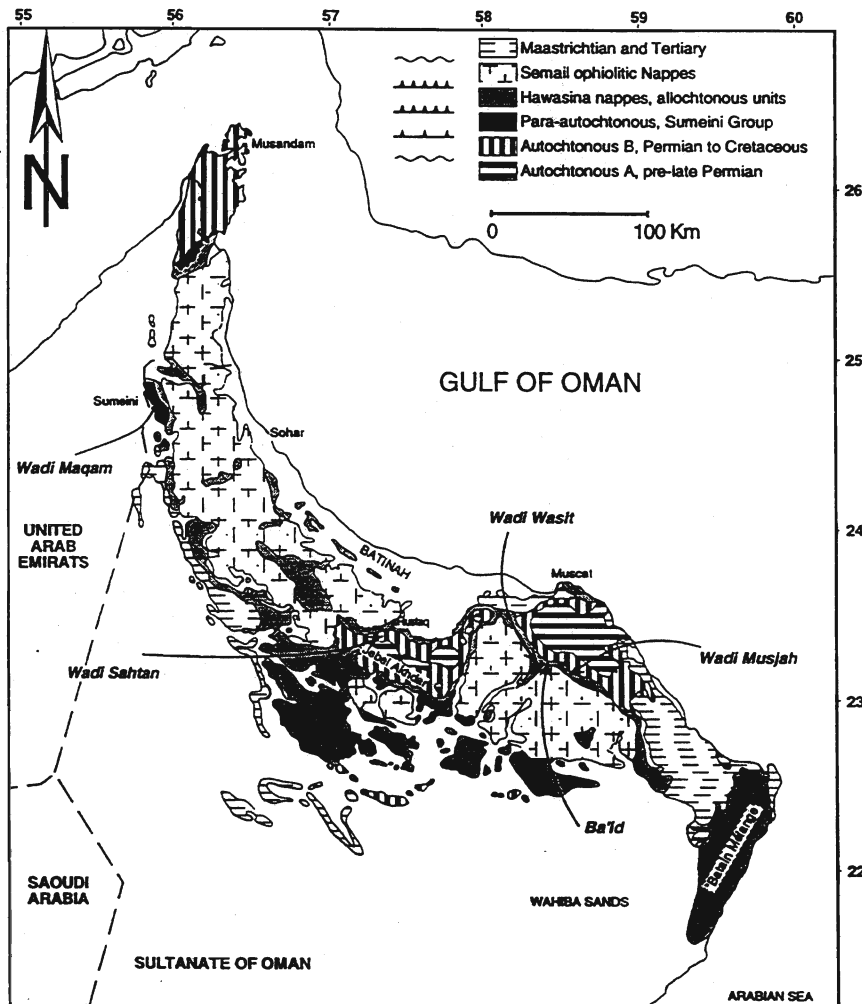


**Fig. 23** Simplified geological map of Oman Mountains (after Glennie, 1974) with the location of the studied sections

In the present study we examined five sections from three major facies zones: shallow water carbonates of the Akhdar Group, slope carbonates of the Sumeini Group and pelagic carbonates deposited on submarine highs or related environments as recorded by the Oman Exotics. The groundwork for this study has been laid by previous studies (Pillevuit, 1993; Pillevuit et al., 1997; Baud, unpublished). The reader is referred to these studies for more detailed and comprehensive information.

## 5.2. Shallow-water settings: the Akhdar Group

The Permian-Triassic sequence deposited on the inner part of the Omanese margin is exceptionally well exposed in the Central Oman Mountains, the Jabal Akhdar Mountains, as part of the "autochthonous" which crops out in a large tectonic window. The Permian and Triassic shallow water carbonate rocks occurring in this area were included into the Akhdar Group (Glennie et al., 1974), with two main lithologic units: the Saiq and Mahil formations.

The Saiq Formation, described in detail by Glennie et al. (1974), Montenat et al. (1976) and Rabu (1988), among others, overlies unconformably Precambrian strata, documenting the late Permian marine transgression. In the Jabal Akhdar Mountains the basal member of the Saiq Formation, made up of terrigenous detritus occur only locally and may reach up to 20 m thick (Rabu et al., 1990). The remainder of the Saiq Formation is made up of an extensive carbonate unit, 450m thick according to the same authors (Rabu et al., 1990). The upper part of the Saiq Formation is affected by pervasive dolomitization which overprinted the primary sedimentary structures, therefore most of the age diagnostic fossil have been recovered from the lower part of the formation. The base of the carbonate sequence of the Saiq Formation was dated by Montenat et al., (1976) as middle Murgabian (*Neoschwagerina schuberti* zone). For the upper part of the Saiq Formation a Dzhulfian age is indicated by *Staffella* cf. *sisonghensis* (Rabu et al., 1990). No paleontologic data for the uppermost Permian stage (Changhsingian) is available. There is a shallowing upwards trend towards the top of the Saiq Formation (Rabu et al., 1990).

There is less information available for the overlying Mahil Formation. It consists of massive to thin bedded gray and whitish dolomites of Triassic age (undifferentiated) formed in intra to supratidal environments (Glennie et al., 1974; Rabu et al., 1990; Béchenec et al., 1992). The Triassic age of the Mahil Formation was attributed on the basis of foraminifera from some levels of oolitic beds, occasionally occurring in the sequence. A Norian-Rhaetian age is suggested for the upper part of the Mahil Formation, an age indicated by the presence of *Aulotortus sinuosus* (Rabu et al., 1990). The top of the Mahil Formation is marked by an exposure surface, overlain by middle Jurassic marine carbonates. We estimate the total thickness of the Mahil Formation to 800 meters.

### 5.2.1 Wadi Sahtan section

For the present study we focused on the transition between the Saiq and Mahil Formation, apparently straddling the Permian-Triassic boundary. The examined section is located in the Wadi Sahtan valley, about 4 km North of Fashah village near the road linking Fabaqah to Fashah villages. In this area the Permian to Cretaceous strata of the "autochthonous" form a normal monoclinial structure dipping to the North. The Wadi Sahtan valley cuts more or less transversally the strata and the succession is very well exposed on both sides of the valley. Samples from the upper part of the Saiq Formation come from previous fieldwork carried out by A. Baud. During the fieldwork we sampled only the part of the Mahil Formation. In addition, we sampled and examined the transition between the limestones and dolomites within the Saiq Formation.

The upper part of the Saiq Formation (120 m) were divided by A. Baud (personal communication) in two main lithologic units (B and C) according to stratal patterns and microfacies (fig. 25). Both units B and C are made up of dolomitized high energy calcareous sands, the main microfacies being represented by grainstones. Some unidentified coral fragments have been observed in B1 unit, while badly preserved calcareous algae and foraminifera were observed in thin sections of samples from unit C.

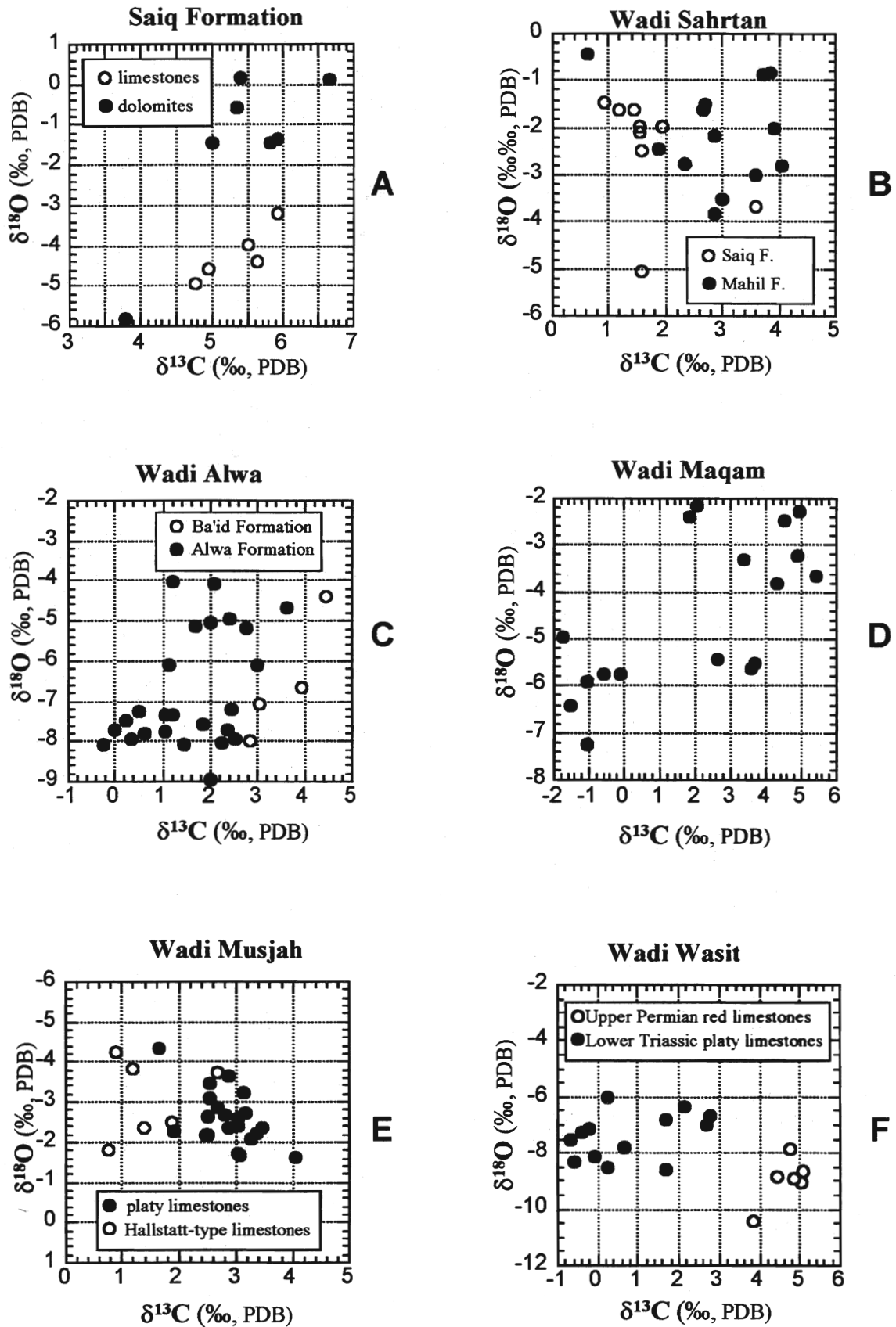


Fig. 24. Cross-plots of  $\delta^{13}\text{C}$  –  $\delta^{18}\text{O}$  values of the sections from Oman.

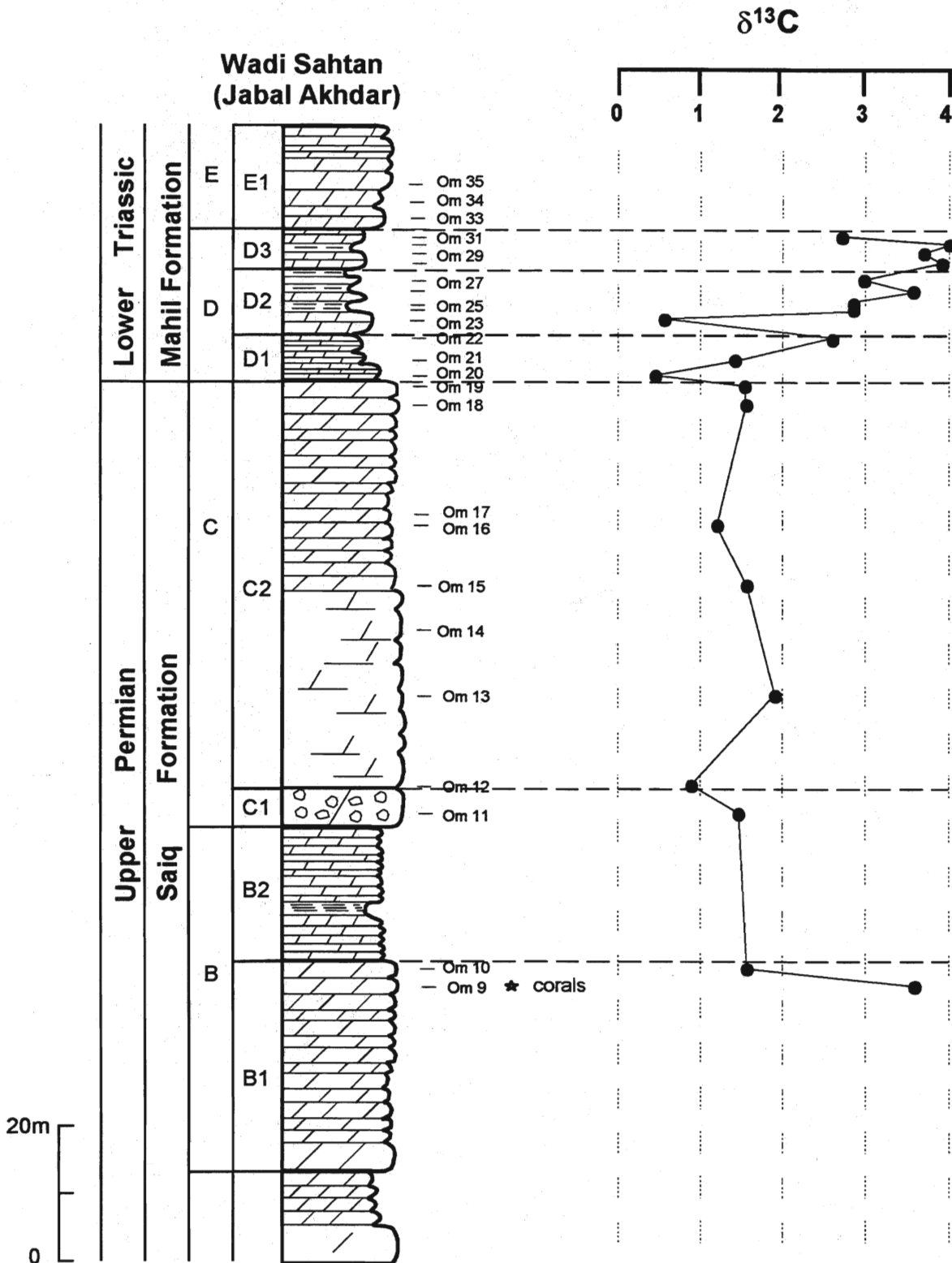


Fig. 25. Carbon isotope profile of Wadi Sahtan section (Jabal Akhdar Mountains).

These scarce fossils suggest, however, a Permian age (corals and calcareous algae have never been reported from lower Triassic strata). The top of Saiq Formation is marked by an irregular surface of hardground type, indicating an interruption in sedimentation, possibly with subaerial exposure.

The lower part of the Mahil Formation, examined herein, is divided in two main lithologic units, D and E, further separated in subunits (see Plate 2, Figs 1 and 2). Overall, both D and E units consist of gray and yellowish peritidal dolomites and dolomitic limestones with fine grained terrigenous sediment. Unit D of the Mahil Formation starts with a bed of flat-pebble conglomerates up to 0.6 m thick, overlaid by a 0.3 m thick bed of black dolomites with columnar stromatolites. These two beds are distinctive for the base of the Mahil Formation.

The sequence grades upward to thinly bedded dolomites with ripple marks structures, yellowish dolomitic marls and several levels of paleosols. Algal-bacterial structures as laminites and stromatolites are common features of the Mahil Formation. Unit E exhibit similar sedimentary structures, however it is more massive and marly interbeds are rare.

Fossils are extremely rare in the Mahil Formation. Foraminifera of *Cyclogira* and *Earlandia* type were identified in three samples from unit D2 (Baud, personal communication) indicating an early Triassic age.

#### **Carbon and oxygen isotope data**

The Wadi Sahtan section is composed mainly of dolomites. It is known from previous studies that dolomitization processes do not affect significantly the carbon isotopic composition of the primary carbonate sediments (Land, 1980; 1992). Dolomites have generally a typical marine carbon isotope signature and many examples showed that dolomites are isotopically indistinguishable by associated calcitic rocks. However, in order to test the influence of dolomitization on the carbon isotopic composition of the carbonates from the Akhdar Group we made a test on the Saiq Formation occurring 3 km North of Fashah village, in the left side of the Wadi Sahtan valley. Here, the contact between the gray bioclastic limestone and the dolomitized limestones is well exposed. The dolomitization front is clearly marked, irregularly cutting the limestone beds.

A number of 13 samples of both limestones and dolomites were collected across the dolomitization front and from a single bed of limestones laterally affected by dolomitization (Plate 1, Figure 3). The  $\delta^{13}\text{C}$  values are shown on the photograph and also plotted together with the  $\delta^{18}\text{O}$  values on a  $\delta^{18}\text{O}$  -  $\delta^{13}\text{C}$  cross-plot (fig. 24a). There is no significant difference in  $\delta^{13}\text{C}$  values between limestones and dolomites. The average  $\delta^{13}\text{C}$  value for the limestone +5.1‰ and for dolomites +5.5‰. For Permian and Triassic shallow water carbonates this difference is considered to be minor. However, the overall range of variation of  $\delta^{13}\text{C}$  values in dolomites appears to be greater than in limestones. In turn,  $\delta^{18}\text{O}$  values of are consistently different between the two phases.  $\delta^{18}\text{O}$  values of limestones (-4.2‰ average) are about 3‰ higher than their counterparts from dolomites (-1.5‰ average). This difference is in agreement with previous reports (e.g. McKenzie, 1981) and with other examples from the present study and it is explained as a result of  $^{18}\text{O}$  enrichment due to evaporation processes in hypersaline environments of sabkha-type, where dolomitization occur frequently. The dolomitization of the Akhdar Group likely occurred in such conditions.

The  $\delta^{13}\text{C}$  values from the section Wadi Sahtan section vary between 0.4‰ and 4‰ (figs. 25; 24b). Two samples from the B1 unit gave different  $\delta^{13}\text{C}$  values, with a 2‰ negative shift from the lower one (Om9) to the second located 2m higher in the section (Om 10). The remainder samples from the Saiq Formation have relatively stable  $\delta^{13}\text{C}$  values comprised between +1‰ and +2‰. Samples from the

Mahil Formation have more variable  $\delta^{13}\text{C}$  values, from 0.4‰ to 4‰, most of them having  $\delta^{13}\text{C}$  values between 2.5‰ and 4‰.  $\delta^{13}\text{C}$  values from the D1 unit show a gradual increase from a value of +0.4‰ to a value of +2.6‰. A similar increase of  $\delta^{13}\text{C}$  values are recorded also in unit D2. It appears that these higher trends are correlated with shallowing upward trends, as observed in the field. Samples from the lower part of the unit D3 gave high  $\delta^{13}\text{C}$  values around +4‰, one sample from the upper part gave a somewhat lower value of +2.8‰.  $\delta^{18}\text{O}$  values are between -0.3‰ and -5‰ and they do covary with the  $\delta^{13}\text{C}$  values (fig. 24b). However, the  $\delta^{18}\text{O}$  -  $\delta^{13}\text{C}$  pairs for the Mahil Formation display a more scattered distribution, which may be explained by the fact that the samples from the Mahil Formation contain some amounts of primary calcite with lower  $\delta^{18}\text{O}$  values than the dolomites.

Overall, there is a well marked stratigraphic trend: whether  $\delta^{13}\text{C}$  values remain constant over the upper part of the Saiq Formation, they display a gradual increase of 2.5‰ over the D unit of the Mahil Formation. If the boundary between upper Permian and lower Triassic deposits coincide with the boundary between the Saiq and Mahil formations, as suggested by sequence stratigraphy and the very scarce paleontologic data (Baud, personal communication), then the carbon isotope pattern appears to be contrary to expectations.

It is well documented that upper Permian carbonates are characterized by high  $\delta^{13}\text{C}$  values (commonly higher than 4‰) and the lower Triassic carbonates usually have low  $\delta^{13}\text{C}$  values (eg Baud et al., 1989; Grossman, 1994; Scholle, 1995; see also a compilation in chapter 8). The Wadi Sahtan section exhibit a contrary pattern: low values in the (supposed) upper Permian carbonates, and high  $\delta^{13}\text{C}$  values in the lower Triassic carbonates. One may believe that the carbon isotope pattern reflects lithologic changes or may reflect marginal marine depositional conditions, influenced by an influx of meteoric waters during subaerial exposure. Subaerial exposure generally lower  $\delta^{13}\text{C}$  values of the carbonate. Sedimentological evidence for more restricted marginal marine environments and subaerial exposure, with paleosoils, mud-cracks and teepee structures (Béchenec et al., 1992; Baud, unpublished), is recorded mainly in the Mahil Formation, characterized by high  $\delta^{13}\text{C}$  values and not lower. We interpret  $\delta^{13}\text{C}$  values as high as 3-4‰ as reflecting a marine signature, even in very shallow water restricted environments.

One possible explanation for the relatively low  $\delta^{13}\text{C}$  values from the upper part of the Saiq Formation would be that the boundary between Permian and Triassic deposits occur lower than currently believed, possibly between B1 and B2 unit. The paleontologic constraints for the upper part of the Saiq Formation are very poor, certain indications for a Permian age are known only from the B1 member. One sample from the top of the B1 unit gave a value of 3.7‰, within the normal range of "Permian values". The fact that high  $\delta^{13}\text{C}$  values, typical for the upper Permian world-wide, are recorded also in the Akhdar Group is proven by the data set acquired lower in the Saiq Formation, at the transition between limestones and dolomites, as shown above. There, the average  $\delta^{13}\text{C}$  values for both dolomites and limestones are higher than 5‰.

However, even if we admit that the Permian-Triassic boundary should be traced lower in the section, the high  $\delta^{13}\text{C}$  values from the base of the Mahil Formation are difficult to explain. Such high  $\delta^{13}\text{C}$  values have not been reported yet from lower Triassic strata. More data from both the middle part of the Saiq Formation and from the remainder of the Mahil Formation would be necessary in order to explain the intriguing stable isotope data set.

### 5.3. Carbonate platform margin settings: the Sumeini Group

The Sumeini Group, as defined by Glennie et al. (1974) is represented by a thick sequence (about 2500 m) of Permian to Cretaceous slope carbonate deposits and crops out near the border between Oman and the United Arab Emirates (Le Métour et al., 1992). A comprehensive stratigraphic and sedimentologic study of the Sumeini Group can be found in Watts (1985, 1990) and Watts and Garrison (1986). The lower part of the Sumeini Group (about 1700 m thick) is included in the Maqam Formation (Upper Permian to Upper Triassic), further subdivided into 6 members (A, B, C, D, E and F). Herein, this nomenclature is used.

#### 5.3.1 Wadi Maqam section

We made a prospective isotopic study on samples from the A, B and C members. Although a limited number of samples were available for this study, the preliminary results appear to be meaningful. The samples were collected by Alain Pillevuit and Aymon Baud from a section located East of Shuayb village. For the precise location see Pillevuit (1993), fig. 27, page 49 and Watts and Garrison (1986), their fig. 3, page 112 (corresponds to their section MS-6).

The Member A of the Maqam Formation (fig. 26), about 80 m thick, is made up of gray and black thinly bedded limestones alternating with marls and locally with sandstones. A Murgabian age was proposed by Pillevuit (1993) on the basis of ammonoids, trilobites and ostracods recovered from the lower half of the unit. The Member B consists of a 365 m thick sequence of predominantly thin-bedded to massive dolomites with numerous calcirudite intervals and locally abundant breccia in the lower part (Watts and Garrison, 1986). According to these authors, the contact with the underlying A Member is irregular. Corals recovered from the lower part indicate a Permian age. The Member C is a very thick unit (455m) made up essentially of platy limestones, calcarenites and calcirudites, the latter being preferentially dolomitized. A Triassic age is inferred, but no conclusive paleontologic evidence is available. The location of the Permian-Triassic boundary is not precisely known, it is tentatively traced between the B and C members.

#### Carbon and oxygen isotope data

The  $\delta^{13}\text{C}$  values vary between -1.7‰ and +5.4‰ and show a distinct stratigraphic pattern (fig. 26). The highest values are recorded in the A and B members.  $\delta^{13}\text{C}$  values drop suddenly at the transition between B and C members, from a value of +4.9‰ recorded at the top of Member B to values around +2‰ at the base of Member C. Higher up in the section the  $\delta^{13}\text{C}$  values continue to decrease gradually to a value of -1.8‰ in the middle part of the Unit C.  $\delta^{18}\text{O}$  values vary between -2‰ and -7.3‰. Pairs of  $\delta^{13}\text{C}$  and  $\delta^{18}\text{O}$  values show a scattered distribution on the  $\delta^{18}\text{O} - \delta^{13}\text{C}$  cross-plot (fig. 24d) although the samples with lower  $\delta^{13}\text{C}$  values have also lower  $\delta^{18}\text{O}$  values. This observation may indicate diagenetic alteration for these samples.

The stratigraphic pattern displayed by the Wadi Maqam section is very similar to the world-wide documented pattern across the Permian-Triassic boundary.  $\delta^{13}\text{C}$  values between +4‰ and +5‰, as recorded in the members A and B are typical for the upper Permian marine carbonates. Likewise, the negative shift of magnitude similar to that recorded at the transition between B and C members is proved to be global. Therefore, the carbon isotope data suggest that for the Wadi Maqam section the Permian-Triassic boundary coincide with the boundary between members B and C. Although a diagenetic overprint cannot be ruled out for the samples from the C member, diagenesis alone can hardly explain a 6‰ shift of  $\delta^{13}\text{C}$  values. It is to note that the magnitude of the Permian/Triassic drop in  $\delta^{13}\text{C}$  values is usually between 3‰ and 4‰. Here it is greater, but there are other examples in the Tethys with shift of this order of magnitude (e.g. Guryul Ravine).



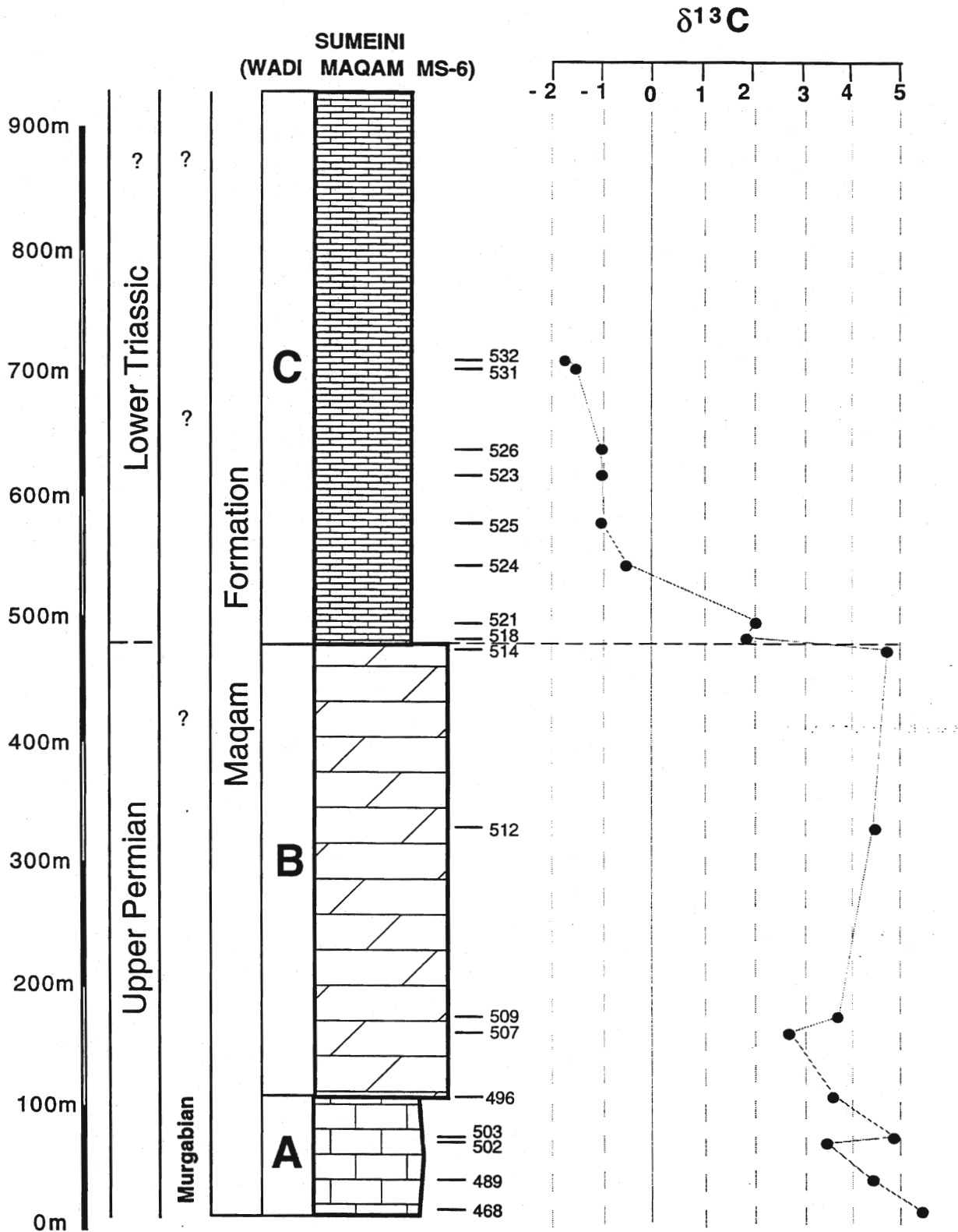


Fig. 26. Carbon isotope profile of Wadi Maqam section (Sumeini Group).

## 5.4. Deeper water settings: the Oman exotics and the Hawasina Group

The sediments deposited in more distal parts of the Oman margin were transported in the front of the Semail Ophiolite during its obduction over the Arabian Platform and they can be found today into the Hawasina Nappes system, tectonically sandwiched between the Autochthonous units and the Semail Ophiolite. A part of the deeper water sediments, mainly those deposited on submarine elevated sectors are present as blocks of various dimensions, the Oman exotic blocks.

For the present study, we examined three of these block, two of them located in the Ba'id area, about 50 km south of Muscat.

### 5.4.1. Wadi Alwa

The Wadi Alwa section is located in the Ba'id exotic, a large block made-up of Permian to Cretaceous limestones, radiolarites and volcanic rocks which occurs in a tectonic window. The Ba'id exotic is well known for its Triassic ammonoid-rich limestones, a particular interest presenting the Hallstatt-type limestones (Tozer and Calon, 1990; Blendinger, 1991; 1995; Orchard, 1995). We examined a section located in the eastern flank of the mountain. For a precise location see Pillevuit (1993), fig. 34, page 63 (the section corresponds to section 4 therein) and Plate 2. Fig. 1. The section is described also by Blendinger (1995), (see section Wadi Alwa II in fig. 7, page 585) and by Pillevuit et al. (1997) (see fig. 10, page 218)

In this section the AlBuda'ah Group occurs (Pillevuit, 1993). The visible sequence starts with massive yellowish dolomites interbedded with gray to black bioclastic limestones, capped by a 1.3 m thick bed with black limestones. This succession, about 23 m thick, is attributed to the Ba'id Formation (Pillevuit, 1993). The limestone interbeds are very rich in foraminifera, on whose basis Pillevuit (1993) dated the upper part of the Ba'id Formation as Dzhulfian. The upper surface of the Ba'id Formation is irregular, likely erosional.

A 25-30m thick sequence of red, pelagic limestones of Hallstatt-type (fig. 27) overlies disconformably the Ba'id Formation. The first 6 m are represented by pinkish microgranular dolomites, probably dolomitized Hallstatt-type limestones. This sequence was included, together with other Hallstatt-type limestones occurring in the Ba'id exotic into a comprehensive unit, the Alwa Formation (Pillevuit, 1993), studied in detail by Blendinger (1995). The succession is often disrupted by low angle faults, Blendinger (1995) proposed that even the contact with the Ba'id Formation is a fault plane. However, a careful examination of sedimentary structures allow a reliable recognition of the stratigraphic relationships. The limestones are rich in ammonoids and microfacially are characterized by wackestones to packstones with thin bivalve filaments, baby-ammonoids and occasionally ostracodes and crinoid elements. They exhibit some particular features comparing to the typical Hallstatt-type limestones. The fossils do not have Fe-Mn oxydes coatings (Tozer and Callon, 1990) and they are filled almost exclusively with white spar (Blendinger, 1995). Hardground surfaces are not common. A prominent characteristic is given by the abundant evidence for microbial activity, which appears to have played an important role in carbonate accumulation. Decimetric layers (probably lenticular) of gray-white thrombolites with radiating crystal sprays (Plate 2, fig. 3.) occur over the section (we identified at least three). Stromatactis-type structures are present at both macro and microscopic scale (Blendinger, 1995, cites even "zebra-rock" structures from the "summit block").

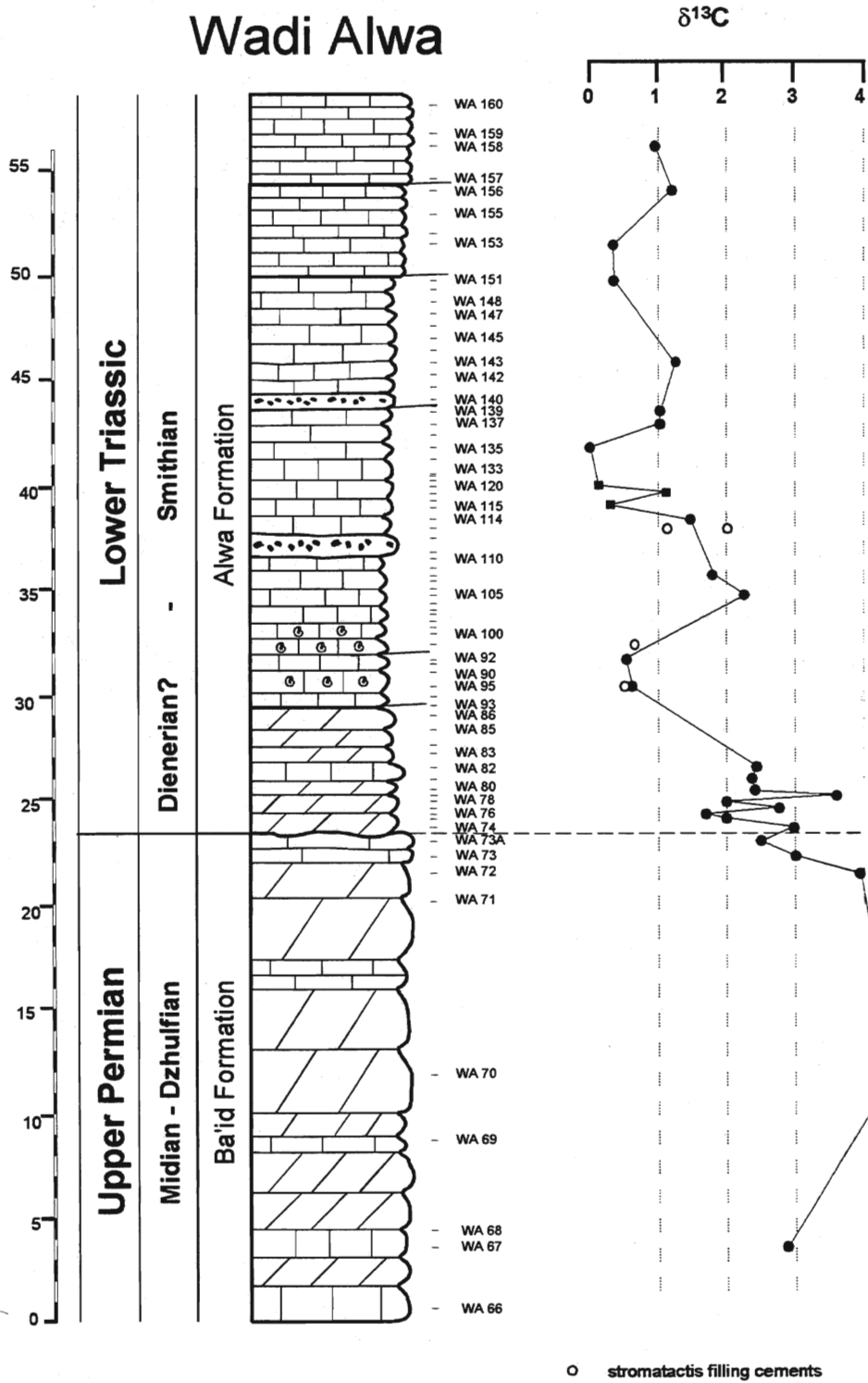


Fig. 27. Carbon isotope profile of Wadi Alwa section (Ba'id exotic).

In thin sections, mainly in samples from the upper part of the section microbial-type structures are abundant (mainly beneath the stromatolite-type voids), as zones with clotted fabric and even well preserved cyanobacterial filament moulds. In the thrombolitic levels, organic remnants of microbial mats are preserved. Another distinctive feature of the red limestones occurring in the studied section is the presence of two interstratified meter thick levels of resedimented limestones including clasts of Permian carbonates (rich foraminifera) and clasts of Hallstatt-type limestones. Pillevuit (1993) interpreted these levels as the result of reworking of unlithified Permian sediments (soft-sediments).

The age of the Hallstatt-type limestones from the Wadi Alwa block is early Smithian (Pillevuit, 1993; Blendinger, 1995), indicated by the presence of the conodonts *Neospathodus waageni* (Krystyn, as cited by Pillevuit, 1993; Blendinger, 1995). Both Late Dienerian and Late Smithian ages are possible for the base and for the top of the section, respectively, but no definite paleontological data are available.

### Carbon and oxygen isotope data

Overall, the  $\delta^{13}\text{C}$  values vary between 0‰ and +4.4‰ (fig.24c), with the higher  $\delta^{13}\text{C}$  values in the Upper Permian Ba'id Formation, as normally expected. The  $\delta^{13}\text{C}$  values from the Alwa Formation vary between 0‰ and +3.6‰ and show a relatively high variability upsection (fig.27). Relatively high  $\delta^{13}\text{C}$  values (comprised between +1.7‰ and +3.6‰) are recorded from the pink dolomites at the base. The  $\delta^{13}\text{C}$  values decrease to values around +0.5‰ in the 6 m of Hallstatt-type, which are particularly rich in ammonoids.  $\delta^{13}\text{C}$  values increase in the overlying strata reaching values up to +2.2‰, below the first level of resediments and then decrease again to values as low as 0‰ (sample WA135). For the remainder of the section  $\delta^{13}\text{C}$  values remain more or less constant with values around +1‰, with a minor excursion to values around +0.3‰.

The magnitude of the shift between the Permian and Triassic beds is about 2‰, considering only samples close to the lithologic boundary, This may be due to a "gap effect": because the earliest Triassic (characterized by the lowermost values) is missing, the amplitude of the shift is diminished because the carbon isotope values already recovered. However, the  $\delta^{13}\text{C}$  values continue to decrease and there are some variability, recorded on both bulk rock and cements.

Two alternative explanations are given in order to explain the high variability:

- they reflect in some extent short term primary variations in surface seawater
- they represent values of re-equilibration with diagenetic fluids which masked the primary values (but not necessarily completely deleted them as suggested by the preservation of the general trend typical for the Permian-Triassic transition).

These two alternatives will be later discussed, together with the other data from the Tethys.

It is interesting to note, however, that these data derive from one of rare occurrence of the Hallstatt-type limestones in the Lower Triassic. Hallstatt-type limestones are considered herein among the best recorders of the Triassic surface waters carbon isotopic composition, because of their pelagic origin, far from any continental input and their high carbonate/organic carbon ratio which makes diagenetic overprint difficult. In addition they are commonly rich in fossils and the isotopic variations can be easier dated.

### 5.4.2. Wadi Wasit

The Wadi Wasit section is also located in the Ba'id area, near the road linking Wadi Ta'yin to Wadi Rahbah (for a detailed location map see Pillevuit et al. (1997), fig. 7, page 215). A more comprehensive description can be found in Pillevuit (1993) (the Permian sequence can be found in fig. 40, page 77, and the lower Triassic one in fig. 41, page 78) and in Pillevuit et al. (1997), fig. 13, page 221.

The main section we examined (Wadi Wasit A) is located on the western side of the hill whose southern flank is exposed in the small gorges near the road (in these gorges the section 2 of Pillevuit et al. (1997) is located. In addition we examined and sampled the platy limestone sequence exposed in front of the gorges (Wadi Wasit B).

The sequence of Wadi Wasit A section, representing a part of the Al Jil Formation, consists of 5 main lithologic units, as depicted on fig. 28 and in Plate 3 fig. 1. Unit 1 (only its uppermost part is represented in fig. 28) is a thick volcano-sedimentary sequence made up of pillow basalts of MORB-type (Pillevuit, 1993), tuffites and interbeds of radiolarites. The overlying unit 2, 19m thick, consists essentially of medium bedded red limestones with some levels of fine-grained resedimented limestones and red shales interbeds. Unit 3 (21m thick) consists of sequence mainly of allodapic limestones and red shales, the latter being more abundant in the upper part. The allodapic limestones are represented either by calcarenites or calcirudites and they include occasionally reddish-whitish chert nodules. Unit 4, about 30 m thick is represented by a massive dolomitized breccia with blocks of reefal limestones (Weidlich et al., 1993). The overlying unit 5 starts with gray platy limestones and thin shales or marlstones interbeds, over a 6 m thickness. The contact with massive dolomitized breccia is marked by a thin layer of marly shales whose deformed nature suggest the presence of a fault between the two units. The platy limestones sequence is overlain by a 12 m thick sequence of light brownish folded radiolarites, which in turn are capped by a 3 m thick sequence of gray platy limestones. The platy limestones from the Wadi Wasit area are also described by Blendinger (1988).

The sequence from the Wadi Wasit B section is very similar with the sequence of the unit 5 from the Wadi Wasit A section, comprising gray platy limestones with shales and marls interbeds. However, some differences are due probably to some low angle faults (observed in the field) which disrupted the stratigraphic succession from the Wadi Wasit A section.

Paleontologic data from the lower part of the succession obtained elsewhere in the Wadi Wasit area (Pillevuit, 1993) suggest an Upper Permian age for units 1 to 4. A Murgabian age was proposed by Pillevuit (1993) for the volcano-sedimentary sequence (our unit 1) on the basis of ammonoids, ostracods and bryozoans. Foraminifera obtained from the blocks of reefal limestones which form the dolomitized breccia (our unit 4) indicate a Murgabian- Dzulfian age. Finally, conodonts obtained from the lower part of the platy limestones (Krystyn as cited by Pillevuit, 1993) indicate a Dienerian age (*kummeli* zone). No age constraints are available for the remainder of the unit 5.

#### Carbon and oxygen isotope data

Carbon and oxygen isotope data were obtained for samples coming from both Wadi Wasit A and Wadi Wasit B sections. Overall,  $\delta^{13}\text{C}$  values vary between -0.7‰ and +5‰ and  $\delta^{18}\text{O}$  values between -10.5‰ and -6‰. The  $\delta^{18}\text{O}$  -  $\delta^{13}\text{C}$  cross-plot (fig. 24e) do not show any covariance between  $\delta^{13}\text{C}$  and  $\delta^{18}\text{O}$  values.  $\delta^{13}\text{C}$  values from units 2 and 3, gave high  $\delta^{13}\text{C}$  values, roughly between +4‰ and +5‰, with a slight increase in  $\delta^{13}\text{C}$  values from a value of +3.9‰ at the base of the unit 2 to background values of

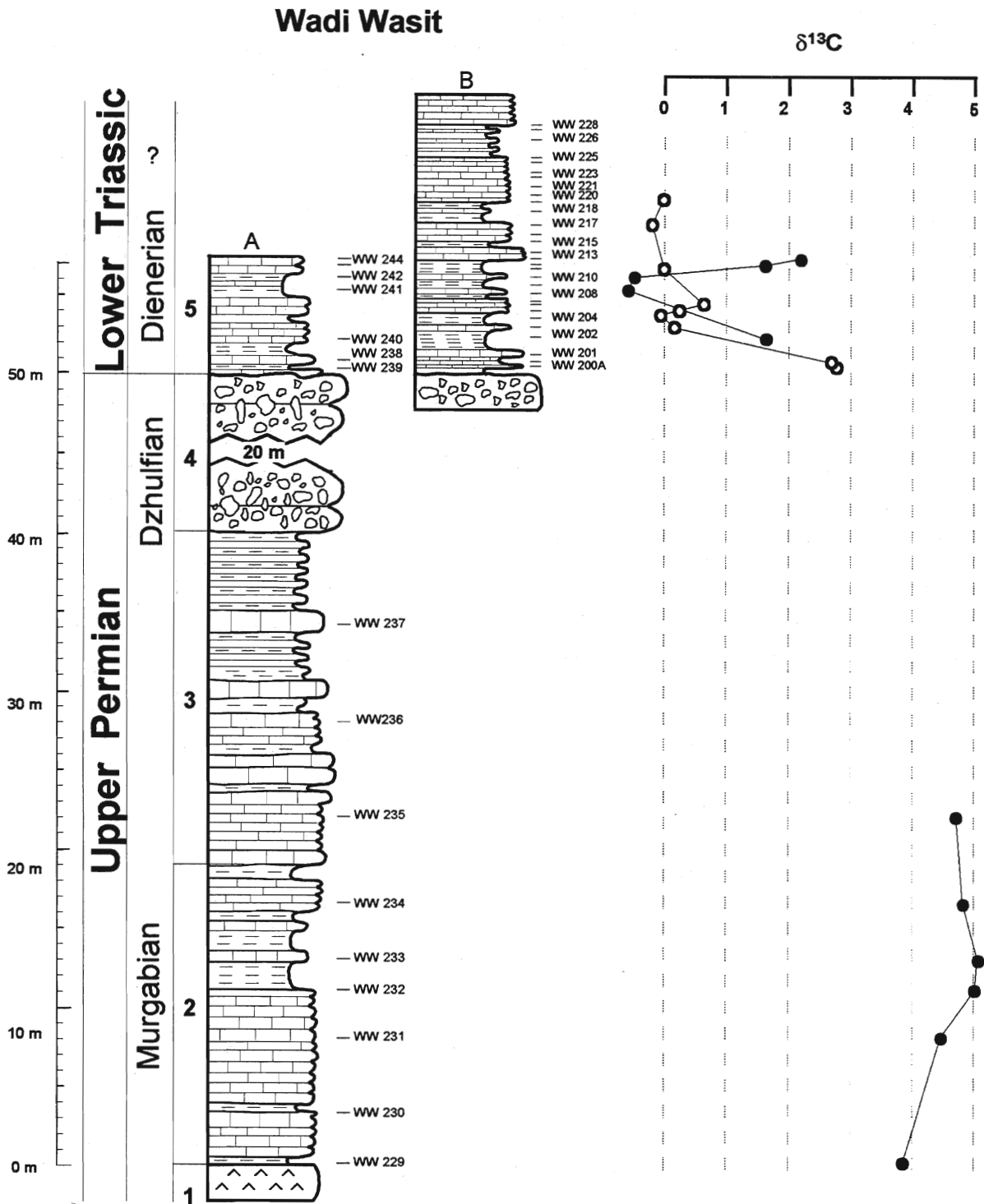


Fig. 28. Carbon isotope profile of Wadi Wasit section.

+5‰ characterizing the remainder of the unit 2 and the lower part of the unit 3. The high  $\delta^{13}\text{C}$  values are consistent with the Late Permian age attributed for these lithologic units by previous works. Samples from the lowermost beds of the platy limestones gave relatively high  $\delta^{13}\text{C}$  values (up to +2.8‰) on both sections examined. The  $\delta^{13}\text{C}$  values decrease (here again on both sections) to values around 0‰ (the lowest  $\delta^{13}\text{C}$  value recorded is of -0.7‰). In the Wadi Wasit B section these  $\delta^{13}\text{C}$  values around 0‰ remain constant over a thickness of 10m. In the Wadi Wasit A section,  $\delta^{13}\text{C}$  values around +2‰ are recorded by the limestones capping the radiolarites. Thus, the stratigraphic plot of  $\delta^{13}\text{C}$  values for the Lower Triassic platy limestones show a distinctive trend, with an initial negative shift of about 2‰, a relatively stable interval and a positive shift of about 2‰.

### 5.4.3. Wadi Musjah

Wadi Musjah is located near the main road linking Muscat to Ibra, north-east of the Rawda village. The section we examined at Wadi Musjah corresponds to "Wadi Musjah nord-est" or section 4 of Pillevuit, 1993 (see fig. 46, page 82 therein, for a precise location).

The base of the sequence we examined at this locality occurs on the western flank of a small hillock (see Plate 3 fig. 2) and is represented by medium bedded gray bioclastic limestones summing 2 meters of thickness (unit 1 in fig. 29). They are overlain by a 10 m thick unit made up of massive, brownish dolomitized breccia (unit 2). Overlying the dolomitized breccia it follows a 15 m thick sequence of platy limestones, thick bedded resedimented limestones and dark gray limestones with siliceous nodules (units 3 and 4). The contact between the units 2 and 3 is sharp and irregular. The base of unit 3 (see Plate 3, fig.3) is represented by two layers of medium bedded (about 0.2 m each) pinkish, micritic limestones similar to the Hallstatt-type limestone, followed by gray platy limestones. The beds of resedimented limestones have often irregular bedding surface due to submarine erosional processes.

The bioclastic limestones from the base of the sequence provided foraminifera which indicate a Late Permian age, without more specific age designation possible. Conodonts recovered from the base of the platy limestones (Krystyn, personal communication to A. Baud) indicate a Dienerian age. Possibly, unit 4 may extend into the Smithian, although there is no definite paleontological data available.

#### Carbon and oxygen isotope data

The  $\delta^{13}\text{C}$  values vary between +1.6‰ and +4‰ and show little variability upsection.  $\delta^{18}\text{O}$  values vary between -4.4‰ and -1.7‰ and do not covary with  $\delta^{13}\text{C}$  values (fig. 24f). Two  $\delta^{13}\text{C}$  values obtained on samples of the gray bioclastic limestones from the base of the section are very close to +4‰, values within the range of variation for the Upper Permian carbonates. All Lower

All Lower Triassic carbonate lithologies gave  $\delta^{13}\text{C}$  values around 3‰, without any marked stratigraphic trend and with low variability for neighbouring samples. Only two samples from the top of the measured section (WM196 and WM198) gave  $\delta^{13}\text{C}$  values around 1.8‰, about 1‰ lower than the average of the samples with a lower position in the section.

We made some tests on samples coming from a small block in the neighbourhood of the section. This block is made up exclusively of Hallstatt-type limestones (it corresponds to Section 5 in Pillevuit (1993), see page 97 therein). The age of the Hallstatt-type limestones occurring in this block is Upper Smithian (*Anasibirites* zone) (H. Bucher, personal communication).

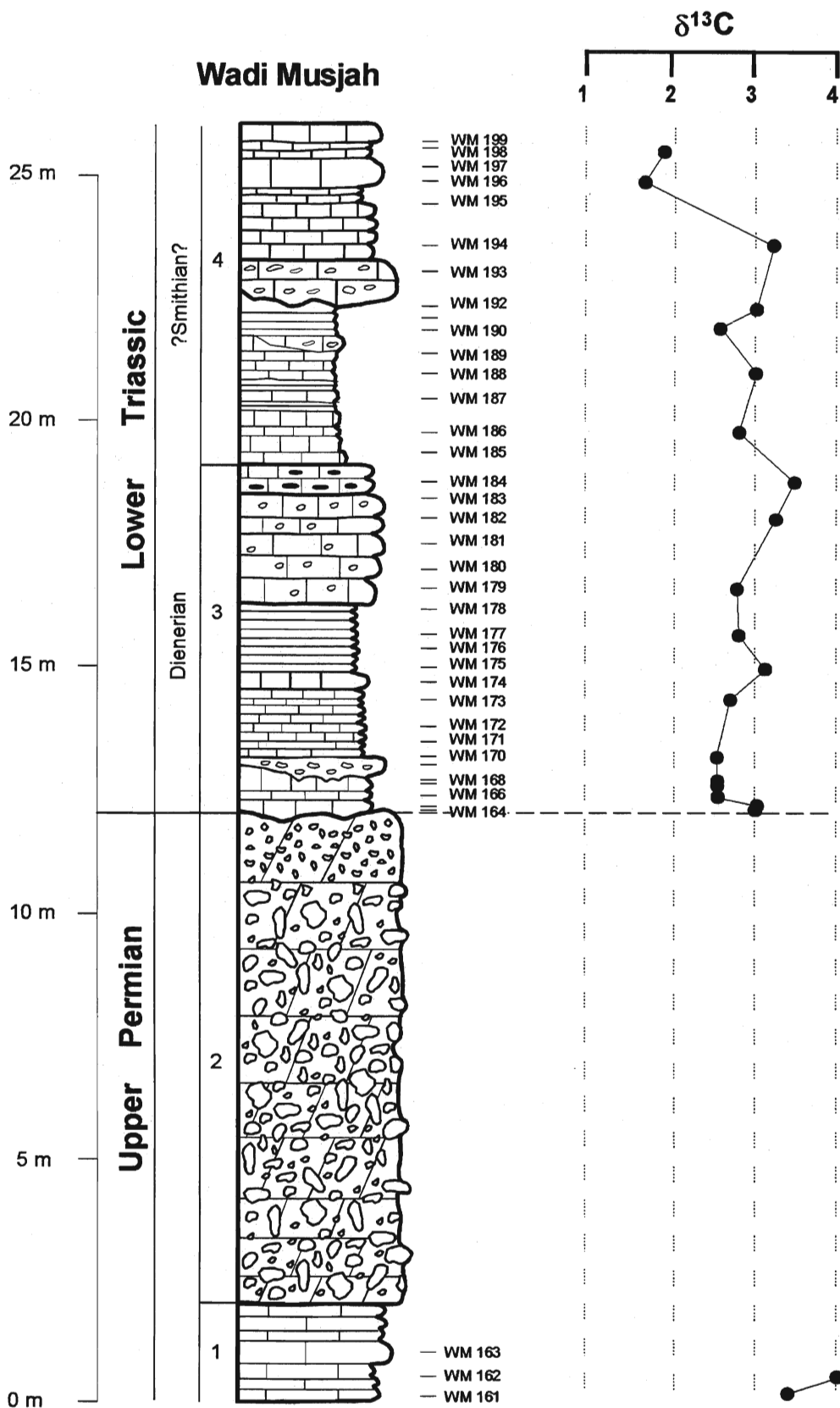


Fig. 29. Carbon isotope profile of Wadi Musjah section.



The  $\delta^{13}\text{C}$  values vary within a relatively wide range, comprised between +0.8‰ and +2.7‰, while the  $\delta^{18}\text{O}$  values are relatively low, varying between -4.2‰ and -1.8‰. Similar high variability of  $\delta^{13}\text{C}$  values in Hallstatt-type limestones have been observed at the Wadi Alwa section. It should be noted, however, that within the *Anasibirites* zone large variations in  $\delta^{13}\text{C}$  values were found in Salt Range and possibly, they are related to changes in seawater chemistry. For the Upper Smithian Hallstatt-type limestones from Wadi Musjah, the number of samples available was too small to define a carbon isotope stratigraphy.

## 5.5. Conclusions

The  $\delta^{13}\text{C}$  values of whole rock carbonates from the Oman vary over a wide range comprised between -2‰ to +6.6‰. The  $\delta^{18}\text{O}$  values also show large variations, between 0‰ and -10‰.

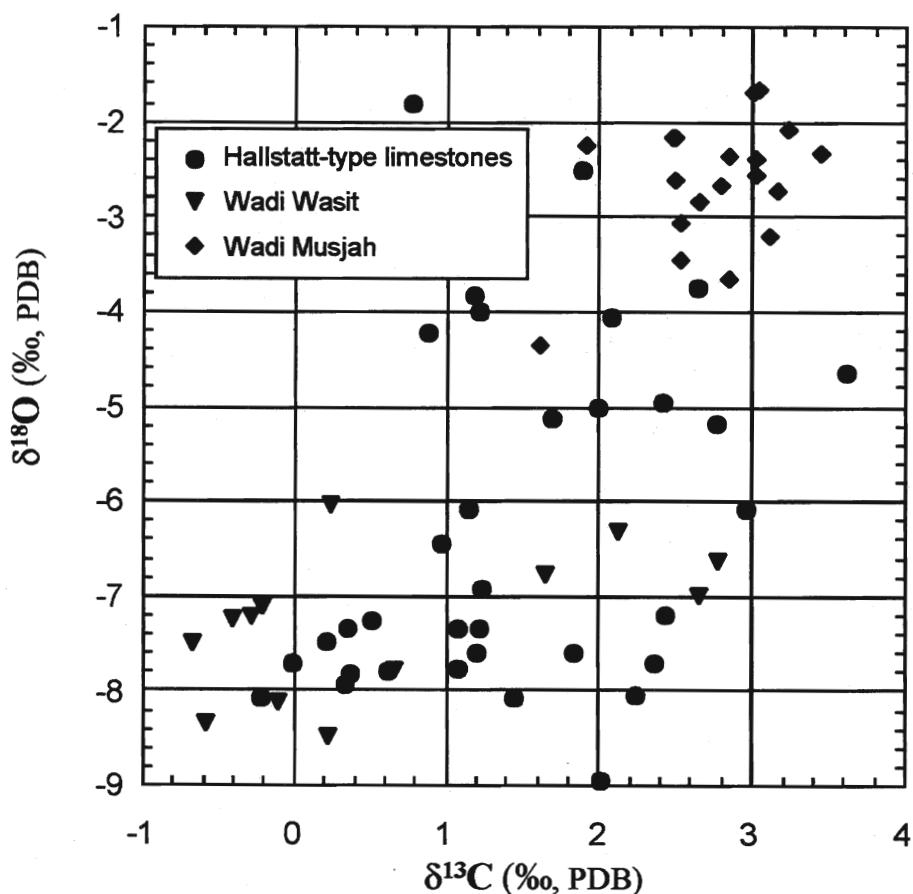


**Fig. 30** The  $\delta^{18}\text{O}$  -  $\delta^{13}\text{C}$  cross-plot for the Lower Triassic carbonates of the Oman exotics

The  $\delta^{13}\text{C}$  values from Permian carbonates, although in a limited number, are high, generally higher than +3‰, confirming thus the observation made by previous studies (e.g. Holser and Magaritz, 1987). The only exception found in Oman comes from the Wadi Sahtan section, where  $\delta^{13}\text{C}$  values from the upper part of Saiq Formation, considered as Upper Permian in age, are roughly close to +1‰. Considering that the overwhelming majority of  $\delta^{13}\text{C}$  values obtained from Upper Permian carbonates world-wide are higher than +3‰, and that carbonates from the lower part of the Saiq Formation gave typical high  $\delta^{13}\text{C}$  values, this might indicate that the upper part of the Saiq Formation may belong to the Lower Triassic.

A prospective carbon isotope profile from the Maqam Formation show variations similar to those reported across the Permian-Triassic boundary world-wide and suggest that the boundary between Permian and Triassic strata should be traced between Units B and C.

The most significant data-set comes from the sections in the Oman exotics and particularly from the Lower Triassic limestones. The interest for the Lower Triassic carbon isotope record is due to the fact that the carbon isotope stratigraphies acquired from the Northern Indian margin showed unusual large variations and negative background values, which contrast with the better established carbon isotope curve for the remainder of the Mesozoic and for the Tertiary.

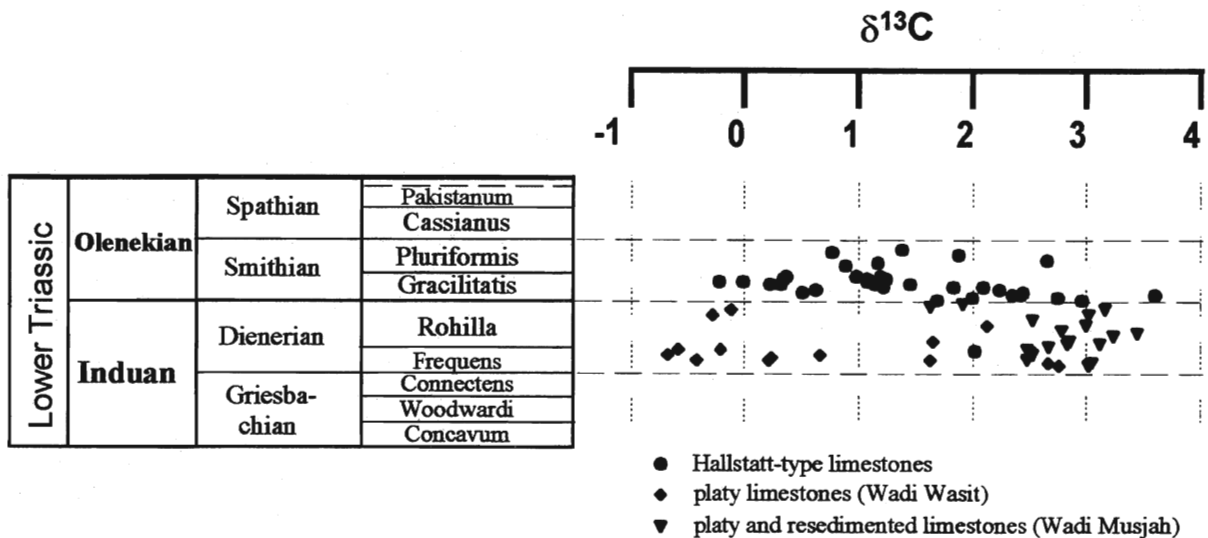


**Fig. 31** Stratigraphic plot of  $\delta^{13}\text{C}$  values for the Lower Triassic carbonates of the Oman exotics

$\delta^{13}\text{C}$  values from the Lower Triassic carbonates from the Oman exotics vary between  $-0.7\text{‰}$  and  $+3.6\text{‰}$ , while  $\delta^{18}\text{O}$  values vary between  $-9\text{‰}$  and  $-1.7\text{‰}$  (fig. 30). There are two significant features provided by the Lower Triassic carbon isotope data-set:

- many  $\delta^{13}\text{C}$  values are relatively high, higher than  $+2\text{‰}$ , which is unexpected for Lower Triassic carbonates; most of the previously published  $\delta^{13}\text{C}$  values from the Lower Triassic are lower than  $+2\text{‰}$  (see review in Grossman, 1994 and Scholle, 1995). It was generally assumed that such high  $\delta^{13}\text{C}$  values were restricted to the Upper Permian, thus reinforcing the contrast between Upper Permian versus Lower Triassic marine signatures.
- the  $\delta^{13}\text{C}$  values show large variability, both for any single section and for various sections compared. The Oman exotics record (fig. 31), for instance, comprise carbonates representing a relatively short period of time (from the Early Dienerian to the Late Smithian) and fairly similar pelagic depositional environments. The  $\delta^{13}\text{C}$  values vary over a range of  $4.5\text{‰}$ , without a clear stratigraphic trend. The Permian and Triassic strata of Oman underwent severe post-depositional diagenetic histories, being tectonically transported in front or beneath the thick Semail Ophiolite Nappe system and it is likely that they were the subject of enhanced fluid circulation or burial. This is also indicated by the covariant trend between the  $\delta^{13}\text{C}$  and  $\delta^{18}\text{O}$  values (fig. 30). However, diagenesis would have lowered the  $\delta^{13}\text{C}$  values, and not only increase their variability. We believe that the high variability of

$\delta^{13}\text{C}$  values is a characteristic of the Lower Triassic carbonate sediments. This may be related to global short term variations in seawater chemistry or local variations of  $\delta^{13}\text{C}$  values of the seawater related to particular paleoceanographic settings. The former alternative is not substantiated by systematic stratigraphic variations, but this may be due to our incapacity to detect them because of the lack of biostratigraphic constraints and the poor chronostratigraphic coverage for single sections.



## CHAPTER 6

# CONSTRAINTS FROM THE TRIASSIC OF NORTH DOBROGEA

The present chapter describes stable isotope data acquired between 1994 and 1998. Basic information related to stratigraphy is based on unpublished data provided by E. Gradinaru (University of Bucharest) and from previous studies carried by the author together with E. Gradinaru. Most of the sections described herein were re-examined and sampled together with A. Baud, S. Bourquin, S. Crasquin-Soleau, B. Galbrun, E. Gradinaru and M. Renard under the frame of the Peri-Tethys Program.

## 6.1 Geological settings and stratigraphy

### 6.1.1. Geological settings

The province of Dobrogea, an elevated area within the Carpathian Foreland, is located in the south-eastern part of Romania, between the lower stream of the Danube River and the Black Sea. In the northern part of Dobrogea a geological distinct unit occur, the North Dobrogean Orogene (NDO), the only geological unit within the Carpathian Foreland to display pronounced Alpine tectonic deformations.

The North Dobrogean Orogene represents the westernmost segment of the Cimmerian fold and thrust belt and in the present day configuration it is bordered northward by the Scythian Platform and southward by the Moesian Platform (Sandulescu, 1984), along the Galati-Sfântul Gheorghe fault and the Peceneaga-Camena fault, respectively (fig.32). It was interpreted either as an intracratonic Early Alpine Orogene (Dumitrescu and Sandulescu, 1968; Sandulescu, 1984), as a Tethyan terrain removed from the main Tethyan areas by post Triassic large scale horizontal displacements (Gradinaru, 1984; Marcoux et al., 1993; Stampfli, 1997).

According to current interpretations, the North Dobrogean Orogene is made up of a pile of north easterly verging thrust-sheets or nappes. From south-west to north-east, one can distinguish Macin, Consul, Niculitel and Tulcea Units (Fig. 32). While the Macin, Consul and Tulcea Units are continental basement-sheared nappes, the Niculitel Unit (a wholly unrooted nappe) represents a Cimmerian suture zone, comprising essentially Late Scythian to Middle Anisian mafic lava flows intercalated with pelagic limestones.

Paleontologic and stratigraphic investigations in the Triassic of North Dobrogea started more than a century ago. Among the early publications one may mention Peters (1867), Anastasiu (1896,1898), Redlich (1896), Kittl (1908), Simionescu (1910, 1911, 1913, 1925) and later Atanasiu (1940) and Mutihac (1964). During the last decades, the Triassic of the NDO was extensively studied by geologists from the Geological Institute of Bucharest (Oreste and Elena Mirauta, Albert Baltres, Doina Gheorghian, among others) and the University of Bucharest (Eugen Gradinaru). Relatively few of their results have been published as journal

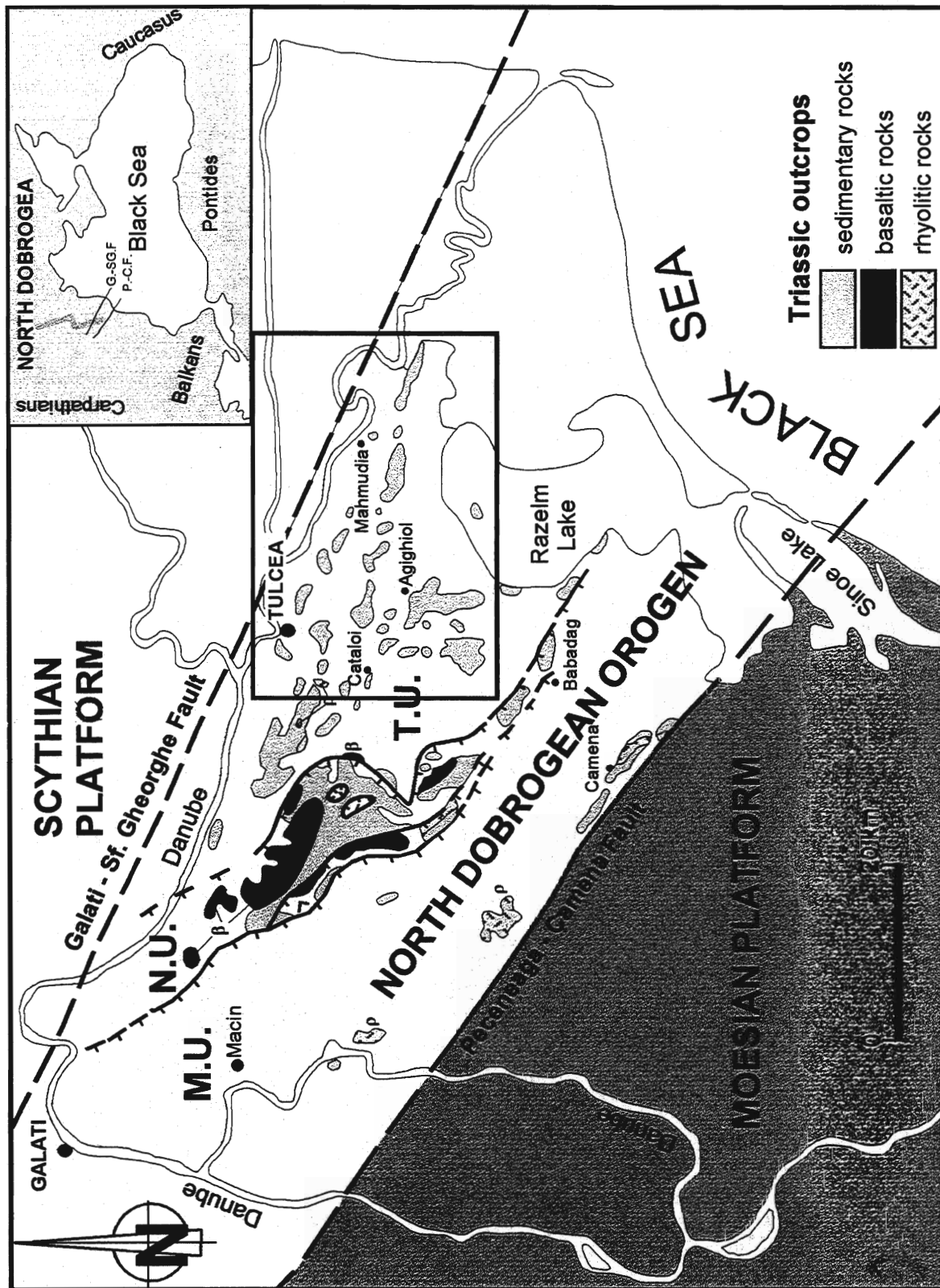


**Fig. 32** Sketch map of the North Dobrogean Orogen showing the location of the study area (rectangle) and the distribution of Triassic deposits. M.U.: Macin Unit; N.U.: Niculitel Unit; T.U.: Tulcea Unit After Gradinaru in Crasquin-Soleau and Gradinaru (1996)

articles, most of the data are presented as internal reports or as field excursion guidebooks with restricted circulation. However, their studies acquired a huge amount of information relative to the Triassic geology of North Dobrogea, established a detailed bio and litho stratigraphical framework and outlined complex stratigraphic relationships between the various lithologic units.

All the above mentioned studies recognized the Tethyan (Alpine) character of the North Dobrogean Triassic. This is a somewhat unexpected feature of the North Dobrogean Orogene given its remote position with respect to the major Tethyan Triassic regions. As a matter of fact, the confining structural units (i.e. Moesian and Scythian platform) exhibit a "Germanic" type Triassic.

Triassic sedimentary rocks occur in all major tectonic units of the NDO (Macin, Niculitel and Tulcea units) showing a high diversity of depositional environments from siliciclastic to dominantly carbonatic. However, the largest development is recorded in the outermost one, that is the Tulcea Unit. During Early and Middle Triassic times the area has been involved in rifting processes, as suggested by the development of basaltic rocks interbedded with marine pelagic sediments (Mirauta, 1982). The Tulcea Unit preserves the sedimentary record of one of the flanks of the newly formed rift basin.

### 6.1.2. The Triassic of the Tulcea Unit

The Triassic sedimentary cover of the Tulcea Unit is overlying unconformably a Hercynian basement. The oldest Triassic deposits are terrigenous and are attributed to the Lower Olenekian on the basis of a bivalve association with *Eumorphotis* (Gradinaru, written communication). The basinal and carbonate platform sedimentation started in the Early Spathian and continued, more or less without interruption, until the end of the Triassic. The sedimentation pattern was closely controlled by rifting related extensional tectonics which resulted in a pronounced submarine topography and in varying subsidence rates across the margin (Gradinaru, 1993). Consequently, the lateral contact of coeval lithological units is usually sharp and the thickness of time equivalent deposits is highly variable. However, due to the detailed biostratigraphic and sedimentologic studies carried out essentially by Romanian geologists, the time-space distribution of the various lithological bodies can be accurately reconstructed.

Accordingly, on the basis of the areal distribution of various carbonate lithofacies it is possible to reconstruct the geometry of the Dobrogean Triassic margin. While uniform sequences of alternating micritic limestones and marls, reflecting basinal sedimentation, are developed in the western part of the Tulcea unit (Cataloi zone), the eastern part record bioclastic limestones deposited in shallow water environments (Murighiol zone). In the central part (Agighiol-Zebil), various types of deeper water carbonate deposits formed (Gradinaru, 1993). Considering the distribution of depositional environments along a shallow water to basin transect, one can recognize that the carbonate sedimentation settings evolved from a homoclinal ramp in the Anisian to a rimmed platform in the Carnian (according to the classification of Tucker, 1993). The geometry of the Spathian carbonate platform is difficult to assess, as there are limited informations relative to the shallow water environments but, judging from the large development of slope carbonate deposits (Baltres, 1993) it could be a distally steepened carbonate ramp.

A particularity of the NDO Triassic is the large development of Spathian and Anisian succession, in various depositional settings and in a very well established biostratigraphical framework (Gradinaru, 1993). There are especially the ammonoid faunas which are characterized by rich and taxonomically diversified assemblages. Consequently, a large number of biozones that were documented either in the Tethyan area or in North America have been recognized here (Gradinaru, unpublished).

### 6.1.3. Lithostratigraphy

The nomenclature and the stratigraphical relationships between the main lithological units of the Tulcea Unit is summarized in fig. 33. The ages and nomenclatures shown in this chart are mainly based on informations provided by Eugen Gradinaru (both oral and written communications). The nomenclature used in this study differs in some respects by that proposed by Baltres and Mirauta (1996). The lateral relationships between the lithological units are much more complicated that it can be deduced from the chart, some of the units having recurrent or diachronous occurrences in the different facies zones. Following are brief descriptions of the lithostratigraphical units that have been considered in this study.

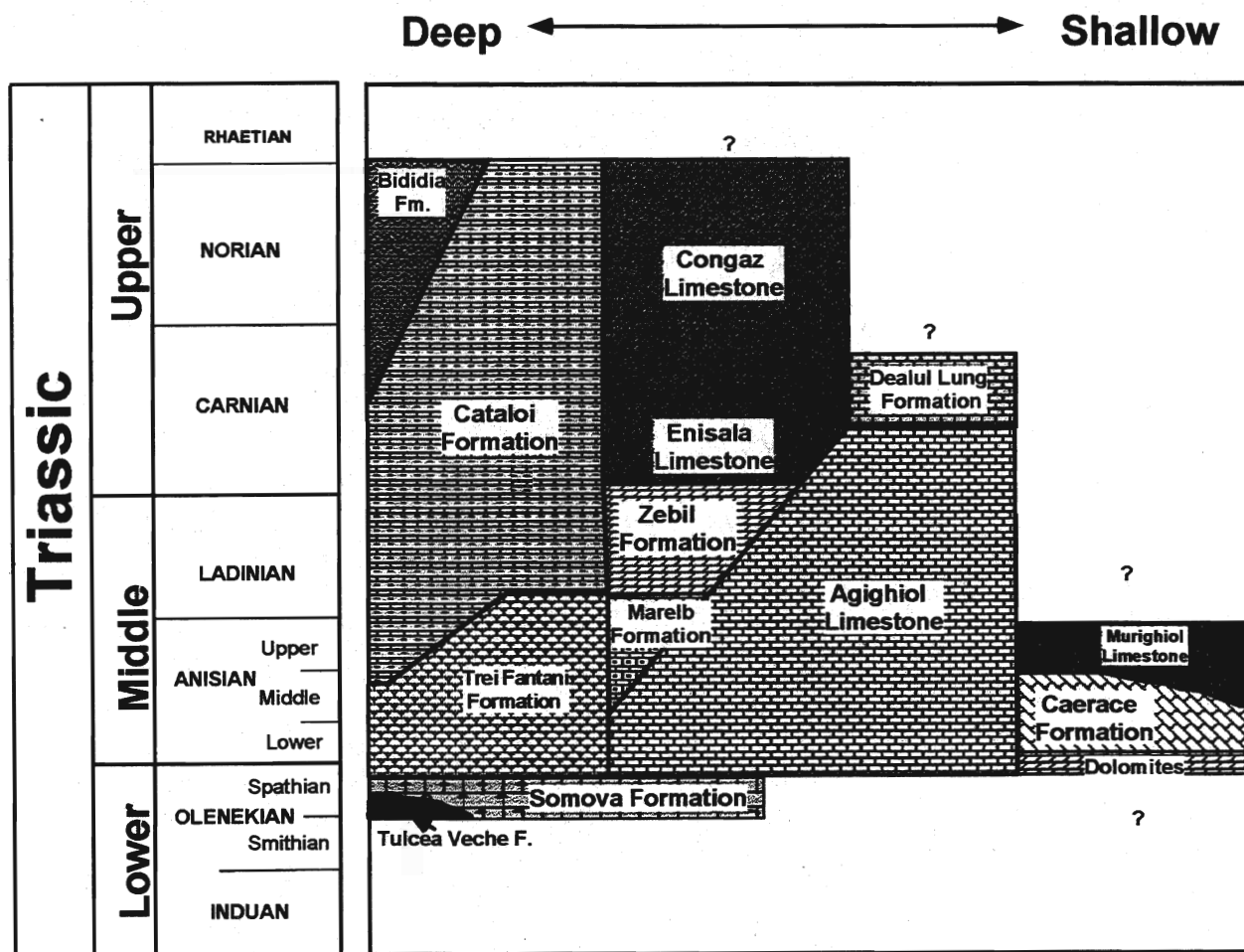


Fig.33 Tentative lithostratigraphical chart showing the time-space relationships between the lithological units used in the present study (based on data from Gradinaru, unpublished)

#### **Tulcea Veche Formation** -Lower Spathian, (Gradinaru, unpublished)

The Tulcea Veche Formation occurs only in an abandoned quarry located about 1 kilometer north-west of main Tulcea railway station. It consists of closely alternating, thinly bedded, dark-coloured, fine-grained turbiditic limestones and shales. These deposits were included by Baltres (1993) to the Somova Formation, as a distinct member. Following Gradinaru (1993) a formational status is preferred herein because it represents a distinctive depositional environment (basinal settings). The age of the Tulcea Veche Formation is Early Spathian (Gradinaru, 1993), on the basis of ammonoids (which include representatives of *Tirolites cassianus*).



**Somova Formation** -Upper Olenekian (Baltres, 1993)

The Somova Formation is recognizable throughout most of the Tulcea Unit (Baltres, 1993), with the best outcrops occurring in the northern part of the Tulcea unit in the Somova - Minerii area. It is made up of thick sequence (up to 1000m) of resedimented (allodapic) limestones, the facies may range from calcilutites to calcrudites, with typical turbiditic sequences. The depositional environment of the Somova Formation is interpreted to be at the base of a carbonate ramp slope, with extremely high sedimentation rates. The Somova Formation is dated as Upper Olenekian (Spathian) on the basis of conodonts and foraminifera (Mirauta, 1982; Baltres, 1993).

**Trei Fântâni Formation** -?Early Anisian - Middle Anisian (Gradinaru and Baltres, unpublished)

The Trei Fântâni Formation is well exposed in the Trei Fântâni quarry, 3 km south of Tulcea. It overlies massive dolomites and it is overlain by the Cataloi Formation. The Trei Fântâni Formation is divided in two members. The lower member, 100 m thick is made up of nodular, red and greenish-gray, massive bedded limestones. The upper member, 30 m thick, consists of dark grey evenly bedded cherty limestones with thin shaly interbeds. On the basis of ammonoids and conodonts, the age of the Trei Fântâni Formation is Middle Anisian. Its base may extend in the Early Anisian. The depositional environment is represented by a deep pelagic carbonate bank. More details can be found in localities description, Trei Fântâni-Bididia quarries section.

**Marelb Formation** Middle Anisian to Upper Anisian (Gradinaru, unpublished)

The Marelb Formation crops out in the Hills between the Zebil and Congaz (Rândunica) villages and it is well exposed in the Dealul Rosu Hill. In this area it overlies the Hallstatt-type limestones of the Agighiol Formation and is overlain by the Zebil Quarry Formation. The Marelb Formation is divided in two members. The lower member is made up of a sequence of thinly bedded reddish, nodular, cherty limestones alternating with reddish marly shales and occasionally with rhyolitic tuffitic rocks. The age of the lower member is Middle Anisian (Gradinaru, 1993), on the basis of ammonoid assemblage recovered from the upper part, correlative with the *constrictus* subzone (Bucher, 1992) of the low latitude North American Triassic. The underlying Hallstatt-type limestones contain Early Anisian ammonoids. The upper member of the Marelb Formation consists of a sequence of gray nodular cherty limestones with black silica nodules followed by black bituminous limestones to the top. Ammonoids collected from a ravine north of Dealul Rosu Hill indicate an early Late Anisian age (*Paraceratites* zone) (Gradinaru, 1993). The upper part of the Marelb Formation is exposed in the Zebil quarry and contain late Anisian conodonts (see localities description, Zebil Quarry section). The thickness of the Marelb Formation is difficult to estimate due to the poor exposure of strata.

**Agighiol Limestone** -Spathian - Lower Carnian (Gradinaru, unpublished)

The Agighiol Limestone occur in many localities in the central part of the Tulcea Unit but the most complete sequence occur in the eastern flank of the Dealul Pietros Hill, just near the Agighiol village. Other localities where the Agighiol Limestone crops out are: Desli Caira, Uzum Bair, Orta Bair, Dealul Rosu, Dealul Mare, Dealul Lung, among many others. In this formation are included the red pelagic limestones commonly described as "Hallstatt-type" limestones. The Agighiol Limestone consists of sequence of thick bedded varicoloured pelagic limestones with subordinate marly partings. They are rich in fossils (mainly cephalopods), strongly bioturbated and locally may exhibit a nodular fabric. Hardground surfaces and Fe-Mn crusts typically occur, as well as neptunian dykes and burial diagenetic features like dissolution seams and stylolites.

Both lateral and vertical relationships with adjacent formations are extremely complex, due to the marked heterochronous character of the Agighiol Limestone. Its thickness is highly variable as well; however, from a composite section (see localities description) we measured over 100 m and this likely represents the higher range of thickness. The oldest age reported from limestones belonging to the Agighiol Limestone is Lower

Spathian on the basis of a conodont association with *Neospathodus triangularis* (see localities description, section Dealul Pietros I) and the youngest is Lower Carnian (Simionescu, 1913, Gradinaru, 1993).

The Hallstatt facies is generally interpreted as a pelagic deposit laid down far from any source of terrigenous sediment. Close juxtaposition of ammonoids zones indicates very low rates of sedimentation. The depth at which Hallstatt-type limestones rocks formed has long been debated, but most likely it lies between 100-300m (Tucker, 1993), on structural submarine highs or on deeper parts of the carbonate ramp.

**Caerace Limestone** -Lower Anisian - ?Upper Anisian (Gradinaru, unpublished)

The Caerace Formation occurs in the Caeracul Mare and the Caeracul Mic Hills, about 4 km south-west of Mahmudia village, with the best exposure in the big quarry located on the south-eastern flank of the Caeracul Mare Hill. As defined herein, the Caerace Formation is divided in two members, with the lower member made up of dark coloured micritic limestones, partially dolomitized and the upper member consisting of a thick sequence of massively bedded, varicoloured (from gray to reddish) micritic limestones with abundant stromatactis structures. The carbonates included in the Caerace Formation were deposited in a mud mound developed on the inner part of the Anisian carbonate ramp. For a more detailed lithological description of the Caerace Formation see the localities description (Mahmudia quarry section). Its age is Middle Anisian, on the basis of ammonoids (Gradinaru, unpublished); however the lower member may extend downward in the Lower Anisian, as it will be discussed below.

**Murighiol Formation** -Middle - Upper Anisian (Gradinaru, unpublished)

The Murighiol Formation crops out exclusively in the eastern part of the Tulcea Unit, in the Hills surrounding the Murighiol village. The bulk of this formation is composed of thick bedded, sometimes massive, white and medium gray bioclastic limestones and locally dolomites. A characteristic feature of the Murighiol Formation is the presence of oncolitic and algal levels, which point to a high energy shallow water carbonate environment. The stratigraphic relationships with adjacent lithological units are not known because of the poor exposure of rocks in the area. North-west of the Dunavatul de Sus village, the limestones belonging to the Murighiol Formation overlain massive dolomites and dolomitic limestones. The thickness of the formation cannot be precisely measured from outcrops, but it likely exceed 100 meters. The Middle-Late Anisian age of the Murighiol Formation was established by Dragastan and Gradinaru (1975) on the basis of calcareous algae (*Oligoporella* - *Physoporella* genera grouping) and confirmed by brachiopod data (Mirauta, personal communication).

**Cataloi Formation** -Upper Anisian - Upper Norian (Gradinaru, 1984)

This formation is best exposed in the Trei Fântâni and in the Bididia quarries but it also occur in the Cataloi area. It consists of evenly bedded, black limestones alternating with marly shales, dark-gray marls with yellowish weathering. For a more detailed lithological description see localities part, Trei Fântâni - Bididia quarries and Cataloi sections. The Late Anisian age of the basal part of the Cataloi Formation is indicated by the presence of *Paraceratites* at the Trei Fântâni Quarry (Gradinaru, written communication) and by conodonts and foraminifera at Cataloi type section (Mirauta et al., 1993). In the Cataloi type section the upper part extends into the Upper Norian, and is covered by the Frecatei Sandstone (Gradinaru, 1984), while in the Bididia quarry its top is not younger than the Early Carnian (on the basis of conodonts) and is covered by the Bididia Formation.

The stratal patterns and microfacies types suggest a deep water, basinal deposition of the Cataloi Formation. The organic carbon concentration and the occurrence of abundant pyrite are consistent with a deposition in anoxic-dysaerobic bottom waters. Episodes of relatively more aerated bottom waters are indicated by bioturbation occurring at some levels.

**Zebil Quarry Formation** –Ladinian (Gradinaru, unpublished)

The Zebil Quarry Formation occurs in Zebil quarry, located about 1km north-east of the Zebil railway station, close to the Dealul Rosu Hill. It includes a 20 m thick sequence of nodular limestones alternating with red shales and probably represent a deeper equivalent of the Agighiol Limestone (part of it). It overlies conformably the Marelb Formation, as it can be seen in the floor of the quarry. Its contact with the overlying Enisala Formation is gradational. The age of the Zebil Quarry Formation is Ladinian, on the basis of ammonoids and conodonts. For more details see localities description (Zebil quarries section).

**Enisala Limestone** -?Upper Ladinian - Lower Carnian (Gradinaru, unpublished)

The Enisala Limestone crops out in some hills in the neighbourhood of the Enisala village, in the two quarries near the Zebil railway station and in the Popina Island. It is represented by massive, light-gray bioclastic limestones, referred to as « Wetterstein-type » limestones. A detailed lithological description can be found in Baltres et al., (1982). Macrofossils are rare within the Enisala Limestone; an ?Upper Ladinian - Lower Carnian age has been attributed on the basis conodont faunas that have been recovered from several levels. In the Zebil railway station - Congaz are the Enisala Limestone overlies progradingly the Zebil Formation and is overlain by the Upper Carnian to Upper Norian Congaz Formation.

**Bididia Formation** Upper Carnian – Norian (Gradinaru, unpublished)

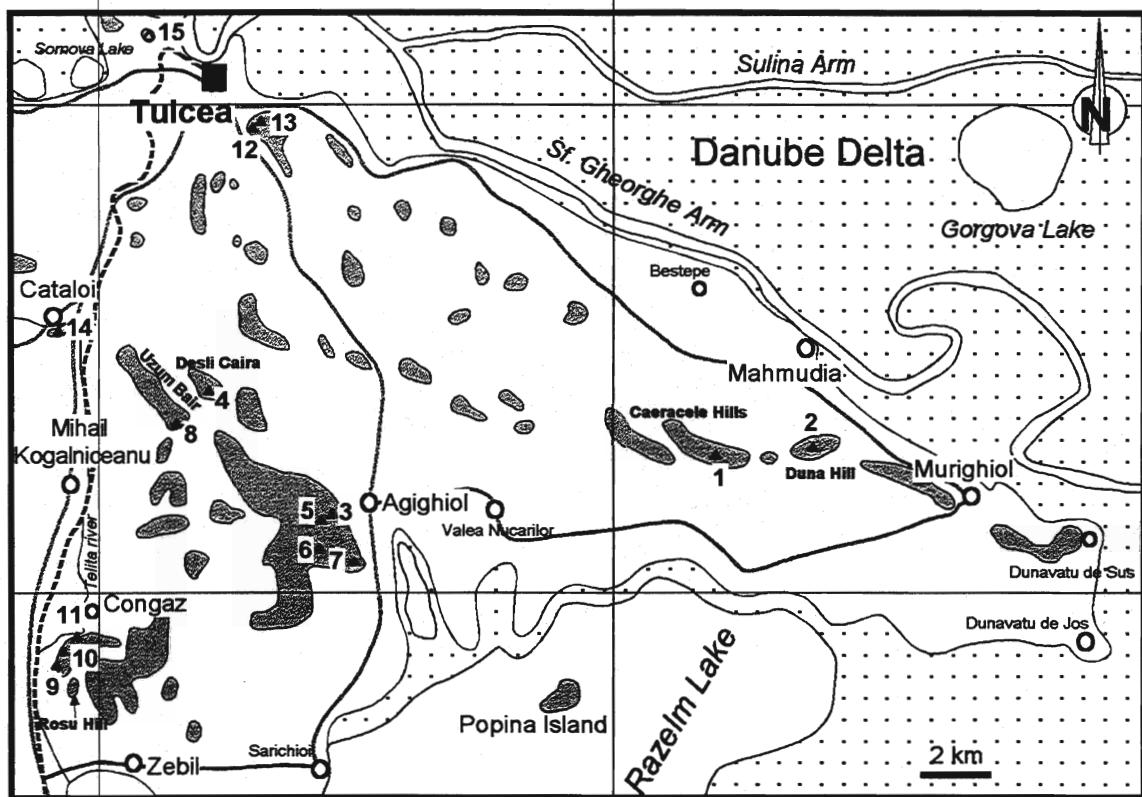
The Bididia Formation occur in the Bididia quarry, 4 km south of Tulcea, close to the Trei Fântâni quarry. It consists of a mixed siliciclastic-carbonate sequence, with calcareous debris flows at the base which grade upwards to terrigenous turbidites alternating with black pelagic limestones. Its thickness can reach several meters. The base of the Bididia Formation is dated as Upper Carnian, on the basis of conodonts and it presumably extends into the Upper Norian.

**Congaz Formation** -Upper Carnian-Upper Norian, (Gradinaru, unpublished)

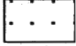
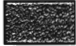




The Congaz Formation is exposed about two kilometers south of the Congaz (Rândunica) village in the small Hills from the left side of the Telita river. It consists of well bedded, dark gray to reddish fine-grained bioclastic limestones interbedded with cherty limestones and shales. The Congaz Formation overlies the Enisala Limestone and its onset indicate the drowning of the "Wetterstein" platform. Conodont and foraminifera faunas (Mirauta and Gheorghian, 1975), as well as ammonoids and halobiid bivalves (Gradinaru, unpublished) support a Late Carnian to Late Norian age of the Congaz Formation.

**Dealul Lung Formation** -Upper Carnian (Gradinaru, unpublished)

The Dealul Lung Formation crops out in the Dealul Lung Hill, near Agighiol village, where it overlies the Agighiol Limestone. It is made up of well bedded, black, finely grained bituminous limestones with whitish weathering and thin intercalations of silty shales. Large euhedral pyrite (up to cm size) crystals occur disseminated in the rock. The sediments belonging to the Dealul Formation are believed to record a sedimentary area developed in the Late Carnian, with restricted circulation and anoxic to dysaerobic bottom waters. Ammonoids fauna recovered from the lower part of the Dealul Lung Formation, including representatives of *Tropites*, point to a Late Carnian age (*dilleri* zone) of the Dealul Lung Formation (Gradinaru, 1993).



### Legend

- |   |  |
|---|--|
|  | area flooded by the Danube Delta complex   |
|  | main outcrops of Triassic deposits (undifferentiated), roughly delineating the topography of the land area |
|  | main roads   |
|  | railways   |
|  | main villages  |
|  | examined localities, as following  |
| 1   | Mahmudia quarry  |
| 2   | Duna Hill  |
| 3   | Dealul Pietros   |
| 4   | Desli Caira  |
| 5-6   | Dealul cu Cununa - Dealul Mare   |
| 7   | Dealul Lung  |
| 8   | Uzum Bair  |
| 9   | Zebil quarry   |
| 10  | Olga quarry  |
| 11  | Congaz   |
| 12  | Trei Fantani quarry  |
| 13  | Bididia quarry   |
| 14  | Cataloi  |
| 15  | Tulcea Veche   |

**Fig. 34** Sketch map of the North-East Dobrogea showing the location of the localities described in the present study

## 6.2. Stratigraphy, carbon and oxygen isotope data

For the present study Triassic carbonate sequences were examined in a number of 14 sites (fig. 34). The selection of these sites was made in order to obtain a good stratigraphical coverage with a good age control, trying to sample a variety of depositional environments over a shallow water to basin transect. In the following section the examined sections are presented according to their position along the transect.

### 6.2.1. Shallow water settings

Anisian shallow water deposits crop out exclusively in the eastern part of the Tulcea Unit, in the Mahmudia -Murighiol area. In the following, two sections from this area are described. Shallow-water carbonates are also known from Carnian, belonging to the Enisala Formation; a sequence comprising these rocks will be described in the "deep water" part, as they have been studied in a sequence that include also deep-water deposits.

#### Mahmudia Quarry

In the big quarry located about 4 km west of Mahmudia village, on the south-eastern flank of the Caeracul Mare Hill, a thick sequence of ?Early -Middle Anisian shallow water limestones (belonging to the Caerace Formation) occur. A 136 m profile, in the front of the lower level of the quarry, (October 1995) has been measured and sampled. Two main lithological units have been recognized from the base to the top, which have been further subdivided in several subunits (fig 35).

The lower one, 40 m thick, named "mottled limestone", is made up of two thickening upward sequences (A1 and A2) of dark coloured bedded limestones which pass laterally (gradually) to white or yellowish dolomites (pure dolomites occur in the upper front of the quarry and in the northern flank of the Caeracul Mare Hill). The limestones are strongly burrowed; the burrowed zones, often anastomosed, are preferentially dolomitized and enriched in Fe oxides, resulting in orange to purple red coloration. Several hardground surfaces were identified, mainly in the A2 sequence. Stromactis-type structures also occur, but they are not as frequent as in the overlying unit. Microfacially they consist of mudstones to wackestones, with bioclasts of ostracods, foraminiferas, rare thin shelled bivalves and crinoid elements.

The rock-sequence grades upward to thick bedded or massive varicoloured limestones, from gray to reddish, with typical stromatactis cavities, therefore named "Stromatactis limestone". The lower part of the "Stromatactis limestone" (B1) is well bedded, strongly affected by dolomitization and contain planar stromatactis cavities. In thin sections, when the primary fabric escaped from dolomitization, it is possible to distinguish the mud-supported fabric (dominantly mudstone), with ostracodes, bivalve debris, foraminiferas and crinoid elements.

The bulk of the "Stromatactis limestone" is made up of thick bedded burrowed micritic limestones (B2 and B3). The limestones are characterized by an extremely high carbonate content (deduced from the small amount of acetic acid insoluble residues) and by the presence (rock-forming) of stromatactis cavities. Microfacially, they are mainly mudstones and wackestones, rarely packstones, display a fenestral fabric and contain ostracodes, thin and thick shelled bivalves, foraminiferas, crinoid elements, siliceous spicules and rare peloids. Microfossils recovered from limestones of the Caerace Formation (acetic acid insoluble residues) include abundant conodonts, fish teeth and scales, few foraminifera and holothurian sclerites.

The size of the stromatactis voids may vary from microscopic to decimetric. They usually have a flat base and a digitate roof (they are typical), most of them are isolated, although at several levels they might be interconnected, displaying a "zebra-rock" texture.

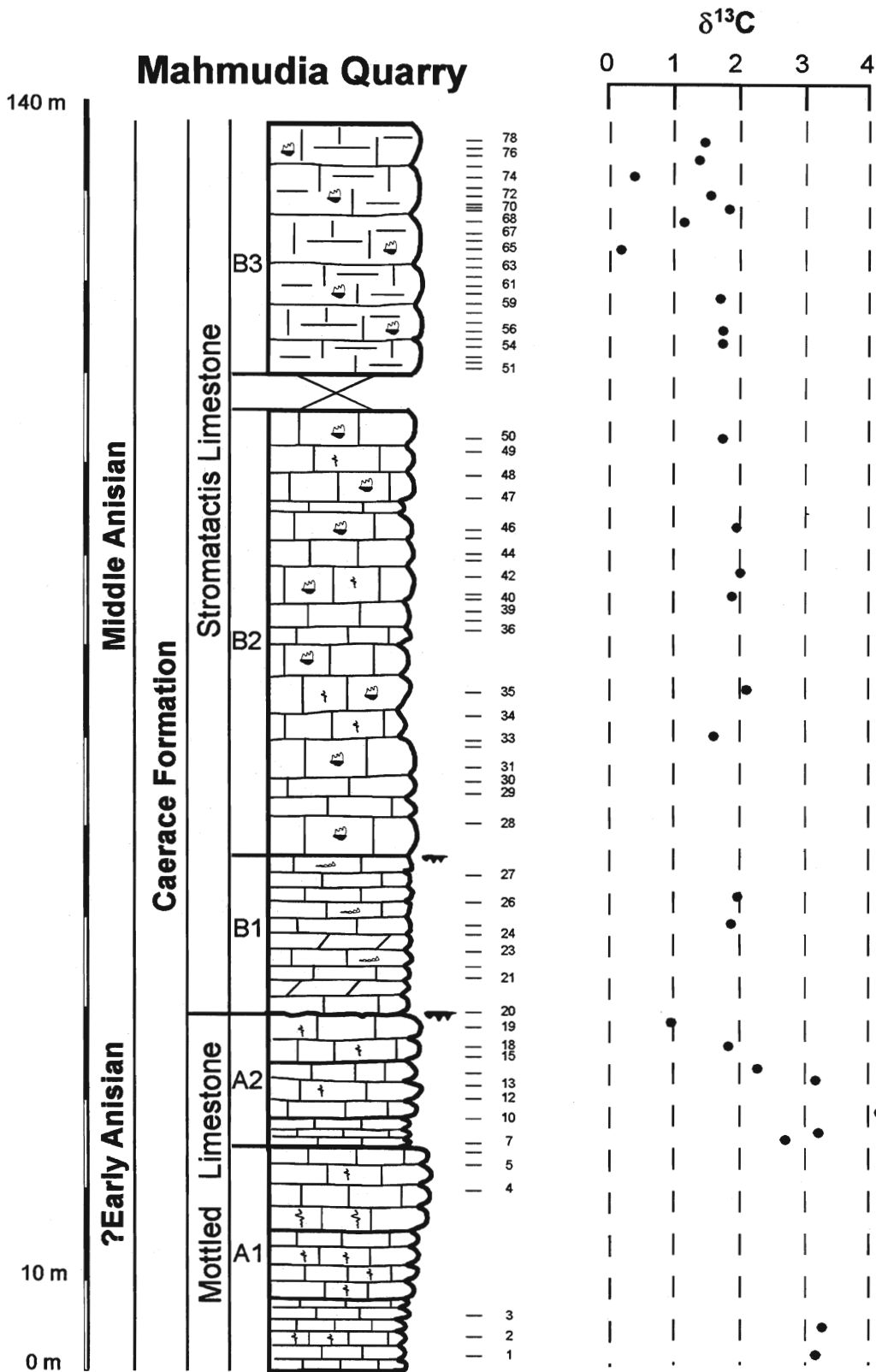


Fig. 35. Carbon isotope profile of Mahmudia quarry section

The calcite filling the stromatactis voids consists generally of two or three types of cement grown concentrically. On the borders of the void, there is usually a thin layer of gray equant spar, while in the inner part, forming the bulk of the void filling there is coarsely grained white blocky calcite. Typically, internal sediment rests on floor of the cavity, thus forming geopetal structures (Plate 5, Fig. 1). Internal sediment was observed also as "clasts" within masses of spar filling the void. Besides the stromatactis cavities, there is important volume of ellipsoidal or irregular shaped voids and fissures filled apparently with the same type of cements as the stromatactis cavities. The presence of the stromatactis structures, together with hardground surfaces, indicates an early lithification of the carbonate sediment (Bathurst, 1980; 1982; Tsien, 1985).

The sedimentological observations outlined above suggest that the carbonates included in the Caerace Formation formed in a shallow water mud mound setting. The most characteristic feature is the abundance of stromatactis cavities in a thick sequence of muddy carbonate-rich sediment. By analogy with other mud mound carbonates (Reitner and Neuweiller, 1995; papers in Monty et al., 1995, and in Neuweiller et al., 1997), the carbonate mud that dominates the microfacies of the Caerace Limestone originated probably from autochthonous precipitation mediated by nonpreserved microbial communities. However, a mound shape could not be discerned in the field, although the strata from the quarry display an antiformal structure.

At the time this chapter is being written, limited diagnostic paleontologic data from the measured section is available (the paleontologic work on conodont fauna is in progress). A conodont fauna was collected from the sample R95-78 (located at the top of the section) and contain *Gondolella bulgarica* (Budurov & Stefanov), *Gondolella constricta* Mosher & Clark and *Gondolella bifurcata* (Budurov & Stefanov), an assemblage indicative for the Upper Middle Anisian (Pelsonian). Ammonoids recovered by E. Gradinaru (oral and written communication) from quarried blocks (which likely come from the upper part of the rock-sequence described herein) indicate a Middle Anisian age (an association correlative with the *Kocaelia* zone). Middle Anisian (and possibly Early Anisian) conodonts have been found from previously collected samples from the quarry (Mirauta, personal communication). From the same quarry, a package of coquinoid limestones, over 5m thick with gastropods, ammonoids, nautiloids and bivalves has also been found (Gradinaru, personal communication).

#### *Stable isotope data*

The carbon and oxygen isotopic composition were measured on some selected samples along the measured section. In addition, for one sample (R95-78) Sr isotopic composition was measured (both whole-rock and stromatactis filling cement).

The  $\delta^{13}\text{C}$  values fall in a range comprised between +0.4‰ to +4.2‰. The highest values are recorded in the dark burrowed limestones from the base of the section, with values ranging from +1‰ to 4.2‰, most of them higher than +2‰. Towards the top of the "Mottled Limestone", the  $\delta^{13}\text{C}$  values decrease gradually, reaching a minimum of +1‰ close to the hardground surface that separates the two members of the Caerace Formation. The "Stromatactis limestone" is characterized by fairly constant  $\delta^{13}\text{C}$  values, around +2‰, with some lower values towards the top of the section. Overall, the  $\delta^{13}\text{C}$  values show a distinct stratigraphic trend, with a gradual but rapid decrease in  $\delta^{13}\text{C}$  values in the vicinity of a lithological change, marked by a hardground surface. Marshall and Ashton (1980) measured  $\delta^{13}\text{C}$  values of carbonates across hardground surfaces and found a slight lowering of  $\delta^{13}\text{C}$  values towards the hardground, however this trend has not been recorded in all sections they analysed. Moreover, the lowering of  $\delta^{13}\text{C}$  values was recorded in a cm scale. Our data show a trend towards lower  $\delta^{13}\text{C}$  values on a meter scale. Data from other sections (all sections from Agighiol Limestone) haven't found variations of carbon isotopes underneath hardground surfaces. Therefore the decrease in  $\delta^{13}\text{C}$  values is not considered to be directly related to the occurrence of the hardground. Whole-rock  $\delta^{18}\text{O}$  values vary from -1.8‰ to -4.35‰, with most of the values between -2‰

and -3‰. The cross-plot of  $\delta^{18}\text{O}$  -  $\delta^{13}\text{C}$  (fig. 36a) values show a positive correlation between the two parameters, which would support a geochemical diagenetic overprint. The lowermost  $\delta^{13}\text{C}$  values are correlated with lowermost  $\delta^{18}\text{O}$  values. However, there are several lines of evidence, that suggest that the general  $\delta^{13}\text{C}$  stratigraphic pattern is not significantly affected:

- carbon isotope variations are higher than the oxygen isotope variations (dismissing the extreme values, the range of variation is about +2‰ for  $\delta^{13}\text{C}$  and +1.5‰ for  $\delta^{18}\text{O}$ )
- the lithological change, correlated with  $\delta^{13}\text{C}$  variations, is not significant in terms of carbonate contents. Moreover, the organic matter is more abundant in the limestone that gave higher  $\delta^{13}\text{C}$ , contrary to what it would be normally expected if a diagenetic overprint is present. Organic diagenesis can lead to higher  $\delta^{13}\text{C}$  values only in the bacterial fermentation zone (Irwin et al., 1977)
- the  $^{87}\text{Sr}/^{86}\text{Sr}$  ratios of both whole-rock and early diagenetic cements are within the range of contemporaneous seawater. Strontium isotopes are more sensitive to diagenesis than carbon isotopes (Banner, 1995)

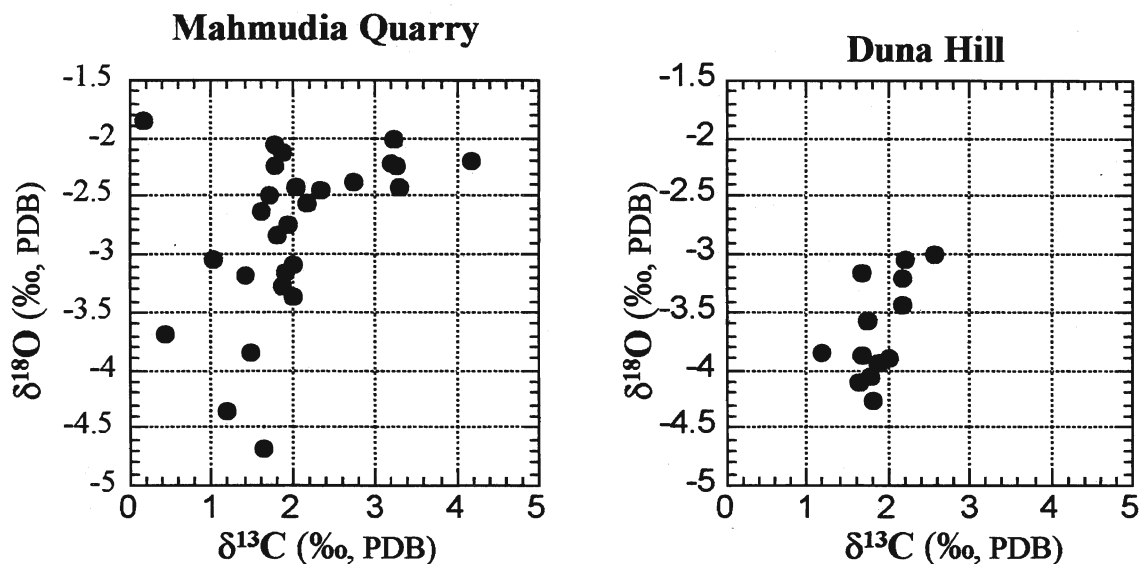


**Fig. 36.**  $\delta^{18}\text{O}$  -  $\delta^{13}\text{C}$  cross-plot for Mahmudia (a) and Duna Hill (b) sections.

An alternative interpretation for the observed stratigraphic trend is that it reflect variations in seawater isotopic composition, as it will be discussed later in the text.

Carbon and oxygen isotope data, as well as  $^{87}\text{Sr}/^{86}\text{Sr}$  ratios support an early lithification of the carbonates included in the Caerace Formation and an early origin of the void filling cements, although a more systematic study would be needed to reinforce this statement.



## Duna Hill

In the Hills from the neighbourhood of the Murighiol village the Middle-Upper Anisian Murighiol Formation is relatively well exposed. However, a representative section through the entire formation cannot be measured from outcrop exposures. The lithology and the stratal pattern is quite uniform, fossils are rare and correlations from one hill to another difficult. We have measured and sampled a 34m thick profile (fig. 37) in an abandoned quarry from the Duna Hill (28°48'08"E; 45°04'27"N), north of Saraturile Lake, 4 km west of Mahmudia village.

The examined sequence comprise thick bedded, monotonous light gray bioclastic limestones with interbedded coarse grained dolomites at the top of the profile. Oncolites can be observed both macro and microscopically. They are essentially grainstones, with bioclasts, oncolites and peloids (which can be micritized bioclasts), locally grapestones, bounded by spar cement or incorporated in a micritic matrix. Bioclasts are mainly calcareous algae, foraminiferas and ostracods. The microfacies is typical for a high-energy shallow water environment. The age of the of the limestones is Upper Middle Anisian - Upper Anisian, on the basis of calcareous algae (Dragastan and Gradinaru, 1975). The facies is very similar to the Steinalm limestone of the Northern Calcareous Alps.

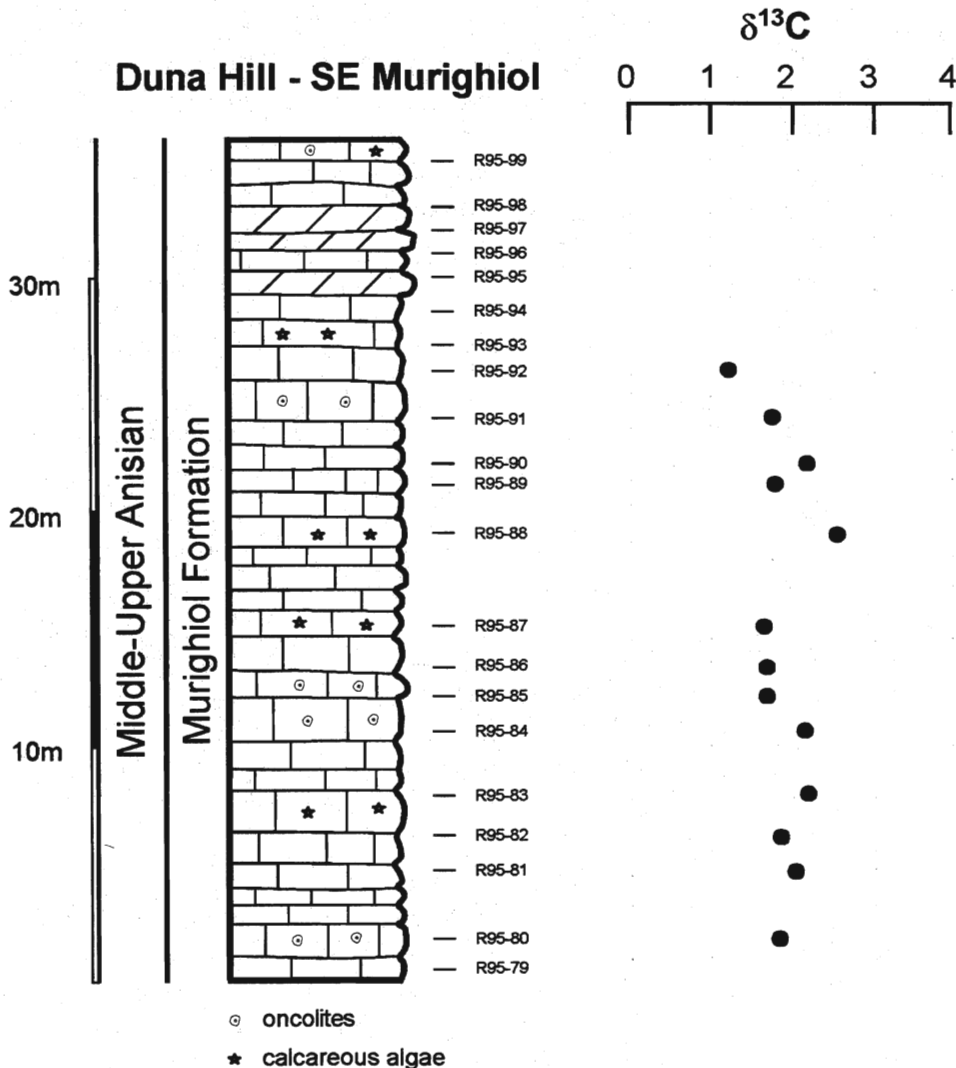


Fig. 37. Carbon isotope profile of Duna Hill section

### *Stable isotope data*

Both  $\delta^{13}\text{C}$  and  $\delta^{18}\text{O}$  values vary in a narrow range ( $\delta^{13}\text{C}$  values vary between +1.2‰ to +2.5‰ and  $\delta^{18}\text{O}$  values between -3 to -4.2) and do not show any significant trend along the section. Mean values are +1.8‰ for  $\delta^{13}\text{C}$  and -3.5‰ for  $\delta^{18}\text{O}$ .  $\delta^{18}\text{O} - \delta^{13}\text{C}$  cross-plot (fig. 36b) show a slight correlative trend, which is accentuated by two extreme points. Discarding these two values, no correlation between  $\delta^{13}\text{C}$  and  $\delta^{18}\text{O}$  values is visible.

## 6.2.2 Deeper water settings

In more distal parts of the carbonate ramp (in the Agighiol-Zebil zone) carbonate sediments were deposited in a complex framework of submarine highs characterized by continuous or intermittent pelagic sedimentation (the fine-grained, usually red, condensed pelagic limestones deposited on submarine highs are very common in the Tethyan Triassic and are termed "Hallstatt-type" limestone). These elevated areas were separated by intra-platform troughs where marly and cherty limestones were deposited concurrently.

In the Agighiol area (Plate 4, Fig.1) the Triassic rocks are present in two major tectonic compartments, which exhibit two distinct lithologic sequences (Gradinaru, 1993). The two compartments are separated by a NW-SE trending and NE verging reverse fault, visible at Dealul Pietros Hill. In the East Agighiol compartment, the sedimentary record is essentially of "submarine high" type, with Hallstatt type limestones, whereas in the West Agighiol compartment the "intra-platform trough" type sequence prevails.

The sections selected for the present study represented both red Hallstatt-type limestones and intra-platform trough-type carbonate sequences and they are well dated by ammonoids (Gradinaru, 1993 and written communication) and conodonts (paleontologic determinations by E. Mirauta).

### **The Hallstatt-type sequence (Agighiol Limestone)**

The Hallstatt-type sequence (represented in Dobrogea by the Agighiol Limestone) is studied through a composite section spanning the Late Olenekian to Late Carnian that includes three sections from the Dealul Pietros Hill, one from Desli Caira Hill and one from Dealul Lung Hill (see Fig. 34 for location).

The lithology and the stratal patterns are similar for the five individual sections, therefore a general characterization of the Agighiol Limestone will be made in the following (see also Baltres, 1976).

The Hallstatt-type limestones represent a facies which is very common in the Tethyan Triassic - and, according to Tozer (1984) restricted to the Tethys - and similar with the Devonian "Griotte" (Wendt and Aigner, 1985) and with the Jurassic "Ammonitico Rosso" (Jenkyns, 1971). Many of the Hallstatt limestones of other localities in the Tethys are known to be "exotic" blocks. Hallstatt-type limestones are rarely found in well ordered stratigraphic sequences (Tozer and Callon, 1990) and in this respect their occurrence in North Dobrogea is of great interest.

In the studied sections, they are thick bedded varicoloured, mainly reddish, pelagic limestones subordinately interlayered with whitish Posidonia-bearing coquinoïd limestones. Often there are differences in color in micrite zones due to local enrichment in Fe and Mn in burrowed sediments (Plate 5, Fig. 2). They have marly partings, are strongly bioturbated and locally may exhibit a nodular fabric. Hardground surfaces, Fe-Mn crusts and neptunian dykes typically occur. Microcavities of stromatolitic-type are commonly present and, to a lesser extent laminitic and stromatolitic structures (Plate 5, Fig. 3). The microfacies is mainly wackestone to packstone with baby-ammonites, thin-shelled bivalves, brachiopods, foraminiferas,

crinoid fragments, calcitized radiolarians, gastropods and ostracodes. Acetic acid insoluble residues contain abundant conodonts, fish teeth and scales, foraminiferas, and occasionally holothurian sclerites. Ammonoids are relatively abundant and well preserved, although difficult to extract from the host rock. Their preservation is locally enhanced by manganese oxides coatings. The ammonoids are filled with sediment and occasionally with white spar.

The development of hardground surfaces and neptunian dykes, the absence of mechanical compaction features support the idea of early lithification of the carbonate sediment (Demicco and Hardie, 1995; Clari and Martire, 1996). Unpreserved microbial mats may have had an important role in trapping and binding the carbonate sediment, as suggested by the presence of stromatactis-type structures and locally laminitic, sometimes stromatolitic structures. In this respect, the limestones share much with the Jurassic "Ammonotico rosso" (Martire, 1996). Burial diagenetic features observed are dissolution seams and stylolites. Stylolites are filled either with sediment and Mn-Fe oxides, locally with bladed cement.

### Agighiol Dealul Pietros

Dealul Pietros, located about 1 km west of Agighiol village, became famous in the paleontological literature due to the classical monographs by Kittl (1908) and Simionescu (1913). It is also the type locality for the Agighiol Limestone, which has here the most extensive development. Both tectonic compartments separated in this area (East Agighiol and West Agighiol, respectively) occur at Dealul Pietros, and in both of them the Agighiol Limestone is present, although at different stratigraphic levels. One of the three sections measured at Dealul Pietros (I) is from the West Agighiol compartment, the others (II and III) are from the East Agighiol compartment. The sections are represented in fig. 38.

#### *Dealul Pietros I*

Located at the top of the Dealul Pietros Hill, on the north-eastern flank, this section consists of a 50 m thick sequence of massive red limestones and subordinate dolomites. This sequence represents the base of the West Agighiol compartment succession and it is followed by closely alternating dark gray platy limestones with stratiform or nodular siliceous nodules and greenish to black marls.

Conodonts have been recovered from three samples, as follows (paleontologic determinations Elena Mirauta):

V97-511

*Neospathodus homeri* (Bender)

*Neohindeodella benderi* Kozur & Mostler

V97-514

*Neospathodus triangularis* (Bender)

*Neospathodus spathi* Sweet

*Neospathodus homeri* (Bender)

*Neohindeodella benderi* Kozur & Mostler

*Ozarkodina turgida* Bender

V97-524

*Neospathodus homeri* (Bender)

*Neospathodus spathi* Sweet

*Neohindeodella benderi* Kozur & Mostler

*Neohindeodella ceweki* (Bender)

*Ozarkodina turgida* Bender

*Enantiognathus mitzopouli* (Bender)

*Anastrophognathus sagittalis* Bender

The conodont faunas from the samples coming from lower half of the measured section (V97-511 and V97-514) are indicative for the lower Spathian, while the fauna recovered from the sample V97-524 indicates the base of the upper Spathian.

### *Dealul Pietros II*

A second section at the Dealul Pietros Hill was logged on the eastern flank of the Hill, at its base (28°51'56"E; 45°01'45"N). It represents the base of the East Agighiol compartment sequence. The first 10 meters are exposed in a E-W orientated ravine (the largest ravine) that cut the loess deposits covering the base of the sequence. The limestones vary in color from pink to red or gray, thick bedded (bed thickness may vary from 30 cm to 1m) and are strongly burrowed. Microbial structures as planar stromatolites or stromatactis-type micro-cavities occur in the upper part of the sequence occurring the ravine. Although numerous ammonoid sections have been observed at several levels, they could not be extracted from the rock and no direct age indication is available from this part. However, in the next ravine, about 50m to the north, two successive ammonoid faunas have been recovered (Gradinaru, unpublished). The rock-sequences of the two ravines are roughly correlative, although bed by bed correlations are uncertain due to the incomplete exposure of strata; therefore, their location on the profile is uncertain. Both ammonoid assemblages (AG1 and AG2) provided ammonoids indicative for the lower Middle Anisian (the Lower Bithynian *Kocaelia* Zone), representing two distinct subzones (Gradinaru, unpublished).

The remainder of the profile was measured in the eastern flank of the Hill. Between the two segments of the section the rock sequence is not exposed, however the missing sequence probably do not exceed 3 meters. The upper part of the sequence is better exposed, the stratal patterns and the facies do not changes significantly, however. For the entire section the microfacies is characterized by mudstones and packstones. Bioclasts are mainly thin bivalve shells, but all others components mentioned in the general description of the Hallstatt-type limestones are present. Microbial structures are observed also in thin sections, with laminites (sample R95-215) and microcavities with fenestral and geopetal fabric (e.g. R95-188 and R95-221). Age indications are given by other two ammonoid assemblages (Gradinaru, unpublished; see their location on the profile AG3 and AG4). The first one (AG3) indicate a late Middle Anisian age (Pelsonian) and the second one (AG4) an early Late Anisian age (the Lower Illyrian *Paraceratites* Zone).

In summary, the rock-sequence from the Agighiol II section represents the Early Middle Anisian to Early Late Anisian time interval.

### *Dealul Pietros III*

This sections includes the upper part of the Hallstatt-type sequence from the Dealul Pietros Hill. It is located on the eastern flank of the hill, at its base, just above the vineyards (28°52'01"E; 45°01'39"N). It is made up of pink to red strongly bioturbated limestones with marly partings and some interlayered levels of coquinoïd limestones (up to decimeter thick) with *Daonella/Posidonia*-type bivalves. Neptunian dykes filled with internal sediment, ammonoids and fibrous calcite were observed in the lower part of the sequence. The microfacies is roughly similar to the other sections, however there are some differences. Although the common microfacial type is mudstone to wackestone, in the upper part the packstones and grainstones prevail. Small-sized gastropods become common among bioclasts (from sample D9060 upwards), sponge spicules and brachiopods are also more frequent.

Age information is based on ammonoids and three conodonts samples. A first level with ammonoids (AG5) contain an assemblage with *Paraceratites* (Gradinaru, unpublished), indicating an Early Late Anisian age (*Paraceratites* Zone of the Illyrian). This level is an equivalent of the level AG4, from the Dealul Pietros II



section, therefore the top of the Dealul Pietros II section overlaps with the base of the Dealul Pietros III section. Three samples from the base of the section provided conodonts assemblages, as follows:

**D9055**

*Gondolella bulgarica* (Budurov & Stefanov)  
*Gondolella constricta*  
*Gondolella bifurcata* (Budurov & Stefanov)  
*Gladigondolella malayensis budurovi*  
*Gondolella cornuta* (Budurov & Stefanov)  
*Gondolella cf. G. hanbulogi* (Sudar & Budurov)  
*Gladigondolella sp. aff. G. malayensis budurovi*

**D9058**

*Gladigondolella malayensis budurovi*  
*Gondolella excelsa* (Mosher)  
*Gondolella constricta*  
*Gondolella cornuta* (Budurov & Stefanov)

**D9060**

*Gondolella liebermani* Kovacs & Krystyn  
*Gondolella excelsa* (Mosher)  
*Gondolella constricta constricta* (abundant)  
*Gondolella constricta cornuta*  
*Gladigondolella tethydis* (Huckriede)  
*Gondolella mombergensis mombergensis* Tatge

These faunas are characteristic for the Late Anisian *Paraceratites* Zone, which is in good agreement with the ammonoid based zones and show that the base of the sections do not extend in the Middle Anisian.

A second level of ammonoids is located in the middle part of the profile (AG6). It contains ammonoids belonging to the Early Ladinian (Late Fassanian) *currioni* zone (Kittl, 1908; Simionescu, 1913). Other two ammonoids assemblages are located in the upper part of the sequence (AG7 and AG8) and belong to the Late Ladinian *archelaus* zone and to the Early Carnian (Early Julian) *aonoides* zone, respectively. Accordingly, the Agighiol III section covers the Late Anisian - Early Carnian time interval. The Ladinian sequence is very condensed (only 10 meters).

## Desli Caira

The Desli Caira Hill, also known as Stânca Mare Hill (Plate 4, Fig. 2), located about 6 km east of Mihail Kogălniceanu village, exposes on its southern flank a 40 m thick sequence of Hallstatt-type limestones. The limestones exposed at the Desli Caira Hill was informatively studied by Kittl (1908) and by Simionescu (1910), who described some new taxa of ammonoids. The sequence presented herein represents only the upper half of the succession, which is relatively better exposed. The sections starts from the bottom of the abandoned quarry located in the central part of the western side of the Hill (28°48'08"E; 45°04'27"N).

The limestones are variously coloured, mainly reddish, and subordinately interlayered with Posidonia-bearing coquinoïd limestones (occurring mainly in the lower part of the sequence). Intercalations of coquina limestones are decimeter thick, white-gray and can be interpreted as distal tempestites. Frequently the micritic limestones are bioturbated, and hard-ground surfaces that indicate short interruptions of sedimentation are also present. Stromatactis-type microcavities filled with sparry calcite are common along the section, but they are more frequent in the upper part. The wackestones and packstones dominate the microfacies, but mudstones and packstones have also been observed. Bioclasts are represented by bivalve shells, baby-ammonites, foraminiferas, ostracodes, and calcitized radiolarians. For the lower part of the section (up to sample D9045), the microfacies is characterized by the abundance of microbivalve shells,

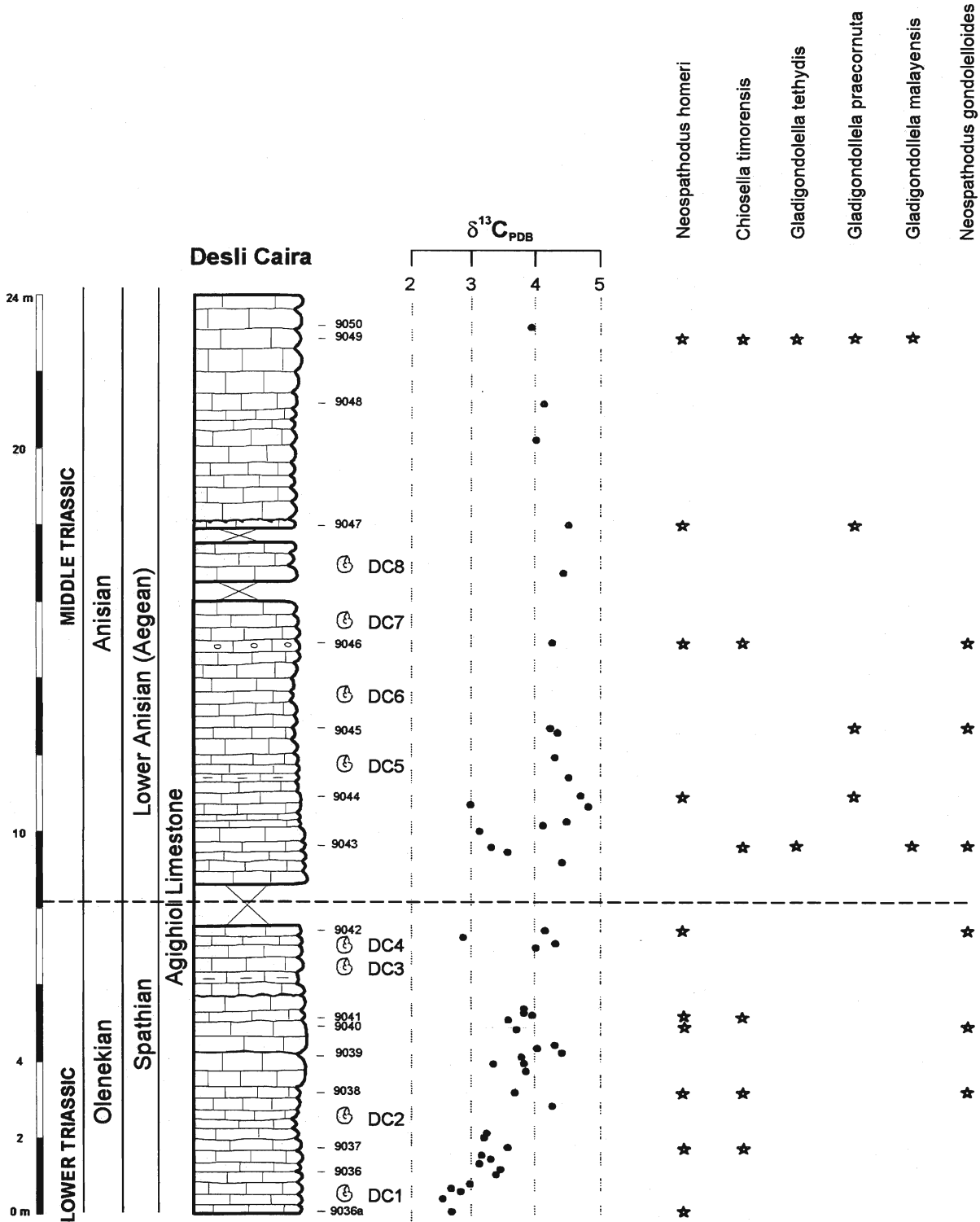


Fig. 39. Carbon isotope profile and conodont biostratigraphy of the Desli Caira section. The location of the Olenekian/Anisian boundary is based on ammonoids (Gradinaru, unpublished)

chaotically orientated. In the upper half they are less abundant although they are commonly present.

Eight levels of stratigraphically successive ammonoid faunas have been identified (Gradinaru, unpublished). The first four levels (DC1, 2, 3 and 4; see figure 39 for their location on the section) contain species of *Procarnites*, *Albanites*, *Proptychitoides*, *Preflorianitoides* (among others), which are representative for the Late Olenekian. The levels DC5, 6, 7 and 8 contain representatives of *Aegeiceras ugra* and *Japonites welteri*, among many others, which indicate an earliest Anisian age. Accordingly the Desli Caira section exposes the transition from the Olenekian to Anisian. The Olenekian/Anisian boundary lies somewhere between the levels DC4 and DC5 (Gradinaru, unpublished). Conodonts have been recovered from 13 samples and taxonomically identified by E. Mirauta. Their distribution along the section is also represented in Fig. 39.

It is noteworthy mentioning that the Desli Caira section is one of the rare places in the world where the transition from the Lower Triassic to the Middle Triassic is apparently continuous, well constrained biostratigraphically and without a major facies change. For these reasons, the Desli Caira section is of an outstanding interest and represents a suitable candidate for the Lower Triassic/Middle Triassic boundary stratotype (Gradinaru, 1993; Gaetani, 1994).

### Agighiol Dealul Lung

The uppermost part of the Agighiol Limestone occurs on the eastern slope of Dealul Lung Hill. The section measured and sampled in this Hill (28°51'56"E; 45°00'54") includes both the upper part of the Agighiol Limestone and the base of the Dealul Lung Formation, which are well exposed in three small quarries. The base of the section coincides with the floor of the lowermost quarry. The Agighiol Limestone occurring in this quarry is made up of thick bedded gray-yellowish to pink bioclastic limestones with ammonoids and brachiopods. Microfacially it is quite different of the limestones occurring at Dealul Pietros and Desli Caira Hill. The main microfacies is grainstone with bioclasts (essentially of the same type as the bulk of the Agighiol Limestone) and peloids, which suggest a shoaling upward trend for the Upper Ladinian - Lower Carnian part of the Agighiol Limestone.

Upwards, the rock sequence change abruptly to evenly bedded black bituminous limestones with thin shaly intercalations belonging to the Dealul Lung Formation. Microfacially they are wackestones with thin bivalve filaments, foraminiferas, calcitized radiolarians, crinoid debris and disseminated organic matter and pyrite. The abundance of pyrite and the preservation of organic matter in the limestones of the Dealul Lung Formation suggest a depositional environment with oxygen-restricted bottom waters. They may have had formed in a lagunar environment that have developed in the inner part of the newly formed rimmed platform, separated from the open sea by the Wetterstein reefs. An alternative interpretation of the depositional environment has been proposed by Baltres (1976), who favoured basinal, euxinic settings. The contact between the Agighiol Limestone and the Dealul Lung Formation is sharp. It represent a shift from an oxic to an anoxic (or dysaerobic) environment.

Two levels with biostratigraphically significant ammonoid faunas are known from the Dealul Lung section. The first one (AG9) is located in the upper part of the Agighiol Limestone and contain a characteristic assemblage for the Late Early Carnian (Late Julian *aonoides* zone). The ammonoids recovered from the lower part of the Dealul Lung Formation (AG10), from the floor of the second quarry, including representatives of *Tropites*, indicate an early Late Carnian age (*dilleri* zone) for the base of the Dealul Lung Formation (Gradinaru, unpublished).



*Carbon and oxygen isotope data*

The Hallstatt-type limestones grouped in the Agighiol Limestone are particularly well suited to carbon isotope analysis because:

- they are pelagic in origin and likely record shallow-water isotopic composition
- they are devoid of organic matter; diagenetic alteration of organic matter may represent a source of contamination with  $^{13}\text{C}$  depleted carbonate cements for the host carbonate
- they escaped severe tectonic deformation and burial diagenesis, as revealed by field observation, microfacies analysis and low Colour Alteration Indices of conodonts (1-2).
- they are particularly rich in fossils and the timing of potential stratigraphic variations can be well constrained

In order to check the reliability of carbon and oxygen isotope data from Hallstatt-type limestones, some tests were attempted. Pairs of "subsamples" were drilled from different types of carbonate (e.g. burrowed/not burrowed) on hand specimen samples. A good correlation was found between the sample pairs for both  $\delta^{13}\text{C}$  and  $\delta^{18}\text{O}$  values (table 1). Generally, the differences between the subsamples are minor; however the burrowed carbonate seems to have slightly higher  $\delta^{13}\text{C}$  values. Void filling cements have  $\delta^{13}\text{C}$  and  $\delta^{18}\text{O}$  values similar to the host rock (although systematically lower). Finally, two samples from the same layer, about 10 m far one from each other, show almost identical  $\delta^{13}\text{C}$  and  $\delta^{18}\text{O}$  values.

Sample	$\delta^{13}\text{C}$ (‰, PDB)	$\delta^{18}\text{O}$ (‰, PDB)	Comments
DC36/2	2.84	-3.2	reddish carbonate
DC36/2	3.08	-3.15	white carbonate (burrow filling)
DC37/1	3.57	-3.1	reddish carbonate(laminae)
DC37/1	3.4	-2.26	reddish carbonate (whole rock)
DC37/1	3.25	-4.51	void filling cement
DC37/3	3.15	-3.23	reddish carbonate
DC37/3	2.95	-3.72	void filling cement
DC39/3	3.9	-2.6	reddish carbonate
DC39/3a	3.8	-2.61	same layer, 10 m laterally
DC39/5	3.87	-2.58	reddish carbonate
DC39/5	4	-2.86	white carbonate (burrow filling)
DC40/6	3.74	-2.55	reddish carbonate
DC40/6a	3.5	-2.18	same layer, 5 m laterally
DC41/2	3.58	-2.52	reddish carbonate
DC41/2	3.96	-2.39	white carbonate (burrow filling)

**Table 1.**  $\delta^{13}\text{C}$  and  $\delta^{18}\text{O}$  results on selected samples from Desli Caira section.

Overall,  $\delta^{13}\text{C}$  values vary from 1.4‰ to 2.9‰ and  $\delta^{18}\text{O}$  values from -2.5‰ and -6.3‰, but most of the samples have  $\delta^{18}\text{O}$  values close to -3‰. The lowermost values (between -4‰ and -6.3‰) are recorded in some isolated samples collected at Dealul Pietros Hill, in the proximity of the reversed fault that separates the two compartments. This is not surprising because these rocks were prone to an enhanced interaction with fluids (possible of a meteoric origin) circulating preferentially along the fault zone. Carbon isotopes do not appear to be significantly affected in these samples. The  $\delta^{18}\text{O}$  -  $\delta^{13}\text{C}$  cross-plot (Fig. 40) show a weak correlation between  $\delta^{13}\text{C}$  values and  $\delta^{18}\text{O}$  values. This correlation is somehow surprising, as the range of variation for  $\delta^{13}\text{C}$  values is much greater than for  $\delta^{18}\text{O}$  values (excluding the extreme  $\delta^{18}\text{O}$  values, which are not representative for the trend). Because oxygen isotopes are much more sensitive to diagenesis than carbon isotopes, this situation is unusual.

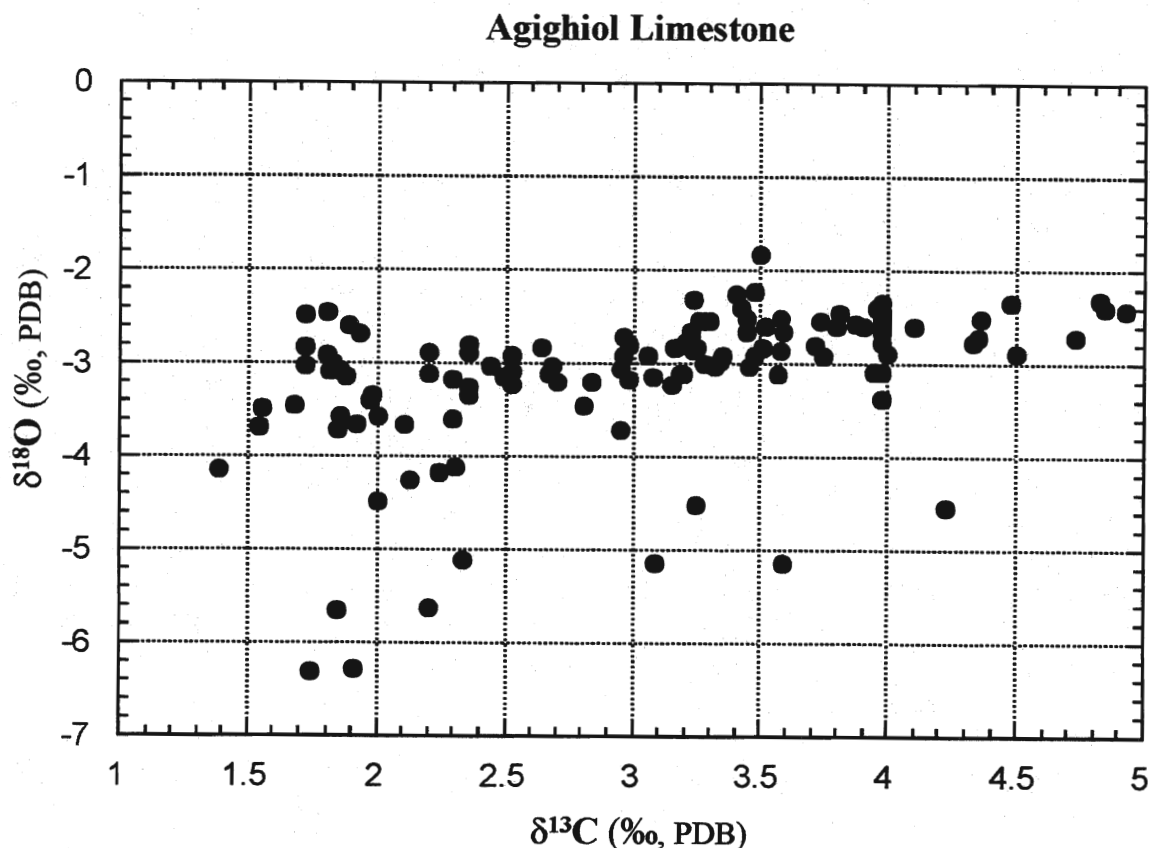


**Fig. 40.**  $\delta^{18}\text{O}$  -  $\delta^{13}\text{C}$  cross-plot for the Hallstatt-type limestones.

When plotting the  $\delta^{13}\text{C}$  data along the composite section (fig. 38) a consistent stratigraphic pattern is observed. The background  $\delta^{13}\text{C}$  values are around +2‰, measured in the sections from Dealul Pietros. For these section there are not significant deviations from the background values, although carbonate was measured from various types of carbonates (different degrees of bioturbation, various distances from hardground surfaces, marly partings, etc.). No correlation was found between the microfacies type and  $\delta^{13}\text{C}$  values.

On this fairly constant trend, there are two distinct positive excursions of  $\delta^{13}\text{C}$  values. The first one is clearly marked in the Desli Caira section, where  $\delta^{13}\text{C}$  values increase gradually from values around +2.5‰ (recorded from the base of the section) to values between +4‰ and +5‰, which characterize the remainder of the Desli Caira section. The increase of  $\delta^{13}\text{C}$  take place in the upper Spathian sequence, while the highest values are recorded in the earliest Anisian *Aegeiceras ugra* beds. The backward trend of this positive excursion is not observed, probably because of a gap in the sedimentary record between the Desli Caira section and Dealul Pietros II section. The upper part of the Early Anisian and the lower part of the Middle Anisian is apparently missing from the record, as documented by ammonoid biostratigraphy (Gradinaru, unpublished).

There are five  $\delta^{13}\text{C}$  values (from a total of 50) which are out of the trend, however higher than the "background" values, for reasons that are not apparent; they might reflect an increase amount of diagenetic cements in the analysed powder, heterogeneities of the original sediment (although the data from table 1 do not support such an hypothesis) or subtle reworkings of older sediments (not confirmed by thin section analysis).

All the remainder of Anisian and the Ladinian is characterized by background values, with only two values out of the trend, which may have a common origin with those from Desli Caira, as discussed above.

A gradual upward trend of  $\delta^{13}\text{C}$  values is noticed at the top of the Dealul Pietros III section. Higher  $\delta^{13}\text{C}$  values are recorded all along the Dealul Lung section. The onset of this upward trend seems to be placed near the Ladinian-Carnian boundary. A more detailed sampling would be needed in order to better constrain the onset of the gradual rise. From the data presented here it cannot be excluded that the rise in  $\delta^{13}\text{C}$  values can start in the late Ladinian.  $\delta^{13}\text{C}$  values are constant through all the Dealul Lung section and the major lithological break between the Agighiol Limestone and Dealul Lung Formation is not associated with any change in  $\delta^{13}\text{C}$  values. It is important to mention that the  $\delta^{13}\text{C}$  pattern parallelize the shoaling upward trend that characterize the upper part of the Agighiol Limestone.

The  $\delta^{13}\text{C}$  values pattern recorded by the Hallstatt-type limestone is interpreted to reflect variations in surface ocean chemistry. This interpretation will be discussed in more detail in subchapter 6.3. Concerning the variations from the Hallstatt-type limestones, there are some lines of evidence which suggest that the  $\delta^{13}\text{C}$  pattern do not represent a diagenetic artifact:

- the major lithological change is not reflected in either  $\delta^{13}\text{C}$  or  $\delta^{18}\text{O}$  values
- $\delta^{18}\text{O}$  values are relatively high, within the range reported from aragonite cements (Scherer, 1977), aragonitic muds (Loreau et al., 1995), well preserved brachiopods (Veizer et al., 1997) and marine calcite cements (Frisia-Bruni et al., 1989). It is not suggested here that these values are primary; they simply reflect little diagenetic overprint
- the correlation between  $\delta^{13}\text{C}$  values and  $\delta^{18}\text{O}$  values is very weak. It is difficult to imagine a diagenetic mechanism which will affect to a greater extent the  $\delta^{13}\text{C}$  values than  $\delta^{18}\text{O}$  values (Marshall, 1992), while both  $\delta^{13}\text{C}$  and  $\delta^{18}\text{O}$  values are within the range of seawater values or close of it.
- the  $\delta^{18}\text{O}$  values remain fairly constant upsection
- the low variability of  $\delta^{13}\text{C}$  and  $\delta^{18}\text{O}$  values upsection; besides the long term stratigraphic variations, the  $\delta^{13}\text{C}$  values vary very little
- there is no correlation between  $^{87}\text{Sr}/^{86}\text{Sr}$  ratios and  $\delta^{13}\text{C}$  values (fig. 53b)

### **Agighiol Dealul cu Cununa - Dealul Mare**

In the Dealul cu Cununa - Dealul Mare hills area the intra-platform through type sequence crops out. The thickness of this sequence is considerably higher than the time equivalent Hallstatt-type sequence. The measured section (fig. 41) is located on the eastern slope of the Dealul cu Cununa Hill; the uppermost part of the sequence (units 11 and 12) was examined in the summit of the Hill and in the pass towards Dealul Mare.

The sequence from Dealul cu Cununa (2 km west of Agighiol village) starts with white - yellowish granular dolomites (unit 1), which make-up two morphologically distinct cupolas in front of the Dealul cu Cununa Hill. Upwards, the dolomites are followed by a sequence made-up by nodular marly limestones and marls with sparse intercalations of massive limestones (unit 2), thin bedded limestones with intercalations of nodular marls and limestones or yellowish shales (unit 3), nodular marly limestones (unit 4), reddish, massive brecciated limestones (unit 5), reddish brecciated limestones with alternations of thin bedded red shales (unit 6), red, micritic limestones with silty limestones and red shales interbeds (unit 7), grey cherty limestones with sparse intercalations of shales (unit 8). The following lithological unit (9), made-up of hard, silicified limestones gives a morphologically distinct crown-like band. It is followed by a close alternance of gray platy limestones and marly shales (10). Following the rock-sequence southwards in the area of Dealul Mare Hill there are reddish to yellowish-cream coloured, nodular

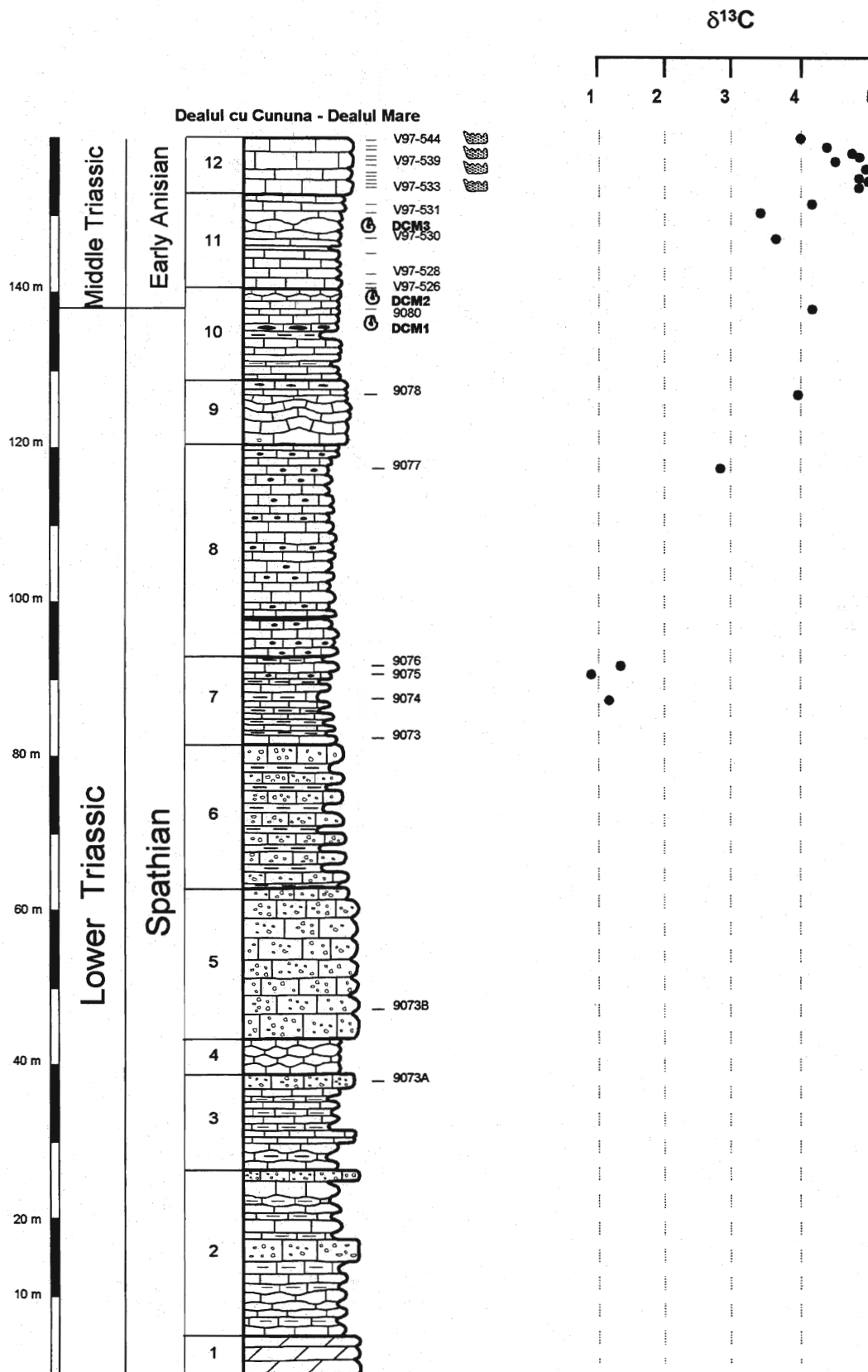


Fig. 41. Carbon isotope profile of Dealul cu Cununa - Dealul Mare section. Lithostratigraphy and biostratigraphy after Gradinaru (unpublished)

limestones with marly joints or thin layers of marly shales and evenly bedded gray limestones (unit 11) which are capped by thick bedded Hallstatt-type limestones (unit 12).

Age constraints are available mainly from the upper part of the examined sequence. A first level of ammonoids (DCM 1) is located just above the crown-like band, in yellowish-gray limestones. It provided an ammonoid assemblage indicative for the late Spathian which includes species of *Leiophyllites*, *Sulioticeras*, *Procarnites*, *Proptychitoides*, *Olenekites* and *Neomeekoceras* (Gradinaru, 1997). Upwards, two successive ammonoid levels (DCM 2 and DCM3) yielded both of them representatives of *Paracrochordiceras*, which is an index fossil for the earliest Anisian (Gradinaru, unpublished).

Four samples from the Hallstatt-type limestone (the topmost unit) provided the following conodonts fauna (E. Mirauta):

V97-533

*Chiosella timorensis* (Nogami)

*Neospathodus gondolelloides* (Bender)

V97-539

*Neospathodus gondolelloides* (Bender)

*Chiosella timorensis* (Nogami)

*Gondolella praecornuta* Budurov & Mirauta

*Gondolella* aff. *G. jubata* (Sweet)

V97-541

*Neospathodus gondolelloides* (Bender)

*Chiosella timorensis* (Nogami)

*Neospathodus homeri* (Bender)

*Gladigondolella malayensis budurovi* Kovacs & Kozur

*Ozarkodina turgida* Bender

*Didymodella alternata* (Mosher)

*Enantiognathus radiatus* (Bender)

V97-544

*Neospathodus gondolelloides* (Bender)

*Chiosella timorensis* (Nogami)

*Gladigondolella malayensis budurovi* Kovacs & Kozur

*Gondolella* cf. *G. mombergensis* (Tatge)

*Gondolella* cf. *G. regale* Bender

*Enantiognathus radiatus* (Bender)

These associations are characteristic for the Early Anisian.

#### Carbon and oxygen isotope data

$\delta^{13}\text{C}$  values vary from +1‰ to +5‰ and  $\delta^{18}\text{O}$  values from -2‰ to -6‰. The  $\delta^{18}\text{O}$  -  $\delta^{13}\text{C}$  cross-plot (fig. 42b) shows a strong positive correlation between the two variables (lower  $\delta^{13}\text{C}$  values are associated with lower  $\delta^{18}\text{O}$  values), which suggest a diagenetic overprint. The plot of  $\delta^{13}\text{C}$  values against depth in section reveals a distinct pattern.  $\delta^{13}\text{C}$  values rise gradually from values around +1‰ recorded in the grey cherty limestones of the unit 7 to values up to +5‰ in the evenly bedded gray limestones of unit 11 and the base of the Hallstatt-type limestones of unit 12. There is a slight trend towards less positive values just at the top of the Hallstatt-type limestones. The rise in  $\delta^{13}\text{C}$  values takes place during the Upper Spathian. The high  $\delta^{13}\text{C}$  values are restricted to the Lower Anisian. Lithology is highly variable through the section; however, the variations in  $\delta^{13}\text{C}$  do not appear to be related to the changing facies. High  $\delta^{13}\text{C}$  values appear to be age related. Thus, the general pattern is very similar with the pattern recorded in the time equivalent Hallstatt-type limestones from Desli Caira.

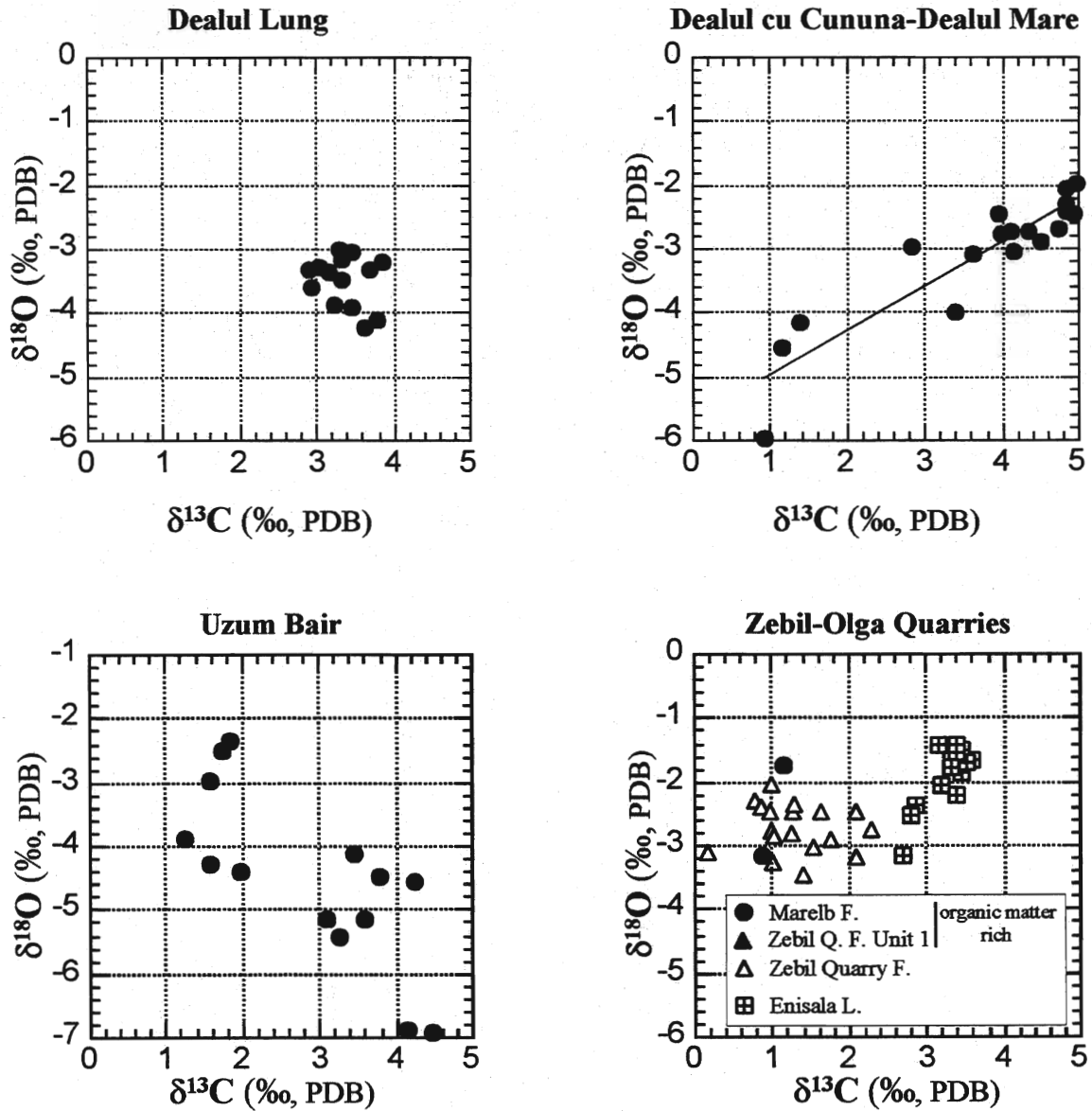


Fig. 42.  $\delta^{18}\text{O}$  -  $\delta^{13}\text{C}$  cross-plot for Dealul Lung (a), Dealul cu Cununa (b), Uzum Bair (c) and Zebil-Olga quarries (d).

## Uzum Bair

The Uzum Bair section (28°46'52"E; 45°03'58"N) is located 4 km east of Mihail Kogălniceanu village. A detailed description of lithology and fossil content is given by Crasquin-Soleau and Gradinaru (1996). The succession (fig. 43) starts with red to pale-pink colored Hallstatt type limestones, partly dolomitized and with episodic occurrence of juvenile bivalves bearing coquinoïd layers (distal tempestites) in the lower part (unit A). Upwards, the sequence grades to closely alternating, cherry-reddish coloured marly clays and thinly bedded platy limestones (unit B), to Amonitico Rosso-type limestones (unit C), closely alternating, thinly bedded marls and nodular chert limestones bearing reddish calcareous nodules (D), thinly bedded gray nodular limestones alternating with marly shales and tuffaceous rocks (E) and further to well bedded, light grey limestone with scattered chert nodules (F). The dominant microfacies is characterized by mudstones to wackestones with bivalves, ostracodes and calcitized radiolarians. Burial diagenetic structures are frequently encountered through the section, but they are more pronounced in units B to F, due to the higher clay content characterizing these units. The vertical distribution of facies show a deepening upward trend, from structural submarine highs type to deeper pelagic environments, suggested by the increasing proportions of shales and cherts upsection. The upper part of the sequence, grouped by Crasquin-Soleau and Gradinaru (1996) in the Uzum Bair Formation, represents a transitional facies between the Hallstatt-type limestone and the basinal deposits of the Cataloi Formation. On the basis of ammonoids and conodonts (Crasquin-Soleau and Gradinaru, 1996) the age of Hallstatt-type limestones is Late Olenekian (Spathian), while C, D and E units have an Early Anisian age (from level C representatives of *Paracrochordiceras americanum* are described). The unit F is assigned by the upmentioned authors to the Middle Anisian on the basis of conodont faunas.

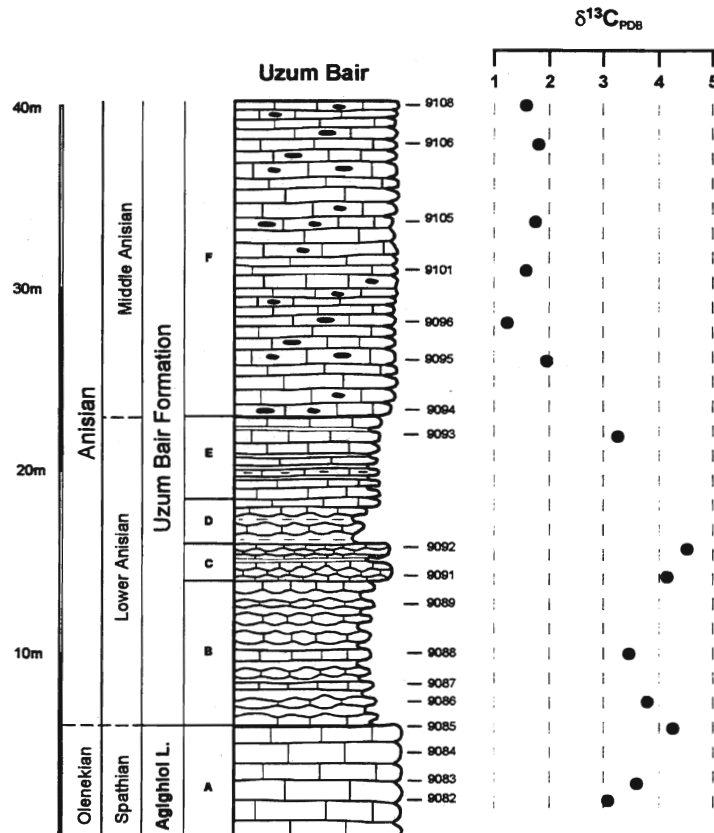


Fig. 43. Carbon isotope profile of the Uzum Bair section. Litho and biostratigraphy after Crasquin-Soleau and Gradinaru (1996).

### Carbon and oxygen isotope data

Isotopic measurements were performed on a limited number of samples, following a scrutiny check, according to their microfacies. Samples affected by recrystallization or dolomitization have not been analysed.  $\delta^{13}\text{C}$  and  $\delta^{18}\text{O}$  values range from +1.2‰ to +4.5‰ and from -2.3‰ to -6.9‰, respectively. Despite the reduced number of points, once again there is a consistent stratigraphic trend at the Lower-Middle Triassic transition. There is an initial increase in  $\delta^{13}\text{C}$  values (+1.2‰), followed by a poorly defined decreasing trend in unit B.  $\delta^{13}\text{C}$  values rise again reaching +4.5‰ in the Ammonitico Rosso type limestones of the unit C, then decrease gradually to values between +1‰ and +2‰ which characterize the unit F. The double peak shape of the carbon isotope profile in the lower part of the section is poorly constrained. However, the general trend from high  $\delta^{13}\text{C}$  values in the lower part to lower  $\delta^{13}\text{C}$  values in the upper part is clearly marked. The  $\delta^{18}\text{O}$  -  $\delta^{13}\text{C}$  cross-plot (fig. 42c) show a strong negative correlation and the primary origin of the stratigraphic pattern could be challenged. This negative correlation between  $\delta^{13}\text{C}$  and  $\delta^{18}\text{O}$  values is rather intriguing as diagenesis results in a positive correlation (Brand and Veizer, 1980; Marshall, 1992). The lowest  $\delta^{18}\text{O}$  values (around -6.9‰) are recorded in samples from the Ammonitico Rosso-type interval and from the Hallstatt-type limestones which are also characterized by the highest  $\delta^{13}\text{C}$  values.

The stratigraphic trend defined in this section is remarkably well correlatable on the basis of biostratigraphic data with the other two sections available for this time-span. High  $\delta^{13}\text{C}$  values are recorded close to the Spathian/Anisian boundary, with the highest values recorded in the lowermost Anisian (here coinciding with beds with *Paracrochordiceras americanum*) while the decreasing trend is confined to the Lower Anisian - Middle Anisian transition. For these reasons, it is considered that the carbon isotope composition is not significantly affected by the diagenesis.

### Zebil and Olga Quarries

In the Hills between the Zebil railway station and Congaz village an Upper Olenekian to Rhaetian rock sequence is exposed. While the Upper Olenekian and Anisian deposits occur mainly in the Dealul Rosu Hill (and in other Hills eastwards), the Ladinian to Rhaetian rock sequence is well exposed in two quarries located north of Dealul Rosu Hill, namely Zebil and Olga quarries, and further to the north in some small ravines south of Congaz village. For this study a composite section was measured and sampled from the two quarries mentioned above.

The Zebil quarry section (28°43'42"E; 44°58'34"N) provides a good exposure of a prograding carbonate platform (the so called "Wetterstein" platform) over deeper water sediments of the Zebil Quarry Formation. To the section represented in fig. 44, a 4m thick rock sequence representing a part of the upper member of the Marelb Formation was added. These rock-sequence was measured and sampled in a small ravine about 400 m North of Dealul Rosu Hill (28°44'16"E; 44°58'24"N) and it is represented by dark gray nodular limestones in the lower part and black bioclastic limestones with black bituminous shales interbeds. Ammonoids identified from the nodular limestones (level Z1) include *Paraceratites* sp., indicating an early Late Anisian (Illyrian) age (Gradinaru, 1993).

The sequence from the quarry starts with black bituminous limestones (occurring in the floor of the quarry), very similar with those occurring in the ravine. The overlying Zebil Quarry Formation comprises a 17m thick rock-sequence, divided in 3 distinct lithological units. The lower unit (1), 5m thick, is made-up of shaly limestones with black calcareous nodules and anastomosed shaly partings, yellowish shales interbeds and gray-yellowish marls to the top. Unit 2, 7m thick, consists of a close alternation of nodular varicolored limestones and reddish shales. The next lithological unit is characterized by thick bedded, nodular medium gray limestones with minor shales interbeds. It is a shallowing upward unit, marking the gradual transition to the overlying Enisala Limestone.



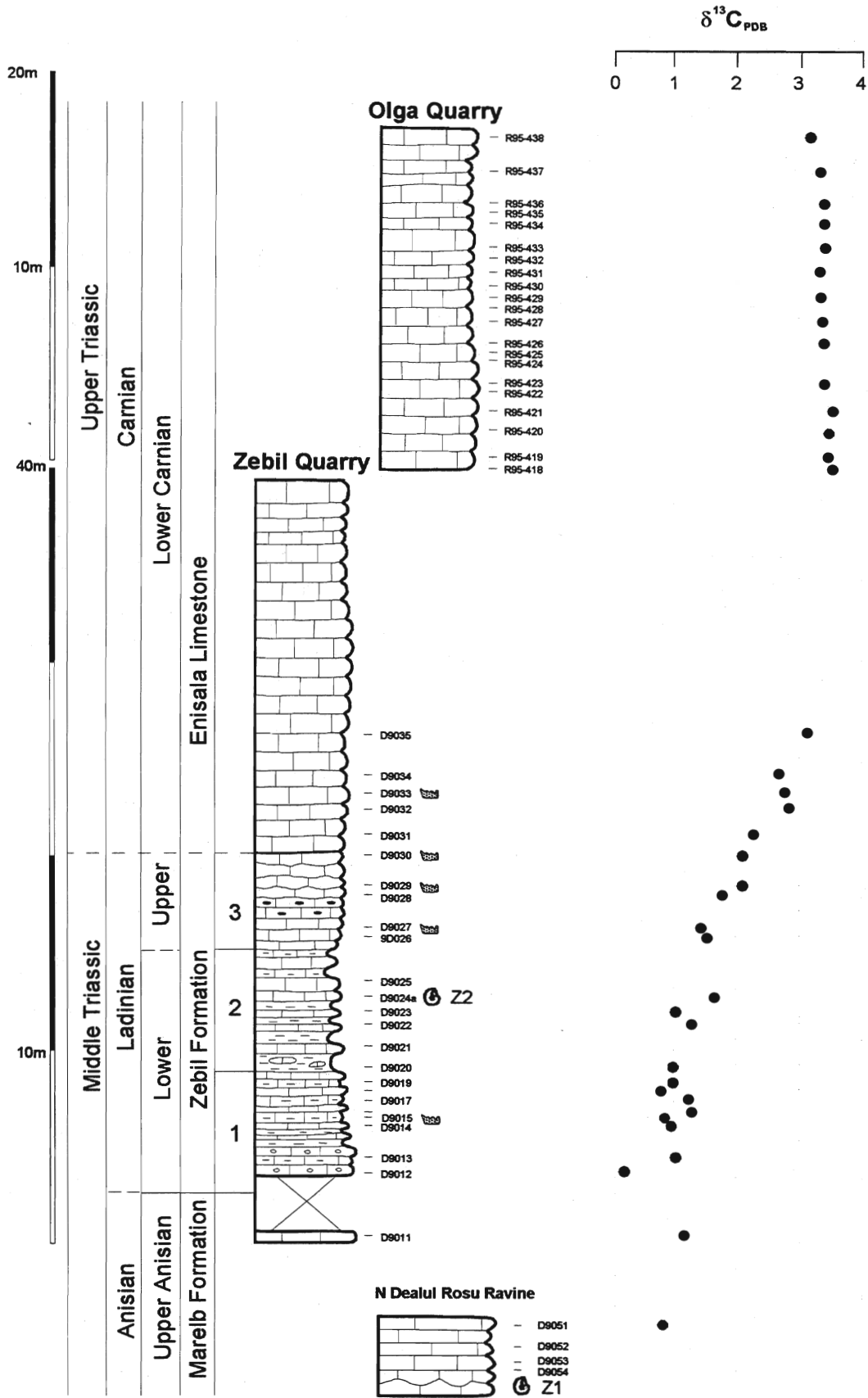


Fig.44. Carbon isotope profile along a composite section including Zebil quarry section and Olga quarry section.

The microfacies of the limestone beds of the Zebil Quarry Formation is represented mainly by wackestones and packstones with thin shelled bivalves, foraminiferas, ostracodes, calcitized radiolarians and microcavities of stromatactis-type showing a close similitude with the Hallstatt-type limestones microfacies. Therefore, the Zebil Quarry Formation is considered as a deeper equivalent of the Agighiol Limestone (part of it).

The Enisala Limestone covers progradingly the Zebil Quarry Formation. In the first quarry only its lower part is exposed, but a thicker sequence occur in the Olga Quarry, several hundred meters to the North. The thickness of the Enisala Formation cannot be measured precisely from outcrop exposures, being partly covered. In the Olga quarry we measured 40 m, but the total thickness is much higher. The Enisala Limestone is made up of thick bedded to massive light gray bioclastic limestones, similar to the Wetterstein-type facies from the Northern Calcareous Alps (Baltres et al., 1982). The microfacies is characterized by packstones with peloids, calcareous algae, fragments of calcisponges, bryozoans, spicules, foraminiferas, indicating a shallow-water high energy environment, probably a fore-reef environment (suggested by the abundance of reef builders debris).

Age diagnostic fossils (ammonoids and conodonts) are available from several levels, mainly from the Zebil Quarry Formation. Sample D9015 from Unit 1 provided *Gondolella trammeri* which is very frequent in the Lower Ladinian, although it was reported also from the uppermost Anisian (sensu Brack and Rieber, 1993). Therefore an Early Ladinian age for the base of the Zebil Quarry Formation is the most likely. Ammonoids faunas recovered from the middle part of unit 2 (level Z2) include *Eoprotrachyceras currionii*, indicative for the Lower Ladinian. Sample 89027, located in the lower part of unit 3, provided the following conodont species: *Budurovignathus mungoensis* (Diebel), *Gondolella foliata inclinata* Kovacs, *Gondolella* aff. *G. polygnatiformis* (Budurov & Stefanov), indicating a Late Ladinian age. Three samples from the upper part of the Zebil Quarry Formation and from the base of the Enisala Limestone provided assemblages that do not permit a distinction between the Upper Ladinian and the Lower Carnian (E. Mirauta, written communication). These assemblages are, as following:

**D 9029***Gondolella foliata inclinata**Gondolella polygnatiformis* (Budurov & Stefanov)**D9030***Gondolella foliata inclinata* (abundant)*Gladigondolella arcuata* Budurov**D9033***Gondolella foliata inclinata* (abundant)*Gladigondolella arcuata* Budurov*Lonchodina hungarica* Kozur & Mostler*Neocavitella tatrca* (Zawidzka)

Finally, a sample from Enisala Limestone (R95-447), collected in the Olga quarry, 8 meters above the top of the section represented in Fig.44, contain the conodont *Gondolella tadpole* which indicates undoubtedly the Lower Carnian.

*Carbon and oxygen isotope data*

Carbon and oxygen isotope composition was determined in samples with high carbonate content. Marly intervals were avoided.  $\delta^{13}\text{C}$  values are between +0.2‰ and +3.6‰ and show a distinctive stratigraphic trend. The lowest  $\delta^{13}\text{C}$  values are recorded in the upper part of the Marelb Formation and in the first unit of the Zebil Quarry Formation. Starting with unit 2 of the Zebil Quarry Formation, the  $\delta^{13}\text{C}$  values increase gradually and reach values up to +3.1‰ at the base of the Enisala Limestone. The shift to more positive values is about +2‰ and it is parallelized with the onset shallowing upward trend. The limestones from the top of the Marelb Formation are rich in organic matter, whose concentrations decrease gradually through

the unit 1 of the Zebil Quarry Formation. Most of the low  $\delta^{13}\text{C}$  values (around +1‰) are thus confined to the organic matter rich beds (Fig. 42d). The increase in  $\delta^{13}\text{C}$  values is correlated with the onset of fully oxic conditions that characterize the depositional environment of the remainder of the Zebil Quarry Formation.  $\delta^{13}\text{C}$  values from the Wetterstein-type limestones from the Olga quarry are remarkably constant upsection, with an average value of +3.4‰.

$\delta^{18}\text{O}$  values vary between -1‰ and -3.5‰ and do not vary systematically with the  $\delta^{13}\text{C}$  values (fig.42d). The highest  $\delta^{18}\text{O}$  values are recorded in samples belonging to the Enisala Limestone, with a mean value of -1.65‰. Three  $\delta^{18}\text{O}$  values are out of the main range of variation, also characterized by lower  $\delta^{13}\text{C}$  values, which may indicate diagenetic overprint.

To sum up, the  $\delta^{13}\text{C}$  profile of the Zebil-Olga quarries section show a gradual increase, correlated with the shallowing upward trend, clearly demonstrated by facies succession. In the lower part, the  $\delta^{13}\text{C}$  values correlates also with the organic carbon content of the rock. These lines of evidence suggest that the stratigraphic trend is facies controlled. However, a possible connection with changes in surface waters isotopic composition cannot be completely ruled out. As a matter of fact, a similar trend was recorded in the Agighiol Limestone (fig. 38). A more comprehensive discussion can be found in subchapter 6.3.

## Congaz

The sequence cropping out in the Hills south of Congaz village, belonging to the Congaz Formation, represents the continuation of the succession described above. The strata overlying the Enisala Limestone are relatively poorly exposed. They are of major interest as one of the rare exposures where Upper Carnian to Rhaetian deposits can be examined in the Zebil- Agighiol area.

The sequence exposed in the main ravine, a tributary of the Telita river, starts with a 10 m thick unit made-up of black, thinly to medium bedded bioclastic limestones interbedded with cherty limestones, belonging to the Congaz Formation (Fig. 45). They are followed by 3.5 meters of gray colored medium bedded bioclastic limestones. From the gray limestones an ammonoids fauna (CG1) with *Tropites acutangulus* indicate a Late Carnian age - *subbulatus* zone (Gradinaru, written communication). A thin level (20 cm thick) of medium gray thin shelled bivalves bearing coquinoïd limestones crops-out upwards, following a 3m thick covered interval. 4m upwards a 0.6m thick interval is exposed, consisting of nodular gray to reddish limestone with ammonoids, brachiopods and halobiid bivalves. A latest Carnian age (*Anatropites* zone) is indicated by the presence of *Anatropites* and *Placites* (ammonoid level CG2). They are followed by a 4m thick interval made up of red nodular limestones with coquinoïd limestones interbeds. The bivalve *Halobia veerbecki*, recovered from the base of this unit (CG3) indicate the transition from the Upper Carnian to the Lower Norian (Gradinaru, written communication).

The overlying rock-sequence can be examined 100m westwards, on the slope of a small Hill, where a thin level of dark gray coquinoïd limestones occur (CG4). It provided *Halobia salinaria*, which indicates an Upper Norian (Sevatian) age. The thickness of the covered interval between the top of the ravine sequence and this level is of about 10m. The uppermost level exposed in the Hill consists of nodular red-cherry limestones with marly partings, showing some similitudes with the Hallstatt-type limestones. This level (CG5) is attributed to the Rhaetian stage on the basis of the bivalve *Otapiria marshalli alpina* and the conodont *Gondolella steinbergensis* (Gradinaru, written communication).

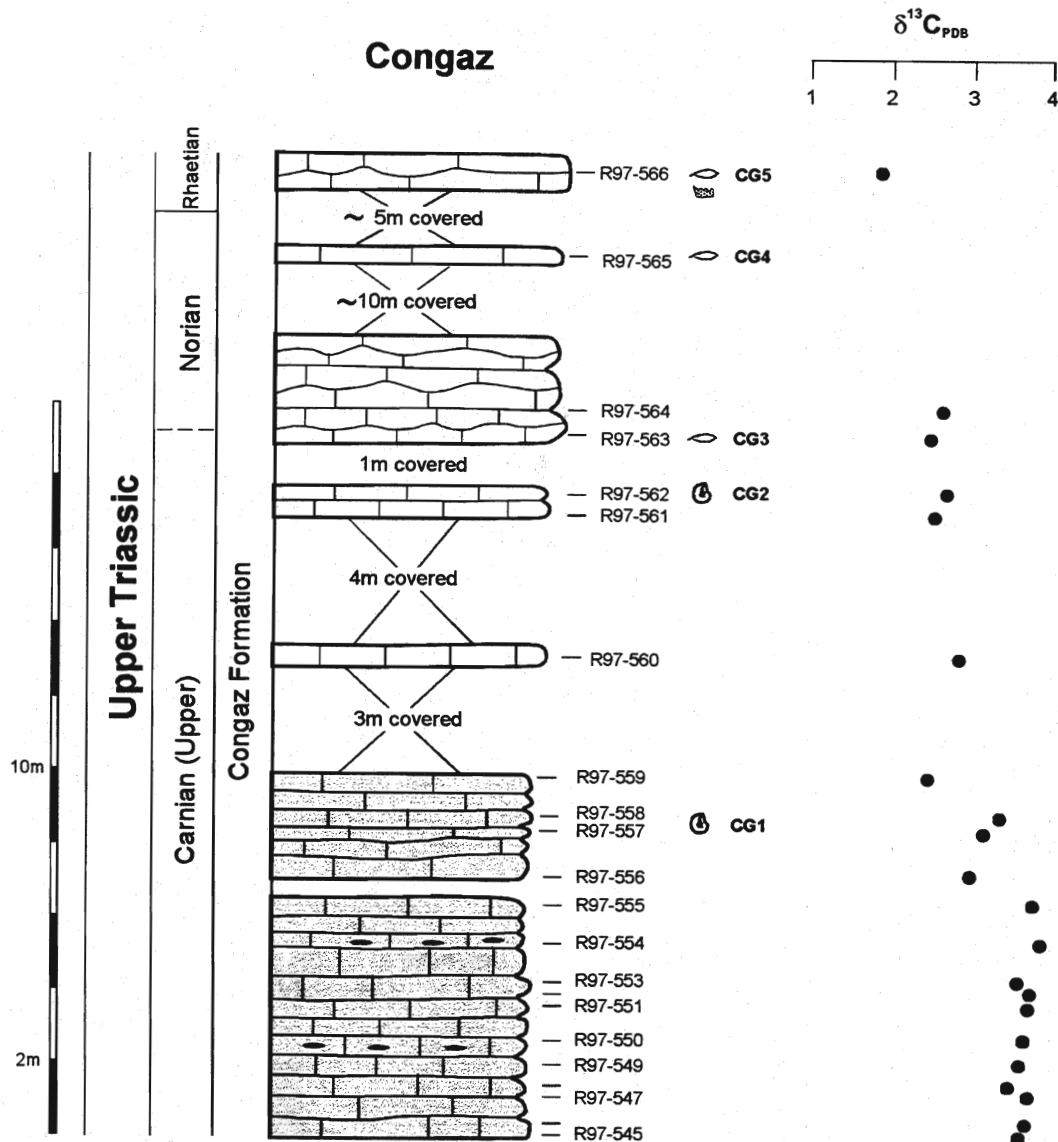


Fig. 45. Carbon isotope profile of Congaz section

#### Carbon and oxygen isotope data

The  $\delta^{13}\text{C}$  values from the limestones described above are between +1.8‰ and +3.9‰ (with a mean value of +3.7‰). The highest  $\delta^{13}\text{C}$  values were recorded in the black limestones from the base of the sequence and they vary very little along the first 6 meters. The remainder of the section is characterized by lower  $\delta^{13}\text{C}$  values, displaying a more scattered distribution, with an average value of +2.6‰. The transition between the two groups of values is more or less gradual, and occur in the level of gray bioclastic limestones located at the top of the Congaz Formation. The  $\delta^{18}\text{O}$  values vary between -2‰ and -6.6‰ and show a strong covariance with the  $\delta^{13}\text{C}$  values (Fig. 46). The bimodal distribution of  $\delta^{13}\text{C}$  and  $\delta^{18}\text{O}$  pairs which is clearly marked on the  $\delta^{18}\text{O}$  -  $\delta^{13}\text{C}$  cross-plot appears to be facies controlled. The black limestones from the base of the section are have higher  $\delta^{13}\text{C}$  and  $\delta^{18}\text{O}$  values, whereas the gray and reddish limestones from the upper part of the section have lower and more scattered  $\delta$  values for both carbon and oxygen.

The well defined stratigraphic pattern (fig. 45) seems to be, therefore, facies controlled. Still, it is noteworthy that both  $\delta^{13}\text{C}$  and  $\delta^{18}\text{O}$  values from the Congaz Formation are close to their counterparts of the underlying Enisala Limestone, although the facies contrast is more significant.

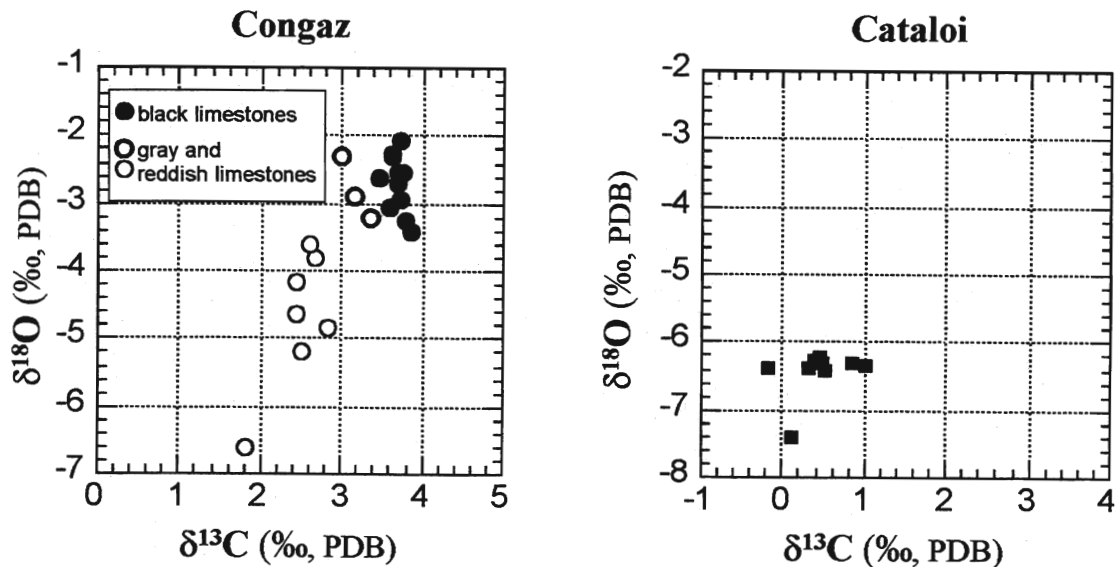


Fig. 46.  $\delta^{18}\text{O}$  -  $\delta^{13}\text{C}$  cross-plot for Congaz (a) and Cataloi (b) sections.

### 6.2.3. Basinal settings

Sediments deposited at the base of the slope and in basinal settings are known mainly in the western part of the Tulcea Unit. Whereas slope apron resedimented carbonates are known only from the Spathian (Somova Formation), true basinal sediments, with rhythmic development of limestone-marl couplets are known from the lower Spathian (Tulcea Veche Formation) and from the Upper Anisian to Upper Norian interval (Cataloi Formation) (Gradinaru and Baltres, unpublished). The base of slope sediments are only briefly discussed in the present study. The best exposures of Triassic sediments deposited in deep-water and basinal settings occur in two quarries south of Tulcea, the Trei Fântâni and Bididia quarries and on the right bank of the Telita river, near the church of Cataloi.

#### Trei Fântâni and Bididia sections

In the Trei Fântâni quarry (28°49'16"E; 44°58'24"N), about 2 km south of Tulcea, an Upper Olenekian to Upper Anisian sequence of carbonate deposits occur, with a total thickness of about 300 m. Four main formations, deeping more or less vertically, occur in this quarry: Somova Formation, a dolomitic complex, Trei Fântâni Formation and Cataloi Formation (fig 47). The succession is apparently continuous, however the dolomitic complex is fault bounded. Only the lower part of the Cataloi Formation is exposed in the Trei Fântâni quarry, however, the upper part of it and the overlying Bididia Formation can be examined in the neighbouring Bididia quarry (28°49'28"E; 45°09'40"N).

The lowermost stratigraphic unit, the **Somova Formation**, crops out in the western flank of the quarry. It is made up of rhythmic calcirudite-calcarenite sequence, totalizing 76 m. Four units have been separated (only the upper two units- 3 and 4 - are represented in fig. 16) according to the relative proportion of fine/coarse size of the calcareous clasts and bed thickness. These resedimented limestones were deposited at the base of the slope and are similar with the Lower - Middle Triassic slope carbonates described in South China (Bao, 1998). There is no direct evidence for the age of the Somova Formation occurring in the Trei Fântâni quarry. The Somova Formation have been dated as Spathian on the basis of conodonts and foraminifera

found elsewhere (Mirauta, 1982; Baltres, 1993). Conodonts recovered from the overlying dolomitic complex indicate a late Spathian or Early Anisian age which support a Spathian age for the Somova Formation. The dolomitic complex overlying the Somova Formation is divided in three units (5-7). Unit 5, about 30 m thick, consists of massive dolomitic limestones and calcirudites with polychrome pebbles partially dolomitized and is overlain by a 23m thick sequence of well bedded polichrome (red, gray or greenish) platy limestones with shales interbeds (unit 6). The latter unit represent the transition from calcarenitic turbidites to nodular limestones. Both units show some similarities with the underlying Somova Formation and probably represents its upper part dolomitized. Generally, the rock-sequence show a shallowing upwards trend.

The uppermost unit of the dolomitic complex (unit 7) is made-up of massive granular dolomites, with thickness estimated to about 50m. This unit is fault bounded, however, because massive dolomites are commonly found at this stratigraphic level in North Dobrogea, it is presumed that these faults are minor and did not disrupted the stratigraphic succession.

A conodont sample (R95-235 and TF1) from the top of unit 6, just beneath the contact with the dolomites provided an association with: *Neospathodus* sp. cf. *N. spathi* Sweet, *Neoplectospathodus muelleri* (Kozur & Mostler), *Neohindeodella aequiramosa* Kozur & Mostler, *Ketinella mexicavata* Gedik, *Prioniodina ? bitorta* (Bender), which suggest a late Spathian or early Anisian age, although diagnostic species are not present.

The overlying **Trei Fântâni Formation**, about 120 m thick, is divided in two members: a lower member informally named "nodular limestones" and an upper member named "cherty limestones" (Gradinaru and Baltres, unpublished). The "nodular limestones" are divided in three units (8-10). Unit 8, 33 m thick, consists of burrowed greenish and mainly red nodular limestones and with marly partings. It is followed by evenly bedded gray-greenish nodular limestones with thin shales interbeds (unit 9) and dark gray nodular limestones with pyrite and rare ellipsoidal cherts (unit 10). The microfacies is characterized by wackestones with thin bivalves shells, calcitized radiolarians and rare ostracods. Conodonts recovered from sample R95-244 (TF2) were identified by E. Mirauta as *Neospathodus homeri* (Bender), *Cornudina* cf. *C. breviramulis minor* Kozur, *Hindeodella stoeppeli* Bender which suggest a late Spathian or early Anisian age. Three successive conodonts samples from the top of unit 8 (R95-258; TF3), the base of unit 9 (R95-264; TF4) and the lower part of unit 10 (R95-282; TF4), all contain associations with *Gondolella bulgarica* (Budurov & Stefanov) and *Gondolella hanbulogi* (Sudar & Budurov), which indicate a middle Anisian age. This age is supported by some rare ammonoids (*Proteusites* sp. and *Acrochordiceras* sp.) recovered from the nodular limestones (Gradinaru, unpublished).

The upper member of the Trei Fântâni Formation, "cherty limestones" (unit 11) consists of thin bedded (from 5 to 10 cm) dark gray limestones with small sized ellipsoidal black cherts. The source of silica in cherts is probably the dissolution of radiolarians or sponge spicules. The microfacies is dominated by wackestones with thin shelled bivalves and calcitized radiolarians. Two conodont samples from the upper part of the "cherty limestones" (R95-306; TF6 and R95-310; Trei Fântâni 7) provided associations with *Gondolella bulgarica* (Budurov & Stefanov), *Gondolella hanbulogi* (Sudar & Budurov) and *Gondolella constricta*, indicative for the Middle Anisian.

The dark gray pelagic limestones with black cherts of the Trei Fântâni Formation grade rapidly upward to black limestone with marls interbeds of the **Cataloi Formation**. Although the sequence of limestone-marl couplets is quite monotonous, it may be interrupted locally by several meters thick layers of massive marls. Limestone bed thickness is usually around 10 cm, but they may reach up 30 cm. The mutual contact between the limestone and marl layers can be sharp or transitional. Bed surfaces can be either planar or wavy. Veins with complicated cross cutting relationships commonly occur. Abundant pyrite occurs either as fine grained, homogeneously disseminated framboids or as euhedral aggregates with massive fabric. The common microfacies of the limestones is represented by mudstone and wackestone containing scattered

thin-shelled bivalves and rare foraminiferas, calcitized radiolarians and ostracods. Five units (12-16) have been separated according to the thickness and the stratal pattern of the marl-limestone couplets (fig. 47).

The limestones contain thin-shelled halobiid-type bivalves throughout the section, more abundant in the upper part, in the Bididia quarry. Abundant in the type locality of the Cataloi Formation, ammonoids are rare in the Trei Fântâni-Bididia quarries. An ammonoid fauna collected from the lower part (TF8), contain representatives of *Paraceratites*, indicating a late Anisian age for the base of the Cataloi Formation, in agreement with conodont based data from the Cataloi type-section (Mirauta et al., 1993). Age indication for the upper part of the Cataloi Formation (occurring in the Bididia quarry) are scarce, and are based on bivalves (Gradinaru, personal communication). They indicate a Lower Carnian age for the upper part of the Cataloi Formation. In the type locality, the Cataloi Formation extends up to the upper Norian.

A basinal depositional setting is considered for the Cataloi Formation. The relatively high organic matter content and the abundance of pyrite suggest that deposition and early diagenesis took place in an oxygen deficient environment.

The last main lithologic unit examined is the **Bididia Formation**, which overlies conformably the Cataloi Formation. It is made up of a rhythmic sequence of black sandstones, limestones and shales. Its age is Carnian to Norian. Only its base has been measured and sampled.

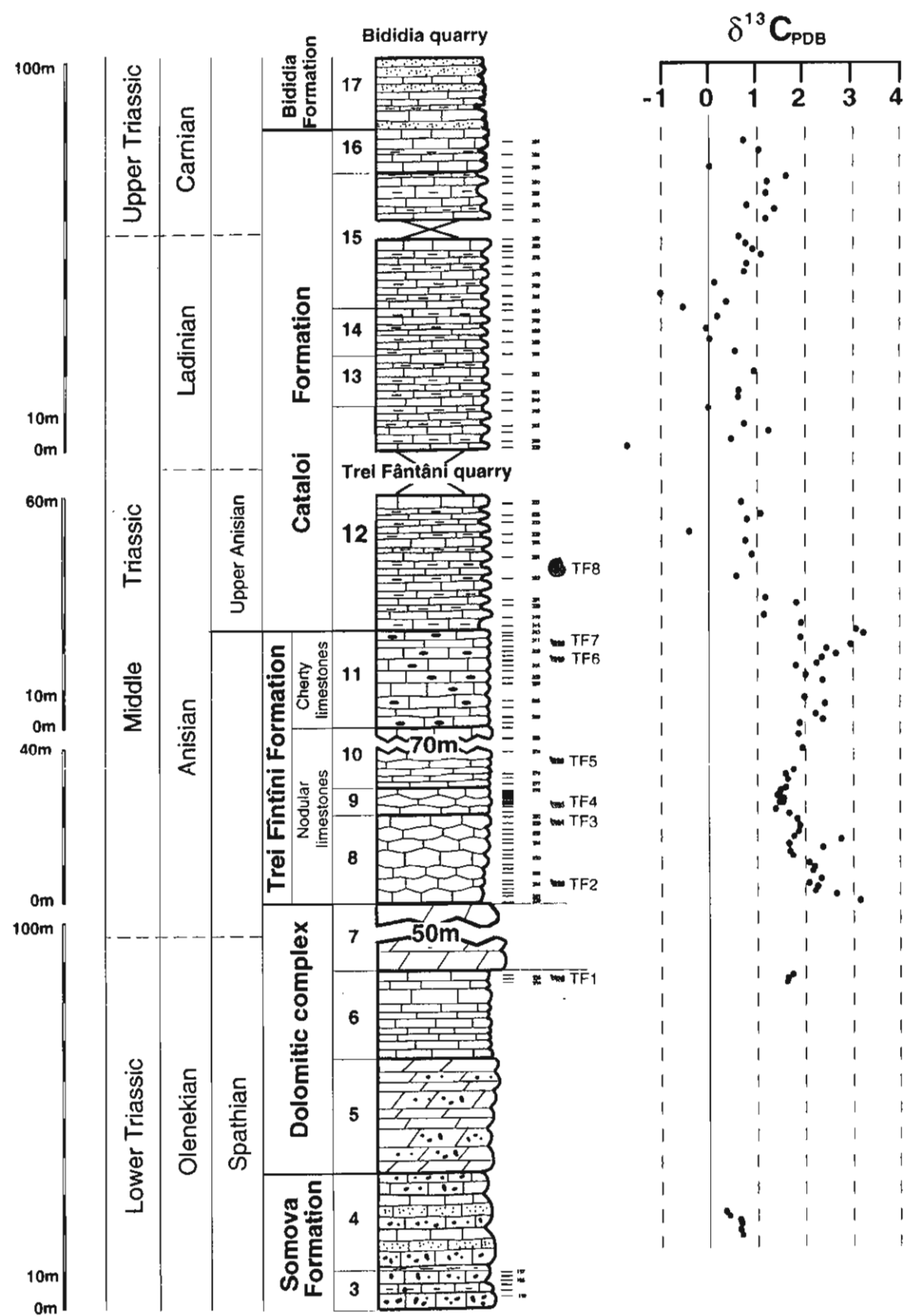
#### *Carbon and oxygen isotope data*

A detailed sampling for stable isotope measurements was carried out in the two quarries. However, the massive dolomites have not been sampled because of their uncertain stratigraphic position (they are confined by faults and do not contain fossils). From the total amount of samples collected from the Somova Formation, only a few were measured. Sampling density is increased for the Trei Fântâni and Cataloi formations.

Overall,  $\delta^{13}\text{C}$  values vary between -1.8‰ and +3.3‰. Only 6 samples gave negative  $\delta^{13}\text{C}$  values and all of them are from the Cataloi Formation. Samples from the Somova Formation gave low but constant  $\delta^{13}\text{C}$  values (between +0.4‰ to +0.7‰). Three samples from the dolomitic complex (from the top of unit 6) have  $\delta^{13}\text{C}$  values around 1.8‰ and show a slight increasing trend.

Above the dolomitic complex, the carbon isotope profile show a gradual decreasing trend from a value of +3.2‰ to background values around +1.5‰. Some minor but coherent variations are delineated in the middle and the upper part of the "nodular limestones" of the Trei Fântâni Formation, with shifts of 0.5‰. Only two samples (out of 30) gave  $\delta^{13}\text{C}$  values out of this trends. Whereas the decreasing trend from the base of nodular limestones can be correlated with the backwards slope of the Spathian/Anisian positive excursion present in other sections (Desli Caira, Uzum Bair, Dealul cu Cununa), the significance of the smaller variations is difficult to asses. They may reflect short term variations in seawater chemistry, for a time interval not sampled elsewhere, but this has to be substantiated by other detailed studies. Within the upper member of the Trei Fântâni Formation the stratigraphic distribution of  $\delta^{13}\text{C}$  values display a more scattered pattern and a progressive increase to values up to +3.2‰.

The transition from the Trei Fântâni Formation to Cataloi Formation is marked by a sharp decrease in  $\delta^{13}\text{C}$  values. The carbon isotopic signature of the Cataloi appears to be particular. Not only the  $\delta^{13}\text{C}$  values are lower than their counterparts of the underlying Trei Fântâni Formation, their distribution is much more scattered as they vary in a range of +3‰. The shift in  $\delta^{13}\text{C}$  values coincides with a major lithological change and is not correlated with any shift in other time equivalent profiles; therefore it is interpreted as a diagenetic artifact, as it will be further discussed in the following chapter. In the upper part of the section,



47 Carbon isotope profile along a composite section including Trei Fantani and Bididia quarries sections (stratigraphy after Gradinaru, unpublished)



the  $\delta^{13}\text{C}$  values show a more random stratigraphic distribution with an gradual trend to higher values towards the top of the Cataloi Formation.

The  $\delta^{18}\text{O}$  values are highly variable, they are between -2‰ to -6‰ and they also show a facies related bimodal distribution as it is clearly shown by the  $\delta^{18}\text{O}$  -  $\delta^{13}\text{C}$  cross-plot (fig.48). A somehow surprising evidence is that, considering the  $\delta^{18}\text{O}$  -  $\delta^{13}\text{C}$  pairs for each major lithological unit, there is no correlation between them. This is probably due to the fact that the Trei Fântâni Formation, which is characterized by "normal"  $\delta^{13}\text{C}$  and  $\delta^{18}\text{O}$  values, behaved differently in response to diagenesis when compared with the Cataloi Formation. Note that the  $\delta^{18}\text{O}$  values for the Somova Formation are "intermediate".

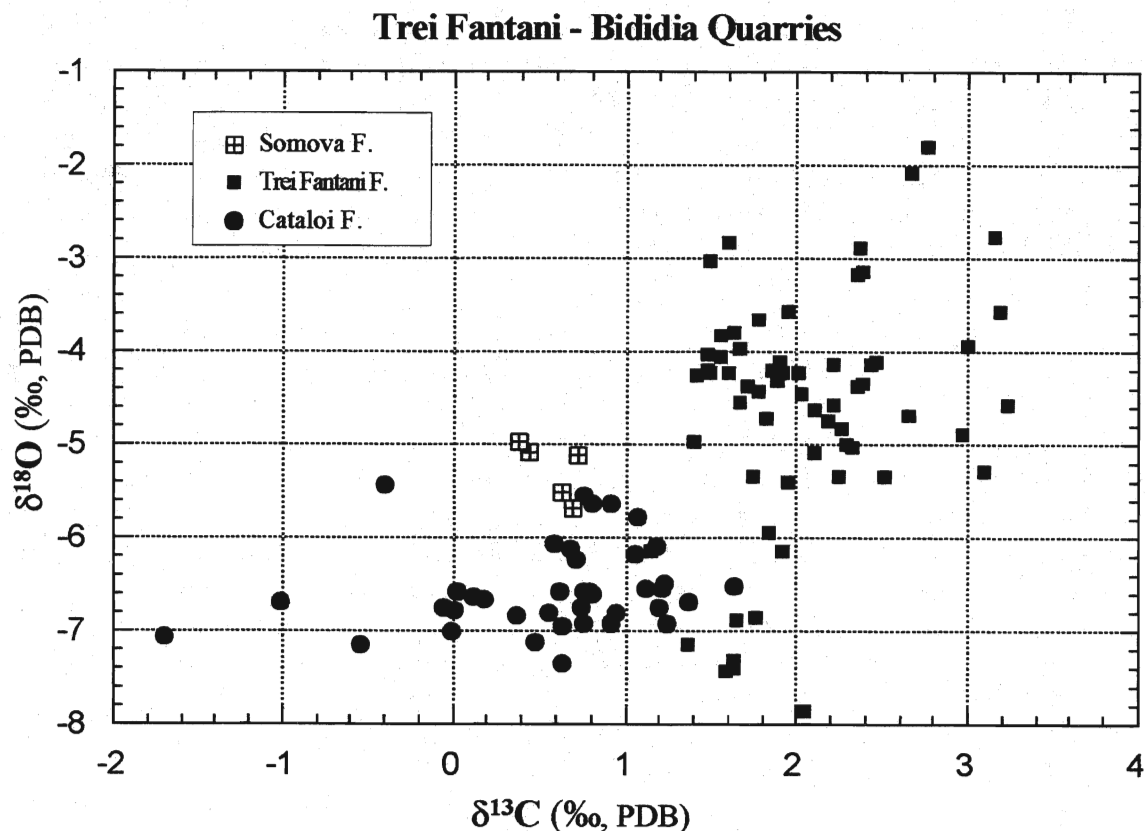


**Fig. 48.**  $\delta^{18}\text{O}$  -  $\delta^{13}\text{C}$  cross-plot for Trei Fântâni and Bididia sections.

In summary, the carbon isotope profile from the Trei Fântâni-Bididia quarries section show variations which coincide with a major lithological change from deep-water pelagic sediments to basinal, anoxic sediments, therefore interpreted as diagenetic in origin (as discussed in detail in subchapter 6.3.1.).

### 6.2.4. Other localities

Some additional analysis have been performed on samples collected from some other localities. They are not presented in detail because they are either too isolated, either do not bring relevant information. Samples collected from Upper Anisian and the Ladinian of the Cataloi Formation at the **Cataloi** village section - the classical section described by Kittl (1908), Simionescu (1925) and Mirauta et al., (1993) - shows the same range of values as at the Trei Fântâni quarry, without any stratigraphic trend.

One sample from the **Tataru Hill**, north of Nicolae Balcescu village, collected from the gray limestones alternating with the basaltic lava flows gave values of +1.1‰ and -12‰ for carbon and oxygen, respectively. The extremely low  $\delta^{18}\text{O}$  value of -12‰ is not surprising as these limestones underwent recrystallisation at elevated temperatures (induced by the lava flows). The evidence that  $\delta^{13}\text{C}$  still preserve marine values provides further confidence in the overall carbon isotope data set. Similar indications are given by another sample collected from the basinal limestones, Early Spathian in age, from the **Tulcea Veche** quarry, with values of +2‰ for  $\delta^{13}\text{C}$  and -10‰ for  $\delta^{18}\text{O}$ . Although isolated, this  $\delta^{13}\text{C}$  value of +2‰ is very important, as the single from undoubtedly Lower Spathian limestones (beds with *Tirolites cassianus*) and shows to be in the same range of values than the Spathian limestones from Dealul Pietros (section I).

## 6.3. Interpretation of the carbon and oxygen stable isotope data

Overall, the  $\delta^{13}\text{C}$  values show a wide range of variation, between -2‰ and +5‰, most of them varying between +2‰ and +4‰, within the range of variation for marine carbonates (Anderson and Arthur, 1983). The range of variation of  $\delta^{13}\text{C}$  values from void and fissure filling cements is similar, which imply that these cements resulted from dissolution and reprecipitation of marine carbonates (Dickson and Coleman, 1980).  $\delta^{18}\text{O}$  values vary between -1.5‰ and -8‰, mostly within -2‰ and -5‰. The latter interval roughly corresponds with the values measured on Triassic aragonitic shells (Scherer, 1977), aragonitic muds (Loreau et al., 1995), well preserved calcitic brachiopods shells (Veizer, 1997) and calcite cements (Frisia-Bruni et al., 1989). However, the  $\delta^{18}\text{O}$  values obtained from whole-carbonates can hardly be interpreted as primary (not overprinted by diagenetic processes).

### 6.3.1 Carbonate platform versus basin isotopic signatures

Figure 49a displays the  $\delta^{18}\text{O}$  -  $\delta^{13}\text{C}$  cross-plot,  $\delta^{18}\text{O}$  -  $\delta^{13}\text{C}$  pairs being presented according to various major depositional environments. The same data-set is represented in figure 49b according to the measured profiles. The major feature revealed by both diagrams is a strongly marked facies related bimodal distribution of  $\delta^{18}\text{O}$  -  $\delta^{13}\text{C}$  pairs. While carbonate platform and pelagic carbonates have  $\delta^{13}\text{C}$  values generally higher than +1‰, the lowest  $\delta^{13}\text{C}$  values, comprised in the range of -1‰ to +1‰, are recorded in the basinal sediments of the Cataloi Formation. Hence, the basinal facies and the various carbonate platform to pelagic facies are isotopically distinguishable. In contrast, the carbon isotopic signature of shallow water carbonates and deep water pelagic carbonates is almost identical. The lower  $\delta^{18}\text{O}$  values recorded by some deep pelagic carbonates appears to be related to burial diagenesis, which apparently did not affected carbon isotope ratios.

The lower  $\delta^{13}\text{C}$  values recorded in the Cataloi Formation are most likely related to the presence of organic material in this sediments which also indicate an oxygen-deficient depositional and diagenetic environment. The modern anoxic basins (as the Black Sea) are characterized by  $^{13}\text{C}$  depleted bottom waters, which result

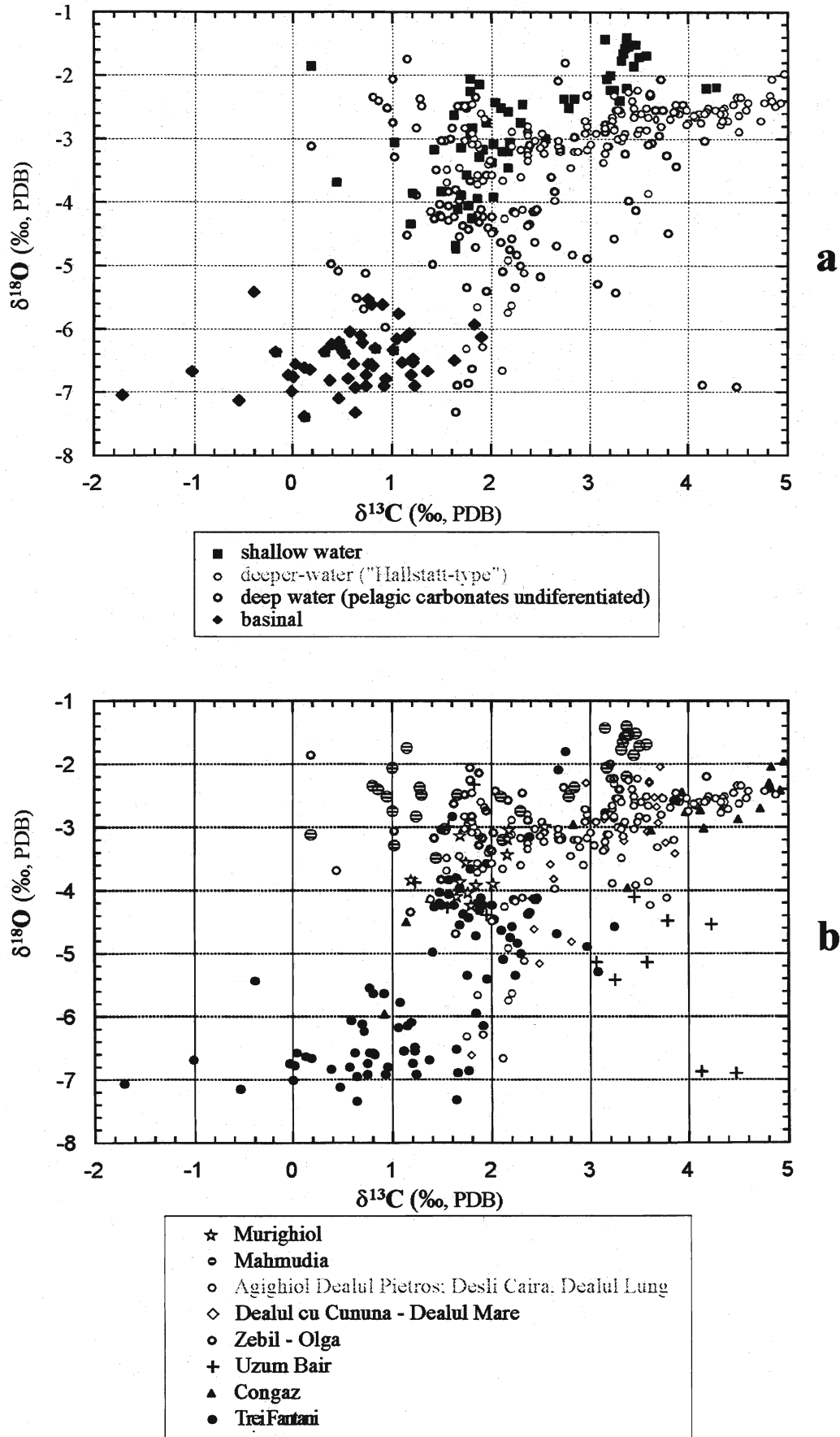


**Fig. 49** Cross-plot of carbon and oxygen isotopic data from Triassic carbonates of North Dobrogea. Pairs of  $\delta^{13}\text{C}$  and  $\delta^{18}\text{O}$  values are plotted according to the main depositional environments (a) and to the sections from which they derive (b).  
depositional environments (a) and to the sections from which they derive (b).

in a surface to deep water  $\delta^{13}\text{C}$  gradient up to 7‰ (Deuser 1970), significantly higher than in the well mixed global ocean - where it is about 2‰ (Kroopnick, 1980). One may expect this gradient to be partly recorded in carbonate sediments, as in deep water sediments, in addition to the carbonate formed in surface waters there may be a fraction of  $^{13}\text{C}$  depleted carbonate formed at greater depth (Berger and Vincent, 1986), which would explain the lower  $\delta^{13}\text{C}$  values of the Cataloi Formation. The scattered distribution of  $\delta^{13}\text{C}$  suggest, however, another (or an additional) explanation of  $\delta^{13}\text{C}$  lowering. Anoxia may be responsible for departures of  $\delta^{13}\text{C}$  values of carbonates by the mean of early diagenesis (Deines, 1980). Anoxic degradation of organic carbon via bacterial sulfate reduction result in porewaters depleted in  $^{13}\text{C}$  (Pisciotta and Mahoney, 1981). These porewaters are highly alkaline (Morse and Mackenzie, 1990), which can cause precipitation of carbonate minerals (Bernier, 1971). The process may involve also dissolution and reprecipitation of the pre-existent carbonate. The resultant carbonate will be depleted in  $^{13}\text{C}$  relative to his precursor, in an extent dependent of various factors such as sulfate reduction rate, sedimentation rate and organic carbon content. Because of the big difference between the anoxic porewaters  $\delta^{13}\text{C}$  values and carbonate carbon, only a small amount of new added carbonate would be sufficient to shift whole-rock carbonate  $\delta^{13}\text{C}$  values.

A similar mechanism could be responsible for the lower  $\delta^{13}\text{C}$  values of the Cataloi Formation, which are organic-rich and undoubtedly suffered anoxic early diagenesis. The stratigraphically scattered distribution of  $\delta^{13}\text{C}$  support such a hypothesis, as the whole process is not expected to shift uniformly the whole mass of sediments (particular conditions may occur for each layer). The same scenario may explain also the lower  $\delta^{18}\text{O}$  values, as the organic matter decomposition in the sulfate reduction zone may results in a  $^{18}\text{O}$  depleted porewaters Sass et al., (1991), although it is questionable whether whole-rock  $\delta^{18}\text{O}$  values can be shifted accordingly to values down to -7‰.

An alternative possibility is to invoke recrystallization during burial diagenesis (e.g. Choquette and James, 1990), which can explain the low and relatively narrow range of variation of  $\delta^{18}\text{O}$  values (-6‰ to -7‰), consistent with the evidence brought by conodonts Color Alteration Index. The CAI is generally low for most of the platform and pelagic sediments, from 1 to 2 on Epstein's (1977) scale, and higher for the basinal deposits of the Cataloi Formation (3 to 4) which indicate a more severe thermal history for the Trei Fântâni-Bididia quarry section. All carbonates occurring at the Trei Fântâni quarry have  $\delta^{18}\text{O}$  values lower than in other sections, therefore the burial diagenesis is likely to be responsible for the low  $\delta^{18}\text{O}$  values. Thus, if the carbon isotope pattern may be easier explain by early diagenetic processes, the low oxygen isotope values can be directly linked to burial diagenesis. A combination of early diagenesis (which shifted  $\delta^{13}\text{C}$  values by +1‰ to +3‰) and burial diagenesis (that affected mainly  $\delta^{18}\text{O}$  values) is the scenario favoured herein in order to explain the bimodal distribution of  $\delta^{18}\text{O}$  -  $\delta^{13}\text{C}$  pairs.

Importantly, not all organic-rich carbonates from Dobrogea show low  $^{13}\text{C}$  values. The limestones of the Dealul Lung Formation are also rich in organic matter and pyrite and likely suffered anoxic early diagenesis. Still,  $\delta^{13}\text{C}$  values are relatively high and identical to the underlying "oxic" carbonates. The same holds true for the Congaz Formation, which is organic-rich and has  $\delta^{13}\text{C}$  values higher than the overlying red limestones. The single  $\delta^{13}\text{C}$  value measured on a sample from the basinal sediments of the Tulcea Veche Formation is of 2‰, while  $\delta^{18}\text{O}$  is as low as -10‰! In turn, the black limestones from the top of the Marelb Formation have  $\delta^{13}\text{C}$  values lower than the average of the contemporaneous sediments. Therefore, no single scenario can explain the relatively wide variations encountered in dobrogean Triassic carbonates. There is no doubt, however, that organic-rich sediments have to be considered "suspect" in the absence of independent criteria to show that diagenesis did not affect their isotopic composition significantly.

### 6.3.2. The preservation of the stable isotope record

Excepting the lowering of  $\delta^{13}\text{C}$  values observed in the Cataloi Formation, most likely resulting from a diagenetic overprint as discussed above, there are some geochemical indicators which suggest that alteration of primary marine values may have affected also the remainder of the samples. For many individual section there is a covariance between  $\delta^{13}\text{C}$  and  $\delta^{18}\text{O}$  values and trace element data are out of normal range of variation for marine carbonates. This is a very intriguing aspect as the Triassic carbonates from North Dobrogea do not show any direct evidence for meteoric diagenesis, which should be invoked to explain both  $\delta^{13}\text{C}$  and  $\delta^{18}\text{O}$  covariance and strontium concentration depletion. In contrast, field observations, conodonts CAI and other geochemical data suggest that these carbonates (with some exceptions) preserved the primary composition.  $\delta^{13}\text{C}$  values are typical marine;  $\delta^{18}\text{O}$  values, although can be hardly interpreted as primary, are within the range reported for Triassic marine values; importantly the  $^{87}\text{Sr}/^{86}\text{Sr}$  are also within (or close of) the range of the Triassic seawater. Can be imagined a diagenetic process that would delete the original Sr concentration but still preserve the  $^{87}\text{Sr}/^{86}\text{Sr}$  ratio?

#### *Insights from trace elements concentrations*

Trace elements concentrations from the same samples were carried out by Sofia Zerrari (Université Paris VI). One of the most surprising feature revealed by trace elements geochemistry is that for some elements concentrations are out of the range commonly reported for seawater (Renard and Zerrari, 1997; Zerrari, in preparation). For example, most of the strontium concentrations are lower than 200 ppm. Because strontium concentrations in the modern carbonate sediments (as well as the majority of ancient carbonates) are higher than 400 ppm, such low concentrations are considered to reflect significant diagenetic overprint; meteoric diagenesis (Veizer, 1983) or continental influence (Renard, 1986) are often invoked in order to explain very low strontium concentrations. The highest Sr contents were measured in limestones of the Cataloi Formation, for which field observations, conodonts CAI and stable isotope data suggest that a more pronounced burial diagenesis. There is little support for freshwater influence; all stable isotope data show typical marine values.

Similar low concentrations have been previously reported from Triassic whole-rocks (Veizer and Demovic, 1974; Carulli et al., 1993); in turn Loreau et al. (1996) reported very high strontium concentration (up to 20.000 ppm) from Middle Triassic aragonite muds.

The Dealul Lung section provide some evidence for a decoupling between stable isotopes and trace elements patterns. The sharp contact between the Agighiol Limestone and the Dealul Lung Formation (from oxic to anoxic in terms of paleoenvironment) is marked by a sharp shift in strontium and manganese concentrations (among others), while both  $\delta^{13}\text{C}$  and  $\delta^{18}\text{O}$  values remain constant. This evidence suggest that the factors which caused the bimodal distribution of trace elements concentration (either oceanographic or diagenetic) did not affected carbon and oxygen isotope composition and provides a good argument against a diagenetic overprint of stable isotope composition.

The strongest argument against a diagenetic overprint of  $\delta^{13}\text{C}$  values is provided by the evidence that stratigraphic carbon isotope profiles are correlative and shifts in  $\delta^{13}\text{C}$  values appear to be synchronous. Therefore, the majority of the carbon isotope data are likely to approximate the primary seawater composition.

While the carbon isotopic composition is typically marine and shifts along profiles seemigly record variation in ocean DIC (with some exceptions), the oxygen isotopic composition likely reflect reequilibration with diagenetic fluids. There is strong correlation between the Color Alteration Index of conodonts, which are believed to record the thermal history of the rocks during burial diagenesis or metamorphism (Epstein et al., 1977; Rejebian et al., 1987) and  $\delta^{18}\text{O}$  values. High CAI (on a scale from 1 to

5) indicate that those rocks experienced transformations at elevated temperatures. In North Dobrogea, conodonts recovered from carbonate platform limestones have generally a low CAI (1 to 2) and  $\delta^{18}\text{O}$  values of those limestones are mostly comprised in a range of -2‰ to -4‰. Conodonts from the Cataloi Formation have CAI of 3-4 and the host rock have  $\delta^{18}\text{O}$  values between -6‰ to -7‰. The most "altered" conodonts (with a CAI around 5) have been recovered from limestones interbedded with basaltic lava flow (samples collected from Tataru Hill) and the limestone  $\delta^{18}\text{O}$  values are as low as -12‰. This observation is in agreement with a re-equilibration of oxygen isotope with diagenetic fluids, the resulting  $\delta^{18}\text{O}$  values being lower as the temperature of the fluids is higher.

### 6.3.4. Stratigraphic trends

When comparing the carbon isotope profiles (fig. 50) some similarities are apparent. Two main trends are revealed: a well marked positive carbon isotope excursion across the Olenekian-Anisian boundary and a gentle rise in  $\delta^{13}\text{C}$  values starting in the Upper Ladinian and attaining maximum in Lower Carnian and in the Lower Upper Carnian.

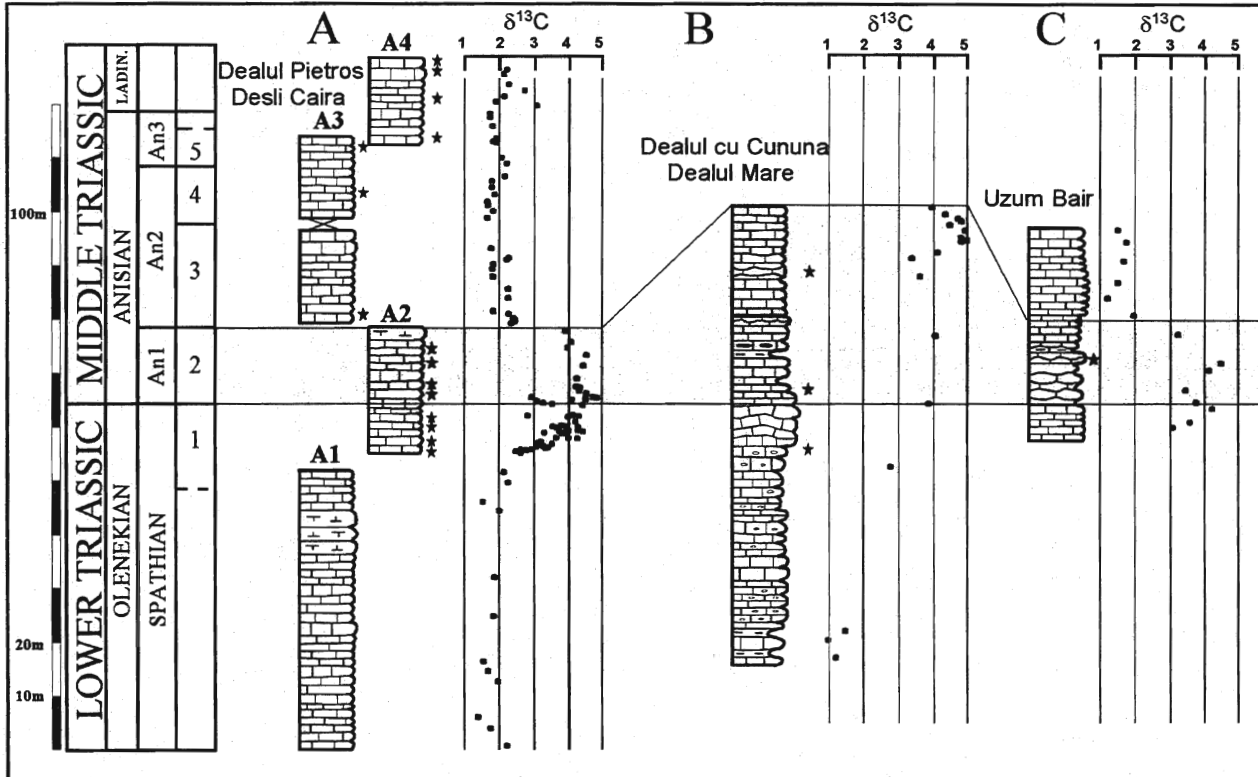
#### *Carbon isotope shifts at the Olenekian/Anisian boundary.*

All examined sections spanning the Upper Olenekian to Anisian time interval display a positive excursion of  $\delta^{13}\text{C}$  values, very well documented in the Agighiol-Desli Caira, Dealul cu Cununa-Dealul Mare and Uzum Bair sections. The biostratigraphic constraints (both ammonoids and conodonts) show that this excursion is perfectly correlative between section in terms of age (Fig.50), which suggest that it reflect variations of seawater chemistry. Its primary origin is further supported by the evidence that it was recorded both in lithologically monotonous sections (Agighiol and Desli Caira) and in sections with highly variable lithologies.

The onset of the rise in  $\delta^{13}\text{C}$  values takes place certainly in the Upper Spathian, most likely in the Uppermost Spathian and the most positive values are attained in the Lowermost Anisian (*Aegeiceras ugra* Zone). The recovery to background values (that are typical to the Lower Spathian and the remainder of the Anisian), takes place somewhere close to the Lower/Middle Anisian boundary. In relation with the conodont faunas, the carbon isotope "anomaly" at least partly overlaps the range of *Chiosella timorensis*, *Neospathodus homeri* and *Neospathodus gondolelloides* and the rise in  $\delta^{13}\text{C}$  values occurs before the first occurrence of *Gladigondolella tethydis*. Also, the backward trend of the carbon isotope profile do not start before the first occurrence of *Gondolella regalae*. This latter species have not been recognized in the samples from Desli Caira prepared for this study, but it was reported from in the upper part of the Desli Caira section (Mirauta, personal communication) and also found in the Dealul Mare section, in limestones characterized by high  $\delta^{13}\text{C}$  values..

In terms of amplitude, the increase is of 2.5‰ in Hallstatt-type limestones, and more than 3‰ in Dealul cu Cununa-Dealul Mare and Uzum Bair sections. It is likely that the former approximate better the magnitude of the shift in seawater DIC, because in the two other sections the amplitude may have been amplified by changes in depositional environment or facies related variable diagenetic overprint.

The significance of the carbon isotope excursion across the Olenekian/Anisian boundary will be discussed in the last chapter. In North Dobrogea there is no evidence for geological events (relevant to this issue) to precisely match the excursion time-interval. This is not surprising as carbon isotope excursions, if global, should primarily reflect global changes in the major carbon reservoir partitioning (Holser, 1997), which are not necessarily recorded worldwide as sedimentary events. However, its potential utility for stratigraphic correlation is apparent from the data-set presented herein.

**Fig. 50**

Plot of  $\delta^{13}\text{C}$  data against thickness for three composite sections covering the Late Olenekian to Late Ladinian time interval. Subdivisions in the time scale column correspond to section A and are based on ammonoids recovered from stratigraphically successive levels (stars). Numbers refer to ammonoid biozones identified in section A. 1. *Procarnites* Zone; 2. *Aegeiceras ugra* Zone; 3. *Kocaelia* Zone; 4. *Balatonites balatonicus* Zone; 5. *Paraceratites* Zone. A. Composite section made up exclusively by red pelagic limestones. A1. Dealul Pietros I. A2. Dealul Pietros II. A3. Dealul Pietros III. A4. Dealul Pietros III. B. Dealul cu Cununa - Dealul Mare section. C. Uzum Bair section. The shaded area represents the extent of Lower Anisian sediments on the basis of biostratigraphic data (ammonoids and conodonts). In North Dobrogea, and perhaps throughout the Tethys, the base of the Anisian is marked by the first appearance of the ammonoids *Aegeiceras ugra*, *Japonites welteri* and *Paracrochordiceras*, and the conodont *Gladigondolella* (see also Orchard and Tozer (1997) for the North American Triassic biochronology).

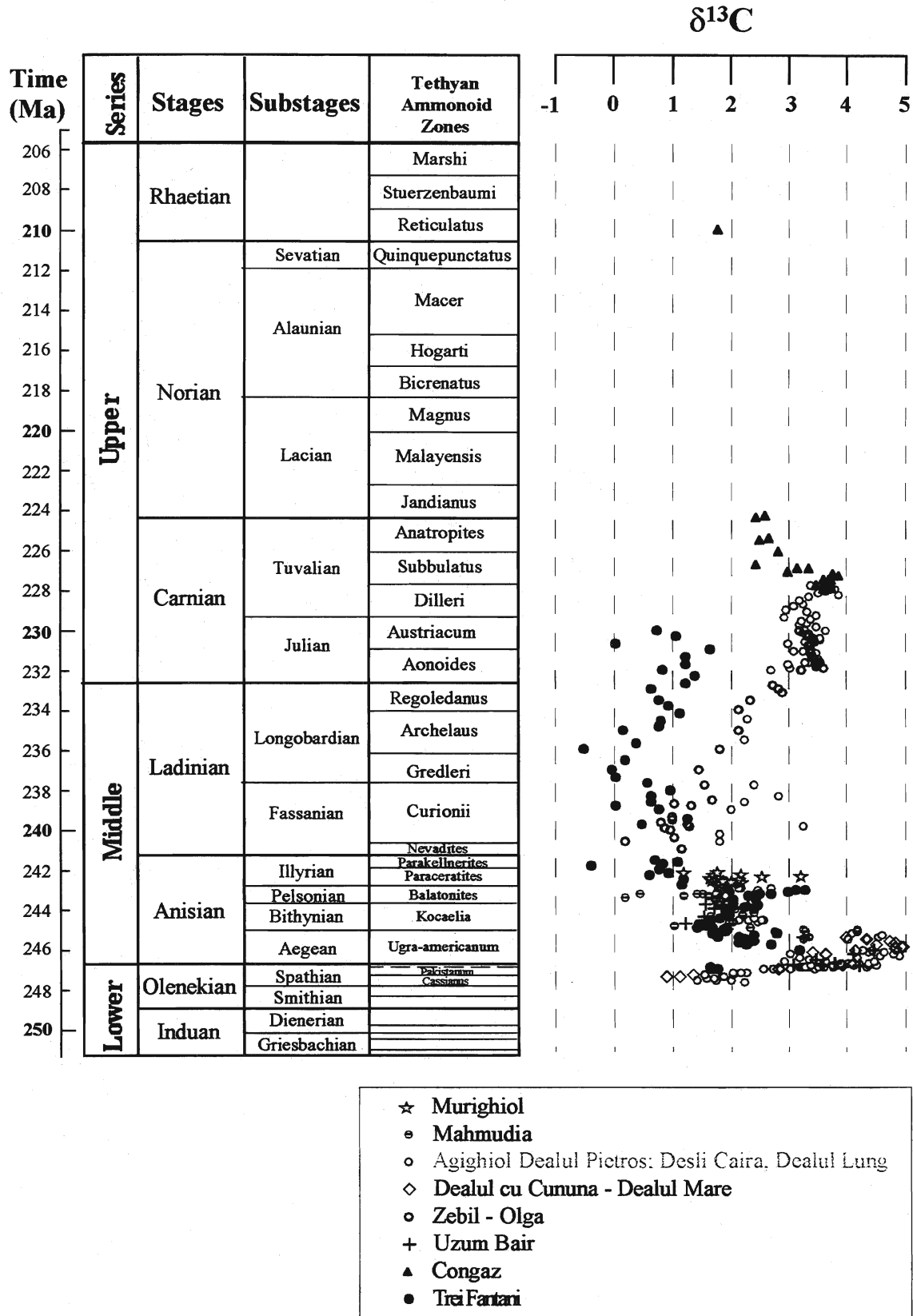
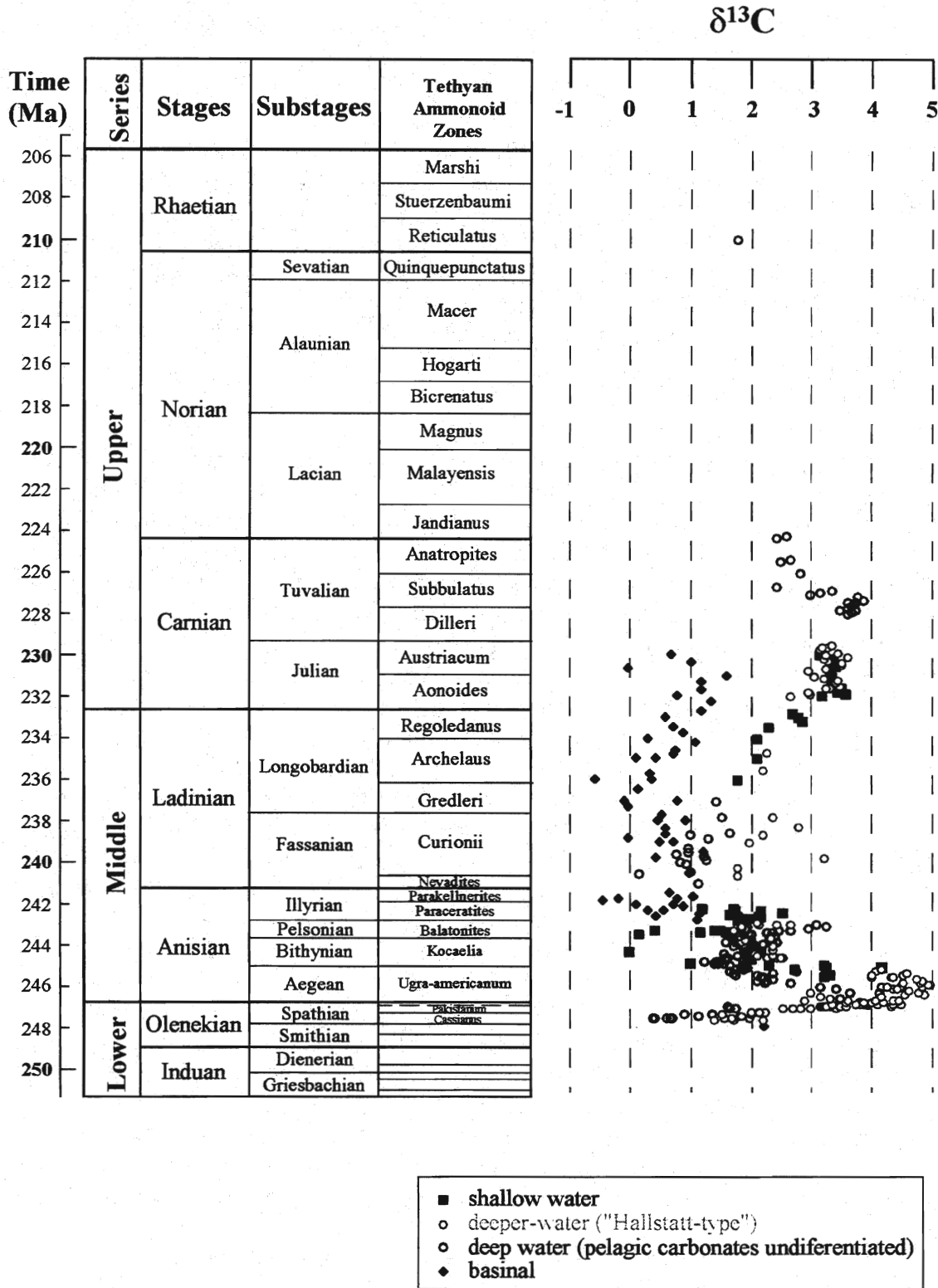


Fig. 51 Secular variations of  $\delta^{13}C$  values of Triassic carbonates from North Dobrogea  
The colors represent the various sections examined





**Fig. 52** Secular variations of  $\delta^{13}\text{C}$  values of Triassic carbonates from North Dobrogea  
The colors represent various depositional environments

From the set of samples analysed from North Dobrogea (over 400),  $\delta^{13}\text{C}$  values higher than +4‰ were obtained only in lower Anisian limestones and for the Middle and Upper Anisian values higher than 3‰ are rarely present (fig. 51). In the light of these observations, one may question whether the high values measured in the limestones from the base of the Mahmudia quarry are not related to the Lower Anisian positive "anomaly". Certainly, carbon isotope stratigraphy within the Triassic is only in its "incipient" phase and this would be one of the first applications. The same reasoning may be followed for the base of the Trei Fântâni Formation occurring in the Trei Fântâni quarry, just above the dolomites. Here, the samples from the lower part gave values around +3‰ and display a downward trend which, at a first glance, may represent the recovery part of the Lower Anisian positive excursion. As it was shown in a previous part of the manuscript, the carbon isotope record of the Trei Fântâni quarry is among the less reliable from North Dobrogea and therefore, this interpretation may be too speculative; however, the existent biostratigraphical data do not exclude such a possibility (nor it confirm).

#### *Carbon isotope trends from Middle Anisian to Upper Carnian*

Following the Upper Olenekian-Lower Anisian carbon isotope excursion, the Middle and Upper Anisian is characterized by relatively constant  $\delta^{13}\text{C}$  values, around 2‰ with no visible trend and regardless the depositional environment (Fig. 52). The Ladinian segment is not well constrained by data, mainly because in the examined sections Ladinian deposits are either condensed, either poorly dated. Consequently the precise age rating for Ladinian samples is sometimes questionable; the errors in age rating do not give, however, potential misleading trends. Acknowledging the problem of poor age control, one may observe a general trend of increase in  $\delta^{13}\text{C}$  values starting from the base of the Upper Ladinian. This trend results from the Dealul Pietros-Dealul Lung and Zebil-Olga profiles. Both sections exhibit a shallowing upward trend which is correlative with the increase in  $\delta^{13}\text{C}$  values. Two alternatives are considered for explaining the correlation between the two parameters.

The first one relates the increasing  $\delta^{13}\text{C}$  values to decreasing paleobathymetry (see chapter 3), assuming that the surface to deep gradient may be recorded by sediments. It is to note here that in the Zebil-Olga section the amplitude of the rise is higher, the background values being lower than in Agighiol ("Hallstatt") section. These lower values correspond to organic matter rich limestones and may be due to the addition of diagenetic  $^{13}\text{C}$  depleted cement resulted from the degradation of organic matter. However, the general increasing trend is not affected even if we discard these "suspect" values, the increase being restricted to limestones devoid of organic matter (the upper part of Zebil Quarry Formation), which do not show any indication of diagenetic overprint. Considering the whole data dobrogean data-set, the correlation of  $\delta^{13}\text{C}$  values with the depositional water depth is not systematic. In the Anisian, for instance, all environments tested showed similar carbon isotope signatures. Therefore, this alternative appears to be unlikely.

The second alternative explains the increase in  $\delta^{13}\text{C}$  values as reflecting a primary increase of shallow water  $\delta^{13}\text{C}$  values of DIC. The primary increase in  $\delta^{13}\text{C}$  values is not necessarily a direct consequence of sea level changes, they might have been driven by a common causal factor, possibly related to the climate.

The carbon isotope profile from the Cataloi Formation also show an increasing trend from the Upper Ladinian to Carnian. This is a quite surprising feature as these limestones undoubtedly carry a diagenetic component in their carbon isotopic signature, as explained in subchapter 6.3.1. It might be a simple coincidence or maybe, despite diagenesis, a primary trend has been conserved.

The Lower Carnian and Lower Upper Carnian sediments are characterized by relatively high  $\delta^{13}\text{C}$  values, between 3‰ and 4‰, regardless the carbonate facies. Wetterstein-type shallow water limestones, Hallstatt-type limestones, organic rich limestones, all gave about the same  $\delta^{13}\text{C}$  values, which proves to be a strong argument for a primary feature of the seawater. There is a trend of lowering in  $\delta^{13}\text{C}$  values in the Upper

Carnian, as recorded by the limestones of the Congaz Formation. As noted in the description of the Congaz section the lowering in  $\delta^{13}\text{C}$  values is correlated with a change in lithology and a correlative lowering of  $\delta^{18}\text{O}$  values. In the absence of other data from different profiles for the same time interval the origin of this trend cannot be well evaluated.

## 6.4. Strontium isotope data

### 6.4.1. Samples

Strontium isotope analyses have been undertaken using both carbonates and conodonts with predominantly low Color Alteration Indices. From the total number of 25 samples measured, 11 are whole-rock carbonate, two are stromatolite-type void fillings and 12 conodonts. Pairs of  $^{87}\text{Sr}/^{86}\text{Sr}_{\text{conodonts}}$  and  $^{87}\text{Sr}/^{86}\text{Sr}_{\text{bulk carbonate}}$  are available for seven samples. Sample preparation and analytical methods are described in chapter two. While carbonate samples are routinely measured, conodont samples require some special preparation because of their extremely small size and limited abundance. Rubidium and strontium concentrations were also measured by ICP-MS. For the conodont samples they could be only roughly approximated because of sample weight uncertainties (the samples weights were between 100 $\mu\text{g}$  to 400 $\mu\text{g}$  and could not be precisely measured). However, the Sr/Rb (as a ratio of absolute concentrations) data are reliable.

### 6.4.2. Results

#### *Whole rock data*

The samples for whole rock analysis were selected mainly from the Hallstatt-type limestones (7 samples), which have proved to be suitable for carbon and oxygen isotope analysis and whose age is well constrained biostratigraphically. Four other samples have been selected from Cataloi Formation (1), Mahmudia Formation (1), Enisala Limestone (1) and Dealul Lung Formation (1) in order to cover a larger range of depositional environments.

The  $^{87}\text{Sr}/^{86}\text{Sr}$  data of bulk carbonates and cements are presented in Table 2, together with information concerning sample provenance.  $^{87}\text{Sr}/^{86}\text{Sr}$  ratios vary over a wide range between 0.7078 and 0.7085. The range of the  $^{87}\text{Sr}/^{86}\text{Sr}$  values in whole-rock carbonates is similar to and more radiogenic than that expected from precipitation for Middle Triassic seawater (Koepnick et al., 1990). The two cement values and only four of the bulk carbonate data are similar to that expected from precipitation from Middle Triassic seawater (Koepnick et al., 1990), the remainder of bulk carbonate values being significantly more "radiogenic". Therefore the  $^{87}\text{Sr}/^{86}\text{Sr}$  ratios for most of samples were possibly shifted during diagenesis, as it is also suggested by the scatter of results.

Previous studies demonstrated that deviations from the original  $^{87}\text{Sr}/^{86}\text{Sr}$  signal are accompanied by systematic changes in trace-element concentrations (e.g. Brand and Veizer, 1980; Denison et al., 1994; Banner, 1995). Denison et al., (1994), for instance, suggested that the most relevant elements are Sr, Mn and Fe and that samples with more than 900 ppm Sr and less than 300 ppm Mn and 3000 ppm Fe, are likely to record original seawater  $^{87}\text{Sr}/^{86}\text{Sr}$  ratios. As a matter of facts, the limestones from Dobrogea have very low Sr concentrations, mostly lower than 200 ppm, much lower than the 900 ppm threshold. In turn, the Mn and Fe contents are well within the range of "likely unaltered" samples, with contents lower than 200 ppm for Mn and lower than 800 ppm for Fe. Sr and Mn contents are very similar, resulting in Sr/Mn ratios close to one, while Denison and colleagues suggested that likely "unaltered samples" should have Sr/Mn ratios higher than two. Therefore, the trace element data are somehow contradictory: the low Sr concentrations indicate alteration, whereas Fe and Mn contents suggest good preservation.

It is well known that higher  $^{87}\text{Sr}/^{86}\text{Sr}$  ratios can also result from the addition of  $^{87}\text{Sr}$  resulted from  $^{87}\text{Rb}$  decay. The older the rocks and the lower Sr/Rb ratio, the higher is the deviation to more radiogenic values. If the addition of radiogenic Sr from Rubidium decay may be important for Precambrian rocks, for Mesozoic it is considered insignificant, as Sr concentrations in sedimentary rocks greatly exceed Rb concentrations and little "young" radiogenic Sr could be produced in only a few hundred million years (McArthur, 1994). The limestones from Dobrogea have relatively low Sr/Rb ratios and the contribution of radiogenic Sr from Rubidium decay could be significant. Some corrections can be applied to minimize the effect of radiogenic Sr resulted from Rb decay, but such corrections bring uncertainties in the data set and are not recommended (Stille and Shields, 1997).

There is no correlation between the bulk carbonate  $^{87}\text{Sr}/^{86}\text{Sr}$  ratios and either  $\text{CaCO}_3$  and Sr contents,  $\delta^{13}\text{C}$  or  $\delta^{18}\text{O}$  values (Fig. 53a, b, c and d). The lack of correlation between  $^{87}\text{Sr}/^{86}\text{Sr}$  ratios and C and O isotopes suggests that if any diagenetic processes affected strontium isotopes, it did not affect significantly C and O isotopes. Both stromatactis void filling cements gave values within the seawater band, which suggest they precipitated during early diagenesis, from fluids dominated by seawater.

#### *Conodont data*

Conodont samples have been selected mostly from ammonoid levels in order to have good stratigraphic control. Only conodonts with a Color Alteration Index lower than 2 have been analyzed, as previous studies had shown that conodonts with higher CAI gave less reliable  $^{87}\text{Sr}/^{86}\text{Sr}$  values (Keto et al., 1987; Bertram et al., 1992; Cummins and Elderfield, 1994).

Additional information concerning the samples and  $^{87}\text{Sr}/^{86}\text{Sr}$  data are presented in Table 3. Two of them (AG1 and CG5) have been donated by Prof. E. Gradinaru, the others have been extracted during the present work. The  $^{87}\text{Sr}/^{86}\text{Sr}$  values vary from 0.7083 to 0.078, a range smaller than for bulk carbonate data. Conodont  $^{87}\text{Sr}/^{86}\text{Sr}$  ratios are consistently lower than their (uncorrected for  $^{87}\text{Rb}$  contribution) bulk carbonate counterparts and, with the exception of the Lower Anisian samples, all are within the Triassic seawater band. There is a positive correlation between  $^{87}\text{Sr}/^{86}\text{Sr}$  ratios from conodonts and  $^{87}\text{Sr}/^{86}\text{Sr}$  ratios for bulk carbonates (fig. 53e); this correlation is due to a stratigraphic trend, as will be shown bellow.

Sr/Rb ratios for conodont samples are much higher than for carbonates, generally higher than 1000, and the corrections for  $^{87}\text{Sr}$  resulted from  $^{87}\text{Rb}$  decay are insignificant relative to analytical uncertainties. Only one sample has a low Sr/Rb ratio (sample D9042); however the correction which must be applied amounts to 0.00005, which is minor compared to the overall range of variation of conodont data.

#### **6.4.3. Stratigraphic trends**

The plot of the  $^{87}\text{Sr}/^{86}\text{Sr}$  data from Dobrogea against the Triassic timescale (fig. 54) displays a stratigraphic trend consistent with previously published Triassic strontium isotope curves (Burke et al., 1982; Koepnick et al., 1990) for both bulk carbonate and conodont data. The  $^{87}\text{Sr}/^{86}\text{Sr}$  ratios decrease gradually from the Upper Spathian-Lower Anisian boundary interval to the Middle Carnian. An isolated conodont sample from the Rhaetian has a  $^{87}\text{Sr}/^{86}\text{Sr}$  ratio considerably higher than the average of the Middle Triassic ratios. While the bulk carbonate data are scattered and the decreasing trend is relatively poorly defined, the conodont data are remarkably well aligned and the decreasing trend is very well constrained.

There is a close (remarkable!) juxtaposition of  $^{87}\text{Sr}/^{86}\text{Sr}$  ratios in samples of the same age. For example, two samples from the same ammonoid biozone but different locations (R95-224 and D9058, both coming from beds with *Paraceratites*) gave identical  $^{87}\text{Sr}/^{86}\text{Sr}$  value of 0.70796, and they overlap in figure 54. The

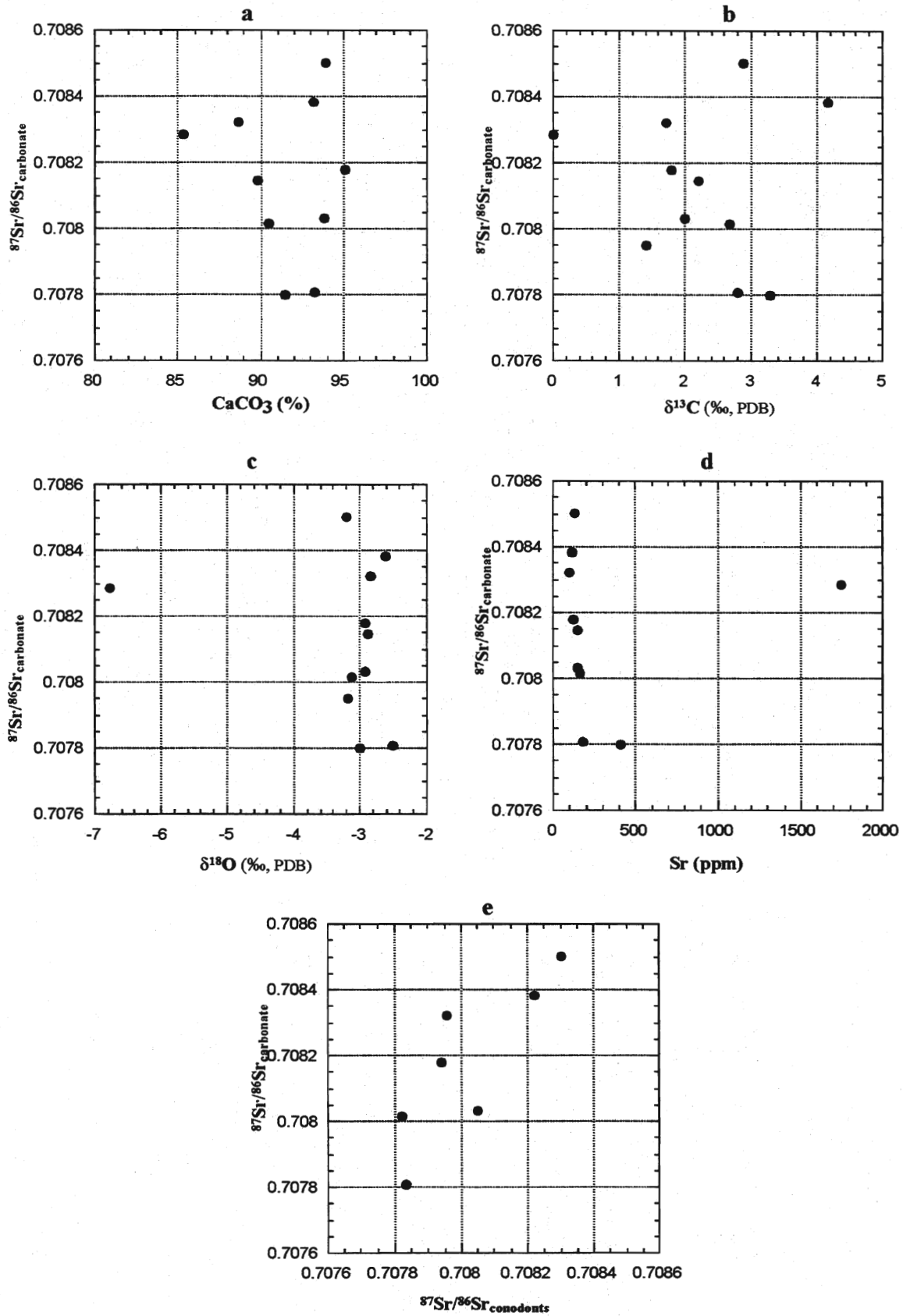


**Fig. 53** Plots of  $^{87}\text{Sr}/^{86}\text{Sr}$  ratio in carbonates versus  $\text{CaCO}_3$  content (a),  $\delta^{13}\text{C}$  values of carbonates (b),  $\delta^{18}\text{O}$  values of carbonates (c), Sr concentrations of carbonates (d) and  $^{87}\text{Sr}/^{86}\text{Sr}$  ratio of conodonts (e).

Sample	Locality	Comments	Relative age <i>Ammonoid zone</i>	Age rating	CaCO <sub>3</sub> (%)	Sr (ppm)	<sup>87</sup> Sr/ <sup>86</sup> Sr	2σ
D9042	Desli Caira	Hallstatt-type limestone	Upper Spathian (" <i>Procarinites</i> " zone)	246.8	94	129	0.70850	10
D9049	Desli Caira	Hallstatt-type limestone	Lower Anisian ( <i>ugra</i> zone)	246	93	116	0.70838	8
R95-77	Mahmudia.	mudstone (mud-mound)	Middle Anisian (? <i>Balatonites</i> zone)	243.2	n.d.	n.d.	0.70795	10
R95-77	Mahmudia.	"stromatactis" cement	Middle Anisian (? <i>Balatonites</i> zone)	243.2	n.d.	n.d.	0.70807	11
D9055	Dealul Pietros	Hallstatt-type limestone	Upper Anisian ( <i>Paraceratites</i> zone)	242.6	94	147	0.70803	10
D9055	Dealul Pietros	"stromatactis" cement	Upper Anisian ( <i>Paraceratites</i> zone)	242.6	n.d.	n.d.	0.70805	14
R95-224	Dealul Pietros	Hallstatt-type limestone	Upper Anisian ( <i>Paraceratites</i> zone)	242.5	88.7	96	0.70832	7
D9063	Dealul Pietros	Hallstatt-type limestone	Upper Anisian-Lower Ladinian	241	95.1	124	0.70818	11
D9067	Dealul Pietros	Hallstatt-type limestone	Upper Ladinian ( <i>currioni</i> zone)	239	89.8	144	0.70815	8
R95-358	Bididia	"basinal" limestone	Ladinian	237	85.2	1750	0.70828	13
D9072	Dealul Pietros	Hallstatt-type limestone	Lower Carnian ( <i>aonooides</i> zone)	232	90.4	160	0.70802	11
D9033	Zebil.	bioclastic limestone	Upper Ladinian - Lower Carnian	233	93.2	183	0.70781	8
DL206	Dealul Lung	black limestone	Upper Carnian ( <i>dilleri</i> zone)	229	91.4	405	0.70780	11

Table 2 *Sr isotope (<sup>87</sup>Sr/<sup>86</sup>Sr) data for the carbonate samples*

Sample	Locality	Relative age <i>Ammonoid zone</i>	Age rating (M.a.)	Sr/Rb (conc.)	$^{87}\text{Sr}/^{86}\text{Sr}$	2 $\sigma$
D9040	Desli Caira	Upper Spathian ("Procarinites" zone)	246.9	3200	0.70829	8
D9042	Desli Caira	Upper Spathian ("Procarinites" zone)	246.8	180	0.70831	11
D9049	Desli Caira	Lower Anisian ( <i>ugra</i> zone)	246	4300	0.70822	8
AG1	Dealul Pietros	Middle Anisian ( <i>Kocaelia</i> zone) ( <i>hyatti</i> )	245	6400	0.70809	10
D9055	Dealul Pietros	Upper Anisian ( <i>Paraceratites</i> zone)	242.6	720	0.70805	11
D9058	Dealul Pietros	Upper Anisian ( <i>Paraceratites</i> zone)	242.5	8500	0.70796	14
R95-224	Dealul Pietros	Upper Anisian ( <i>Paraceratites</i> zone)	242.5	3200	0.70796	20
D9061	Dealul Pietros	Upper Anisian ( <i>Paraceratites</i> zone)	242	n.d.	0.70797	17
D9063	Dealul Pietros	Upper Anisian-Lower Ladinian	241	1600	0.70794	8
D9033	Zebil q.	Upper Ladinian - Lower Carnian	233	1200	0.70783	11
D9072	Dealul Pietros	Lower Carnian ( <i>aonoides</i> zone)	232	600	0.70782	10
CG5	Congaz	?Rhaetian ( <i>steinbergensis</i> )	210	5100	0.70823	11

Table 3 Sr isotope ( $^{87}\text{Sr}/^{86}\text{Sr}$ ) data and Sr/Rb ratios for conodont samples

two early cements samples have  $^{87}\text{Sr}/^{86}\text{Sr}$  ratios within the trend of conodont data, as do four bulk carbonate values. Importantly, the bulk carbonate samples which fit on the conodont trend have relatively high Sr/Rb ratios and the  $^{87}\text{Rb}$  corrections are minor for these samples. All these features suggest that the decreasing trend of  $^{87}\text{Sr}/^{86}\text{Sr}$  ratios from the Upper Olenekian/Lower Anisian to Carnian reflect primary variations of  $^{87}\text{Sr}/^{86}\text{Sr}$  ratio of the Triassic seawater. The age plot of data from Fig. 54 show that the decrease of  $^{87}\text{Sr}/^{86}\text{Sr}$  ratios was very rapid during the Early and Middle Anisian; however (see McArthur, 1994), the apparently variable rates of variation may be determined by the uncertain estimates of the relative duration of stages and substages, as discussed in chapter 2.

It should be mentioned, however, that despite the very well defined stratigraphic trend which most likely parallels primary variations of seawater, the measured  $^{87}\text{Sr}/^{86}\text{Sr}$  ratios of conodonts do not necessarily represent original seawater values. Previous studies (e.g. Kürschner et al., 1992; Diener et al., 1996; Ebner et al., 1997; Qing et al., 1998) convincingly demonstrated that  $^{87}\text{Sr}/^{86}\text{Sr}$  ratios recorded by conodonts are systematically higher than original seawater as recorded by well preserved brachiopods shells (Popp et al., 1986). This may be due to a diagenetic exchange of conodont strontium with surrounding porewaters and/or carbonate strontium which shifted all the  $^{87}\text{Sr}/^{86}\text{Sr}$  values by a relatively constant degree. This may partly explain why the conodonts from the lowermost Anisian have  $^{87}\text{Sr}/^{86}\text{Sr}$  values out of the seawater trend. It may be also argued that the uppermost Olenekian to lowermost Anisian segment of Koepnick et al., 1990 seawater curve is poorly constrained. Well dated lowermost Anisian sediments are rare and the data set of Koepnick et al., (1990) do not include any paleontologic evidence for this particular time span, which apparently coincide with a major inflexion point of the strontium isotope seawater curve (see below).

The Middle Triassic decrease of  $^{87}\text{Sr}/^{86}\text{Sr}$  ratios is apparent from the previously reported seawater curves and it followed a steep rise of  $^{87}\text{Sr}/^{86}\text{Sr}$  ratios during the Late Permian and the Early Triassic. A large amount of data have been acquired recently by the "Bochum-Ottawa Group" but the totality of Triassic strontium isotope data are not included in the recent paper by Veizer et al., (1997) and no clear trend is visible for the Triassic in their Phanerozoic curve. However, a more comprehensive curve was made available via Internet by the "Bochum-Ottawa Group" on the Geochemical Earth Reference Model site see also Korte et al. (1998). Although the timing of the shifts apparent from this curve cannot be assessed because of the condensed timescale used, similar variations during the Lower and Middle Triassic are clearly delineated, with a sharp inflexion point following the Late Permian to Early Triassic steeply increasing trend.

The data set presented herein, when added to by the conodont based data set for the late Permian and early Triassic of Martin and Macdougall (1995) allow us to constrain the timing that this major inflexion point of the strontium isotope seawater curve. It is restricted to the upper Olenekian as it will be further discussed in chapter 8.

The above mentioned seawater strontium isotope curve of the "Bochum-Ottawa Group" reveals a new feature of the Triassic curve, only vaguely suggested by Koepnick's et al., (1990) data: a relatively broad rise towards more radiogenic values during the Upper Triassic. The single conodont value from the Rhaetian (sample CG5, fig. 54) appears to be consistent with this trend. Certainly, more data are needed for the Upper Carnian and Norian interval in order to confirm this trend.



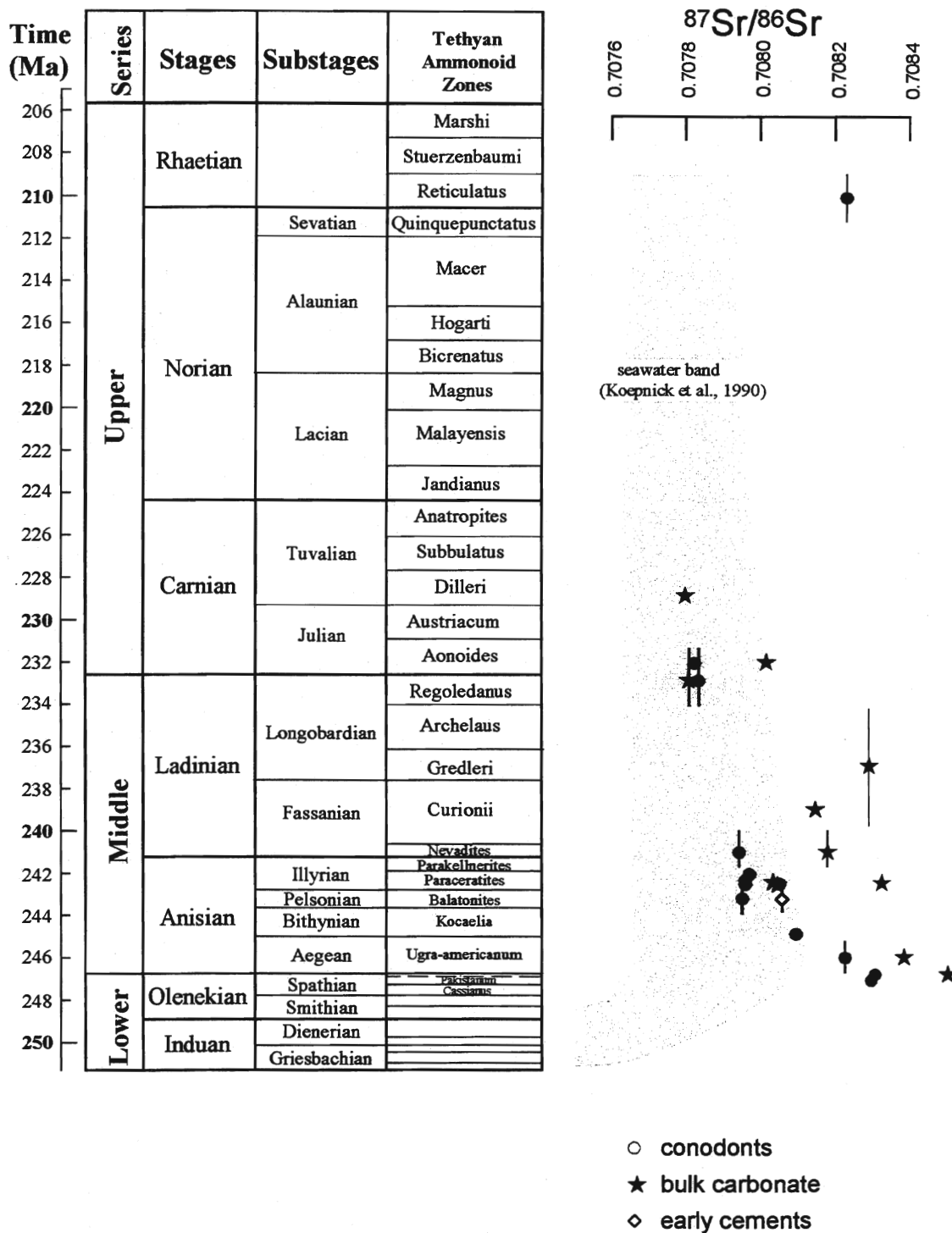


Fig. 54  $^{87}\text{Sr}/^{86}\text{Sr}$  data versus age for conodonts, bulk carbonate and early cements. Vertical bars show the uncertainty in age assignment. The shaded area delineates the seawater band proposed by Koepnick et al. (1990).

## CHAPTER 7

# CONSTRAINTS FROM THE TRIASSIC OF ALBANIA

This short chapter describes the carbon and oxygen isotope data obtained from a section from Albania (Kçira section) during the final stage of preparation of the present work. The samples were kindly provided by Prof. M. Gaetani (Milano).

### 7.1. Kçira section

The interest in analyzing samples from the Kçira section resides in the fact that it is one of the few sections where the Lower/Middle Triassic transition is well constrained by biostratigraphical data, and represents a suitable point of comparison for the stable isotope data set acquired in North Dobrogea in terms of correlation potential. The section is known from the beginning of the century (see Germani, 1997) and it was recently re-examined in detail for biostratigraphy and magnetostratigraphy (Muttoni et al., 1996; Germani, 1997). For location and a more detailed description the reader is referred to these studies.

The samples analyzed come exclusively from the section Kçira A of Muttoni et al. (1996), which comprise a 42m thick sequence of reddish nodular Han-Bulog limestones, which represents a close equivalent of the Hallstatt-type limestones. Biostratigraphical data available for the Kçira section includes ammonoids, conodonts and benthic foraminiferas (Germani, 1997, Nicora and Rettori in Muttoni et al., 1996). Ammonoids are more abundant in the lower part of the section (Spathian in age) and only scarce faunas were recovered from the beds close to the Spathian/Anisian boundary. Therefore, the Spathian/Anisian boundary is defined on the basis of conodonts, it is approximated by the FAD of *Chiosella timorensis*. However, typical lower Anisian ammonoids have not been recovered from the Kçira section. Instead, from beds attributed to the Lower Anisian the *Procarnites kokeni* was identified (Germani, 1997), ammonoid which commonly occur in Spathian beds.

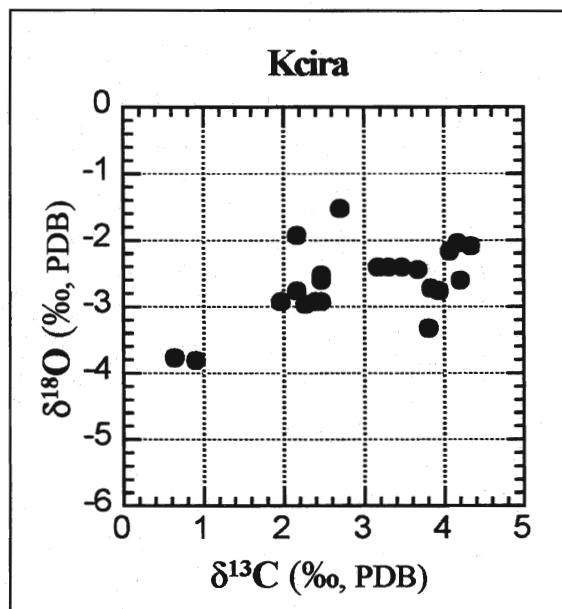


Fig. 55  $\delta^{13}\text{C}$ - $\delta^{18}\text{O}$  cross-plot for the Kçira section (Albania)

27 samples were analysed for carbon and oxygen isotope composition.  $\delta^{13}\text{C}$  values vary between +0.9‰ and +4.2‰ and  $\delta^{18}\text{O}$  values between -3.9‰ and -1.5‰. The  $\delta^{18}\text{O}$  -  $\delta^{13}\text{C}$  cross-plot (fig. 55) show a weak correlation between the two parameters. When plotted against thickness  $\delta^{13}\text{C}$  values display a well defined stratigraphic trend.  $\delta^{13}\text{C}$  values increase gradually from baseline values around +2.2‰ in the 17 meters to values as high as +4.2‰ recorded at meter 24, just above the FAD of *Chiosella timorensis*. Higher-up in the section the  $\delta^{13}\text{C}$  values decrease gradually to the same baseline values around +2‰ in the upper part of the section.

Thus, the carbon isotope excursion displayed at Kçira appears to be correlative with the carbon isotope excursion recorded in Dobrogea across the Lower-Middle Triassic boundary (see chapter 6.3.2) and in Spiti (see chapter 4.4.). It is noteworthy that both  $\delta^{13}\text{C}$  and  $\delta^{18}\text{O}$  values for the Kçira section vary within the same range as in Dobrogea, in similar facies, and  $\delta^{18}\text{O}$  values are relatively low (averaging -2.5‰), close to the values reported from Middle Triassic aragonite (Loreau et al., 1995). Therefore the weak correlation between  $\delta^{13}\text{C}$  and  $\delta^{18}\text{O}$  values (also noted in the Hallstatt-type limestones from Dobrogea) appears to be a surprising feature.

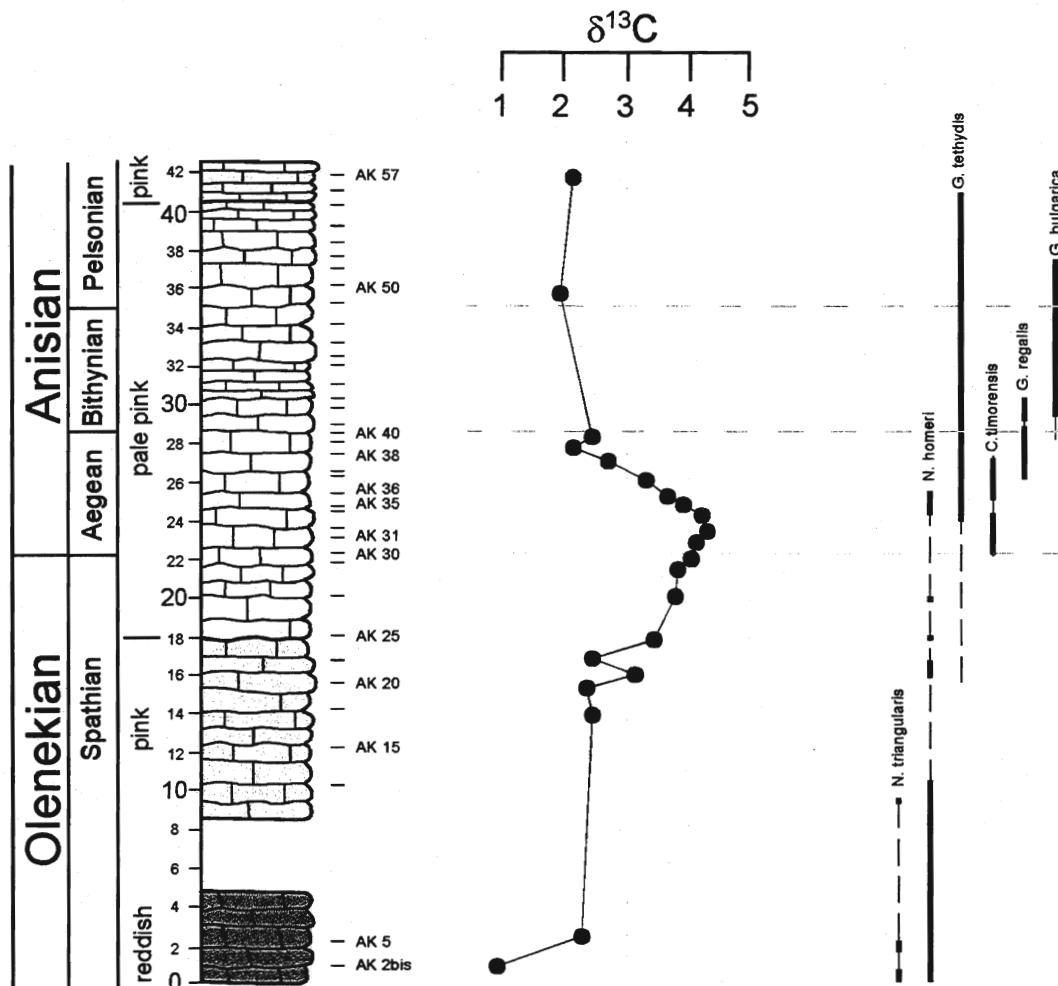


Fig. 56 Carbon isotope profile and conodont biostratigraphy for Kçira section. (conodont biostratigraphy from Nicora in Muttoni et al., 1996).

# CHAPTER 8

## THE UPPER PERMIAN TO UPPER TRIASSIC CARBON ISOTOPE CURVE

### CONCLUSIONS

The data reported in the present study, corroborated with previously published data emphasize new features of the Upper Permian to Upper Triassic carbon isotope curve. Most of the carbon isotope data acquired in the present study are plotted against age in fig. 57 and a tentative  $\delta^{13}\text{C}$  curve is proposed in fig. 58. In addition, data derived from Tethyan carbonates are compiled, specifically data from Baud et al. (1989), Chen et al. (1991) and van Shootbrugge (1997). An evaluation of the major features revealed by the compilation presented in fig. 57 is presented below, following 5 time-windows, selected according to the pattern displayed by the carbon isotope data. These time windows are: the Late Permian, the Permian/Triassic boundary interval, the Early Triassic, the Lower/Middle Triassic boundary interval and the Middle to Late Triassic.

#### 8.1. Late Permian

Previous studies revealed that Upper Paleozoic marine carbonates are characterized by high  $\delta^{13}\text{C}$  values (Keith and Weber, 1964; Veizer et al., 1980; Lindh, 1983; Holser, 1984; Holser and Magaritz, 1987; Popp et al., 1986; Baud et al., 1989a; Grossman, 1994; Scholle, 1995; Veizer et al., 1997a). The Late Permian high  $\delta^{13}\text{C}$  levels is apparently a continuation of a general high level of  $\delta^{13}\text{C}$  values starting in the Carboniferous (Veizer et al., 1980; Holser, 1984; Popp et al., 1986; Grossman, 1994; Scholle, 1995; see fig. 1). However, the compilation by Scholle (1995) revealed that Upper Permian carbonates appears to be particularly enriched in  $^{13}\text{C}$ , with anomalously high  $\delta^{13}\text{C}$  values (as high as +8‰). Thus, a well marked peak is displayed in the Upper Permian (see fig. 2).

The data set from the Tethys (fig. 57) confirm the general high  $\delta^{13}\text{C}$  values levels for the Upper Permian but do not exhibit any marked positive peak in the Upper Permian. Higher  $\delta^{13}\text{C}$  values are observed in the Murgabian (Oman data) and in the Midian (Salt Range data), but considering the whole data set for that time period a positive excursion cannot be unequivocally proposed. It should be mentioned that the positive excursion outlined by Scholle's compilation is characterized by  $\delta^{13}\text{C}$  values as high as +8‰, while data from the Tethys only occasionally exceed +5‰. A re-assessment of the existing  $\delta^{13}\text{C}$  data from the Upper Permian, revealed that the overwhelming majority of anomalously high  $\delta^{13}\text{C}$  values derive from carbonates occurring in evaporitic sequences as in the Delaware Basin (Magaritz et al., 1983), European Zechstein (Magaritz and Turner, 1982; Magaritz and Peryt, 1994), East Greenland (Clemmensen et al., 1985; Scholle et al., 1991) and from brachiopod shells (Gruszczynski et al., 1989; see also Mii et al., 1997).  $\delta^{13}\text{C}$  values recorded in carbonates from evaporitic sequences usually reflect marine signatures; however primary  $^{13}\text{C}$  enrichment can be encountered in isolated basins through

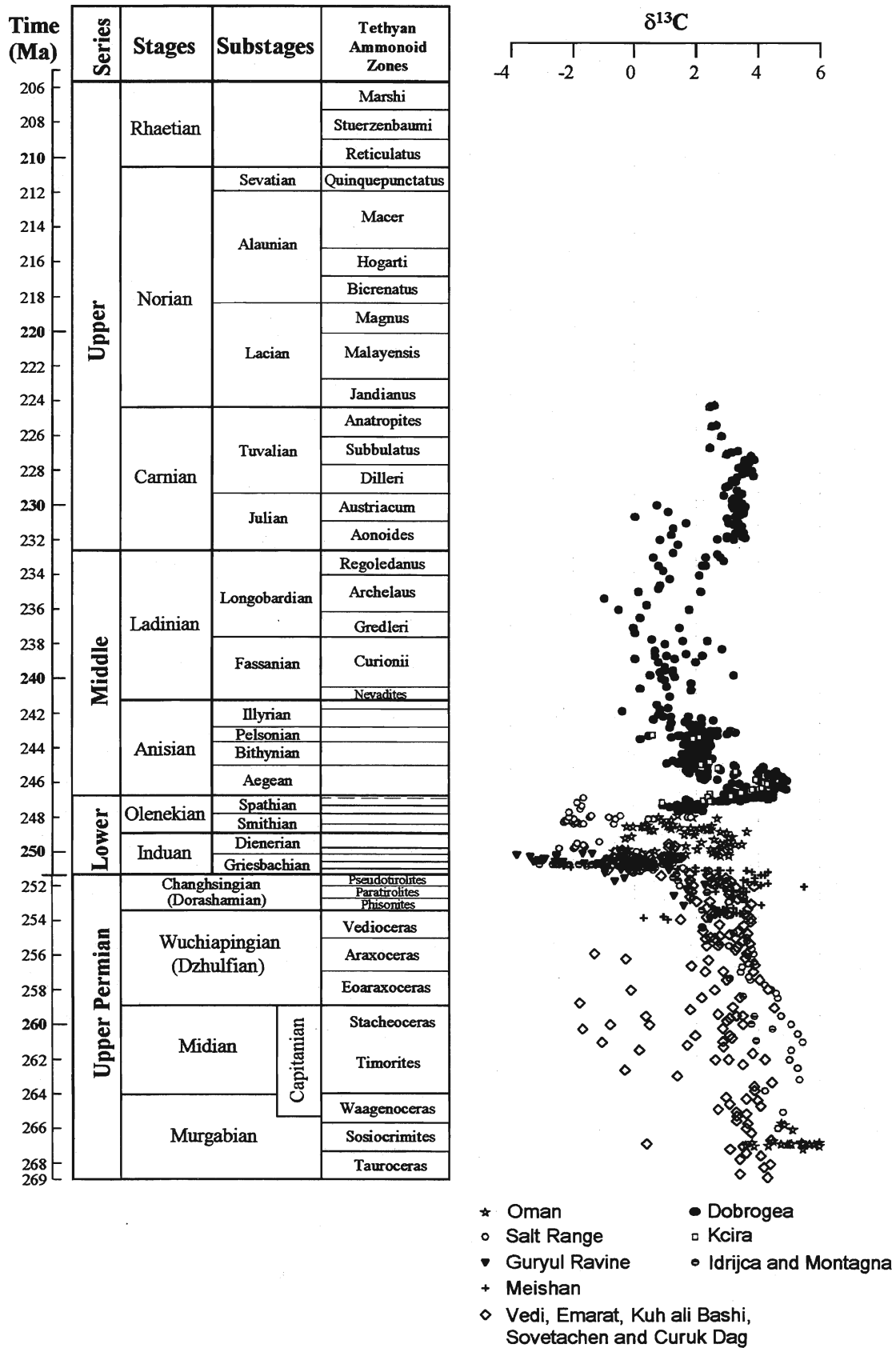


Fig. 57 Secular variations of  $\delta^{13}\text{C}$  values of Upper Permian to Upper Triassic Tethyan carbonates. Data from Baud et al. (1989), Chen et al. (1991), van de Schootbrugge (1997) and the present study.

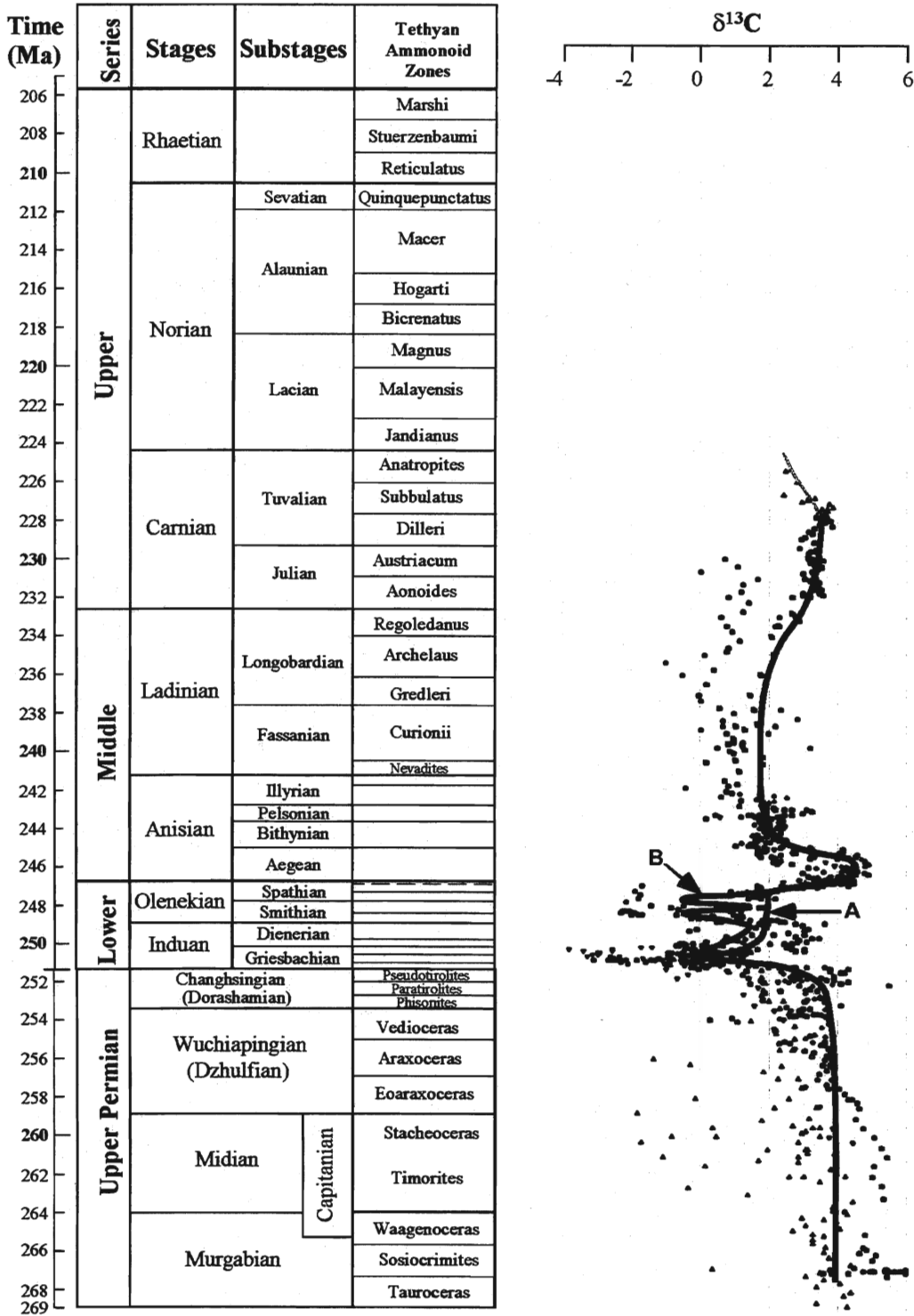


Fig. 58 Proposed carbon isotope curve for the Late Permian to the Late Triassic time interval. See text for details. For the Early Triassic two alternatives are suggested (A and B).

extensive evaporation (Stiller, 1985). The observation that marine carbonates from the Tethys do not show anomalously high  $\delta^{13}\text{C}$  values, these values being rather restricted to particular environments do not support a positive excursion of  $\delta^{13}\text{C}$  values in the Late Permian. There are no reasons to believe that all Tethyan  $^{13}\text{C}$  data were shifted to relatively lower  $\delta^{13}\text{C}$  values by diagenetic processes, and those from marginal marine environments were not; in principle, the carbonates associated with evaporites, deposited in restricted environments are prone to diagenetic exchange with meteoric waters during early stages of diagenesis, therefore it would be more likely to find diagenetic lowering of  $\delta^{13}\text{C}$  values in these carbonates.

The sharp rise of 7‰ reported by Magaritz (1983) in the Delaware Basin and thought to represent the onset of high  $\delta^{13}\text{C}$  values, is likely to reflect diagenetic alteration as the low  $\delta^{13}\text{C}$  values from the base of the section are correlated with high organic carbon contents (2-4%). Diagenetic alteration is likely to be responsible also for the unusual low  $\delta^{13}\text{C}$  values from the base of the Reppwand section (Holser and Magaritz, 1985), interpreted as correlative with the low values from the base of the Delaware Basin section.

It should be emphasized that this aspect is very important since recently emerged models invoke a Late Permian anoxic ocean relying on the pattern of the carbon isotope curve. Malkowski et al. (1989) proposed that the mass extinction has been triggered by an overturn from a Late Permian stratified stagnant ocean to an Early Triassic well mixed one. Similarly, Knoll et al. (1995) and Grotzinger and Knoll (1995) suggested that the end-Permian mass-extinction have been driven by the poisoning of surface waters with high concentrations of carbon dioxide (depleted in  $^{13}\text{C}$ ) formed previously in deep anoxic waters. Both models require the existence of widespread oceanic anoxia during the Late Permian and use the Late Permian high  $\delta^{13}\text{C}$  levels as evidence. In the author's view there is little evidence for a Late Permian stratified ocean, or at least not a long lasting one, which would be responsible for the high  $\delta^{13}\text{C}$  values characterizing most of the Late Permian. The deep sea record do not show evidence of anoxia for the Upper Permian, only the upper part of the Upper Permian contain organic matter rich sediments (Isozaki, 1997; Kakuwa, 1996; but see also Kajiwarra et al., 1994 for a dissenting view). The duration of the Late Permian is estimated to 20 Ma. Such a long lasting anoxia, coupled with a relatively high marine productivity would leave unequivocal traces in the geologic record and lead to notable accumulations of organic carbon. There is no evidence for unusual accumulations of organic carbon during the Late Permian. Petroleum source rocks or coals are not particularly developed in Upper Permian strata (Ulmishek and Klemme, 1990; Klemme and Ulmishek, 1991). As a matter of fact, the amount of Upper Permian (and Permian in general) coals or petroleum source rocks are insignificant when compared with their Carboniferous counterparts.

If the onset of high  $\delta^{13}\text{C}$  values started in the Late Carboniferous as suggested by previous studies, we can rather relate them to the massive accumulations of coals that occurred at that time and assume that the marine  $\delta^{13}\text{C}$  level was set to higher values because  $^{13}\text{C}$  depleted carbon was removed from the system for a long period of time (until the end-Permian, judging from the  $\delta^{13}\text{C}$  curve pattern).

## 8.2 The Permian/Triassic boundary

Both carbonate carbon and organic carbon isotopic curves across the Permian/Triassic boundary show a dramatic drop in  $\delta^{13}\text{C}$  values in the Upper Permian. The negative excursion of  $\delta^{13}\text{C}$  values was also found in terrestrial mammal fossils (Thackeray et al, 1990), non-marine organic carbon (Morante and Herbert, 1994) and coals (Faure et al., 1994). The decrease of  $\delta^{13}\text{C}$  values at the end of the Permian is a well established feature of the carbon isotope curve and it is clearly marked on the plot from fig. 57. The data acquired for the present study do not bring new information, but they confirm its ubiquity.

The drop in  $\delta^{13}\text{C}$  values at the Permian/Triassic boundary, with a magnitude of 3-4‰ is interpreted to have resulted from the oxidation of organic matter on continental shelves due to exposure during regression coupled with a drop in primary productivity (Holser and Magaritz, 1987; Baud et al., 1989a), from reduction of the rate of burial of organic carbon due to the warming and drying of the Earth (Bernier, 1989) or from a sudden release of  $^{13}\text{C}$  depleted  $\text{CO}_2$  previously formed in deep anoxic waters (Knoll et al., 1995; Grotzinger and Knoll, 1995) among many other hypothesis (see discussion in Erwin, 1993 and in Bowring et al., 1998). The drop in  $\delta^{13}\text{C}$  values appears to be extremely rapid, as suggested by Bowring et al. (1998). The magnitude and the global nature of the carbon isotope excursion suggest that a huge quantity of  $^{12}\text{C}$  enriched carbon was introduced into the ocean-atmosphere system. A productivity collapse alone cannot account for 3-4‰ lowering of surface  $\delta^{13}\text{C}$  values because the amount of organic carbon represented by the living biomass is just a small fraction of the total carbon present in the ocean-atmosphere system (Kump, 1991). The general pattern of the Carboniferous to Late Permian carbon isotope curve suggest that the drop in  $\delta^{13}\text{C}$  values was driven by a sudden transfer of previously stocked  $^{13}\text{C}$  depleted carbon, rather than by the overturn of a Late Permian stratified ocean.

### 8.3. Early Triassic

The Early Triassic carbon isotope record is not easily interpreted. The  $\delta^{13}\text{C}$  values vary within a wide range, both in individual sections and in geographically distant sections. Whereas in the Himalayan sections the background  $\delta^{13}\text{C}$  values are very low, reaching values as low as -3‰, in Oman sections  $\delta^{13}\text{C}$  values may be higher than +3‰. There are some lines of evidence which suggest diagenetic (metamorphic) alteration for the Himalayan section. For some of them the  $\delta^{13}\text{C}$  profiles correlate with lithology (although not always) and  $\delta^{18}\text{O}$  values are extremely low. However, the carbon isotope profiles display seemingly correlative fluctuations. For instance, the section from Spiti, although strongly affected by diagenetic/metamorphic processes, preserves the positive excursion across the Lower/Middle Triassic boundary well documented in other areas. Consequently, the interpretation of the carbon isotope record for this Early Triassic is not straightforward.

For these reasons two possible curves are proposed for the Early Triassic period (fig. 58). Alternative A imply a rapid recovery of  $\delta^{13}\text{C}$  values and a relatively constant baseline over most of the Lower Triassic. It is supported by the data of Magaritz and Holser (1991) from the Gartnerkopf core section, which do not show any significant variation over the portion of Lower Triassic covered. Alternative B gives credit to Himalayan sections and implies an increase in  $\delta^{13}\text{C}$  values over the Dienerian, a decrease in the Lower Smithian followed by a rapid and short positive excursion near the Smithian/Spathian boundary. Alternative A is favoured, although there is no compelling evidence for either one alternative. Alternative B, with high amplitude and abrupt variations of  $\delta^{13}\text{C}$  values appears to be very difficult to explain in terms of mass balance. In fig. 58 the peaks are smoothed and the amplitudes are diminished, comparing with their real amplitudes in the sections. In both Salt Range and Spiti sections the variations may reach 4‰, which is about the same as the end-Permian drop in  $\delta^{13}\text{C}$  values. It is very difficult to explain such large variations by any of the usually invoked mechanisms. Likewise, a pattern with rapid and abrupt variations would be a unique feature of the Phanerozoic. Only for the Cambrian highly variable carbon isotope profiles have been reported (Ripperdan, 1994; Brasier et al., 1996). However, the Early Triassic is characterized by many other unique features.

There are some possible fluctuations of the carbon isotope curve for the Griesbachian segment. Magaritz and Holser (1991) detected a multiple peak shape in the Gartnerkopf core section, possibly correlative with the  $\delta^{13}\text{C}$  profile of the Guryul Ravine section (Baud et al., 1996). However, in the



Gartnerkopf core sections these fluctuations correlate with the organic carbon content and their primary origin is therefore questionable (Scholle, 1995). Generally, the carbon isotope record from Griesbachian is highly variable, even in individual sections.

## 8.4. The Lower-Middle Triassic boundary

The data presented in this work outline a positive excursion across the Lower/Middle Triassic boundary, globally developed since it was detected in various paleogeographic settings: in many sections in North Dobrogea, in Kçira section from Albania and in Losar section from Spiti (see fig. 59). The rise in  $\delta^{13}\text{C}$  values starts in the Uppermost Spathian and the most positive values are attained in the Lowermost Anisian (*Aegeiceras ugra* Zone). The recovery to background values (that are typical to the Lower Spathian and the remainder of the Middle Triassic), takes place somewhere close to the Lower/Middle Anisian boundary.

Short term variations in carbon isotope compositions are usually interpreted as reflecting the changing rate of organic carbon burial and/or significant changes in primary productivity. For pre-Cretaceous periods, interpretations of carbon isotope fluctuations are somewhat speculative because: 1) the lack of direct methods to reconstruct vertical  $\delta^{13}\text{C}$  gradients - as a proxy for the efficiency of the productivity pump (Berger and Vincent, 1986); and 2) most of the pre-Cretaceous deep-sea sediments that would potentially record evidence for increased burial of organic carbon were consumed by plate subduction processes.

In Tethyan sediments there is no evidence of significant accumulations of organic carbon that would precisely match the Upper Olenekian-Lower Anisian time interval. However, Anisian deposits host important hydrocarbon source rocks (Moerck and Byoroey, 1983; Riediger et al., 1990; Riediger et al., 1997; Isacksen and Bohacs, 1995). Generally, these source rocks are associated with the global Early Anisian transgressive cycle that followed the Upper Olenekian regression (Embry, 1997). Whether these organic-rich deposits are related to the carbon isotope excursion has to be proved yet.

However, it is likely that the carbon isotope excursion reflect an increase in primary productivity of surface waters. Assuming positive correlation between biodiversity and biomass, there seems to be a consistency with the contemporaneous biotic turnover. The Early Triassic biotic recovery lag is well known, but its nature, timing and rate are not fully understood (Schubert and Bottjer, 1995; Erwin, 1996).

Although ammonoids and conodonts underwent a significant turnover near the Smithian-Spathian boundary (Guex; Orchard, personal communication), it appears that the major step in biotic diversification took place during the Anisian (Erwin, 1996; Wiedmann, 1996). Indeed, plots of diversity in Triassic ammonoids (House, 1988) show a significant explosion in the number of genera at the Lower-Middle Triassic boundary. The Anisian also marked the initial stage in the Mesozoic evolutionary history of reef communities (Stanley, 1988; Senowbari-Darian et al., 1993) and the recovery from the coal gap (Retallack et al., 1996).

Regardless of the implications relating to the recovery from the mass extinction, it appears that the Spathian/Anisian carbon isotope event is a reliable stratigraphical marker and may assist in the correlation of Triassic carbonate deposits.

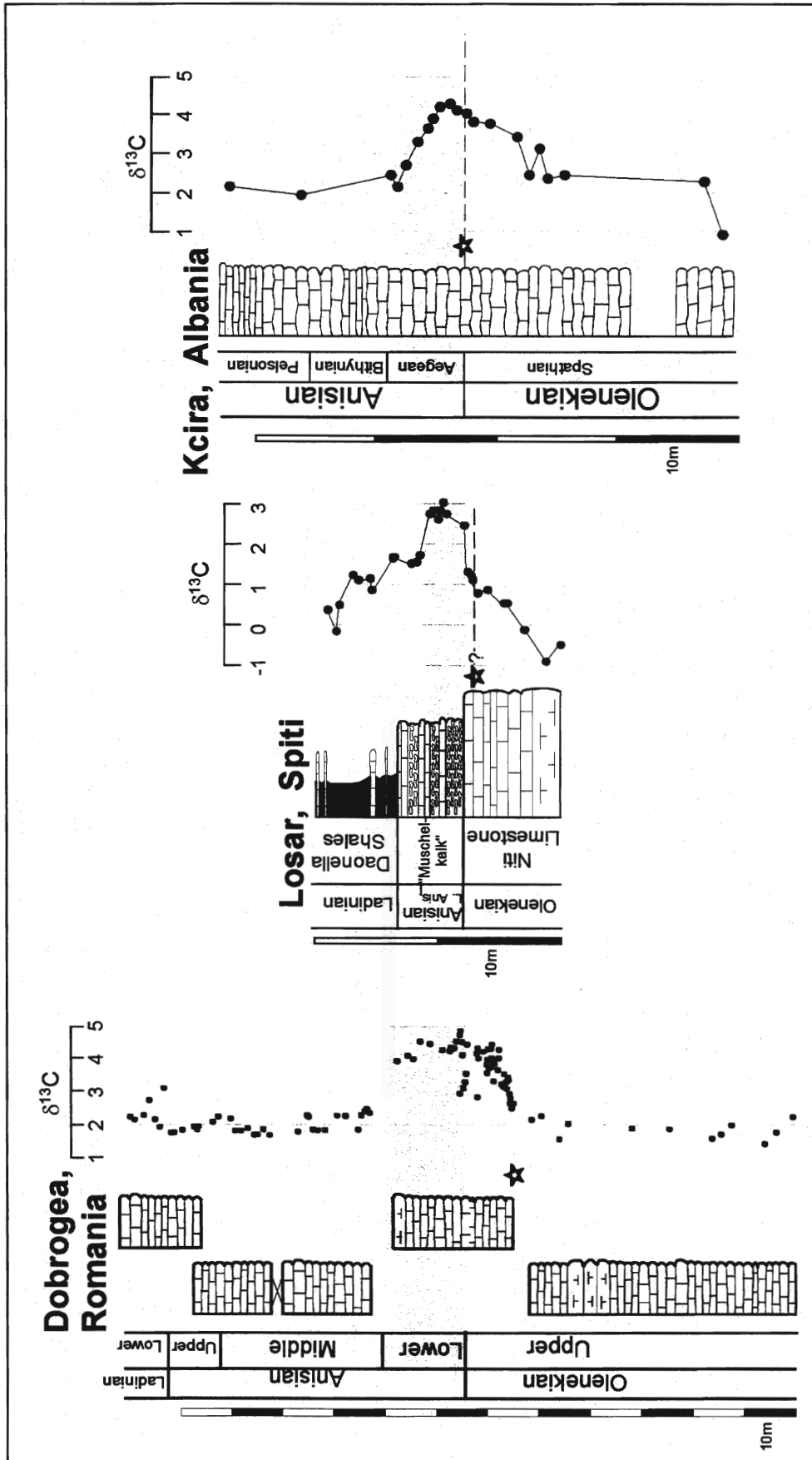


**Fig. 59** Comparison of the carbon isotope profiles (Dobrogea, Spiti and Albania) across the Lower-Middle Anisian boundary. Note that for the section from Albania the boundary is traced by the FAD of *Chiosella timorensis*, while in Dobrogea and Spiti it is made on the basis of ammonoids. *Chiosella timorensis*'s FAD is derived from the present study for Dobrogea (identifications by E. Mirauta), Nicora in Garzanti et al. (1995) for Spiti and in Muttoni et al. (1997) for Albania. Stars indicate the FAD of *Chiosella timorensis*.

## 8.5. Middle - Late Triassic

The carbon isotope record from North Dobrogea also exhibit a gradual and gentle rise in  $\delta^{13}\text{C}$  values starting with the Late Ladinian or Early Carnian. Unfortunately, our data set do not include enough data from the Upper Triassic to better define this trend. Böhm and Gawlick (1997) studied the carbon isotope profile for the Upper Triassic from a section in the Northern Alps, analysing also Hallstatt-type limestones. They reported high  $\delta^{13}\text{C}$  values for the Upper Carnian and a positive excursion in the Lower Norian. Combining our data-set with the one reported by Böhm and Gawlick (1997), a consistent trend can be defined, with a gradual rise in  $\delta^{13}\text{C}$  values from the Lower Carnian to Lower Norian, followed by a decrease in  $\delta^{13}\text{C}$  values starting with the Upper Lower Norian. The data from Spiti also display a gradual rise in  $\delta^{13}\text{C}$  values in the Upper Ladinian. Certainly, this pattern needs further constraints; however, as a first approximation, it seems to be in agreement with Steuber (1991), who reported a gradual increase in  $\delta^{13}\text{C}$  values of organic matter from Ladinian to Norian.

## 8.6. Strontium and sulfur isotope curves

Strontium isotope ratio ( $^{87}\text{Sr}/^{86}\text{Sr}$ ) of the seawater, as recorded by carbonates and biogenic phosphates, underwent large variations during the Upper Permian to Upper Triassic time-interval (Burke et al., 1982; Holser and Magaritz, 1987).  $^{87}\text{Sr}/^{86}\text{Sr}$  ratios increased abruptly from a minimum recorded in the Late Permian without any major change across the Permian/Triassic boundary. The steep increase in  $^{87}\text{Sr}/^{86}\text{Sr}$  ratios is currently explained as the result of increased continental erosion (Martin and Macdougall, 1995). However, it is unclear why anomalously high continental erosion rates occurred during times of high continentality and dry climates, unfavourable for chemical weathering. From previously published data, it appears that the increase of  $^{87}\text{Sr}/^{86}\text{Sr}$  ratios ended somewhere close to the Lower/Triassic boundary, then  $^{87}\text{Sr}/^{86}\text{Sr}$  ratios started to decrease gently. The timing of the inflexion point of the strontium isotope curve is not well constrained by previously published data.

The strontium isotope data obtained on well preserved conodonts from North Dobrogea, coupled with the data published by Martin and Macdougall (1995), also based on the the analysis of conodonts (fig. 60), allow a good age calibration of the inflexion point (which is a major feature of the Phanerozoic curve, see fig. 1). It appears that it occur during the Late Spathian and coincide with the onset of the carbon isotope excursion reported in this work.

One of the most intriguing features of the Phanerozoic sulfate  $\delta^{34}\text{S}$  curve (Holser et al., 1988) is an abrupt positive shift in the Late Early Triassic (fig. 61), the so-called Röt event. There are some uncertainties as to the precise timing of this event due to the difficulties in dating evaporite deposits. Based on data from the Western US, Holser and Magaritz (1987) placed the onset of high  $\delta^{34}\text{S}$  values near the Smithian-Spathian boundary. Recent data reported by Worden et al. (1997) suggest that the onset of high  $\delta^{34}\text{S}$  values may have occurred earlier in the Triassic. However, most of the unusual high  $\delta^{34}\text{S}$  values were reported from samples in the close vicinity of the Olenekian-Anisian boundary (Claypool et al., 1980; Wilgus, 1981; Cortecchi et al., 1981; Chen and Chu, 1988; Spötl, 1988; Spötl and Pak, 1996). The Röt Member of the Buntsandstein, where the  $\delta^{34}\text{S}$  jump was first described is currently interpreted to be Upper Olenekian-Lower Anisian in age (Menning, 1995). It is therefore likely that the carbon isotope excursion at Olenekian-Anisian boundary overlaps in time at least partly with the sulfur isotope excursion.

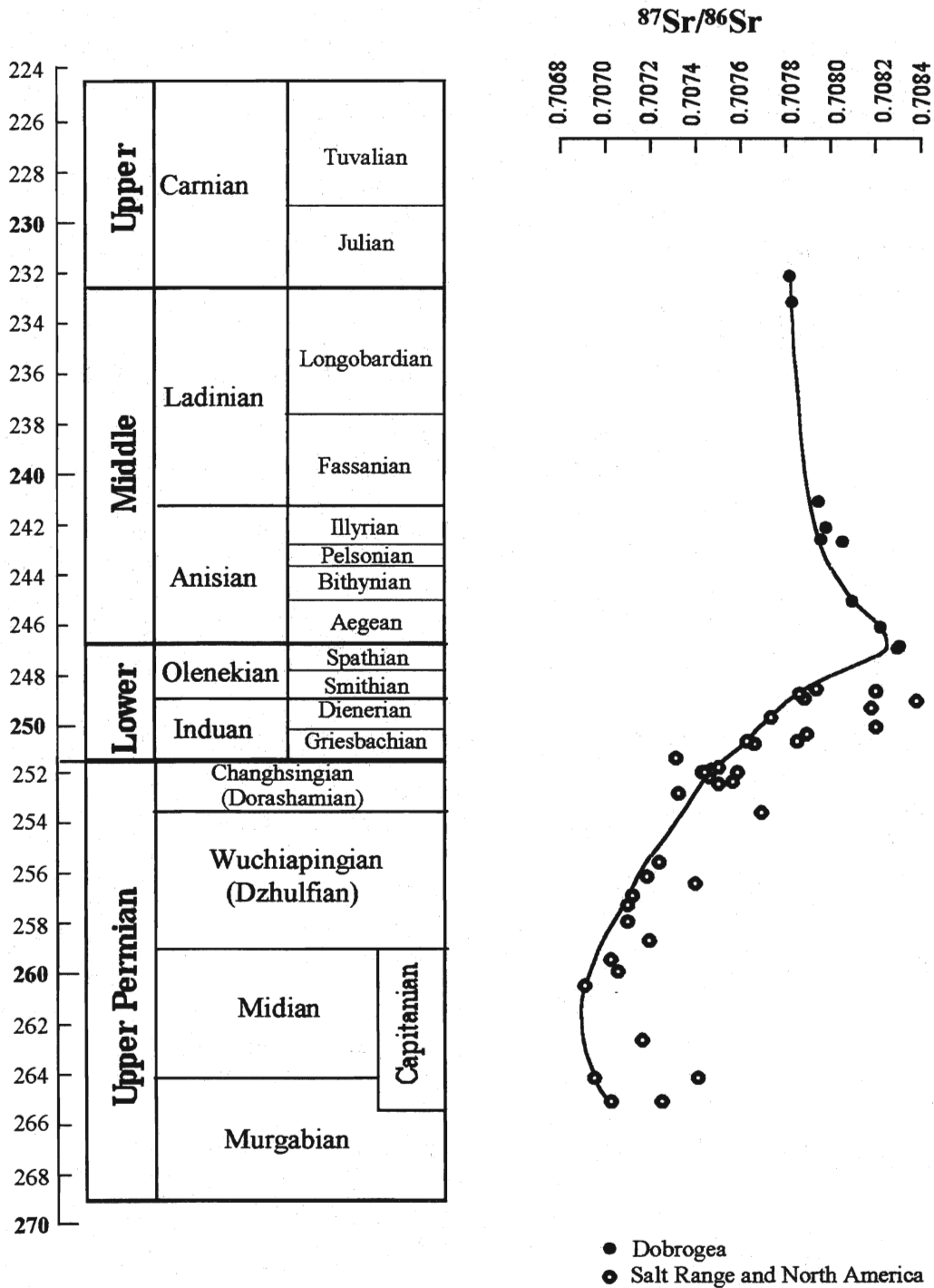


**Fig. 60** Late Permian to Late Triassic  $^{87}\text{Sr}/^{86}\text{Sr}$  age curve based on data obtained on conodonts. Data from Martin and Macdougall (1995) and the present study.

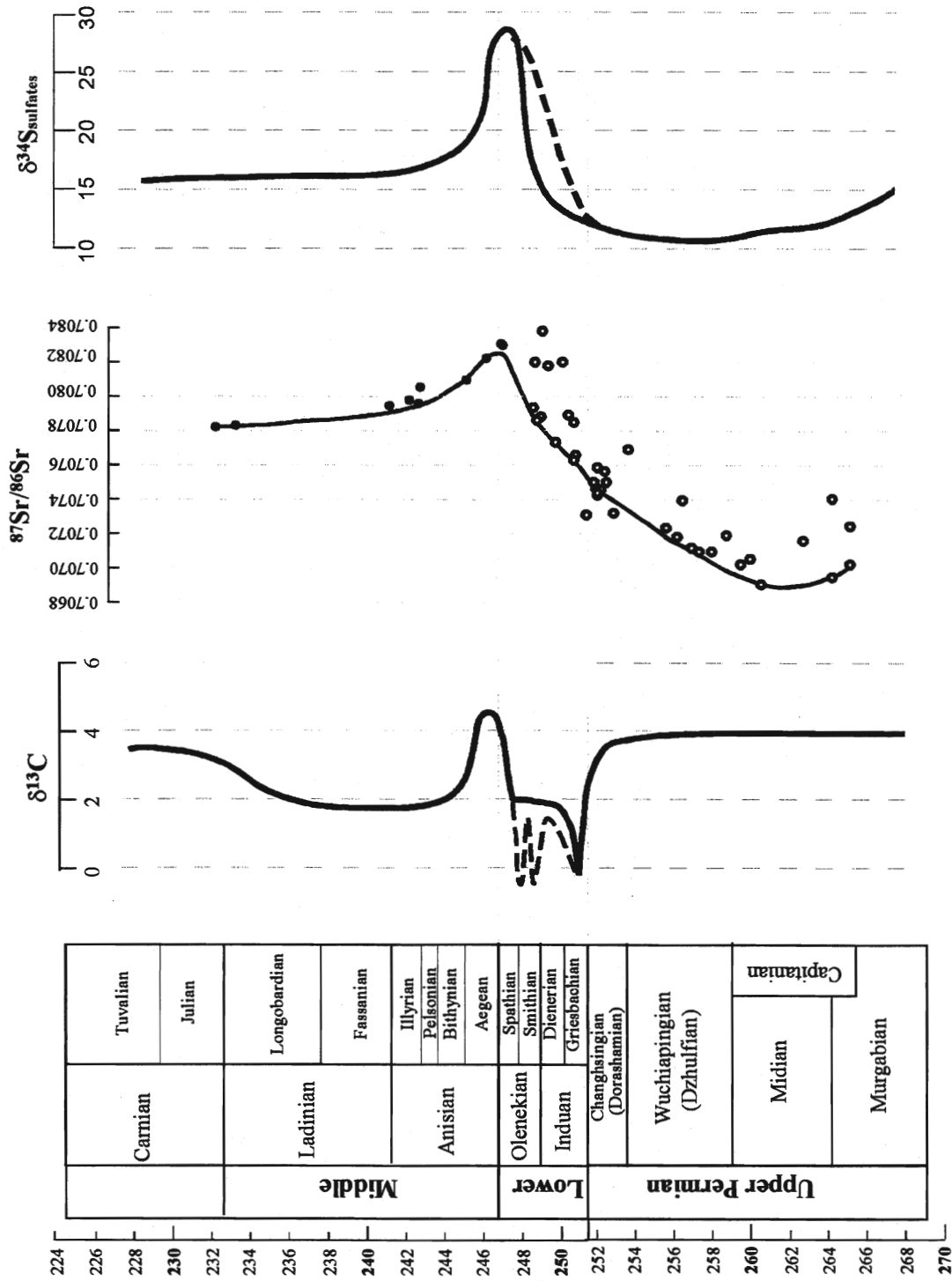


Fig. 61 Late Permian to Late Triassic age curves of carbon isotopes ( $\delta^{13}\text{C}$ ) in carbonates, strontium isotopes ( $^{87}\text{Sr}/^{86}\text{Sr}$ ) in conodonts and sulfur isotopes ( $\delta^{34}\text{S}$ ) in sulfates. The sulfur isotope curve is modified after Claypool et al. (1980).

However, as previously noted by Holser (1977), because of the long residence time of sulfur in seawater the sulfur isotope excursion appears to be much too short to reflect a change in the sulfate of the entire ocean. Holser (1977) suggested that the extremely high  $\delta^{34}\text{S}$  values recorded in marine sulfates near the Lower-Middle Triassic boundary can be explained by the release during ventilation of residual high  $\delta^{34}\text{S}$  brines previously formed in stratified water masses. This explanation is compatible with some recent models proposing that oxygen-deficient conditions characterized most of the Early Triassic (Isozaki, 1997). The geochemical data presented and/or evaluated in the present study are consistent with the development of a stratified, anoxic ocean during the Early Triassic and with a major change in the oceanic circulation patterns at the Lower-Middle Triassic transition. The Early Triassic anoxia is the only scenario that would explain the sulfur isotope anomaly and it may explain the intriguing steep rise of strontium isotope ratios during the Early Triassic through a model similar by that proposed by Malkowski et al. (1989). A chemical stratification of the Early Triassic ocean would make the surface waters more sensitive to the riverine input of more radiogenic strontium. The onset of upwelling currents towards the end of the Early Triassic may have driven nutrient-rich deep waters to the surface, resulting in an increase in ocean productivity and biotic diversification (Martin, 1996), mirrored by carbon isotope changes (fig. 62). The mixing of deep and surface waters would also lower the  $^{87}\text{Sr}/^{86}\text{Sr}$  ratios of surface waters. However, there are some difficulties in applying this model. Although the development of oxygen deficient conditions could be considered on the basis of the North-American Panthalasian margin record and from what we know from the Panthalasian deep-sea record (Isozaki, 1997), it is difficult to reconcile it with the Tethyan sedimentary record.

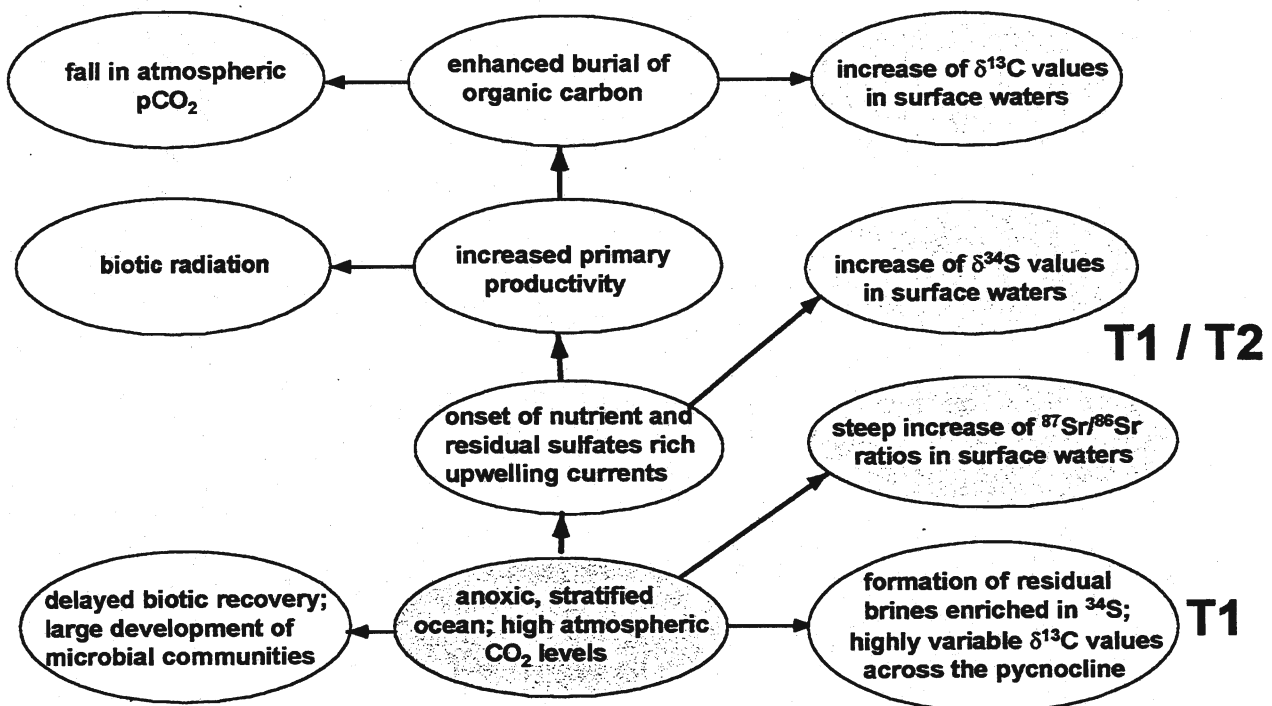


Fig. 62 Flow chart showing a possible scenario for the events that followed the end-Permian mass extinction.

The geochemical perturbations reported in this work suggest that the transition from Lower to Middle Triassic was a time of major global changes that followed the end-Permian mass-extinction, and represents a significant step in the Mesozoic evolution of marine environments. It is foreseen that this distinct carbon isotope excursion may be used as a stratigraphical marker and further assist in the correlation of Triassic carbonate deposits.

## References

- Adlis, D.S., Grossman, E.L., Yancey, T.E., and McLerran, R.D., 1988, Isotope Stratigraphy and Paleodepth Changes of Pennsylvanian Cyclical Sedimentary Deposits: *Palaios*, v. 3, p. 487-506.
- Al-Aasm, I.S., Coniglio, M., and Desrochers, A., 1995, Formation of complex fibrous calcite veins in Upper Triassic strata of Wrangellia Terrain, British Columbia, Canada: *Sedimentary Geology*, v. 100, p. 83-95.
- Al-Aasm, I.S., Taylor, B.E., and South, B., 1990, Stable isotope analysis of multiple carbonate samples using selective acid extraction: *Chemical Geology (Isotope Geoscience Section)*, v. 80, p. 119-125.
- Allan, J.R., and Matthews, R.K., 1977, Carbon and oxygen isotopes as diagenetic and stratigraphic tools: Surface and subsurface data, Barbados, West Indies: *Geology*, v. 5, p. 16-20.
- Allan, J.R., and Matthews, R.K., 1982, Isotope signatures associated with early meteoric diagenesis: *Sedimentology*, v. 29, p. 797-817.
- Anastasiu, V., 1896, Note préliminaire sur la constitution géologique de la Dobrogea: *Bull. Soc. Géol. France*, v. 24, p. 595-601.
- Anastasiu, V., 1898, Contribution à l'étude géologique de la Dobrogea (Roumanie). Terrains secondaires: Paris, *Carré et Naud*, 135 p.
- Anderson, T.F., and Arthur, M.A., 1983, Stable isotopes of oxygen and carbon and their application to sedimentologic and paleoenvironmental problems, in Arthur, M.A., Anderson, T.F., Kaplan, I.R., Veizer, J., and Land, L.S., eds., *Stable isotopes in sedimentary geology*, Volume 10: SEPM Short Course: Dallas, p. 1-151.
- Arthur, M.A., Anderson, T.F., Kaplan, I.R., Veizer, J., and Land, L.S., 1983, *Stable Isotopes in Sedimentary Geology*, SEPM Short Course, Volume 10: Dallas, SEPM.
- Atanasiu, V., 1940, Privire generala asupra geologiei Dobrogei: *Lucr. Soc. Geogr. "D.Cantemir"*, v. 3, 89 p.
- Atudorei, V., and Baud, A., 1997, Carbon isotope events during the Triassic: *Albertiana*, v. 20, p. 45-49.
- Atudorei, V., Baud, A., Gradinaru, E., and Sharp, Z., 1996, Spatial and temporal variations of the carbon isotope in an ancient carbonate platform-basin system (Triassic, North Dobrogea, Romania), in Mutti, M., Simo, T., Weissert, H., and Backer, P., eds., *Carbonate and Global Change: an interdisciplinary approach*: Wildhaus, Switzerland, p. 14.
- Balini, M., and Krystyn, L., 1997, Middle Triassic ammonoids from Spiti Himalayas - A chance for major improvements in Tethyan Anisian subdivisions?: *Albertiana*, v. 19, p. 37-40.
- Balini, M., Krystyn, L., and Torti, V., 1998, In search of the Ladinian/Carnian boundary: perspectives from Spiti (Tethys Himalaya): *Albertiana*, v. 21, p. 26-32.
- Baltres, A., 1976, Triassic Platform and Basinal Carbonate Sedimentation in North Dobrogea, in Patrușiu, D., Drăganescu, A., Baltres, A., Popescu, B., and Radan, S., eds., *Carbonate Rocks and Evaporites*, Volume 15: Guidebook Series: Bucharest, Institute of Geology and Geophysics, p. 43-54.
- Baltres, A., 1993, *Formațiunea de Somova. Studiu sedimentologic* (Unpublished PhD thesis): Universitatea București, 167 p.
- Baltres, A., and Mirauta, E., 1996, Lithostratigraphic and biostratigraphic studies in North Dobrogea: *Romanian Journal of Stratigraphy*, p. 58-60.



- Baltres, A., Mirauta, E., and Gheorghian, D., 1979, The Triassic limestones from Popina Island, North Dobrogea: *D.S. Inst. geol. geofiz.*, v. LXVI/4, p. 89-108.
- Banner, J., 1995, Application of the trace element and isotope geochemistry of strontium to studies of carbonate diagenesis: *Sedimentology*, v. 42, p. 805-824.
- Banner, J.L., and Hanson, G.N., 1990, Calculation of simultaneous isotopic and trace element variations during water-rock interaction with applications to carbonate diagenesis: *Geochimica et Cosmochimica Acta*, v. 54, p. 3123-3137.
- Bao, Z., 1998, Continental slope limestones of Lower and Middle Triassic, South China: *Sedimentary Geology*, v. 118, p. 77-93.
- Bartolini, A., Baumgartner, P.O., and Hunziker, J., 1996, Middle and Late Jurassic carbon stable-isotope stratigraphy and radiolarite sedimentation of the Umbria-Marche Basin (Central Italy): *Eclogae geol. Helv.*, v. 89, p. 811-844.
- Bassoulet, J.P., and Colchen, M., 1976, La limite Permien-Trias dans le domaine tibétain de l'Himalaya du Nepal (Annapurnas-Ganesh Himal): *Colloques Internationaux du C.N.R.S.*, v. 268, p. 41-52.
- Bassoulet, J.P., Colchen, M., Guex, J., Lys, M., Marcoux, J., and Mascle, G., 1978, Permien terminal néritique, Scythien pélagique et volcanisme sous-marin, indices de processus tectono-sédimentaires distensifs à la limite Permien-Trias dans un bloc exotique de la suture de l'Indus (Himalaya du Ladakh): *C.R. Acad.Sc. Paris*, v. 287, p. 675- 678.
- Bathurst, R.G.C., 1980, Stromatactis - origin related to submarine-cemented crusts in Paleozoic mud-mounds: *Geology*, v. 1980, p. 131-134.
- Bathurst, R.G.C., 1982, Genesis of stromatactis cavities between submarine crusts in Paleozoic carbonate mud buildups: *Journal of the Geological Society of London*, v. 139, p. 165-181.
- Baud, A., 1996, The Permian-Triassic boundary: recent developments, discussion and proposal: *Albertiana*, v. 20, p. 6-9.
- Baud, A., Atudorei, V., and Sharp, Z.D., 1995, The Upper Permian of the Salt Range area revisited: new stable isotope data: *Permophyles*, v. 27, p. 39-41.
- Baud, A., Atudorei, V., and Sharp, Z.D., 1996, Late Permian and Early Triassic evolution of the Northern Indian margin: carbon isotope and sequence stratigraphy: *Geodinamica Acta*, v. 9, p. 57-77.
- Baud, A., Cirilli, S., and Marcoux, J., 1997, Biotic response to mass extinction: the Lowermost Triassic microbialites: *Facies*, v. 36, p. 238-242.
- Baud, A., and Magaritz, M., 1988, Carbon Isotope Profile in the Permian - Triassic of the Central Tethys: The Kashmir Sections (India). Abstract: *Berichte der Geologisch. Bundesanst.*, Band 1, p. 2.
- Baud, A., Magaritz, M., and Holser, W.T., 1989a, Permian-Triassic of the Tethys: carbon isotope studies: *Geologische Rundschau*, v. 78, p. 649-677.
- Baud, A., Marcoux, J., Guiraud, R., Ricou, L.E., and Gaetani, M., 1993, Late Murgabian (266-264 Ma), in Dercourt, J., Ricou, L.E., and Vrielynck, B., eds., *Atlas Tethys, Palaeoenvironmental maps, explanatory notes*: Paris, Gauthier-Villards, p. 9-21.
- Baud, A., Marcoux, J., and Stampfli, G., 1989b, Late Permian-Early Triassic Tethyan margin of India: Evolution from rifting to drifting (Salt Range, Kashmir, Zaskar traverse): 28th Int. Geol. Congress. Washington., v. Abstract 1, p. 103.
- Baum, J.S., Baum, G.R., Thompson, P.R., and Humphrey, J.D., 1994, Stable isotopic evidence for relative and eustatic sea-level changes in Eocene to Oligocene carbonates, Baldwin County, Alabama: *Geological Society of America Bulletin*, v. 106, p. 824-839.
- Béchenec, F., Roger, J., Le Métour, J., and Wyns, R., 1992, Explanatory notes to the Geological map of Seeb, Sheet NF40-03: Muscat, Oman Ministry of Petroleum and Minerals, 104 p.
- Bellanca, A., Di Stefano, P., and Neri, R., 1995, Sedimentology and isotope geochemistry of Carnian deep-water marl/limestones deposits from the Sicani Mountains, Sicily:

- Environmental implications and evidence for a planktonic source of lime mud: *Palaeogeography, Palaeoclimatology, Palaeoecology*, v. 114, p. 111-129.
- Berger, W.H., and Vincent, E., 1986, Deep-sea carbonates: Reading the carbon-isotope signal: *Geologische Rundschau*, v. 75, p. 249-269.
- Bernasconi, S.M., 1994, *Geochemical and Microbial Controls on Dolomite Formation in Anoxic Environments: A Case Study from the Middle Triassic (Ticino, Switzerland)*: Stuttgart, E. Schweizerbart'sche Verlagsbuchhandlung, 109 p.
- Berner, R.A., 1971, Bacterial processes effecting the precipitation of calcium carbonate in sediments, *in* Bricker, O.P., ed., *Carbonate Cements, Volume 19: Studies in Geology*, The John Hopkins University, p. 247-251.
- Berner, R.A., 1984, Sedimentary pyrite formation: An update: *Geochimica et Cosmochimica Acta*, v. 48, p. 605-615.
- Berner, R.A., 1989, Drying, O<sub>2</sub>, and mass extinction: *Nature*, v. 340, p. 603-604.
- Bertram, C.J., Elderfield, H., Aldridge, R.J., and Conway Morris, S., 1992, <sup>87</sup>Sr/<sup>86</sup>Sr, <sup>143</sup>Nd/<sup>144</sup>Nd and REEs in Silurian phosphatic fossils: *Earth and Planetary Science Letters*, v. 113, p. 239-249.
- Blendinger, W., 1988, Permian to Jurassic deep water sediments of the Eastern Oman Mountains: Their significance for the evolution of the Arabia margin of South Tethys: *Facies*, v. 19, p. 1-32.
- Blendinger, W., 1991, Upper Triassic (Norian) cephalopod limestones of the Hallstatt-type, Oman: *Sedimentology*, v. 38, p. 223-242.
- Blendinger, W., 1995, Lower Triassic to Lower Jurassic cephalopod limestones of the Oman Mountains: *N. Jb. Geol. Paläont. Mh.*, v. 10, p. 577-593.
- Bodenhausen, J.W.A., De Booy, T., Egeler, C.G., and Nijhuis, H.J., 1964, On the Geology of Central-West Nepal. A preliminary note, *in* Sundaram, S.K., ed., 22nd Intern. Geol. Congress, sect. 11, Himalayan and Alpine orogeny, Volume 11, p. 101-122.
- Böhm, F., and Gawlick, H.-J., 1997, Late Triassic carbon isotope excursion in pelagic limestones of the Northern Calcareous Alps (Abstract 18th Regional European Meeting of Sedimentology): *Gaea heidelberg.*, v. 3, p. 79.
- Bowen, R., 1991, *Isotopes and Climates*, Elsevier Applied Science Publishers, 483 p.
- Bowring, S.A., Erwin, D.H., Jin, Y.G., Martin, M.W., Davidek, K., and Wang, W., 1998, U/Pb Zircon Geochronology and Tempo of the End-Permian Mass Extinction: *Science*, v. 280, p. 1039-1045.
- Brack, P., Mundil, R., Oberli, F., Meier, M., and Rieber, H., 1996, Biostratigraphic and radiometric age data question the Milankovitch characteristics of the Latemar cycles (Southern Alps, Italy): *Geology*, v. 24, p. 371-375.
- Brack, P., and Rieber, H., 1993, Towards a better definition of the Anisian/Ladinian boundary: new biostratigraphic data and correlations of boundary sections from the Southern Alps: *Eclogae geol. Helv.*, v. 86, p. 415-527.
- Brand, U., and Veizer, J., 1981, Chemical diagenesis of a multicomponent carbonate system -2: Stable isotopes: *Journal of Sedimentary Petrology*, v. 51, p. 987-997.
- Brand, W.A., 1996, High Precision Isotope Ratio Monitoring Techniques in Mass Spectrometry: *Journal of Mass Spectrometry*, v. 31, p. 225-235.
- Brasier, M.D., Shields, G., Kuleshov, V.N., and Zhegallo, E.A., 1996, Integrated chemo- and biostratigraphic calibration of early animal evolution: Neoproterozoic-early Cambrian of southwest Mongolia: *Geological Magazine*, v. 133, p. 445-485.
- Broecker, W.S., and Peng, T.H., 1982, *Tracers in the Sea*: New York, Eldigio Press, 690 p.
- Broglio Loriga, C., Cirilli, S., De Zanche, V., di Bari, D., Gianolla, P., Laghi, G.F., Lowrie, W., Manfrin, S., Mastandrea, A., Mietto, P., Muttoni, G., Neri, C., Posenato, R., Rechichi, M.,

- Rettori, R., and Roghi, G., 1998, A GSSP candidate for the Ladinian/Carnian boundary: the Prati di Stuares/Stuares Wiesen section: *Albertiana*, v. 21, p. 2-18.
- Bucher, H., 1989, Lower Triassic Ammonoids from the northern Humboldt Range (northwestern Nevada, USA) and their bearing upon the Lower-Middle Triassic boundary: *Eclogae geol. Helv.*, v. 82, p. 945-1002.
- Bucher, H., 1992a, Ammonoids of the Anisian transgression in the Triassic Star Peak Group, Northwestern Nevada, USA: *Palaeontographica Abt. A*, v. 223, p. 137-166.
- Bucher, H., 1992b, Ammonoids of the Shoshonensis Zone (Middle Anisian, Middle Triassic) from Northwestern Nevada (USA): *Jb.Geol. B.-A.*, v. 135, p. 425-465.
- Bucher, H., Nassichuck, W.W., and Spinosa, C., 1997, Upper Permian *Stacheoceras* from the Himalayas: *Eclogae geol. Helv.*, v. 90, p. 599-604.
- Burke, W.H., Denison, R.E., Hetherington, E.A., Koepnick, R.B., Nelson, H.F., and Otto, J.B., 1982, Variation of seawater  $^{87}\text{Sr}/^{86}\text{Sr}$  throughout Phanerozoic time: *Geology*, v. 10, p. 516-519.
- Canfield, D.E., 1991, Sulfate reduction in deep-sea sediments: *American Journal of Science*, v. 291, p. 177-188.
- Canfield, D.E., 1994, Factors influencing organic carbon preservation in marine sediments: *Chemical Geology*, v. 114, p. 315-329.
- Canfield, D.E., and Teske, A., 1996, Late Proterozoic rise in atmospheric oxygen concentration inferred from phylogenetic and sulphur-isotope studies: *Nature*, v. 382, p. 127-132.
- Carpenter, S.J., and Lohmann, K.C., 1989,  $\delta^{18}\text{O}$  and  $\delta^{13}\text{C}$  variations in late Devonian marine cements from the Golden Spike and Nevis Reefs Alberta, Canada: *Journal of sedimentary Petrology*, v. 59, p. 792-814.
- Carpenter, S.J., and Lohmann, K.C., 1997, Carbon isotope ratios of Phanerozoic marine cements: Re-evaluating the global carbon and sulfur systems: *Geochimica et Cosmochimica Acta*, v. 61, p. 4831-4846.
- Carulli, G.B., Longo Salvador, G., Pistolato, M., and Rampazzo, G., 1993, Stratigraphy and Geochemical Characterization of the Middle Triassic- Carnian Sequence of the Lumiei Valley (Carnia, Northeastern Italy): *Geol. Croat.*, v. 46, p. 9-24.
- Chen, J.-S., and Chu, X.-L., 1988, Sulfur isotope composition of Triassic marine sulfates of South China: *Chemical Geology (Isotope Geoscience Section)*, v. 72, p. 155-161.
- Chen, J.-S., Chu, X.-L., Shao, M.-R., and Zhong, H., 1991, Carbon isotope study of the Permian-Triassic boundary sequences in China: *Chemical Geology (Isotope Geoscience Section)*, v. 89, p. 239-251.
- Chester, R., 1990, *Marine Geochemistry*: London, Chapman & Hall, 698 p.
- Choquette, P.W., and James, N., 1990, *Limestones - The burial diagenetic environment*: *Geoscience Canada Reprint Series*, v. 4, p. 75-111.
- Claoué-Long, J.C., Zichao, Z., Guogan, M., and Shaohua, D., 1991, The age of the Permian-Triassic boundary: *Earth and Planetary Science Letters*, v. 105, p. 182-190.
- Clari, P.A., and Martire, L., 1996, Interplay of cementation, mechanical compaction, and chemical compaction in nodular limestones of the Rosso Ammonitico Veronese (Middle-Upper Jurassic, Northeastern Italy): *Journal of Sedimentary Research*, v. 66, p. 447-458.
- Clark, D.L., and Hatleberg, E.W., 1983, Paleoenvironmental factors and the distribution of conodonts in the Lower Triassic of Svalbard and Nepal: *Fossils and Strata*, v. 15, p. 171-175.
- Clauer, N., and Chaudhuri, S., 1992, *Isotopic Signatures and Sedimentary Record*, Lecture Notes in Earth Sciences, 43, Springer Verlag, 529 p.
- Claypool, G.E., Holser, W.T., Kaplan, I.R., Sakai, H., and Zak, I., 1980, The age of sulfur and oxygen isotopes in marine sulfate and their mutual interpretation: *Chemical Geology*, v. 28, p. 199-260.

- Clemmensen, L., Holser, W.T., and Winter, D., 1985, Stable isotope study through the Permian-Triassic boundary in east Greenland: *Bull. geol. Soc. Denmark*, v. 33, p. 253-260.
- Colchen, M., 1971, Les formations paléozoïques de la Thakkhola., *in* Bordet, P.e.a., ed., *Recherche géologique dans l'Himalaya du Népal, région de la Thakkhola.*: Paris, Edition du CNRS, p. 67-96.
- Colchen, M., 1975, Palaeogeographic and structural evolution of the Tibetan area of the Nepal Himalaya (Annapurna region): *Himalayan Geology (Dehra Dun)*, v. 5, p. 83-103.
- Colchen, M., Le Fort, P., and Pêcher, A., 1986, *Recherches géologiques dans l'Himalaya du Népal. Annapurna, Manaslu, Ganesh Himal.*: Paris, Edition du CNRS, 136 p.
- Cortecchi, G., Reyes, E., Berti, G., and Casati, P., 1981, Sulfur and oxygen isotopes in Italian marine sulfates of Permian and Triassic ages: *Chemical Geology*, v. 34, p. 65-79.
- Crasquin-Soleau, S., and Gradinaru, E., 1996, Early Anisian ostracode fauna from the Tulcea Unit (Cimmerian North Dobrogean Orogen, Romania): *Annales de Paléontologie*, v. 82, p. 59-116.
- Crowley, T.H., Hyde, W.T., and Short, D.A., 1989, Seasonal cycle variations on the supercontinent of Pangea: implications for Early Permian vertebrate extinction: *Geology*, v. 17, p. 457-460.
- Cummins, D.I., and Elderfield, H., 1994, The strontium isotopic composition of Brigantian (late Dinantian) seawater: *Chemical Geology (Isotope Geoscience Section)*, v. 118, p. 255-270.
- Curtis, C.D., and Coleman, M.L., 1986, Controls on the precipitation of early diagenetic calcite, dolomite and siderite concretions in complex depositional sequences, *in* Gautier, D.L., ed., *Roles of Organic Matter in Sediment Diagenesis*, Volume 38: SEPM Special Publication: Tulsa, p. 23-34.
- De Leeuw, J.W., Frewin, N.L., Bergen, P.F.V., Sinninghe Damsté, J.S., and Collinson, M.E., 1995, Organic carbon as a palaeoenvironmental indicator in the marine realm, *in* Bosence, D.W.J., and Alison, P.A., eds., *Marine palaeoenvironmental analysis from fossils*, Vol. 83: Geological Society Special Publication, p. 43-71.
- Dean, W.E., and Gorham, E., 1998, Magnitude and significance of carbon burial in lakes, reservoirs, and peatlands: *Geology*, v. 26, p. 535-538.
- Deines, P., 1980, The isotopic composition of reduced organic carbon, *in* Fritz, P., and Fontes, J.C., eds., *Handbook of Environmental Isotope Geochemistry. The Terrestrial Environment*, A, Volume 1, Elsevier Scientific Publishing Company, p. 329-434.
- Demicco, R.V., and Hardie, L.A., 1995, *Sedimentary Structures and Early Diagenetic Features of Shallow Marine Carbonate Deposits*: Tulsa, SEPM, 265 p.
- Denison, R.E., and Koepnick, R.B., 1995, Variation in  $^{87}\text{Sr}/^{86}\text{Sr}$  of Permian Seawater: An Overview, *in* Scholle, P.A., Peryt, T.M., and Ulmer-Scholle, D.S., eds., *The Permian of Northern Pangea*, Volume 1, Springer Verlag, p. 124-132.
- Denison, R.E., Koepnick, R.B., Fletcher, A., Howell, M.W., and Callaway, W.S., 1994, Criteria for the retention of original seawater  $^{87}\text{Sr}/^{86}\text{Sr}$  in ancient shelf limestones: *Chemical Geology (Isotope Geoscience Section)*, v. 112, p. 113-143.
- Deuser, W.G., 1970, Carbon-13 in Black Sea Waters and Implications for the Origin of Hydrogen Sulfide: *Science*, v. 168, p. 1575-1577.
- Dickson, J.A.D., and Coleman, M.L., 1980, Changes in carbon and oxygen isotope during limestone diagenesis: *Sedimentology*, v. 27, p. 107-118.
- Diener, A., Ebner, S., Veizer, J., and Buhl, D., 1996, Strontium isotope stratigraphy of the Middle Devonian: Brachiopods and conodonts: *Geochimica et Cosmochimica Acta*, v. 60, p. 639-652.
- Diener, C., 1912, The Trias of the Himalayas: *Mem. Geol. Surv. India*, v. 36/3.
- Dragastan, O., and Gradinaru, E., 1975, Asupra unor alge, foraminifere, sphinctozoare si microproblematică din Triasicul din Carpatii Orientali si Dobrogea de Nord: *St. Cerc. Geol., Geofiz., Geogr., Geologie*, v. 20, p. 247-254.

- Dumitrescu, I., and Sandulescu, M., 1968, Problèmes structuraux fondamentaux des Carpates roumaines et de leur avant-pays: *Ann. Com. Géol.*, v. 36, p. 195-218.
- Ebner, S., Diener, A., Buhl, D., and Veizer, J., 1997, Strontium isotope systematics of conodonts: Middle Devonian, Eifel Mountains, Germany: *Palaeogeography, Palaeoclimatology, Palaeoecology*, v. 132, p. 79-96.
- Elderfield, H., 1986, Strontium isotope stratigraphy: *Palaeogeography, Palaeoclimatology, Palaeoecology*, v. 57, p. 71-90.
- Embry, A.F., 1997, Global sequence boundaries of the Triassic and their identification in the Western Canada Sedimentary Basin: *Bulletin of Canadian Petroleum Geology*, v. 45, p. 415-433.
- Emrich, K., Ehhalt, D.H., and Vogel, J.C., 1970, Carbon Isotope Fractionation During the Precipitation of Calcium Carbonate: *Earth and Planetary Science Letters*, v. 8, p. 363-371.
- Epstein, A.G., Epstein, J.B., and Harris, L.D., 1977, Conodont Color Alteration - an Index to Organic Metamorphism: *Geological Survey Professional Paper*, v. 995, 26 p.
- Erwin, D.H., 1993, *The Great Paleozoic Crisis: life and death in the Permian*: New York, Columbia University Press, 327 p.
- Erwin, D.H., 1996a, The Mother of Mass Extinctions: *Scientific American*, v. 275, p. 56-62.
- Erwin, D.H., 1996b, Understanding Biotic Recoveries: Extinction, Survival, and Preservation during the End-Permian Mass Extinction, *in* Jablonski, D., Erwin, D.H., and Lipps, J.J., eds., *Evolutionary Paleobiology*, The University of Chicago Press, p. 398-418.
- Eshet, Y., Rampino, M.R., and Visscher, H., 1995, Fungal event and palynological record of ecological crisis and recovery across the Permian-Triassic boundary: *Geology*, v. 23, p. 967-970.
- Ettensohn, F.R., 1994, Marine, organic-rich, dark-shale deposition on North American parts of Pangea, Carboniferous to Jurassic: effect of supercontinent organization, *in* Embry, A.F., Beauchamp, B., and Glass, D.J., eds., *Pangea. Global Environments & Resources*, Canadian Society of Petroleum Geologists Memoir 17, p. 743-762.
- Fantini Sestini, N., 1981, Lower Anisian (Aegean) Ammonites from Chios Island (Greece): *Riv. it. Paleont. Strat.*, v. 87, p. 41-66.
- Faure, G., 1977, *Principles of Isotope Geology*, John Wiley & Sons, 464 p.
- Faure, K., de Witt, M.J., and Willis, J.P., 1995, Late Permian global coal hiatus linked to <sup>13</sup>C-depleted CO<sub>2</sub> flux into the atmosphere during the final consolidation of Pangea: *Geology*, v. 23, p. 507-510.
- Fawcett, P.J., Barron, E.J., Robison, V.D., and Katz, B.J., 1994, The Climatic Evolution of India and Australia from the Late Permian to Mid-Jurassic: A Comparison of Climate Model Results with the Geologic Record, *in* Klein, G.D., ed., *Pangea, Paleoclimate, Tectonics, and Sedimentation During Accretion, Zenith and Breakup of a Supercontinent*: Geological Society of America Special Paper: Volume 288, p. 139-158.
- Flügel, E., 1994, Permian Shelf Carbonates: Controls and Paleoclimatic Significance of Permian and Triassic Reefs, *in* Klein, G.D., ed., *Pangea, Paleoclimate, Tectonics, and Sedimentation During Accretion, Zenith and Breakup of a Supercontinent*: Geological Society of America Special Paper: Volume 288, p. 247-266.
- Flügel, E., and Senowbari-Daryan, B., 1996, Evolution of Triassic Reef Biota: State of the Art: *Göttinger Arb. Geol. Paläont.*, v. SB2, p. 285-294.
- Fölmli, K.B., Weissert, H., Bisping, M., and Funk, H., 1994, Phosphogenesis, carbon-isotope stratigraphy, and carbonate platform evolution along the Lower Cretaceous northern Tethyan margin: *Geological Society of America Bulletin*, v. 106, p. 729-746.
- Foster, C.B., Logan, G.A., Summons, R.E., Gortner, J.D., and Edwards, D.S., 1997, Carbon isotopes, kerogen types and the Permian-Triassic boundary in Australia: implications for exploration: *APPEA Journal*, p. 472-489.

- Frisia-Bruni, S., Jadoul, F., and Weissert, H., 1989, Evinosponges in the Triassic Esino Limestone (Southern Alps): documentation of early lithification and late diagenetic overprint: *Sedimentology*, v. 36, p. 685-699.
- Gaetani, M., 1992, Report on the Symposium on Triassic Stratigraphy (Lausanne, October, 20-23, 1991): *Albertiana*, v. 10, p. 6-9.
- Gaetani, M., 1994, Working group on the Anisian, Ladinian and Carnian stage boundaries. Annual Report.: *Albertiana*, v. 14, p. 49-51.
- Gaetani, M., Jacobshagen, V., Nicora, A., Kauffmann, G., Tselepidis, V., Fantini Sestini, N., Mertmann, D., and Skourtsis-Coroneou, V., 1992, The Early-Middle Triassic boundary at Chios (Greece): *Riv. it. Paleont. Strat.* v. 98, p. 181-204.
- Garzanti, E., Gorza, M., Martellini, L., and Nicora, M., 1994a, Transition from diagenesis to metamorphism in the Paleozoic to Mesozoic succession of the Dolpo-Manang Synclinorium and Thakkhola Graben (Nepal Tethys Himalaya): *Eclogae geol. Helv.*, v. 87, p. 613-632.
- Garzanti, E., Jadoul, F., Nicora, A., and Berra, F., 1995, Triassic of Spiti (Tethys Himalaya, North India): *Riv. it. Paleont. Strat.* v. 101, p. 267-300.
- Garzanti, E., Nicora, A., and Tintori, A., 1994b, Triassic stratigraphy and sedimentary evolution of the Annapurna Tethys Himalaya (Manang Area, Central Nepal): *Riv. It. Paleont. Strat.*, v. 100, p. 195-226.
- Garzanti, E., Nicora, A., Tintori, A., Sciunnach, D., and Angiolini, L., 1994c, Late Paleozoic stratigraphy and petrography of the Thini Chu Group (Manang, Central Nepal): sedimentary record of Gondwana glaciation and rifting of Neotethys: *Riv. It. Paleont. Strat.*, v. 100, p. 155-194.
- Germani, D., 1997, New data on ammonoids and biostratigraphy of the classic Spathian Kçira sections (Albania): *Riv. it. Paleont. Strat.* v. 103, p. 267-292.
- Glennie, K.W., Boeuf, M.G.A., Hughes Clarke, M.W., Moody-Stuart, M., Pilaart, W.F.H., and Reinhart, B.M., 1974, Geology of the Oman mountains: *Verh. Konink. Neder. Mijnb. Genoot.*, v. 31, p. 1-423.
- Gonzales, A., and Lohmann, K.C., 1985, Carbon and oxygen isotopic composition of Holocene reefal carbonates: *Geology*, v. 13, p. 811-814.
- Gradinaru, E., 1984, Jurassic rocks of North Dobrogea. A depositional-tectonic approach.: *Rev. Roum. Geol. Geophys. Geogr.*, ser. Geol., v. 28, p. 61-72.
- Gradinaru, E., 1993, Mesozoic rocks in Central and North Dobrogea: an overview. Guidebook to Field Excursion, International Meeting and Field Excursion IGCP Project 343: Bucharest.
- Gradstein, F.M., Agterberg, F.P., Ogg, J., Hardenbol, J., Van Veen, P., Thierry, J., and Huang, Z., 1995, A Triassic, Jurassic and Cretaceous Time Scale, in Berggren, W.A., Kent, D., Aubry, M.-P., and Hardenbol, J., eds., *Geochronology Time Scales and Global Stratigraphic Correlation: SEPM Special Publication, Volume 54*, p. 95-126.
- Grant, S.W.F., 1992, Carbon isotopic vital effect and organic diagenesis, Lower Cambrian Forteau Formation, northwest Newfoundland: Implications for  $\delta^{13}\text{C}$  chemostratigraphy: *Geology*, v. 20, p. 243-246.
- Gregor, C.B., Garrels, R.M., Mackenzie, F.T., and Maynard, J.B., 1988, *Chemical Cycles in the Evolution of the Earth*, John Wiley & Sons, p. 276.
- Grossman, E., 1992, Isotope Studies of Paleozoic Paleooceanography - Opportunities and Pitfalls: *Palaios*, v. 7.
- Grossman, E.L., 1994, The Carbon and Oxygen Isotope record During the Evolution of Pangea: Carboniferous to Triassic, in Klein, G.D., ed., *Pangea: Paleoclimate, Tectonics, and Sedimentation during Accretion, Zenith, and Breakup of a Supercontinent, Volume 288: The Geological Society of America Special Paper*, p. 207-228.

- Grossman, E.L., and Ku, T.-L., 1986, Oxygen and carbon isotope fractionation in biogenic aragonite: Temperature effects: *Chemical Geology (Isotope Geoscience Section)*, v. 59, p. 59-74.
- Grotzinger, J.P., and Knoll, A., 1995, Anomalous Carbonate Precipitates: Is the Precambrian the Key to the Permian?: *Palaios*, v. 10, p. 578-596.
- Gruszczynski, M., Halas, S., Hoffman, A., and Malkowski, K., 1989, A brachiopod calcite record of the oceanic carbon and oxygen at the Permian-Triassic transition: *Nature*, v. 337, p. 64-68.
- Guex, J., 1978, Le Trias inférieur des Salt Range (Pakistan): problèmes biochronologiques: *Eclogae Geologicae Helveticae*, v. 71, p. 105-141.
- Haag, M., 1989, Magnetostratigraphische und gesteinsmagnetische Untersuchungen an Sedimenten des späten Paläozoikum und frühen: (unpublished PhD dissertation) Zürich, ETH.
- Haag, M., and Heller, F., 1991, Late Permian to Early Triassic magnetostratigraphy: *Earth and Planetary Science Letters*, v. 107, p. 42-54.
- Habicht, K.S., and Canfield, D.E., 1997, Sulfur isotope fractionation during bacterial sulfate reduction in organic-rich sediments: *Geochimica et Cosmochimica Acta*, v. 61, p. 5351-5361.
- Hallam, A., 1991, Why was there a delayed radiation after the end-Paleozoic extinctions?: *Historical Biology*, v. 5, p. 257-262.
- Hallam, A., 1994, The Earliest Triassic as an anoxic event, and its relationship to the End-Paleozoic mass extinction, in Embry, A.F., Beauchamp, B., and Glass, D.J., eds., *Pangea. Global Environments & Resources, Volume 17: Canadian Society of Petroleum Geologists Memoir*, p. 797-804.
- Hallam, A., 1996, Major Bio-Events in the Triassic and Jurassic, in Walliser, O.H., ed., *Global Events and Event Stratigraphy in the Phanerozoic*, Springer Verlag, p. 265-283.
- Hallam, A., and Wignall, P.B., 1997, *Mass Extinctions and Their Aftermath*, Oxford University Press, 320 p.
- Haq, B.U., Hardenbol, J., and Vail, P.R., 1988, Mesozoic and Cenozoic eustatic cycles., in Wilgus, C.K., ed., *Sea-Level changes: an integrated approach.*, Volume 42: SEPM Special Publication, p. 71-107.
- Hardie, L.A., and Hinnov, L.A., 1997, Biostratigraphic and radiometric age data question the Milankovitch characteristics of the Latemar cycles (Southern Alps, Italy): *Comments and Reply: Geology*, v. 25, p. 470-472.
- Hayden, H.H., 1904, The Geology of Spiti, with parts of Barshar and Rupshu: *Mem. geol. Surv. India*, v. 36, p. 1-129.
- Hayes, J.M., 1993, Factors controlling <sup>13</sup>C contents of sedimentary organic compounds: Principles and evidence: *Marine Geology*, v. 113, p. 111-125.
- Hayes, J.M., Kaplan, I.R., and Wedeking, K.W., 1983, Precambrian Organic Geochemistry, Preservation of the Record, in Schopf, J.W., ed., *Earth's Earliest Biosphere: Its Origin and Evolution*, Princeton University Press, p. 93-134.
- Hayes, J.M., Popp, B.N., Takigiku, R., and Johnson, M.W., 1989, An isotopic study of biogeochemical relationships between carbonates and organic carbon in the Greenhorn Formation: *Geochimica et Cosmochimica Acta*, v. 53, p. 2961-2972.
- Hellmann, K., and Lippolt, H.J., 1981, Calibration of the Middle Triassic timescale by conventional K-Ar and Ar-Ar dating of alkali feldspars: *Journal of Geophysics*, v. 50, p. 73-86.
- Henrich, R., and Zankl, H., 1986, Diagenesis of Upper Triassic Wetterstein Reefs of the Bavarian Alps, in Schroeder, J.H., and Purser, B.H., eds., *Reef Diagenesis*, Springer Verlag, p. 245-268.
- Heydari, E., 1997, Hydrotectonic models of burial diagenesis in platform carbonates based on formation water geochemistry in North American sedimentary basins, *Basin-Wide Diagenetic*

- Patterns: Integrated Petrologic, Geochemical, and Hydrological Considerations: SEPM Special Publication, Volume 57, p. 53-79.
- Hoefts, J., 1987, Stable Isotope Geochemistry, Springer Verlag, 241 p.
- Holser, W.T., 1977, Catastrophic Chemical Events in the History of the Ocean: *Nature*, v. 267, p. 403-408.
- Holser, W.T., 1984, Gradual and abrupt shifts in ocean chemistry during Phanerozoic time, *in* Holland, H.D., and Trendall, A.F., eds., *Patterns of Change in Earth Evolution*, Springer-Verlag, p. 123-143.
- Holser, W.T., 1997, Geochemical events documented in inorganic carbon isotopes: *Palaeogeography, Palaeoclimatology, Palaeoecology*, v. 132, p. 173-182.
- Holser, W.T., and Magaritz, M., 1985, The Late Permian Carbon Isotope Anomaly in the Belerophon Basin, Carnic and Dolomite Alps: *Jb. Geol. B.-A.*, v. 128, p. 75-82.
- Holser, W.T., and Magaritz, M., 1987, Events near the Permian-Triassic boundary: *Modern Geology*, v. 11, p. 155-180.
- Holser, W.T., Magaritz, M., and Ripperdan, R.L., 1995, Global Isotopic Events, *in* Walliser, O.H., ed., *Global Events and Event Stratigraphy in the Phanerozoic*, Springer Verlag, p. 63-88.
- Holser, W.T., Schidlowski, M., Mackenzie, F.T., and Maynard, J.B., 1988, Geochemical cycles of carbon and sulfur, *in* Gregor, B.C., Garrels, R.M., Mackenzie, F.T., and Maynard, J.B., eds., *Chemical Cycles in the Evolution of the Earth*, John Wiley & Sons, p. 105-173.
- Holser, W.T., and Schönlaub, H.P., 1991, The Permian-Triassic boundary in the Carnic Alps of Austria (Gartnerkofel Region), *Abh. Geol. B.-A.*, Volume 45, p. 232.
- House, M.R., 1988, Extinction and survival in the Cephalopoda, *in* Larwood, G.P., ed., *Extinction and Survival in the Fossil Record*, Volume 34: The Systematics Association Special Volume, Oxford Science Publications, p. 139-154.
- Hudson, J.D., 1977, Stable isotopes and limestone lithification: *Journal of the Geological Society of London*, v. 133, p. 637-660.
- Irwin, H., Curtis, C., and Coleman, M., 1977, Isotopic evidence for source of diagenetic carbonates formed during burial of organic-rich sediments: *Nature*, v. 269, p. 209-213.
- Isaksen, G.H., and Bohacs, K.M., 1995, Geological Controls of Source Rock Geochemistry Through Relative Sea Level; Triassic, Barents Sea, *in* Katz, B., ed., *Petroleum Source Rocks: Casebooks in Earth Sciences*, Springer Verlag, p. 25-50.
- Isozaki, Y., 1994, Superanoxia across the Permo-Triassic boundary: Record in accreted deep-sea pelagic cherts in Japan, *in* Embry, A.F., Beauchamp, B., and Glass, D.J., eds., *Pangea. Global Environments & Resources: Canadian Society of Petroleum Geologists Memoir 17*, p. 805-812.
- Isozaki, Y., 1997, Permo-Triassic Boundary Superanoxia and Stratified Superocean: Records from Lost Deep Sea Ocean: *Science*, v. 276, p. 235-238.
- James, N.P., and Choquette, P.W., 1984, Diagenesis 9. Limestones - The Meteoric Diagenetic Environment: *Geoscience Canada*, v. 11, p. 161-194.
- Jenkyns, H.C., 1996, Relative sea-level change and carbon isotope: data from the Upper Jurassic (Oxfordian) of Central and Southern Europe: *Terra Nova*, v. 8, p. 75-85.
- Jenkyns, H.C., and Clayton, C.J., 1997, Lower Jurassic epicontinental carbonates and mudstones from England and Wales: chemostratigraphic signals and the early Toarcian anoxic event: *Sedimentology*, v. 44, p. 687-706.
- Joachimski, M.M., 1997, Comparison of organic and inorganic carbon isotope patterns across the Frasnian-Famennian boundary: *Palaeogeography, Palaeoclimatology, Palaeoecology*, v. 132, p. 133-145.
- Kajiwara, Y., Kaiho, K., and Ohkouchi, N., 1997, An invitation to the sulfur isotope study of marine sediments: implications and constraints for the exogenic sulfur cycle: *Ann. Rep., Inst. Geosci., Univ. Tsukuba*, v. 23, p. 69-74.



- Kajiwara, Y., Yamakita, S., Ishida, K., Ishiga, H., and Imai, A., 1994, Development of a largely anoxic stratified ocean and its temporary massive mixing at the Permian/Triassic boundary supported by the sulfur isotopic record: *Palaeogeography, Palaeoclimatology, Palaeoecology*, v. 111, p. 367-379.
- Kakuwa, Y., 1996, Permian-Triassic mass extinction event recorded in bedded chert sequence in southwest Japan: *Palaeogeography, Palaeoclimatology, Palaeoecology*, v. 121, p. 35-51.
- Kampschulte, A., Buhl, D., and Strauss, H., 1998, The sulfur and strontium isotopic compositions of Permian evaporites from the Zechstein basin, northern Germany: *Geologische Rundschau*, v. 87, p. 192-199.
- Kaufman, A.J., and Knoll, A.H., 1995, Neoproterozoic variations in the C-isotopic composition of seawater: stratigraphic and biogeochemical implications: *Precambrian Research*, v. 73, p. 27-49.
- Keith, M.L., 1982, Violent volcanism, stagnant oceans and some inferences regarding petroleum, strata-bound ores and mass extinctions: *Geochimica et Cosmochimica Acta*, v. 46, p. 2621-2637.
- Kempe, S., and Kazmierczak, J., 1994, The Role of Alkalinity in the Evolution of Ocean Chemistry, Organization of Living Systems, and Biocalcification Processes, in Doumenge, F., ed., *Past and Present Biomineralization Processes. Considerations about the Carbonate Cycle, Volume 13: Bulletin de l'Institut océanographique: Monaco*, p. 61-117.
- Kent, D.V., and Olsen, P.E., 1998, Astronomically Calibrated Geomagnetic Polarity Time-Scale for the Late Triassic, *Epicontinental Triassic International Symposium Abstracts Book: Halle*, p. 88-89.
- Keto, L.S., and Jacobsen, S.B., 1987, Nd and Sr isotopic variations of Early Paleozoic oceans: *Earth and Planetary Science Letters*, v. 84, p. 27-41.
- Klemme, H.D., and Ulmishek, G.F., 1991, Effective Petroleum Source Rocks of the World: Stratigraphic Distribution and Controlling Factors: *American Association of Petroleum Geologists Bulletin*, v. 75, p. 1809-1851.
- Knoll, A.H., Bambach, R.K., Canfield, D.E., and Grotzinger, J.P., 1996, Comparative Earth History and Late Permian Mass Extinction: *Science*, v. 273, p. 452-457.
- Koepnick, R.B., Denison, R.E., Burke, W.H., Hetherington, E.A., and Dahl, D.A., 1990, Construction of the Triassic and Jurassic portion of the Phanerozoic curve of the seawater  $^{87}\text{Sr}/^{86}\text{Sr}$ : *Chemical Geology (Isotope Geoscience Section)*, v. 80, p. 327-349.
- Korte, C., Kozur, H., and Veizer, J., 1998,  $^{87}\text{Sr}/^{86}\text{Sr}$ ,  $\delta^{18}\text{O}$  and  $\delta^{13}\text{C}$  of the Muschelkalk: Comparison to Tethys, *Epicontinental Triassic International Symposium Abstracts Book: Halle*, p. 93-94.
- Kroopnick, P., 1980, The distribution of  $^{13}\text{C}$  in the Atlantic Ocean: *Earth and Planetary Science Letters*, v. 49, p. 469-484.
- Kroopnick, P., Deuser, W.G., and Craig, H., 1970, Carbon 13 Measurements on Dissolved Inorganic Carbon at the North Pacific (1969) Geosecs Station: *Journal of Geophysical Research*, v. 75, p. 7668-7671.
- Krystyn, L., and Orchard, M.J., 1996, Lowermost Triassic ammonoid and conodont biostratigraphy of Spiti: *Albertiana*, v. 17, p. 10-21.
- Kummel, B., and Teichert, C., 1970, Stratigraphic boundary problems: Permian and Triassic of West Pakistan, Department of Geology, University of Kansas. Special Publication, Volume 4, 474 p.
- Kump, L.R., 1991, Interpreting carbon-isotope excursions: Strangelove Oceans: *Geology*, v. 19, p. 299-303.
- Kürschner, W., Becker, R.T., Buhl, R.T., and Veizer, J., 1992, Strontium isotopes in conodonts: Devonian-Carboniferous transition, the Northern Rhenish Slate Mountains, Germany: *Annales de la Société géologique de Belgique*, v. 115, p. 595-621.

- Kyser, T.K., 1987, Stable Isotope Geochemistry of Low Temperature Fluids, *in* Canada, M.A.o., ed., Short Course Handbook, Volume 13: Saskatoon, Mineralogical Association of Canada, p. 452.
- Land, L.S., 1980, The isotopic and trace element geochemistry of dolomite: the state of the art, *in* Zenger, D.H., Dunham, J.B., and Ethington, R.L., eds., Concepts and Models of Dolomitization: SEPM Special Publication, Volume 28, p. 87-110.
- Land, L.S., 1992, The dolomite problem: stable and radiogenic isotope clues, *in* Clauer, N., and Chaudhuri, S., eds., Isotopic Signatures and Sedimentary Records: Lecture Notes in Earth Sciences, Volume 43, pp. 256-280.
- Le Métour, J., Béchenec, F., Chevremont, P., Roger, J., and Wyns, R., 1992, Explanatory notes to the Geological map of Burayimi, Sheet NF40-14: Muscat, Oman Ministry of Petroleum and Minerals, 108 p.
- Lindh, T.B., 1983, Temporal variations in the  $^{13}\text{C}$  and  $^{34}\text{S}$  and global sedimentation during the Phanerozoic [M.S. thesis thesis]: Miami, Florida, University of Miami.
- Lintnerova, O., and Hladikova, J., 1992, Distribution of stable O and C isotopes and microelements in Triassic limestones of the Veterlin Unit, the Malé Karpaty Mts.: their diagenetic interpretation: *Geologica Carpathica*, v. 43, p. 203-212.
- Lohmann, K.C., 1987, Geochemical patterns of meteoric diagenetic systems and their applications to studies of paleokarst, *in* James, N.P., and Choquette, P.W., eds., Paleokarst: Springer-Verlag, p. 58-80.
- Longinelli, A., 1989, Oxygen-18 and Sulphur-34 in Dissolved Oceanic Sulphate and Phosphate, *in* Fritz, P., and Fontes, J.C., eds., Marine Environment, Volume 3A: Handbook of Environmental Geochemistry, Elsevier, p. 219-256.
- Loreau, J.-P., Sabbadini, S., Brosse, E., and Frixia, A., 1995, Aragonite triasique dans des roches-mères carbonatées du bassin de Ragusa (Sicile): géochimie, comparaison avec des sédiments actuels et origine: *C.R. Acad. Sci. Paris*, v. 321, s.II a, p. 111-118.
- Magaritz, M., 1983, Carbon and Oxygen Isotope Composition of Recent and Ancient Coated Grains, *in* Peryt, T.M., ed., Coated Grains: Springer Verlag, p. 27-37.
- Magaritz, M., 1989,  $^{13}\text{C}$  minima follow extinction events: A clue to faunal radiation: *Geology*, v. 17, p. 337-340.
- Magaritz, M., Anderson, R.Y., Holser, W.T., Saltzman, E.S., and Garber, J., 1983, Isotope shifts in the Late Permian of the Delaware Basin, Texas, precisely timed by varved sediments: *Earth and Planetary Science Letters*, v. 66, p. 111-124.
- Magaritz, M., and Holser, W.T., 1991, The Permian-Triassic of the Gartnerkofel-1 Core (Carnic Alps, Austria): Carbon and Oxygen Isotope Variation: *Abh. Geol. B.-A.*, v. 45, p. 149-163.
- Magaritz, M., Krishnamurthy, R.V., and Holser, W.T., 1992, Parallel trends in organic and inorganic carbon isotopes across the Permian/Triassic boundary: *American Journal of Science*, v. 292, p. 727-739.
- Magaritz, M., and Peryt, T.M., 1994, Mixed evaporite and meteoric water dolomitization: isotope study of the Zechstein Limestone (Upper Permian), southwestern Poland: *Sedimentary Geology*, v. 92, p. 257-272.
- Malkowski, K., Gruszczynski, M., Hoffman, A., and Halas, S., 1989, Oceanic stable isotope composition and a scenario for the Permo-Triassic crisis: *Historical Biology*, v. 2, p. 289-309.
- Marcoux, J., and Baud, A., 1996, Late Permian to Late Triassic, Tethyan Paleoenvironments - Three Snapshots: Late Murgabian, Late Anisian, Late Norian, *in* Nairn, A.E.M., Ricou, L.-E., Vrielynck, B., and Dercourt, J., eds., The Tethys Ocean, Volume 8: The Ocean Basins and Margins: New York, Plenum Press, p. 153-190.
- Marcoux, J., Baud, A., Ricou, L.E., Gaetani, M., Krystyn, L., Bellion, Y., Guiraud, R., Besse, J., Gallet, Y., Jaillard, E., Moreau, C., and Theveniaul, H., 1993a, Late Norian (212-234 Ma),

- in Dercourt, J., Ricou, L.E., and Vrielynck, B., eds., Atlas Tethys, Palaeoenvironmental maps, explanatory notes: Paris, Gauthier-Villars, p. 21-34.
- Marcoux, J., Baud, A., Ricou, L.E., Gaetani, M., Krystyn, L., Bellion, Y., Guiraud, R., Moreau, C., Besse, J., Gallet, Y., Jaillard, E., and Theveniaul, H., 1993b, Late Anisian (237-234 Ma), in Dercourt, J., Ricou, L.E., and Vrielynck, B., eds., Atlas Tethys, Palaeoenvironmental maps, Explanatory notes: Paris, Gauthier-Villars, p. 21-34.
- Marshall, J.D., 1992, Climatic and oceanographic isotopic signals from the carbonate rock record and their preservation: *Geological Magazine Mag.*, v. 129, p. 143-160.
- Marshall, J.D., and Ashton, M., 1980, Isotopic and trace element evidence for submarine lithification and hardgrounds in the Jurassic of eastern England: *Sedimentology*, v. 27, p. 271-189.
- Martin, E.E., and Macdougall, J.D., 1995, Sr and Nd isotopes at the Permian/Triassic boundary: A record of climate change: *Chemical Geology (Isotope Geoscience section)*, v. 125, p. 73-99.
- Martin, R.E., 1996, Secular Increase in Nutrient Levels Through the Phanerozoic: Implications for Productivity, Biomass, and Diversity of the Marine Biosphere: *Palaios*, v. 11, p. 209-219.
- Martire, L., 1992, Sequence stratigraphy and condensed pelagic sediments. An example from the Rosso Ammonitico Veronese, northeastern Italy: *Palaeogeography, Palaeoclimatology, Palaeoecology*, v. 94, p. 169-191.
- Marzolf, J.E., 1998, High-Frequency Mudstone/Limestone Cycles in the Lower Triassic Moenkopi Formation: The Record of Sea-Level Change in an Early Triassic Ocean?, *Epicontinental Triassic International Symposium Abstracts Book: Halle*, p. 112.
- Matthews, D.E., and Hayes, J.M., 1978, Isotope-ratio-monitoring gas chromatography -mass spectrometry: *Analytical Chemistry*, v. 50, p. 1465-1473.
- McArthur, J.M., 1994, Recent trends in strontium isotope stratigraphy: *Terra Nova*, v. 6, p. 331-358.
- McConnaughey, T., 1989,  $^{13}\text{C}$  and  $^{18}\text{O}$  disequilibrium in biological carbonates I. Patterns: *Geochimica et Cosmochimica Acta*, v. 53, p. 151-162.
- McCrea, J.M., 1950, On the Isotopic Chemistry of Carbonates and a Paleotemperature Scale: *The Journal of Chemical Physics*, v. 18, p. 849-857.
- McKenzie, J.A., 1981, Holocene dolomitization of calcium carbonate sediments from the coastal sabkhas of Abu Dhabi, U.A.E. a stable isotope study: *Journal of Geology*, v. 89, p. 185-198.
- Mei, S., 1996, Conodont succession around the Permian-Triassic boundary and the natural Permian-Triassic boundary: 30th IGC Beijing. Abstr. Vol., v. 2, p. 57.
- Menning, M., 1995, A Numerical Time Scale for the Permian and Triassic Periods: An Integrative Time Analysis, in Scholle, P.A., Peryt, T.M., and Ulmer-Scholle, D.S., eds., *The Permian of Northern Pangea, Volume 1*, Springer Verlag, p. 77-97.
- Meyers, P.A., 1994, Preservation of elemental and isotopic source identification of sedimentary organic matter: *Chemical Geology*, v. 114, p. 289-302.
- Meyers, P.A., 1997, Organic geochemical proxies of paleoceanographic, paleolimnologic, and paleoclimatic processes: *Organic Geochemistry*, v. 27, p. 213-250.
- Mietto, P., and Manfrin, S., 1995, A high resolution Middle Triassic ammonoid standard scale in the Tethys Realm. A preliminary report: *Bull. Soc. géol. Fr.*, v. 166, p. 539-563.
- Mii, H.-S., Grossman, E.L., and Yancey, T.E., 1997, Stable carbon and oxygen isotope shifts in Permian seas of West Spitsbergen - Global change or diagenetic artifact: *Geology*, v. 25, p. 227-230.
- Mirauta, E., 1982, Biostratigraphy of the Triassic deposits in the Somova-Sarica Hill zone (North Dobrogea) with special regard on the eruption age: *D.S. Inst. Geol. Geofiz.*, v. 67, p. 63-78.
- Mirauta, E., and Gheorghian, D., 1975, Norian conodonts and foraminifers from North Dobrogea: *D.S. Inst. Geol. Geofiz.*, v. LXI/3, p. 47-76.

- Mirauta, E., Gheorgian, D., and Badiceanu, M., 1993, Données biostratigraphiques sur la Formation de Cataloi (Dobrogea du Nord, Roumanie): *Rom. J. Stratigraphy*, v. 75, p. 21-27.
- Mirauta, O., 1966, Paleozoicul de la Cataloi si cuvertura lui Triasica: *D. S. Com. Geol., Inst. Geol.*, v. 52, p. 275-289.
- Mitchell, S.F., Paul, C.R.C., and Gale, A.S., 1996, Carbon isotopes and sequence stratigraphy, *in* Howell, J.A., and Aitken, J.F., eds., *High Resolution Sequence Stratigraphy: Innovations and Applications*, Volume 104: Geological Society Special Publication, p. 11-24.
- Moerck, A., and Bjoroe, M., 1983, Mesozoic source rocks on Svalbard, *in* Spencer, A.M., ed., *Petroleum Geology of the North European Margin*, Graham and Trotman Ltd, p. 371-382.
- Montenat, C., Lapparent, A.F., Lys, M., Termier, H., Termier, G., and Vachard, D., 1976, La transgression permienne et son substratum dans le jebel Akhdar (Montagnes d'Oman, Peninsule Arabique): *Ann. Soc. Geol. Nord*, v. XCVI / 3, p. 239-258.
- Monty, C.L.V., Bosence, D.W.J., Bridges, P.H., and Pratt, B.R., 1995, Carbonate Mud-Mounds. Their Origin and Evolution, IAS Special Publication, Volume 23, Blackwell Science, p. 537.
- Morante, R., 1996, Permian and Early Triassic isotopic records of carbon and strontium in Australia and a scenario of events about the Permian-Triassic boundary: *Historical Biology*, v. 11, p. 289-310.
- Morante, R., and Hallam, A., 1996, Organic carbon isotopic record across the Triassic-Jurassic boundary and its bearing on the cause of the mass extinction: *Geology*, v. 24, p. 391-394.
- Morante, R., and Herbert, C., 1994, Carbon isotope and sequence stratigraphy about the Permian-Triassic boundary in the Sydney Basin, Newcastle Symposium on Advances in the Study of Sydney Basin, Volume 28: University of Newcastle, Australia, p. 102-109.
- Morse, J.W., and Mackenzie, F.T., 1990, *Geochemistry of Sedimentary Carbonates*, Elsevier, 707 p.
- Mouterde, R., 1971, Les formations Mésozoïques de la Thakkhola, *Recherches Géologiques dans l'Himalaya du Nepal, Région de la Thakkhola*, p. 124-186.
- Mundil, R., Brack, P., Meier, M., Rieber, H., and Oberli, F., 1996, High resolution U-Pb dating of Middle Triassic volcanoclastics: Time-scale calibration and verification of tuning parameters for carbonate sedimentation: *Earth and Planetary Science Letters*, v. 141, p. 137-151.
- Mundil, R., Meier, M., and Oberli, F., 1997, Single crystal U/Pb dating of Permian/Triassic boundary in SE China: Implications for mass extinction and timescale calibration: *Terra Nova Abstract Supplement*, v. 9, p. 66.
- Mutihac, V., 1964, Zona Tulcea si pozitia acesteia in cadrul structural al Dobrogei: *An. Com. Geol.*, v. 31, p. 215-263.
- Mutti, M., and Weissert, H., 1995, Triassic monsoonal climate and its signature in Ladinian-Carnian carbonate platforms (Southern Alps, Italy): *Journal of Sedimentary Research*, v. B65, p. 357-367.
- Muttoni, G., Kent, D.V., Meço, S., Nicora, A., Gaetani, M., Balini, M., Germani, D., and Rettori, R., 1996, Magnetobiostratigraphy of the Spathian to Anisian (Lower to Middle Triassic) Kçira section, Albania: *Geophys. J. Int.*, v. 127, p. 503-514.
- Nakazawa, K., 1993, Stratigraphy of the Permian-Triassic transition and the Paleozoic/Mesozoic boundary: *Bulletin of the Geological Survey of Japan*, v. 44, p. 425-445.
- Nakazawa, K., and Kapoor, H.M., 1981, The Upper Permian and Lower Triassic faunas of Kashmir, *Memoirs of the Geological Survey of India*, Volume XLVI.
- Nakazawa, K., Mohan Kapoor, H., Ishii, K., Bando, Y., Okimura, Y., and Tokuoka, T., 1975, The Upper Permian and Lower Triassic in Kashmir, India: *Mem. Fac. Sci., Kyoto Univ., Ser. Geol. & Min.*, v. XLII, p. 1-106.
- Neuweiller, F., Reitner, J., and Monty, C., 1997, Biosedimentology of Microbial Buildups: *Facies*, v. 36, p. 195-284.

- Nicora, A., Gaetani, M., and Garzanti, E., 1984, Late Permian to Anisian in Zaskar (Ladakh, Himalaya): , v. 7, p. 27-30.
- Nicora, A., Garzanti, E., and Tintori, A., 1993, Early Triassic sequence stratigraphy of the Nepal Tethys Himalaya., *in* Beauchamp, B., and Embry, A., eds., Carboniferous to Jurassic Pangea, Volume Program and Abstract: Calgary, Can. Soc. Petrol. Geol., p. 221.
- Nielsen, H., 1989, Local and Global Aspects of the Sulphur Isotope Age Curve of Oceanic Sulphate, *in* Brimblecombe, P., and Lein, A.Y., eds., Evolution of the Global Biogeochemical Sulphur Cycle: SCOPE, John Wiley & Sons Ltd, p. 57-64.
- Orchard, M., 1996, Conodont fauna from the Permian-Triassic boundary: observations and reservations: *Permophyles*, v. 28, p. 29-35.
- Orchard, M., and Bucher, H., 1992, Conodont-ammonoid intercalibration around the Lower-Middle Triassic boundary: Nevadan clocks help tell British Columbian time: Geological Survey of Canada, v. 92-1E, p. 133-140.
- Orchard, M.J., and Tozer, E.T., 1997a, Triassic conodont biochronology and intercalibration with the canadian ammonoid sequence: *Albertiana*, v. 20, p. 33-44.
- Orchard, M.J., and Tozer, E.T., 1997b, Triassic conodont biochronology, its calibration with the ammonoid standard, and a biostratigraphic summary for the Western Canada Sedimentary Basin: *Bulletin of Canadian Petroleum Geology*, v. 45, p. 675-692.
- Pakistani-Japanese Working Group, 1985, Permian and Triassic Systems in the Salt Range and Surghar Range, Pakistan., *in* Nakazawa, K. and Dickins, J.M., eds., *The Tethys*: Tokai University Press, p. 221-312.
- Parrish, J.T., 1993, Climate of the Supercontinent Pangea: *Journal of Geology*, v. 101, p. 215-233.
- Patrulius, D., 1971, Introduction in the Triassic Geology of the Romania, *in* Patrulius, D.e.a., ed., *The Triassic Formation of the Apuseni Mountains and the Carpathians Bend*. Guide book to the excursions of the 2nd Triassic Coll. Carpatho-Balkan Association, Volume 8: Bucuresti, Geol. Inst., p. 5-54.
- Patterson, W.P., and Walter, L.M., 1994, Depletion of  $^{13}\text{C}$  in seawater  $\text{CO}_2$  on modern carbonate platforms: Significance for the carbon isotopic record of carbonates: *Geology*, v. 22, p. 885-888.
- Pedersen, T.F., and Calvert, S.E., 1990, Anoxia vs. Productivity: What Controls the Formation of Organic-Carbon-Rich Sediments and Sedimentary Rocks: *The American Association of Petroleum Geologists Bulletin*, v. 74, p. 454-466, 8 figs.
- Peters, K.F., 1867, Grunlinien zur Geographie und Geologie der Dobrudscha: *Denkschr. d. kais. Akad. d. Wiss. math.-naturw. Klasse*, v. 27, p. 83-207.
- Pillevuit, A., 1993, Les Blocs Exotiques du Sultanat d'Oman. Evolution paléogéographique d'une marge passive flexurale: *Mémoires de Géologie (Lausanne)*, v. 17, p. 249.
- Pillevuit, A., Marcoux, J., Stampfli, G., and Baud, A., 1997, The Oman Exotics: a key to the understanding of the Neotethyan geodynamic evolution: *Geodinamica Acta*, v. 10, p. 209-238.
- Pisciotta, K.A., and Mahoney, J.J., 1981, Isotopic survey of diagenetic carbonates, Deep Sea Drilling Project Leg 63: Initial Reports of the Deep Sea Drilling Project, v. LXIII, p. 595-609.
- Popp, B.N., Anderson, T.F., and Sandberg, P.A., 1986, Brachiopods as indicators of original isotopic compositions in some Paleozoic limestones: *Geological Society of America Bulletin*, v. 97, p. 1262-1269.
- Popp, B.N., Parekh, P., Tilbrook, B., Bidigare, R.R., and Laws, E.A., 1997, Organic carbon  $\delta^{13}\text{C}$  variations in sedimentary rocks as chemostratigraphic and paleoenvironmental tools: *Palaeogeography, Palaeoclimatology, Palaeoecology*, v. 132, p. 119-132.

- Qing, H., Barnes, C., Buhl, D., and Veizer, J., 1998, The strontium isotopic composition of Ordovician and Silurian brachiopods and conodonts: Relationships to geological events and implications for coeval seawater: *Geochimica et Cosmochimica Acta*, v. 62, p. 1721-1733.
- Rabu, D., 1988, Géologie de l'autochtone des montagnes d'Oman : La fenêtre du jabal Akdar. La semelle métamorphique de la Nappe ophiolitique de Semail dans les parties orientales et centrale des Montagnes d'Oman : une revue: Documents du Bureau de Recherches Géologiques et Minières, Orléan, v. 130, p. 1-582.
- Rabu, D., Le Métour, J., Béchenec, F., Beurrier, F., Villey, M., and Bourdillon-de-Grissac, C., 1990, Sedimentary aspects of the Eo-Alpine cycle on the northeast edge of the Arabian Platform (Oman Mountains), in Robertson, A.H.F., Searle, M.P., and Ries, A.C., eds., *The Geology and tectonics of the Oman Region*, Geological Society Special Publication, Volume 49, p. 49-68.
- Raup, D.M., 1979, Size of the Permian-Triassic Bottleneck and Its Evolutionary Implications: *Science*, v. 206, p. 217-218.
- Raup, D.M., and Sepkoski, J.J.J., 1986, Periodic Extinction of Families and Genera: *Science*, v. 231, p. 833-836.
- Redlich, K., 1896, Geologische Studien in Rumänien. II: *Verh. k.k. geol.R.-A.*, Wien, v. 17, p. 492-502.
- Reeder, R.J., 1983, Carbonates: Mineralogy and Chemistry, in Ribbe, P.H., ed., *Reviews in Mineralogy*, Volume 11, Mineralogical Society of America, 394 p.
- Reitner, J., and Neuweiler, F., 1995, Mud Mounds: A Polygenetic Spectrum of Fine-grained Carbonate Buildups: *Facies*, v. 32, p. 1-70.
- Rejebian, V.A., Harris, A.G., and Huebner, J.S., 1987, Conodont color and textural alteration: An index to regional metamorphism, contact metamorphism, and hydrothermal alteration: *Geological Society of America Bulletin*, v. 99, p. 471-479.
- Renard, M., 1979, Aspect géochimique de la diagenèse des carbonates: *Bull. B.R.G.M.* (2), v. IV, 2, p. 133-152.
- Renard, M., 1985, La chimiostratigraphie: *Geochronique*, v. 13, p. 16-20.
- Renard, M., 1986, Pelagic Carbonate Chemostratigraphy (Sr, Mg,  $^{18}\text{O}$ ,  $^{13}\text{C}$ ): *Marine Micropaleontology*, v. 10, p. 117-164.
- Renard, M., Delacotte, O., and Létolle, R., 1982, Le strontium et les isotopes stables dans les carbonates totaux de quelques sites de l'Atlantique et de la Téthys: *Bull. Soc. géol. France*, v. 24, p. 519-534.
- Renard, M., and Zerrari, S., 1997, Rapport préliminaire sur les éléments traces des carbonates, in Baud, A., ed., *The Triassic of North Dobrogea*: Lausanne, p. 49-53.
- Retallack, G.J., Veevers, J.J., and Morante, R., 1996, Global coal gap between Permian-Triassic extinction and Middle Triassic recovery of peat-forming plants: *Geological Society of America Bulletin*, v. 108, p. 195-207.
- Reuber, I., and Colchen, M., 1987, The geodynamic evolution of the South Tethyan margin in Zaskar, NW Himalaya, as revealed by the Spongtag ophiolitic melanges: *Geodinamica Acta*, v. 1, p. 283-296.
- Riediger, C.L., 1997, Geochemistry of potential hydrocarbon source rocks of Triassic age in the Rocky Mountain Foothills of northeastern British Columbia and west-central Alberta: *Bulletin of Canadian Petroleum Geology*, v. 45, p. 719-741.
- Riediger, C.L., Brooks, P.W., Fowler, M.G., and Snowdon, L.R., 1990, Lower and Middle Triassic source rocks, thermal maturation, and oil-source rock correlations in the Peace River Embayment area, Alberta and British Columbia: *Bulletin of Canadian Petroleum Geology*, v. 38, p. 218-235.
- Ripperdan, R., 1994, Global variations in carbon isotope composition during the Latest Neoproterozoic and Earliest Cambrian: *Annu. Rev. Earth Planet. Sci.*, v. 22, p. 385-417.

- Ripperdan, R.L., Magaritz, M., Nicoll, R.S., and Shergold, J.H., 1992, Simultaneous changes in carbon isotopes, sea-level, and conodont biozones within the Cambrian-Ordovician boundary interval at Black Mountain, Australia: *Geology*, v. 20, p. 1039-1042.
- Romanek, C.S., Grossman, E.L., and Morse, J.W., 1992, Carbon isotopic fractionation in synthetic aragonite and calcite: Effects of temperature and precipitation rate: *Geochimica et Cosmochimica Acta*, v. 56, p. 419-430.
- Rosenbaum, J., and Shepard, S.M.F., 1986, An isotopic study of siderites, dolomites and ankerites at high temperatures: *Geochimica et Cosmochimica Acta*, v. 50, p. 1147-1150.
- Ross, C., Baud, A., and Menning, M., 1994, A Timescale for Project Pangea, in Embry, A.F., Beauchamp, B., and Glass, D.J., eds., *Pangea. Global Environments & Resources, Volume 17: Canadian Society of Petroleum Geologists Memoir*, p. 81-83.
- Sackett, W.M., 1989, Stable carbon isotope studies on organic matter in the marine environment, in Fritz, P., and Fontes, J.C., eds., *The Marine Environment, Volume 3A: Handbook of Environmental Isotope Geochemistry*, Elsevier, p. 139-170.
- Saltzman, M.R., Runnegar, B., and Lohmann, K.C., 1998, Carbon isotope stratigraphy of Upper Cambrian (Steptoean Stage) sequences of the eastern Great Basin: Record of a global oceanographic event: *Geological Society of America Bulletin*, v. 110, p. 285-297.
- Sandulescu, M., 1984, *Geotectonica României: Bucuresti, Ed. Tehnica*, 336 p.
- Sano, H., and Nakashima, K., 1997, Lowermost Triassic (Griesbachian) Microbial Bindstone-cementstone Facies, Southwest Japan: *Facies*, v. 36, p. 1-24.
- Sass, E., Bein, A., and Almogi-Labin, A., 1991, Oxygen-isotope composition of diagenetic calcite in organic rich-rocks: Evidence for  $^{18}\text{O}$  depletion in marine anaerobic pore water: *Geology*, v. 19, p. 839-842.
- Scherer, M., 1977, Preservation, Alteration and Multiple Cementation of Aragonitic Skeletons from the Cassian Beds (U. Triassic, Southern Alps): Petrographic and Geochemical Evidence: *N. Jb. Geol. Paläont. Abh.*, v. 154, p. 213-262.
- Schidlowski, M., Hayes, J.M., and Kaplan, I.R., 1983, Isotopic Inferences of Ancient Biochemistries: Carbon, Sulfur, Hydrogen, and Nitrogen, in Schopf, W.F., ed., *Earth's Earliest Biosphere: Its Origin and Evolution*, Princeton University Press, p. 149-186.
- Scholle, P.A., 1995, Carbon and Sulfur Isotope Stratigraphy of the Permian and Adjacent Intervals, in Scholle, P.A., Peryt, T.M., and Ulmer-Scholle, D.S., eds., *The Permian of Northern Pangea, Volume 1*, Springer Verlag, p. 133-149.
- Scholle, P.A., and Arthur, M.A., 1980, Carbon Isotope Fluctuations in Cretaceous Pelagic Limestones: Potential Stratigraphic and Petroleum Exploration Tool: *The American Association of Petroleum Geologists Bulletin*, v. 64, p. 67-87, 12 Figs., 1 Table.
- Scholle, P.A., Stemmerik, L., and Ulmer, D.S., 1991, Diagenetic History and Hydrocarbon Potential of Upper Permian Carbonate Buildups, Wegener Halvo Area, Jameson Land Basin, East Greenland: *The American Association of Petroleum Geologists Bulletin*, v. 75, p. 701-725.
- Schönlaub, H.P., 1991, The Permian-Triassic of the Gartnerkofel-1 Core (Carnic Alps, Austria): Conodont Biostratigraphy: *Abh. Geol. B.-A.*, v. 45, p. 79-98.
- Schubert, J.K., and Bottjer, D., 1992, Early Triassic stromatolites as post-mass extinction disaster forms: *Geology*, v. 20, p. 883-886.
- Schubert, J.K., and Bottjer, D.J., 1995, Aftermath of the Permian-Triassic mass extinction event: Paleocology of Lower Triassic carbonates in the western USA: *Palaeogeography, Palaeoclimatology, Palaeoecology*, v. 116, p. 1-39.
- Senowbari-Daryan, B., Zühlke, R., Bechstädt, T., and Flügel, E., 1993, Anisian (Middle Triassic) Buildups of the Northern Dolomites (Italy): The Recovery of Reef Communities after the Permian/Triassic Crisis: *Facies*, v. 28, p. 40-65.

- Shackelton, N.J., and Kennett, J.P., 1975, Paleotemperature history of the Cenozoic and the initiation of the Antarctic glaciation: oxygen and carbon isotope analysis in DSDP Sites 277, 279 and 281, in Kennett, J.P., and Houtz, R.E., eds., Initial Reports of the Deep Sea Drilling Project, Volume 29: U.S. Government Printing Office, p. 743-755.
- Sharma, T., and Clayton, R.N., 1965, Measurement of  $^{18}\text{O}/^{16}\text{O}$  ratios of total oxygen of carbonates: *Geochimica et Cosmochimica Acta*, v. 29, p. 1347-1353.
- Sharp, Z.D., Frey, M., and Livi, K.J.T., 1995, Stable isotope variations (H, C, O) in a prograde metamorphic Triassic red bed formation, Central Swiss Alps: *Schweiz. Mineral. Petrogr. Mitt.*, v. 75, p. 147-161.
- Shields, G., Stille, P., Brasier, M., and Atudorei, N.-V., 1997, Stratified oceans and oxygenation of the late Precambrian environment: a post glacial geochemical record from the Neoproterozoic of W. Mongolia: *Terra Nova*, v. 9, p. 218-222.
- Simionescu, I., 1908, Über das Vorkomen der Werfener Schichten in Dobrogea (Rumänien): *Verh. k.k. geol. R.-A., Wien*, v. 7, p. 159-161.
- Simionescu, I., 1910, La faune triassique de Desli-Caira (Dobrogea): *Publ. Fond. V. Adamachi*, v. 26, p. 465-494.
- Simionescu, I., 1911, Studii geologice si paleontologice din Dobrogea. V. Fauna triasica inferioara din Dobrogea: *Acad. Rom., Publ. Fond. V. Adamachi, Bucuresti*, v. 5, p. 63-79.
- Simionescu, I., 1913, Les ammonites Triasiques de Hagighiol (Dobrogea): *Publ. Fond. V. Adamachi*, v. 34, p. 271-370.
- Simionescu, I., 1925, Les couches à Daonella de Dobrogea: *Publ. Fond. V. Adamachi*, v. 43.
- Simon, V., and Steuber, T., 1993, Stratigraphie und stabile isotope ( $\text{d}^{13}\text{C}$ ,  $\text{d}^{18}\text{O}$ ,  $\text{d}^{13}\text{Corg}$ ) der Domvrena-Schichtengruppe (Trias-Jura) im Helikon-Gebirge, Bötien/Griechland: *Sonderveröffentlichungen, Geologisches Institut der Universität zu Köln*, v. 70, p. 259-275.
- Spero, H.J., Bijma, J., Lea, D.W., and Bemis, B.E., 1997, Effect of seawater carbonate concentration on foraminiferal carbon and oxygen isotopes: *Nature*, v. 390, p. 497-500.
- Spötl, C., 1988, Sedimentologisch-fazielle Analyse Tektonisierter Evaporitserien - eine Fallstudie am Beispiel des Alpenen Haselgebirges (Permoskith, Nördliche Kalkalpen): *Geol. Paläont. Mitt. Innsbruck*, v. 15, p. 59-69.
- Spötl, C., and Burns, S.J., 1991, Formation of  $^{18}\text{O}$ -depleted dolomite within a marine evaporitic sequence, Triassic Reichenhall Formation, Austria: *Sedimentology*, v. 38, p. 1041-1057.
- Spötl, C., and Pak, E., 1996, A strontium and sulfur isotopic study of Permo-Triassic evaporites in the Northern Calcareous Alps, Austria: *Chemical Geology*, v. 131, p. 219-234.
- Srikantia, S.V., 1981, The lithostratigraphy, sedimentation and structure of Proterozoic-Phanerozoic Formations of Spiti basin in the Higher Himalaya of the Himachal Pradesh, India, in Sinha, A.K., ed., *Contemporary geoscientific researches in Himalaya, Volume 1: Dehra Dun*, p. 31-48.
- Stampfli, G., Marcoux, J., and Baud, A., 1991, Tethyan margins in space and time: *Palaeogeography, Palaeoclimatology, Palaeoecology*, v. 87, p. 373-409.
- Stampfli, G.M., 1996, The Intra-Alpine terrain: A Paleotethyan remnant in the Alpine Variscides: *Eclogae geol. Helv.*, v. 89, p. 13-42.
- Stampfli, G.M., Mosar, J., Favre, P., Pillecuit, A., and Vannay, J.C., in press, Permo-Triassic evolution of the western Tethyan realm. The Neotethys/East-Mediterranean connection in Cavazza, W.; Robertson, A.H.F.; & Ziegler, P.A., eds.: *Peritethyan rift/wrench basins and passive margins: Bull. Museum Nat. Hist. Nat., Paris*.
- Stanley Jr., G.D., 1988, The History of Early Mesozoic Reef Communities: A Three-Step Process: *Palaios*, v. 3, p. 170-183.
- Steck, A., Epard, J.-L., Vannay, J.-C., Hunziker, J., Girard, M., Morard, A., and Robyr, M., 1998, Geological transect across the Tso Morari and Spiti areas: The nappe structures of the Tethys Himalaya: *Eclogae geol. Helv.*, v. 91, p. 103-121.



- Steuber, T., 1991, Conodont stratigraphy, depositional environments and stable isotope composition of the Triassic in the Helicon Mountains (Beotia, Greece): *Bulletin of the Geological Society of Greece*, v. 25, p. 515-528.
- Stille, P., and Shields, G., 1997, *Radiogenic Isotope Geochemistry of Sedimentary and Aquatic Systems*, Springer Verlag, 217 p.
- Stiller, M., Rounick, J.S., and Shasha, S., 1985, Extreme carbon-isotope enrichments in evaporating brines: *Nature*, v. 316, p. 434-435.
- Strauss, H., 1997, The isotopic composition of sedimentary sulfur through time: *Palaeogeography, Palaeoclimatology, Palaeoecology*, v. 132, p. 97-118.
- Stutz, E., 1988, Géologie de la chaîne de Nyimaling aux confins du Ladakh et du Rupshu (NW-Himalaya, Inde) - évolution paléogéographique et tectonique d'un segment de la marge nord-indienne: *Lausanne*, 149 p.
- Thackeray, J.F., van der Merwe, N.J., Lee-Thorp, J.A., Sillen, A., Lanham, J.L., Smith, F., Keyser, A., and Monteiro, P.M.S., 1990, Changes in carbon isotope ratios in the late Permian recorded in therapsid tooth apatite: *Nature*, v. 347, p. 751-753.
- Thiede, J., and Suess, E., 1983, Sedimentary Record of Ancient Coastal Upwelling: Episodes, p. 15-18.
- Tozer, E.T., 1967, A standard for Triassic time: *Bulletin of the Geological Survey of Canada*, v. 156, p. 103.
- Tozer, E.T., 1980, Triassic Ammonoidea: Classification, Evolution and Relationship with Permian and Jurassic Forms, *in* House, M.R., and Senior, J.R., eds., *The Ammonoidea, Volume 18: Systematics Association Special Volume*, Academic Press, p. 66-100.
- Tozer, E.T., 1984, The Trias and its ammonoids: the evolution of a time scale, 171 p.
- Tozer, E.T., 1988, Towards a Definition of the Permian-Triassic Boundary: Episodes, v. 11, p. 251-255.
- Tozer, E.T., 1993, Triassic chronostratigraphic divisions considered again: *Albertiana*, v. 11, p. 32-37.
- Tozer, E.T., 1994a, Age and correlation of the *Otoceras* beds at the Permian-Triassic Boundary: *Albertiana*, v. 14, p. 31-37.
- Tozer, E.T., 1994b, Canadian Triassic Ammonoid Faunas: *Geological Survey of Canada Bulletin*, v. 467, 663 p.
- Tsien, H.H., 1985, Origin of Stromatactis - a Replacement of Colonial Microbial Accretions, *in* Toomey, D.F., and Nitecki, M.H., eds., *Paleoalgology: Contemporary Research and Applications*, Springer-Verlag, p. 274-289.
- Tucker, M.E., 1993, Carbonate diagenesis and sequence stratigraphy, *in* Wright, V.P., ed., *Sedimentology Review: Oxford, Blackwell Scientific Publications*, p. 51-72.
- Tyson, R.V., 1995, *Sedimentary Organic Matter. Organic Facies and Palynofacies*, Chapman & Hall.
- Ulmishek, G.F., and Klemme, H.D., 1990, Depositional Controls, Distribution and Effectiveness of World's Petroleum Source Rocks: *U.S. Geological Survey Bulletin*, v. 1931, 59 p.
- Vahrenkamp, V.C., 1996, Carbon Isotope Stratigraphy of the Upper Kharab and Shuiba Formations: Implications for the Early Cretaceous Evolution of the Arabian Gulf Region: *The American Association of Petroleum Geologists Bulletin*, v. 80, p. 647-662.
- Van Cappellen, P., and Ingall, E.D., 1994, Benthic phosphorus regeneration, net primary production, and oceanic anoxia: A model of the coupled marine biogeochemical cycles of carbon and phosphorous: *Paleoceanography*, v. 9, p. 677-692.
- van de Schootbrugge, B., 1997, Sedimentological and Palynological Investigation of the Montan Section. The Permian-Triassic boundary in the Western Dolomites, Italy [MSc thesis], Utrecht University.

- Veizer, J., 1983, Trace elements and isotopes in sedimentary carbonates, *in* Reeder, R.J., ed., *Min. Soc. Amer. Reviews in mineralogy. Carbonates: mineralogy and chemistry*, Volume 11, p. 265-299.
- Veizer, J., Bruckschen, P., Pawellek, F., Diener, A., Podlaha, O.G., Carden, G.A.F., Jasper, T., Korte, C., Strauss, H., Azmy, K., and Ala, D., 1997a, Oxygen isotope evolution of Phanerozoic seawater: Palaeogeography, Palaeoclimatology, Palaeoecology, v. 132, p. 159-172.
- Veizer, J., Buhl, D., Diener, A., Ebner, S., Podlaha, O.G., Bruckschen, P., Jasper, T., Korte, C., Schaaf, M., Ala, D., and Azmy, K., 1997b, Strontium isotope stratigraphy: potential resolution and event correlation: Palaeogeography, Palaeoclimatology, Palaeoecology, v. 132, p. 65-77.
- Veizer, J., and Demovic, R., 1974, Strontium as a tool in facies analysis: *Journal of Sedimentary Petrology*, v. 44, p. 93-115.
- Veizer, J., Fritz, P., and Jones, B., 1986, Geochemistry of brahiopods: Oxygen and carbon isotopic records of Paleozoic oceans: *Geochimica et Cosmochimica Acta*, v. 50, p. 1679-1696.
- Veizer, J., Holser, W.T., and Wilgus, C., 1980, Correlation of  $^{13}\text{C}/^{12}\text{C}$  and  $^{34}\text{S}/^{32}\text{S}$  secular variations: *Geochimica et Cosmochimica Acta*, v. 44, p. 579-587.
- Visscher, H., Brinkhuis, H., Dilcher, D.L., Elsik, W.C., Eshet, Y., Looy, C.V., Rampino, M.R., and Traverse, A., 1996, The terminal Paleozoic fungal event: Evidence of terrestrial ecosystem destabilization and collapse: *Proc. Natl. Acad. Sci. USA*, v. 93, p. 2155-2158.
- von Rad, U., Dürr, S.B., Ogg, J.G., and Wiedmann, J., 1994, The Triassic of the Thakkhola (Nepal). I: Stratigraphy and paleoenvironment of a north-east Gondwanan rifted margin: *Geol. Rundsch.*, v. 83, p. 76-106.
- Wang, C., 1990, Some problems on the Guryul Ravine section of Kashmir as Permian-Triassic boundary stratotype: *Palaeontologia Cathayana*, v. 5, p. 263-266.
- Wang, K., Geldsetzer, H.H.J., and Krouse, H.R., 1994, Permian-Triassic extinction: Organic  $\delta^{13}\text{C}$  evidence from British Columbia, Canada: *Geology*, v. 22, p. 580-584.
- Waterhouse, J.B., 1979, Permian rocks of the Kali Gandaki Area (Thakkhola), North Central Nepal, *in* Gupta, V.J., ed., *Upper Paleozoics of the Himalaya*: Delhi, India, Hindustan Publ. Corp, p. 195-213.
- Waterhouse, J.B., 1987, Aspects of the Permian Tethys: its definition, interface with Gondwana, original disposition, and subsequent deformation., *in* McKenzie, K.G., ed., *Shallow Tethys 2*: Rotterdam, Balkema, p. 131-148.
- Watts, K.F., 1985, Evolution of a carbonate slope facies along a South Tethyan continental margin : the Mesozoic Sumeini group and the Qumayrah facies of the Muti formation, Oman.: (unpublished PhD thesis), University of California, Santa Cruz.
- Watts, K.F., 1990, Mesozoic carbonate slope facies marking the Arabian platform margin in Oman: depositional history, morphology and paleogeography, *in* Robertson, A.H.F., Searle, M.P., and Ries, A.C., eds., *The Geology and tectonics of the Oman Region*, Volume 49: Geological Society Special Publication, p. 139-160.
- Watts, K.F., and Garrison, R.E., 1986, Sumeini Group, Oman - Evolution of a Mesozoic Carbonate Slope on a South Tethyan Continental Margin: *Sedimentary Geology*, v. 48, p. 107-168.
- Wefer, G., and Berger, W.H., 1991, Isotope paleontology: growth and composition of extant calcareous species: *Marine Geology*, v. 100, p. 207-248.
- Weidlich, O., Bernecker, M., and Flügel, E., 1993, Combined quantitative analysis and microfacies studies of ancient reefs: An integrated approach to upper Permian and upper Triassic reef carbonates (Sultanate of Oman): *Facies*, v. 28, p. 115-144.
- Weissert, H., and Lini, A., 1991, Ice Age Interludes During the Time of Cretaceous Greenhouse Climate, *in* Müller, D.W., McKenzie, J.A., and Weissert, H., eds., *Controversies in Modern Geology*, Academic Press, p. 173-192.

- Weissert, H., and Mohr, H., 1996, Late Jurassic climate and its impact on carbon cycling: Palaeogeography, Palaeoclimatology, Palaeoecology, v. 122, p. 27-43.
- Wendt, J., 1973, Cephalopod accumulations in the Middle Triassic Hallstatt Limestone of Yugoslavia and Greece: N. Jb. Geol. Paläont. Mh., v. 28, p. 189-206.
- Wenzel, B., and Joachimski, M.M., 1996, Carbon and oxygen isotopic composition of Silurian brachiopods (Gotland/Sweden): palaeoceanographic implications: Palaeogeography, Palaeoclimatology, Palaeoecology, v. 122, p. 143-166.
- Wiedmann, J., and Kullmann, J., 1996, Crises in Ammonoid Evolution, *in* Landman, N., ed., Ammonoid Paleobiology, Volume 13: Topics in Geobiology: New York, Plenum Press, p. 795-813.
- Wignall, P.B., and Hallam, A., 1993, Griesbachian (Earliest Triassic) palaeoenvironment changes in the Salt Range, Pakistan and southeast China and their bearing on the Permo-Triassic mass extinction: Palaeogeography, Palaeoclimatology, Palaeoecology, v. 102, p. 215-237.
- Wignall, P.B., Morante, R., and Newton, R., 1998, The Permo-Triassic transition in Spitsbergen:  $\delta^{13}\text{C}_{\text{org}}$  chemostratigraphy, Fe and S geochemistry, facies, fauna and trace fossils: Geological Magazine, v. 135, p. 47-62.
- Wilgus, C.K., 1981, A stable isotope study of Permian and Triassic marine evaporite and carbonate rocks, Western Interior, U.S.A., PhD thesis, University of Oregon, Eugene, 131 p.
- Wilson, K.M., Pollard, D., Hay, W.W., Thompson, S.L., and Wold, C.N., 1994, General circulation simulations of Triassic climates: Preliminary results, *in* Klein, G.D., ed., Pangea, Paleoclimate, Tectonics, and Sedimentation During Accretion, Zenith and Breakup of a Supercontinent, Volume 288: Geological Society of America Special Paper, p. 91-116.
- Woodruff, F., and Savin, S.M., 1985,  $\delta^{13}\text{C}$  values of Miocene Pacific benthic foraminifera: Correlations with sea level and biological productivity: Geology, v. 13, p. 119-122.
- Worden, R.H., Smalley, P.C., and Fallick, A.E., 1997, Sulfur cycle in buried evaporites: Geology, v. 25, p. 643-646.
- Wright, J., Schrader, H., and Holser, W.T., 1987, Paleoredox variations in ancient oceans recorded by rare earth elements in fossil apatite: Geochimica et Cosmochimica Acta, v. 51, p. 631-644.
- Xu, D.-Y., and Yan, Z., 1993, Carbon isotope and iridium event markers near the Permian/Triassic boundary in the Meishan section, Zhejiang Province, China: Palaeogeography, Palaeoclimatology, Palaeoecology, v. 104, p. 171-176.
- Yang, Z., and Li, Z., 1992, Permo-Triassic boundary relations in South China, *in* Sweet, W.C., Zunyi, Y., Dickins, J.M., and Hongfu, Y., eds., Permo-Triassic Events in the Eastern Tethys (Stratigraphy, Classification, and Relations with the Western Tethys), Cambridge University Press, p. 9-20.
- Yin, H., 1996, The Paleozoic-Mesozoic boundary candidates of the Global Stratotype Section and Point of the Permian-Triassic boundary, China University of Geosciences Press, 137 p.
- Yugan, J., Wardlaw, B.R., Glenister, B.F., and Kotlyar, G.V., 1997, Permian chronostratigraphic subdivisions: Episodes, v. 20, p. 10-15.
- Zeeh, S., Bechstädt, T., McKenzie, J., and Richter, D.K., 1995, Diagenetic evolution of the Carnian Wetterstein platforms of the Eastern Alps: Sedimentology, v. 42, p. 199-222.
- Zeeh, S., Walter, U., Kuhlemann, J., Herlec, U., Keppens, E., and Bechstädt, T., 1997, Carbonate cements as a tool for fluid flow reconstruction: a study in parts of the Eastern Alps (Austria, Germany, Slovenia), Basin-Wide Diagenetic Patterns: Integrated Petrologic, Geochemical, and Hydrological Considerations: SEPM Special Publication, Volume 57, p. 167-181.

# **Appendix**

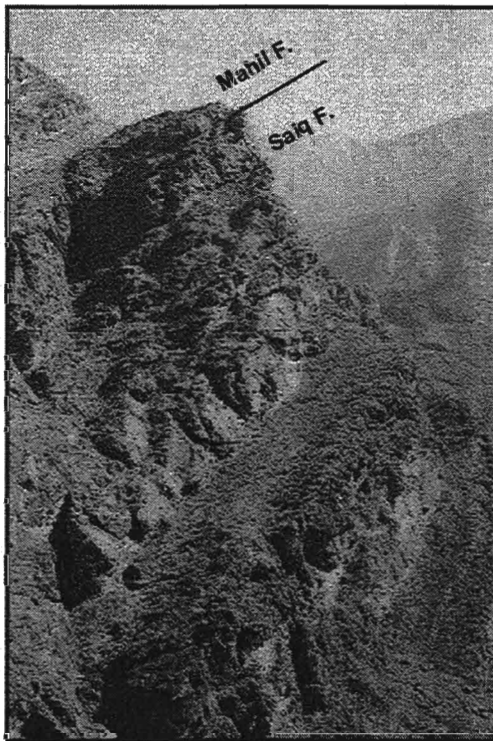
**Plates (1 to 5)**

**Tables (1 to 27)**



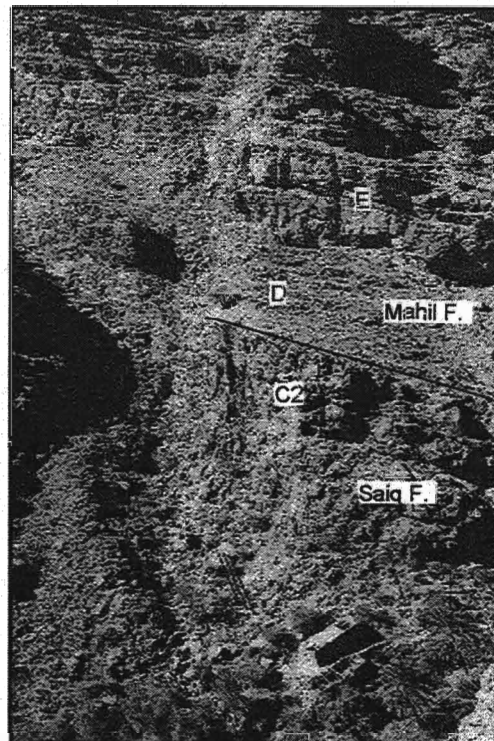
# Plate 1

Fig. 1



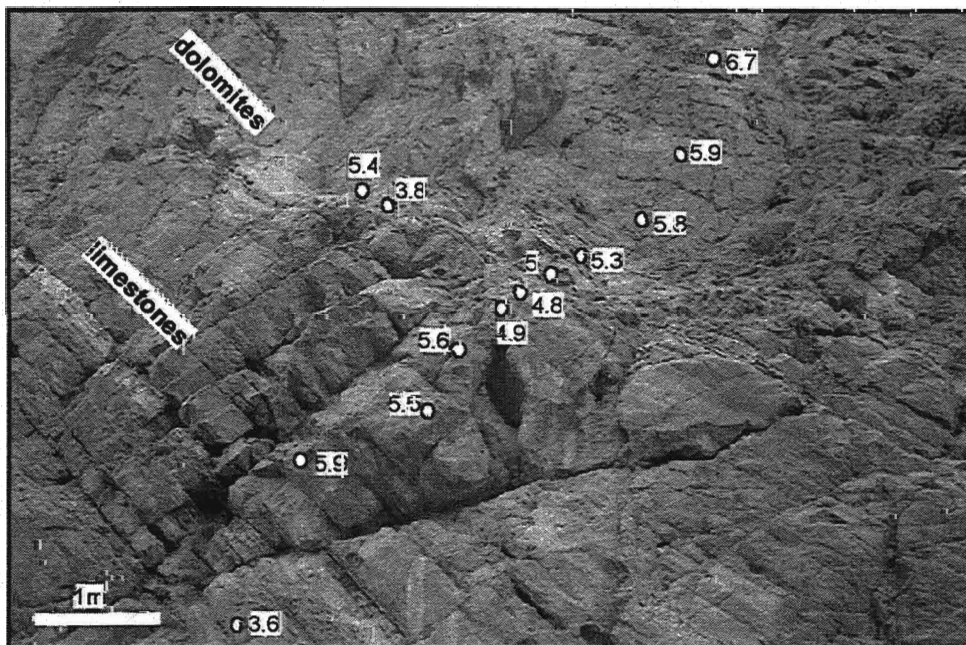
The contact between the Saiq and Mahil formations at Wadi Sahtan

Fig. 2



The contact between the Saiq and Mahil formations at Wadi Sahtan and the main lithological units.

Fig. 3



The irregular front of dolomitization affecting the Saiq Formation. Circles show the location of samples and numbers the corresponding  $\delta^{13}\text{C}$  values.



## Plate 2

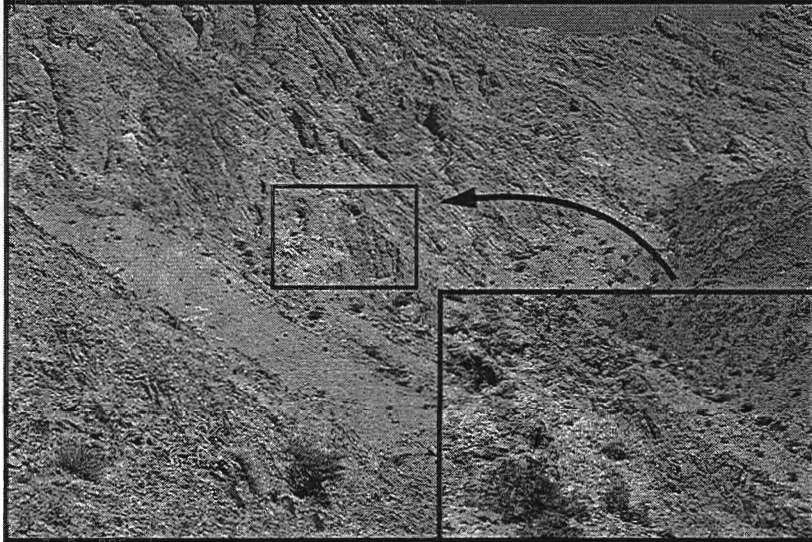


**Fig. 1**

View of the south-eastern side of the Ba'id exotic and the location of the Wadi Alwa section (arrow)

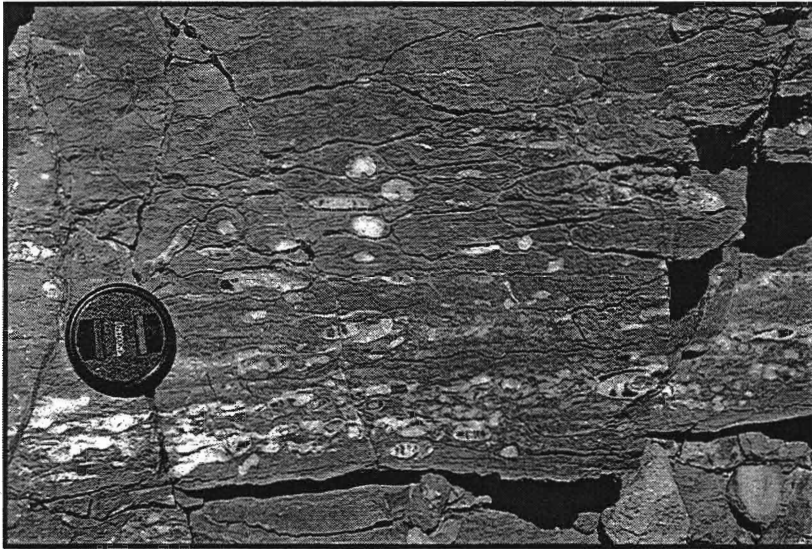


**Fig. 2**

The Hallstatt-type ammonoid-rich limestones of the Alwa Formation

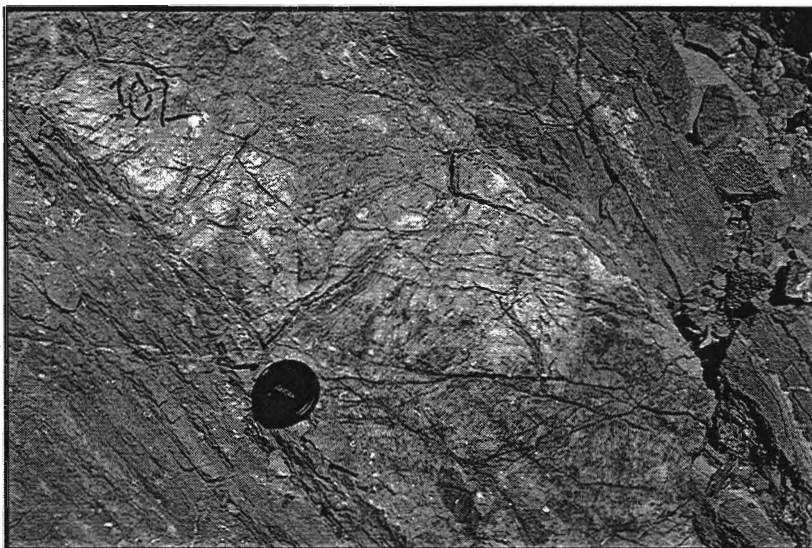


**Fig. 3**

Thrombolitic layer interbedded with the Hallstatt-type limestones  
(Alwa Formation)

(Alwa formation)





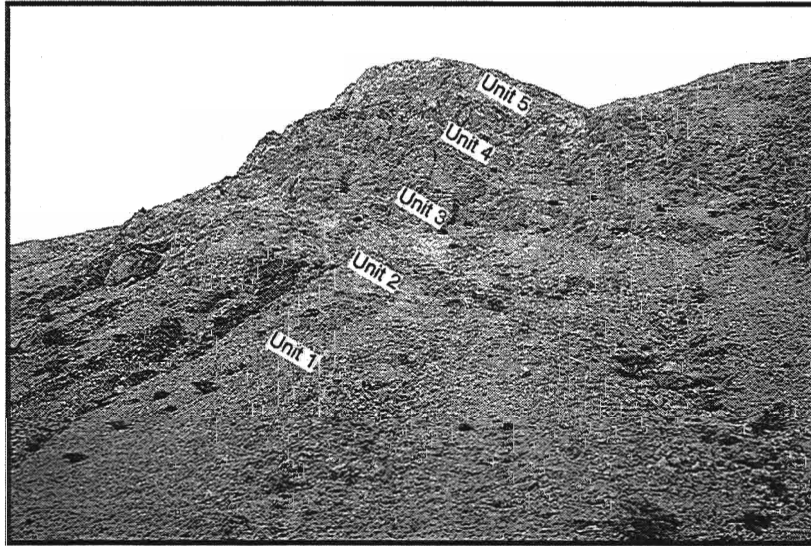


Fig. 1

The Wadi Wasit section A, with the main lithological units separated. (Upper Permian to Lower Triassic, Oman Mountains)

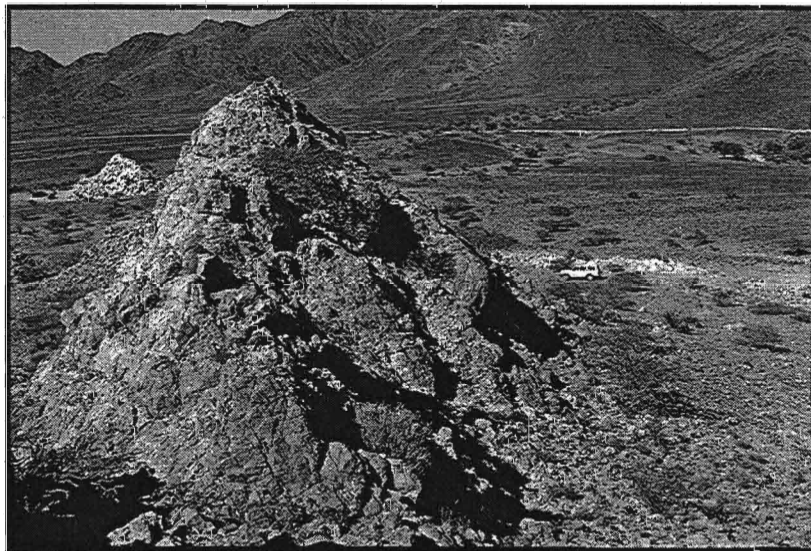


Fig. 2

The Wadi Musjah section, showing in the left side the Upper Permian dolomitized breccia



Fig. 3

The contact between the Upper Permian dolomitic breccia and the Lower Triassic platy limestones (Wadi Musjah, Oman Mountains)



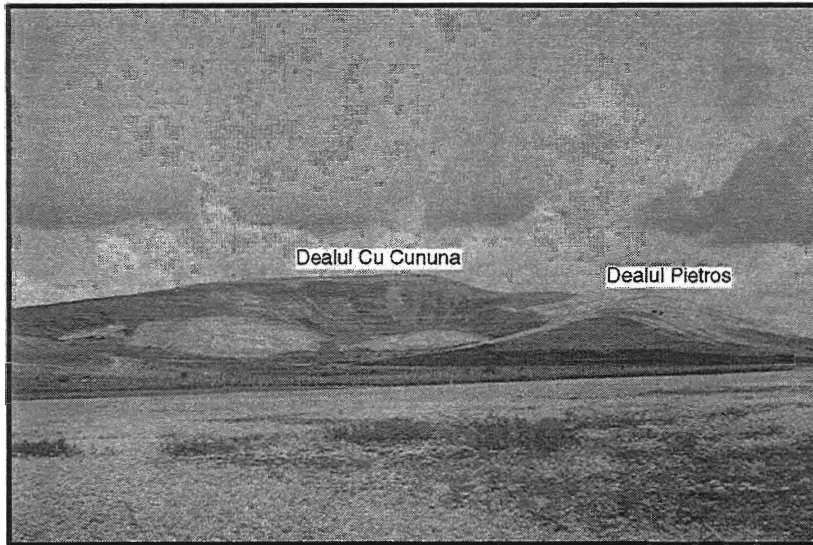


Fig. 1

Panoramic view of the Dealul Pietros and Dealul cu Cununa area, made-up of Early Spathian to Early Carnian carbonate deposits (North Dobrogea, Romania)



Fig. 2

Panoramic view of the Desli Caira Hill, where the Lower - Middle Triassic boundary is exposed (North Dobrogea, Romania)

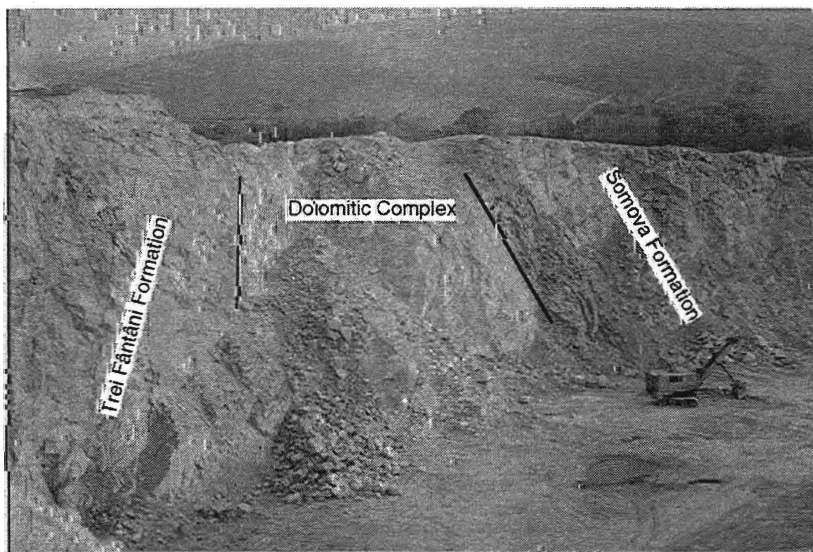


Fig. 3

Panoramic view of the Trei Fântâni Quarry, exposing Upper Spathian to Anisian carbonate deposits of various types.

Anisian carbonate deposits of various types.



# Plate 5

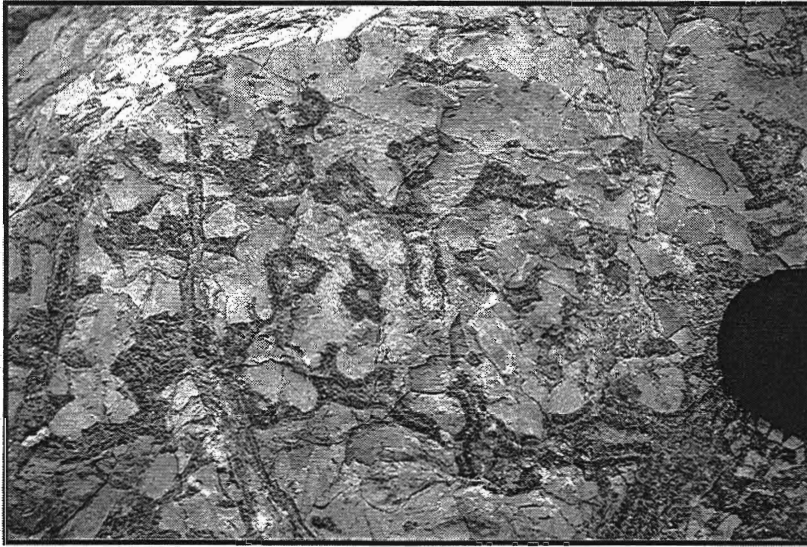


**Fig. 1**

Stromatactis cavities with geopetal structures (Caerace Limestone, Mahmudia Quarry). North Dobrogea, Romania

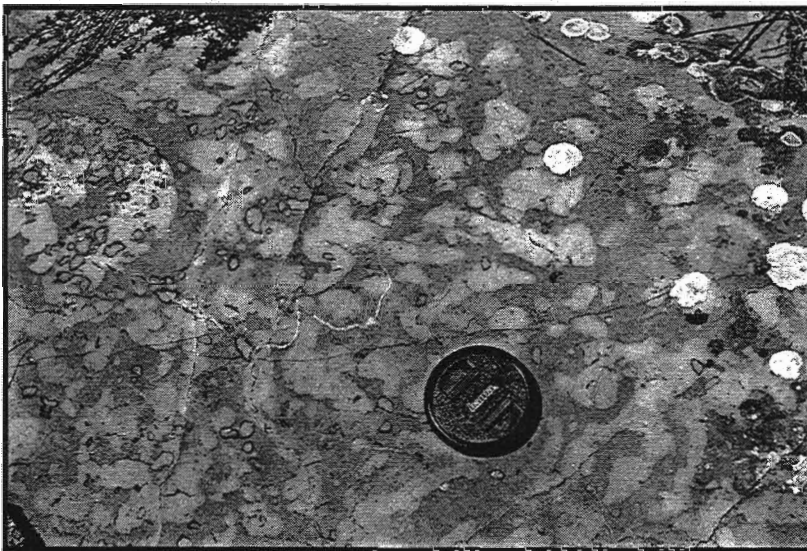


**Fig. 2**

Typical bed surface with burrows of the Agighiol Limestone (Hallstatt-type limestones). Dealul Pietros, North Dobrogea, Romania



**Fig. 3**

Planar stromatolites associated with Hallstatt-type limestones. Dealul Pietros, North Dobrogea, Romania

Dealul Pietros, North Dobrogea, Romania



**Table 1 Nammal Gorge** (position is in meters, relative to the Permian-Triassic boundary)

Sample	$\delta^{13}\text{C}$	$\delta^{18}\text{O}$	Position
N3a1	-0.24	-5.5	0.3
N3a1'	-0.28	-5.08	0.32
N3a1''	-0.21	-5.84	0.35
N3a1'''	-0.19	-5.61	0.4
N3c	1.6	-4.33	1.2
N4a	1.57	-6.11	1.9
N5b	1.22	-6.41	2.7
N6a1	0.28	-9.41	3.3
N6b1	0.12	-8.99	3.8
N6b4	0.57	-7.32	4
N6c2	0.3	-6.22	4.2
N6c3	0.22	-6.06	4.3
N7a	-0.12	-5.3	4.6
N7b	-0.61	-7.65	5.1
N7c	0.09	-5.34	5.7
N8a	-0.44	-7.58	6.3
N8b	0.66	-5.31	7.2
N8c	0.18	-4.29	7.8
N8d	1.04	-5.16	8.8
N8e	0.72	-5.56	10
N8f	0.98	-5.18	10.9
N8g	0.78	-5.17	12.3
N8i	1.53	-5.57	14
N16a1	-0.64	-8.11	49
N16a2	-1.8	-8.43	52.4
N16c1	-1.77	-8.97	57.5
N16c3	-1.66	-8.69	57.9
N17a5	-1.99	-8.36	61
N17b3	-1.89	-7.91	62.3
N17c1	-1.95	-7.61	62.8
N18a1	-2.3	-7.54	63.4
N18a3	-2.32	-8.55	64.5
N18b1	-2.24	-8.62	64.8
N19a1	-2.16	-8.18	66.6
N19a2	-2.18	-8.31	67.2
N19b3	-2.06	-8.56	69
N19c1	-0.6	-7.52	69.4
N20a1	0.59	-6.97	69.9
N20a2	0.45	-8.62	70.3
N20b1	0.68	-6.66	70.9
N20b4	1.19	-6.53	71.4
N20c2	1.84	-7.25	72.2
N21a3	1.74	-9.18	73.7
N21b1	-0.82	-6.94	74.4
N21b2	0.48	-8.81	75.1
N21b3	-0.46	-6.27	75.8
N22b	-1.38	-7.39	82
N26c	-2.13	-7.47	104.2
N26d	-1.8	-7.22	104.8
N27a2	-1.72	-7.49	107
N27a5	-1.89	-7.54	110
N27e3	-1.66	-3.61	118.5

Sample	$\delta^{13}\text{C}$	$\delta^{18}\text{O}$	Position
W 214	4.61	-6.45	-163
W 208	4.77	-6.65	-161
W 189	4.23	-7.44	-137.5
W 175	5.29	-9.18	-132
W 162	5.27	-8.14	-128
W 151	5.01	-6.94	-120
W 146	5.07	-7.53	-112.5
W 134	5.41	-8.23	-99
W 126	5.27	-8.56	-92.5
W 118	5.03	-7.98	-84
W 113	4.71	-8.26	-79
W 108	4.63	-8.03	-74.5
W 103	4.55	-6.96	-71
W 98	4.43	-8.14	-68
W 92	4.21	-7.22	-63
W 80	3.72	-3.33	-56
W 72	3.67	-5.78	-49.5
CH 65	3.43	-3.23	-38.5
CH 63	3.47	-5.61	-37.5
CH 62	3.66	-4.51	-36
CH 60	3.77	-5.79	-34.5
CH 59	3.85	-5.31	-33
CH 57	3.68	-6.7	-31.5
CH 53	3.78	-5.67	-27.5
CH 49	3.06	-7.83	-25
CH 43	3.64	-8.99	-20.5
CH 42	3.64	-7.44	-19
CH 37	3.21	-7.68	-17
CH 36	2.17	-8.87	-15
CH 35	3.09	-7.54	-14
CH 33	3.05	-7.35	-12
CH 25	2.33	-8.9	-7.5
CH 13	1.47	-9.55	-2.5



**Table 2 Guryul Ravine**

Sample	$\delta^{13}\text{C}$	$\delta^{18}\text{O}$	Position
GU 44	2.44	-11.31	-75
GU 42	2.95	-11.05	-73
GU 41	2.69	-10.86	-72
GU 40	1.63	-10.36	-71
GU 35	3.13	-12.05	-19.5
GU 34	1.27	-11.34	-14.7
GU 32	1.7	-10.59	-8
GU 31	2.28	-11.01	-5.6
GU 30	-0.59	-10.8	-2.5
GU 29	-0.31	-10.09	-0.5
GU 1	-0.93	-9.93	-0.05
GU 2	-0.4	-9.79	0.05
GU 4	1.14	-10.9	0.2
GU 5	-1	-10.19	0.25
GU 8	-0.85	-10.95	0.4
GU 9	-0.14	-10.16	1
GU 10	0.04	-11.17	1.5
GU 11	-1.23	-11.14	2.3
GU 48	-1.05	-11.25	3.4
GU 13	-1.12	-11.14	3.9
GU 15	-1.61	-11	5.3
GU 16	-2.32	-11.51	6.2
GU 17	-2.57	-11.58	7.2
GU 18	-3.24	-11.24	7.8
GU 19	-2.94	-11.02	8.2
GU 20	-3.09	-10.79	8.7
GU 21	-2.89	-10.89	9.5
GU 22	-2.94	-11.07	10.2
GU 23	-2.49	-10.78	11
GU 24	-3.38	-10.25	12.8
GU 25	-3.78	-10.31	14
GU 26	-2.5	-10.62	15
GU 27	-1.36	-10.52	15.8
GU 28	-1.69	-9.62	17.3

**Table 3 Landu Nala**

Sample	$\delta^{13}\text{C}$	$\delta^{18}\text{O}$	Position
L7a	0.79	-7.6	22
L8a	0.83	-8.32	25
L8b	0.66	-8.49	29
L9a2	-1.43	-8.78	32
L9b3	-1.55	-8.66	33.5
L10b3	-2.11	-8.26	36.5
L10c1	-1.99	-8.6	38
L10c3	-1.92	-8.46	39
L10c4	-2.17	-8.23	39.5
L11a	-1.42	-7.98	41.5
L11b	-1.58	-8.32	42.5
L11c	-1.36	-8.73	43.5
L13a	4.74	-4.79	47
L13b	3.75	-4.68	47.5
L14a	3.41	-7.04	48.5
L14b1	3.47	-6.22	49.5
L14 b3	2.3	-7.84	51.5

**Table 4 Palgham**

P1	1.92	-11.82	-13
P2	1.54	-12.1	-8
P3	0.63	-11.9	-6
P4	1.14	-11.47	-0.3
P5	-2.07	-11.95	0.1
P6	-2.63	-11.59	2
P7	-3.04	-10.9	8
P8	-2.84	-10.82	10
P9	-4.29	-11.38	17.5
P10	-3.56	-10.88	22
P12	-2.59	-11.21	23.5
P 11	-2.78	-10.73	26

**Table 5 Thini Chu**

T4	-0.15	-12.61
T5	-0.95	-9.88
T6	-0.53	-10.03
T7	-0.9	-10.67
T8	-0.55	-9.36
T9	-0.77	-23.16
T10	-0.16	-18.83
T11	-1.07	-20.69
T15	-1.34	-21.31
T16	-0.3	-13.11
T17	-0.26	-11.54

**Table 6 Losar, Spiti** (position is in meters relative to the Permian-Triassic boundary)

Sample	$\delta^{13}\text{C org}$	$\delta^{13}\text{C}$	$\delta^{18}\text{O}$	Position
1276		1.8	-7.65	85.1
1275		1.85	-7.44	84.75
1273	-23.84	1.89	-7.45	83.2
1271		1.78	-7.32	81.9
1270		1.59	-7.13	81.4
1269		1.46	-8.36	80.9
1268		1.48	-8.52	80.55
1267	-23.75	1.49	-10.4	79.9
1266		1.45	-7.92	79.6
1265		1.23	-10.4	79.3
1264		1.12	-8.68	79.05
1262		0.8	-8.45	78.6
1258	-24.7	0.79	-9.88	77.8
1256		0.57	-9.75	77.45
1254	-25.23	0.93	-9.38	77.1
1251		0.93	-9.57	76.5
1249		0.9	-9.21	76.35
1247	-24.75	0.51	-9.91	74.9
1245		0.8	-9.94	72.9
1243		1.15	-11.37	72.3
1240	-23.02	1.02	-10.56	71.9
1238	-26.39	1.32	-9.21	69.4
1236		1.34	-9.09	68.7
1233		1.36	-9.56	67.95
1232	-26.01	1.34	-9.53	67.35
1229		1.13	-10.15	66.5
1228		1.25	-9.14	64.7
1226		0.81	-9.76	64.25
1225		0.8	-9.68	64
1224	-25.52	0.46	-9.61	63.5
1223	-25.91	-0.17	-9.81	63.1
1222		0.34	-10.08	60.6
1221		-0.17	-10.1	59.9
1220	-25.24	0.47	-10.2	59.6
1219		1.21	-9.19	58.6
1218	-23.91	1.11	-10.21	58.1
1217		1.13	-9.53	57.2
1216		0.84	-9.73	57
1215	-24.76	nd	nd	56.1
1298		1.63	-9.43	55.35
1296		1.67	-9.56	55.3
1328		1.67	-9.56	55.15
1288	-23	1.49	-8.8	53.8
1286		1.55	-9.5	53.4
1285	-23.76	1.71	-9.71	53.15
1282		2.75	-9.34	52.25
1281	-22.24	2.82	-8.95	52.05
1278		2.6	-9.36	51.65
1277		2.8	-9.44	51.45
1214		3	-10.36	51.2
1213	-21.57	2.74	-11.18	50.9
1210		2.45	-10.71	49.5
1305		1.29	-8.94	49.1
1304		1.21	-9.47	48.95
1209		1.11	-9.85	48.7
1208		0.76	-10.89	48.3
1206		0.85	-11.21	47.5
1204	-23.32	0.54	-11.4	46.2
1203		0.51	-11.84	45.9
1201	-23.68	-0.13	-11.94	44.5
1199	-24.74	-0.92	-9.28	42.8
1197	-22.92	-0.49	-11.61	41.6

Sample	$\delta^{13}\text{C org}$	$\delta^{13}\text{C}$	$\delta^{18}\text{O}$	Position
1195	-25.5	-0.64	-12.51	39.8
1194	-25.06	-0.04	-11.78	38.2
1193		0.39	-12.02	36.9
1192		0.81	-11.26	36.4
1191	-26.4	0.96	-11.79	36
1190	-24.26	2.4	-11.04	35.2
1189	-23.85	2.01	-11.1	34.6
1188	-23.58	2.6	-12.14	33.9
1187		1.98	-11.16	33.7
1186	-25.34	1.26	-11.7	33.3
1184	-25.07	0.59	-12.12	32.3
1183		-0.42	-12.15	31.9
1182		-2.05	-12.51	31.75
1181		-0.56	-10.94	31.7
1179	-25.47	-1.83	-11.63	31.1
1177		-1.78	-12.98	30.4
1175	-24.97	-2.08	-12.12	29.4
1173	-24.86	-2.11	-12.23	28.8
1171	-25.91	-2.4	-13.35	27.6
1170	-26.25	-2.76	-13.4	27
1168	-24.3	-2.35	-13.12	26
1164		-2.89	-12.18	24.85
1163	-25.3	-2.54	-12.62	24.5
1159		-2.82	-12.86	22.5
1158	-24.95	-2.59	-12.63	22.1
1155	-29.35	-2.72	-12.89	20.9
1154		-2.45	-12.78	20.6
1152		-2.58	-12.48	19.55
1151		-2.6	-12.42	19.2
1150	-26.25	-2.331	-12.52	18.9
1148	-25.06	-2.37	-12.65	18.2
1147		-2.42	-12.35	18.1
1146	-26.1	-2.19	-12.86	17.45
1143	-25.55	-1.88	-12.75	16
1141	-25.51	-2.05	-12.72	15.7
1139	-25.4	-2.11	-12.62	15
1136	-24.64	-1.91	-13.03	13.8
1134	-27.4	-1.83	-12.49	11.9
1133	-24.8	-1.71	-10.34	11.4
1130	-23.67	-1.42	-13.19	9.5
1122	-24.55	-0.84	-14.33	6.45
1121	-26.16	-0.46	-14.22	5.95
1118		0.31	-14.63	4.7
1117	-26.7	0.52	-14.35	4.25
1115	-23.6	0.6	-8.67	3.4
1114	-24.63	2.59	-12.99	3.2
1113	-23.96	1.74	-14.38	2.9
1111		0.96	-15.31	2
1215		0.75	-13.11	1.45
1110		-1.31	-8.36	1.2
1109		-0.04	-14.45	0.95
1108	-25.35	-0.93	-15.02	0.9
1107		-1.31	-14.7	0.75
1106		-1.77	-12.5	0.65
1105	-26.22	-1.63	-11.32	0.55
1104		0.64	-5.21	0.45
1103		1.34	-4.91	0.35
1102	-25.86	-0.78	-7.48	0.28
1101	-26.62	0.71	-5.73	0.15
1100		-0.89	-8.1	0.05

**Table 7 Wadi Sahrtan**

Sample	$\delta^{13}\text{C}$	$\delta^{18}\text{O}$
Om 9	3.57	-3.65
Om 10	1.57	-5.05
Om 11	1.46	-1.61
Om 12	0.92	-1.46
Om 13	1.93	-1.96
Om 15	1.54	-1.95
Om 16	1.17	-1.6
Om 18	1.59	-2.47
Om 19	1.55	-2.01
Om 20	1.88	-2.43
Om 21	2.33	-2.75
Om 22	2.65	-1.62
Om 23	0.62	-0.44
Om 24	2.87	-3.83
Om 25	2.86	-2.16
Om 26	3.59	-3.01
Om 27	2.99	-3.52
Om 28	3.86	-0.81
Om 28a	3.92	-2.02
Om 29	3.72	-0.85
Om 30	4.03	-2.78
Om 31	2.7	-1.51

**Table 9 Wadi Musjah 1**

WM161	3.35	-2.21
WM162	4.04	-1.61
WM164	3.03	-2.4
WM165	3.05	-1.67
WM166	2.5	-2.19
WM167	2.53	-3.08
WM168	2.51	-2.62
WM170	2.48	-2.18
WM173	2.67	-2.85
WM175	3.12	-3.22
WM177	2.85	-3.67
WM179	2.86	-2.38
WM182	3.25	-2.1
WM184	3.45	-2.35
WM186	2.8	-2.67
WM188	3.02	-1.71
WM190	2.54	-3.47
WM192	3.04	-2.58
WM194	3.17	-2.73
WM196	1.63	-4.36
WM198	1.92	-2.26

**Table 8 Wadi Alwa**

Sample	$\delta^{13}\text{C}$	$\delta^{18}\text{O}$
WA 67	2.84	-7.98
WA 70	4.46	-4.4
WA 72	3.94	-6.67
WA 73	3.01	-7.08
WA 73A	2.5	-7.92
WA 74	2.97	-6.09
WA 75	2.01	-8.93
WA 76	1.7	-5.11
WA 77	2.76	-5.17
WA 78	1.99	-5.02
WA 79	3.61	-4.66
WA 80	2.41	-4.95
WA 81	2.36	-7.72
WA 82	2.44	-7.19
WA 92	0.51	-7.25
WA 95	0.62	-7.79
WA 105	2.24	-8.03
WA 108	1.83	-7.58
WA 113a	2.081	-4.07
WA 113b	1.212	-4.01
WA 114	1.45	-8.08
WA 119	0.33	-7.92
WA 121	1.15	-6.09
WA 123	0.22	-7.48
WA 129	1.21	-7.34
WA 132	-0.23	-8.06
WA 136	-0.01	-7.72
WA 137	1.07	-7.76
WA 140	1.07	-7.35
WA 144	1.23	-6.91
WA 152	0.35	-7.35
WA 154	0.37	-7.83
WA 157	1.2	-7.59
WA 159	0.97	-6.45

**Table 10 Wadi Musjah 2**

WM 61	0.89	-4.23
WM 62	1.18	-3.83
WM 63	2.65	-3.76
WM 64	1.88	-2.51
WM 65	0.77	-1.81
WM 67	1.39	-2.35

**Table 11 Wadi Wasit**

Sample	$\delta^{13}\text{C}$	$\delta^{18}\text{O}$
WW229	3.85	-10.42
WW231	4.45	-8.85
WW232	5.02	-9.02
WW233	5.08	-8.61
WW234	4.83	-8.89
WW235	4.74	-7.85
WW240	1.65	-8.55
WW241	-0.67	-7.51
WW242	-0.57	-8.34
WW243	1.66	-6.78
WW244	2.13	-6.32
WW 200A	2.78	-6.64
WW200	2.67	-7
WW203	0.23	-8.49
WW204	-0.4	-7.25
WW206	0.25	-6.04
WW207	0.67	-7.78
WW211	-0.2	-7.11
WW217	-0.28	-7.24
WW219	-0.1	-8.12

**Table 12 Wadi Maqam**

Sample	$\delta^{13}\text{C}$	$\delta^{18}\text{O}$
468	4.31	-3.82
489	5.4	-3.67
496	3.58	-5.63
502	3.39	-3.32
503	4.95	-2.29
507	2.64	-5.43
509	3.7	-5.5
512	4.5	-2.47
514	4.89	-3.21
518	1.83	-2.39
521	2.07	-2.16
523	-1.06	-5.89
524	-0.56	-5.75
525	-0.1	-5.73
526	-1.05	-7.25
531	-1.53	-6.42
532	-1.72	-4.95

Table 13 Mahmudia

Sample	$\delta^{13}\text{C}$	$\delta^{18}\text{O}$
R95-1	3.2	-2.22
R95-2	3.3	-2.41
R95-7	2.73	-2.37
R95-8a	3.25	-2.23
R95-10	4.17	-2.2
R95-13	3.21	-2.01
R95-14	2.32	-2.44
R95-17	1.88	-3.27
R95-19	1.01	-3.05
R95-25	1.94	-2.75
R95-26	2.01	-3.36
R95-33	1.64	-4.68
R95-35	2.17	-2.56
R95-40	1.92	-3.16
R95-42	2.04	-2.42
R95-46	2.02	-3.09
R95-50	1.8	-2.84
R95-54	1.78	-2.24
R95-56	1.79	-2.05
R95-59	1.72	-2.48
R95-65	0.17	-1.84
R95-68	1.18	-4.35
R95-70	1.88	-2.13
R95-72	1.61	-2.63
R95-74	0.43	-3.68
R95-76	1.41	-3.18
R95-78	1.49	-3.84

Table 14 Duna Hill

R95-80	1.8	-4.26
R95-81	2.02	-3.9
R95-82	1.86	-3.94
R95-83	2.19	-3.05
R95-84	2.16	-3.44
R95-85	1.69	-3.15
R95-86	1.69	-3.88
R95-87	1.65	-4.11
R95-88	2.55	-2.99
R95-89	1.77	-4.06
R95-90	2.17	-3.2
R95-91	1.74	-3.58
R95-92	1.19	-3.85

Table 15 Desli Caira

Sample	$\delta^{13}\text{C}$	$\delta^{18}\text{O}$
9036a	2.7	-3.21
36/1	2.53	-3.23
36/2	2.84	-3.2
36/3	2.7	-3.2
36/4	2.98	-3.17
37/1	3.4	-2.26
37/2	3.48	-2.92
37/3	3.15	-3.23
37/4	3.32	-3.04
37/5	3.19	-3.12
37/6	3.58	-2.85
38/1	3.22	-2.65
38/2	3.25	-2.84
38/3	4.33	-2.76
38/4	3.72	-2.79
39/3	3.9	-2.6
39/5	3.87	-2.56
39/5a	3.35	-2.91
9039	3.81	-2.68
40/1	4.48	-2.33
40/2	4.1	-2.6
40/3	4.36	-2.5
40/6	3.74	-2.55
41/2	3.58	-2.52
41/4	3.98	-2.54
41/5	3.86	-2.46
41/6	3.85	-2.58
42/1	4.06	-2.65
42/2	4.34	-2.53
9042	2.88	-3.21
42/3	4.19	-2.51
43/1	4.45	-2.45
9043	3.6	-3.85
43/3	3.32	-2.61
43/6	3.14	-3.38
43/7	4.17	-2.58
44/1	4.53	-2.35
9044	4.87	-2.48
44/3	3	-3.09
44/4	4.77	-2.43
45/1	4.6	-2.43
45/2	4.36	-2.6
9045	4.4	-2.71
45/4	4.26	-2.54
9046	4.33	-2.6
9047	4.5	-2.63
49/1	4.58	-2.54
9048	4.05	-2.62
49/2	4.16	-2.61
9050	3.99	-2.74

**Table 16 Dealul Pietros I**

Sample	$\delta^{13}\text{C}$	$\delta^{18}\text{O}$
V97-504	2.2	-5.62
V97-506	1.74	-6.3
V97-507	1.39	-4.15
V97-510	1.97	-3.41
V97-511	1.68	-3.46
V97-512	1.55	-3.49
V97-515	1.82	-3
V97-518	1.86	-3.58
V97-520	2	-3.56
V97-521	1.54	-3.68
V97-523	2.24	-4.18
V97-524	2.13	-4.25
V97-525	2	-4.47

**Table 17 Dealul Pietros II**

"Hyatti"	$\delta^{13}\text{C}$	$\delta^{18}\text{O}$
R95-184	2.44	-3.02
R95-185	2.53	-3.07
R95-186(1)	2.52	-2.9
R95-186(2)	2.29	-3.6
R95-187	2.49	-3.14
R95-188	2.36	-3.26
R95-189	1.92	-3.64
R95-201	2.36	-2.8
R95-203	2.36	-2.88
R95-204	1.88	-3.15
R95-205	1.86	-3.08
R95-206	1.91	-6.27
R95-207	2.31	-4.1
R95-208	2.34	-5.12
R95-209	1.81	-3.07
R95-210	1.72	-2.48
R95-211	1.89	-2.59
R95-212	1.72	-3.04
R95-213	1.72	-2.84
R95-214	1.93	-2.69
R95-216	1.85	-3.7
R95-217	1.85	-5.65
R95-219	2.44	-3.02
R95-220	2.16	-4.9
R95-221	2.65	-3.98
R95-222	2.16	-5.73
R95-223	2.12	-6.65

**Table 18 Dealul Pietros III**

Sample	$\delta^{13}\text{C}$	$\delta^{18}\text{O}$
D 9063	1.8	-2.91
D 9064	1.8	-2.46
D 9065	3.2	-2.76
D 9066	1.98	-3.35
D 9067	2.2	-2.88
D 9068	2.81	-3.46
D 9069	2.36	-3.33
D 9070	2.2	-3.12
D 9071	2.29	-3.17
D 9072	2.67	-3.12

**Table 19 Dealul Lung**

DL	$\delta^{13}\text{C}$	$\delta^{18}\text{O}$
DL 1	2.68	-3.03
DL 4	2.98	-2.8
DL 6	2.96	-2.91
DL 7	3.3	-2.54
DL 8	3.24	-2.32
DL 10	3.48	-2.22
DL 12	3.42	-2.39
DL 13	3.44	-2.52
DL 14	3.22	-2.7
DL 16	3.06	-2.92
DL 18	2.96	-2.7
DL 20	3.26	-2.55
DL 21	3.52	-2.59
DL 22	3.51	-2.82
DL 23	3.28	-2.55
DL 24	3.21	-2.8
DL 25	3.59	-2.64
DL 26	3.24	-2.86
DL 27	3.44	-2.66
DL 30	3.16	-2.82
DL 31	3.28	-3.01
DL 32	3.18	-3.1
DL 33	3.34	-2.97
DL 200	2.89	-3.31
DL 201	3.45	-3.03
DL 206	3.29	-3
DL 209	2.93	-3.6
DL 210	3.04	-3.29
DL 38	3.23	-3.87
DL 39	3.16	-3.34
DL 40	3.31	-3.47
DL 43	3.84	-3.21
DL 46	3.47	-3.9
DL 49	3.61	-4.23
DL 52	3.78	-4.11
DL 54	3.69	-3.3
DL 58	3.33	-3.15

**Table 20 Dealul cu Cununa – Dealul Mare**

Sample	$\delta^{13}\text{C}$	$\delta^{18}\text{O}$
D 9074	1.15	-4.52
D 9075	0.92	-5.96
D 9076	1.38	-4.14
D 9077	2.84	-2.97
D 9078	3.94	-2.45
D 9080	4.12	-2.74
V97-530	3.63	-3.06
V97-531	3.4	-3.97
V97-532	4.16	-3.03
V97-533	4.83	-2.05
V97-534	4.97	-1.97
V97-535	4.82	-2.3
V97-538	4.93	-2.43
V97-539	4.5	-2.87
V97-540	4.84	-2.39
V97-541	4.73	-2.7
V97-542	4.35	-2.71
V97-544	3.98	-2.76

**Table 21 Uzum Bair**

D 9082	3.09	-5.14
D 9083	3.59	-5.14
D 9085	4.23	-4.54
D 9086	3.79	-4.49
D 9088	3.46	-4.1
D 9091	4.14	-6.88
D 9092	4.49	-6.91
D 9093	3.26	-5.43
D 9095	1.96	-4.41
D 9096	1.24	-3.88
D 9101	1.57	-4.28
D 9105	1.74	-2.5
D 9106	1.84	-2.35
D 9108	1.59	-2.99

**Table 22 Zebil Quarry**

Sample	$\delta^{13}\text{C}$	$\delta^{18}\text{O}$
D9012	0.18	-3.12
D9013	1	-2.06
D9014	0.94	-2.5
D9015	0.85	-2.41
D9016	1.28	-2.37
D9017	1.24	-2.83
D9018	0.79	-2.34
D9019	0.99	-2.75
D9020	0.99	-2.75
D9022	1.29	-2.49
D9023	1.02	-3.27
D9024	1.65	-2.47
D9026	1.53	-3.02
D9027	1.43	-3.47
D9028	1.78	-2.93
D9029	2.11	-3.21
D9030	2.1	-2.5
D9031	2.3	-2.75
D9032	2.85	-2.36
D9033	2.79	-2.51
D9034	2.69	-3.17
D9035	3.18	-2.05

**Table 23 Olga Quarry**

R95-418	3.57	-1.67
R95-419	3.45	-1.84
R95-420	3.46	-1.51
R95-421	3.51	-1.7
R95-422	3.4	-1.52
R95-423	3.38	-2.21
R95-424	3.35	-1.57
R95-425	3.33	-1.66
R95-426	3.32	-1.76
R95-427	3.4	-1.55
R95-428	3.38	-1.4
R95-429	3.38	-1.54
R95-430	3.31	-1.77
R95-431	3.16	-1.42

Tabel 24 Trei Fantani and Bididia Quarries

Sample	$\delta^{13}\text{C}$	$\delta^{18}\text{O}$
R 95-152	0.7	-5.67
R 95-153	0.63	-5.52
R 95-154	0.73	-5.1
R 95-155	0.63	-5.5
R 95-156	0.44	-5.09
R 95-157	0.38	-4.96
R 95-157a	0.5	-7.04
R 95-227	3	-3.93
R 95-230	1.37	-7.15
R 95-232	1.63	-7.39
R 95-234	1.63	-7.3
R 95-235a	1.58	-7.42
R 95-235b	1.65	-6.89
R 95-236	1.76	-6.86
R95- 237	2.04	-7.86
R 95-239	3.15	-2.78
R95-240a	2.51	-5.33
R95-240b	3.19	-3.57
R 95-241a	2.67	-2.07
R 95-241b	2.32	-5.02
R 95-242	2.24	-5.33
R 95-243	2.29	-5
R 95-244	2.11	-5.08
R 95-245	2.36	-3.17
R 95-246	2.18	-4.74
R 95-248	2.21	-4.57
R 95-249	2.1	-4.64
R 95-250	1.75	-5.33
R 95-251	1.71	-4.38
R 95-252	2.37	-2.87
R 95-253	1.67	-4.54
R 95-254	2.76	-1.8
R 95-255	1.77	-4.42
R 95-256	1.89	-4.2
R 95-257	1.91	-4.22
R 95-258	1.86	-4.19
R 95-260	1.67	-3.97
R 95-261	1.4	-4.97
R 95-262	1.56	-4.05
R 95-264	1.48	-4.2
R 95-265	1.56	-3.83
R 95-267	1.49	-4.24
R 95-268	1.42	-4.25
R 95-270	1.47	-4.04
R 95-273	1.49	-3.03
R 95-275	1.61	-4.22
R 95-277	1.64	-3.8
R 95-278	1.6	-2.83
R 95-279	1.78	-3.65
R 95-284	1.95	-3.56
R 95-285	1.88	-4.3
R 95-286	1.9	-4.11
R 95-287	2.38	-4.34

R 95-287	2.38	-4.34
----------	------	-------

Sample	$\delta^{13}\text{C}$	$\delta^{18}\text{O}$
R 95-295	2.01	-4.22
R 95-298	2.39	-3.13
R 95-300	2.03	-4.44
R 95-302	1.83	-4.7
R 95-304	2.26	-4.82
R 95-306	2.36	-4.37
R 95-307	2.66	-4.69
R 95-308	2.46	4.12
R 95-310	2.97	-4.88
R 95-311	1.94	-5.41
R 95-312	3.24	-4.57
R 95-313	3.09	-5.29
R 95-315	1.92	-6.131
R 95-318	1.15	-6.13
R 95-320	1.84	-5.95
R 95-321	1.18	-6.07
R 95-322	0.58	-6.05
R 95-324	0.91	-5.63
R 95-326	0.76	-5.53
R 95-330	-0.4	-5.43
R 95-333	0.8	-5.62
R 95-335	1.07	-5.78
R 95-337	0.68	-6.1
R 95-338	-1.71	-7.06
R 95-340	0.47	-7.12
R 95-343	1.24	-6.91
R 95-345	0.75	-6.91
R 95-348	-0.01	-6.99
R 95-349	0.63	-7.35
R 95-351	0.63	-6.93
R 95-353	0.94	-6.81
R 95-355	0.55	-6.81
R 95-358	0.01	-6.78
R 95-360	-0.05	-6.73
R 95-362	0.18	-6.65
R 95-363	-0.54	-7.13
R 95-364	0.37	-6.83
R 95-366	-1.01	-6.69
R 95-368	0.12	-6.64
R 95-370	0.74	-6.74
R 95-373	0.79	-6.58
R 95-376	1.11	-6.55
R 95-378	0.92	-6.91
R 95-380	0.76	-6.56
R 95-382	0.61	-6.58
R 95-383	1.21	-6.54
R 95-385	1.37	-6.68
R 95-386	0.81	-6.6
R 95-388	1.2	-6.74
R 95-390	1.22	-6.48
R 95-391	1.63	-6.52
R 95-393	0.02	-6.56
R 95-396	1.05	-6.17

R 95-396	1.05	-6.17
----------	------	-------



**Table 25 Congaz, Dobrogea**

Sample	$\delta^{13}\text{C}$	$\delta^{18}\text{O}$
R97-545	3.61	-2.3
R97-546	3.68	-2.69
R97-547	3.72	-2.05
R97-548	3.47	-2.61
R97-549	3.61	-2.28
R97-550	3.67	-2.54
R97-551	3.71	-2.93
R97-552	3.74	-2.53
R97-553	3.59	-3.07
R97-554	3.86	-3.42
R97-555	3.77	-3.24
R97-556	2.98	-2.3
R97-557	3.15	-2.88
R97-558	3.36	-3.22
R97-559	2.43	-4.14
R97-560	2.82	-4.83
R97-561	2.5	-5.18
R97-562	2.65	-3.82
R97-563	2.45	-4.63
R97-564	2.6	-3.61
R97-566	1.8	-6.62

**Table 26 Cataloi, Dobrogea**

D9122	0.46	-6.24
D9123	0.32	-6.37
D9124	0.12	-7.39
D9125	-0.17	-6.37
D9126	1.02	-6.33
D9127	0.52	-6.4
D9128	0.49	-6.3
D9129	0.83	-6.31
D9130	0.39	-6.26
D9131	0.46	-6.24
D9132	0.32	-6.37

**Table 27 Kcira, Albania**

Sample	$\delta^{13}\text{C}$	$\delta^{18}\text{O}$
AK2a	0.9	-3.81
AK5	2.27	-2.96
AK17	2.46	-2.93
AK20	2.39	-2.91
AK21	3.16	-2.41
AK22	2.45	-2.61
AK25	3.47	-2.41
AK27	3.8	-3.33
AK29	3.85	-2.73
AK30	4.07	-2.14
AK31	4.15	-2.02
AK32	4.33	-2.07
AK33	4.21	-2.58
AK35	3.93	-2.77
AK36	3.68	-2.45
AK37	3.31	-2.4
AK38	2.71	-1.52
AK39	2.17	-2.75
AK40	2.45	-2.53
AK50	1.95	-2.9
AK57	2.16	-1.93
AK62	0.62	-3.77